UNIVERSITÀ DI PARMA

PhD in Biotechnology and Life Science

Ciclo XXXIV

# POTENTIAL HEALTH RISKS AND BIOMEDICAL APPLICATIONS OF ENGINEERED INORGANIC NANOPARTICLES


**PhD Coordinator**

Prof. Marco Ventura

**Tutors**

Prof. Nelson Marmiroli

Prof.ssa Roberta Ruotolo

**PhD student**

Giuseppe De Giorgio


**2019 - 2021**

# ABSTRACT

Synthetic amorphous silica (SAS) is widely used in different fields including the food industry as the additive E551. Since the beginning of its commercialization in the 1950s, SAS is made by two manufacturing methods resulting in the pyrogenic form (NM-203) produced by the thermal route or the hydrated products (precipitated silica, NM-200) produced by the wet route. These manufacturing processes lead to the production of SAS nanoparticles (NPs) that interact to form larger agglomerates and aggregates. In the first part of this work, we evaluated the toxicity of NM-200 and NM-203 in different human cell lines. Especially in THP-1 cells, a human monocytic cell line differentiated into macrophages, NM-203 exhibited greater cytotoxicity than NM-200. An *in vitro* NP-binding assay was performed using protein extracts obtained from THP-1 cells to identify cellular proteins interacting with high-affinity to SAS NPs and forming the so-called 'Hard Protein Corona' (hPC), the composition of which is crucial for the NP bioactivity. We have observed that NM-203 adsorbed a higher amount of proteins on their surface than NM-200 (two-fold increment), although the hPC composition determined by liquid chromatography analysis coupled to mass spectrometry (LC-MS/MS) was the same for both SAS NPs. Hydrophilic and hydrophobic interactions seem to promote the tight adsorption on the surface of SAS NPs of several proteins involved in crucial metabolic pathways. Many of these proteins exhibited a high frequency of intrinsically disordered regions that could drive the protein interaction to SAS NPs by hydrophobic interactions, especially for NM-203, which has a more hydrophobic surface due to the presence of siloxane bridges created during the thermal synthesis method. The interactomic analysis revealed that most of the proteins identified in hPC are constituents of specialized actin-rich structures called 'podosomes' that play important roles in phagocytosis, migration, and adhesion to the extracellular matrix. Confocal microscope and western blot analysis were conducted to evaluate the effects of SAS NP treatment on the abundance of representative podosome proteins. We have observed a de-localization and destructuration of actin filaments, with the formation of punctuate structures, and a reduced abundance of hnRNP K, a RNA-binding protein playing a role in the nuclear metabolism of RNAs but also highly represented in the podosomes. To evaluate the effects of SAS NPs on macrophage functionality we performed a phagocytic assay based on the internalization of fluorescent latex beads by the THP-1 cells. The confocal microscopy analysis showed a nearly complete block of the phagocytic process also at low dosage of both silica NPs. In conclusion, we have observed an increased cytotoxicity of NM-203 compared to NM-200 that could be attributed to a higher surface reactivity of NM-203.

In the second part of my PhD project, we focused on the effects of engineered inorganic NPs in a yeast model of Parkinson's disease (PD) that overexpresses human alpha-synuclein (α-syn), an intrinsically disordered protein (IDP) representing the major component of Lewy bodies (LB), a histological hallmark of PD. In pathological conditions, α-syn undergo a series of lipid-dependent conformational changes leading to the formation of β-sheet-rich aggregates (α-syn oligomers), considered the most neurotoxic forms of α-syn. The overexpression of human α-syn in our yeast model of PD under the control of a galactose-inducible promoter caused a dose-dependent toxicity and a global cellular dysfunction, associated to the formation of α-syn intracellular foci, reminiscent of human LBs. Recent studies showed that SAS NPs promote the process of α-syn aggregation, whereas docking studies revealed that $CeO_2$ NPs best fit in the active site of α-syn. A redox switch between Ce(3+) and Ce(4+) state on the NP surface confers an autoregenerative antioxidant activity to $CeO_2$ NPs making these NPs promising for many biomedical applications. In our yeast PD model, the treatment with SAS NPs did not ameliorate cell viability, but at high doses we observed further toxic effects. Conversely, $CeO_2$ NPs strongly counteracted α-syn-induced toxicity. Microscopic analysis shows that the treatment with $CeO_2$ NPs re-localize α-syn at the plasma membrane level and strongly counteract α-syn foci formation. In line with these results, dot blot analysis revealed that $CeO_2$ NP treatment did not affect the total protein expression levels, but drastically reduced the amount of toxic oligomeric forms of α-syn. We have also observed that the treatment with $CeO_2$ NP restored the mitochondrial morphology, decreased ROS accumulation and strongly counteract the formation of aberrant aggresomes, proteinaceous cytoplasmic inclusions formed when the protein degradation system of the cell is overwhelmed. Analysis of the composition of the hPC formed on the surface of $CeO_2$ NPs showed a direct interaction between these NPs and α-syn, in addition to other yeast proteins involved in metabolic pathways altered by α-syn oligomerization, as the Unfolded Protein Response (UPR) pathway. UPR is a stress response pathway induced by accumulation of misfolded proteins in the endoplasmic reticulum (ER). A chronic activation of this pathway is highly triggered in many neurodegenerative diseases and can lead to programmed cell death. Immunological analysis revealed an increase in the abundance of Kar2, the negative regulator of UPR, after few hours of the treatment with $CeO_2$ NPs, indicating that $CeO_2$ NPs can counteract the chronical activation of UPR pathway. These results are in line with the observations that the upregulation of BiP (the human homolog of Kar2) significantly prevented loss of dopaminergic neurons. In conclusion, $CeO_2$ NPs represent a promising candidate with multi-target mode-of-action which could be used in drug discovery pipelines for the treatment of PD and related disorders.

# 1. INTRODUCTION

## 1.1 Nanotechnology, an overview

Nanotechnology represents one of the most innovative and promising disciplines born in the 21st-century. The first reference to nanotechnology was given in 1959 by Richard Feynman, in a lecture entitled "*There's Plenty of Room at the Bottom",* indicating that soon the manipulation of the matter at atomic level would have been possible and crucial for scientific progress. Nanotechnology involves applied science and technology and deals with the understanding, control, and application of sub-micrometric matter originating nanoparticles (NPs) with dimensions ranging between 1 and 100 nm (**Fig. 1**) (Steckiewicz and Inkielewicz-Stepniak, 2020; Hulla et al., 2015). NPs and nanomaterials (NMs) are distinguished by structural determinants, in fact NMs are defined as materials with any structural dimension in the range between 1 and 100 nm, thus they can be synthetized or structured as nanofibers, nanocomposites or nanostructures. NPs instead are nano-objects organized in particles or aggregates having all the three dimensions in the nanoscale (Sudha et al., 2018; Buzea et al., 2007). The high surface volume ratio of NMs compared to the bulk material confers unique characteristics and properties exploited for many applications (Sharma et al., 2018). During the last decades the use of the most disparate NMs or NPs interested different fields e.g.: biomedical, pharmaceutical, agriculture, cosmesis, food. The enormous development of this new scientific branch led to the employment of more than 7 million workers with a turnover of $1 trillion in 2015 (Kim et al., 2011).

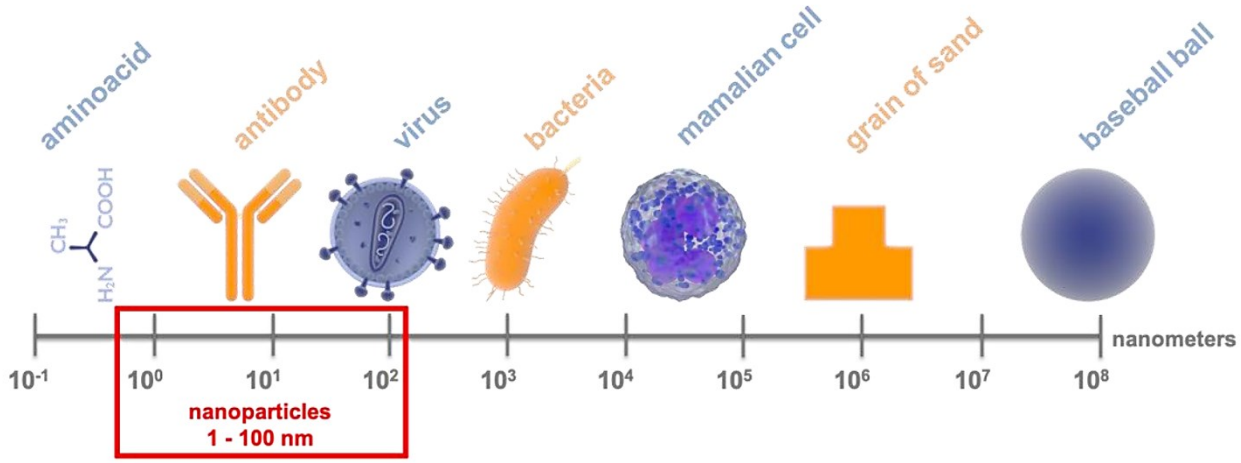


***Figure 1.*** Comparison scale between NPs and other entities. Figure adapted from *(Steckiewicz and Inkielewicz-Stepniak, 2020).*

## 1.2 Synthesis methods

The synthesis methods of NMs are principally two, Bottom-up and Top-down (**Fig. 2**). Top-down synthesis consist in breaking down a large molecule or bulk material using different techniques for example: grinding/milling, physical vapor deposition (PVD), nanolithography, laser ablation, sputtering. The larger starting molecule (or material) is decomposed until converted into nanosized NM or NP; this approach represents a destructive approach and is relatively simple and often used in the industrial field, one of the weak points of this approach is the difficulty in the control of the homogeneity of the final products that could maintain imperfections in the surface structure. (Ealia and Saravanakumar, 2017; Khan et al., 2019). Bottom-up approach consist in a constructive method of synthesis and consist in the building of the NM or NP starting from small precursors consisting in atoms, molecules or clusters. This approach is more economical, thanks to the optimization and control of the synthesis process that produce less waste, and includes different techniques as: Sol-gel, spinning, chemical vapor deposition (CVD) and pyrolysis. One of the most interesting and raising techniques that employs Bottom-up approach is the biosynthesis, also called green synthesis; this method takes advantage of different biological organisms to produce NMs or NPs (Hussain et al., 2016). For example, for the synthesis of metal NPs different bacteria or multicellular eukaryotes are utilized to reduce the metal precursor into NPs in this process the control of growth parameters, media composition, pH or the employ different organisms allow to change the morphology or the size of the final product (Thakkar et al., 2010). Green synthesis generates sustainable, low-cost and nontoxic NPs of various genres.

## 1.3 NPs in the environment: natural or human sources

NPs are also present in nature deriving from different sources and natural events such as volcanic eruptions, wildfires, erosion, dust storms that can produce NPs of various genres and composition. The dispersion of NPs in the environment it may also be due by human activities e.g., engine combustions or chemical industry (Buzea et al., 2007). All this NPs dispersed in the environment from different sources, can by internalized in different ways by human organism and have health implications (Kreyling et al., 2006).

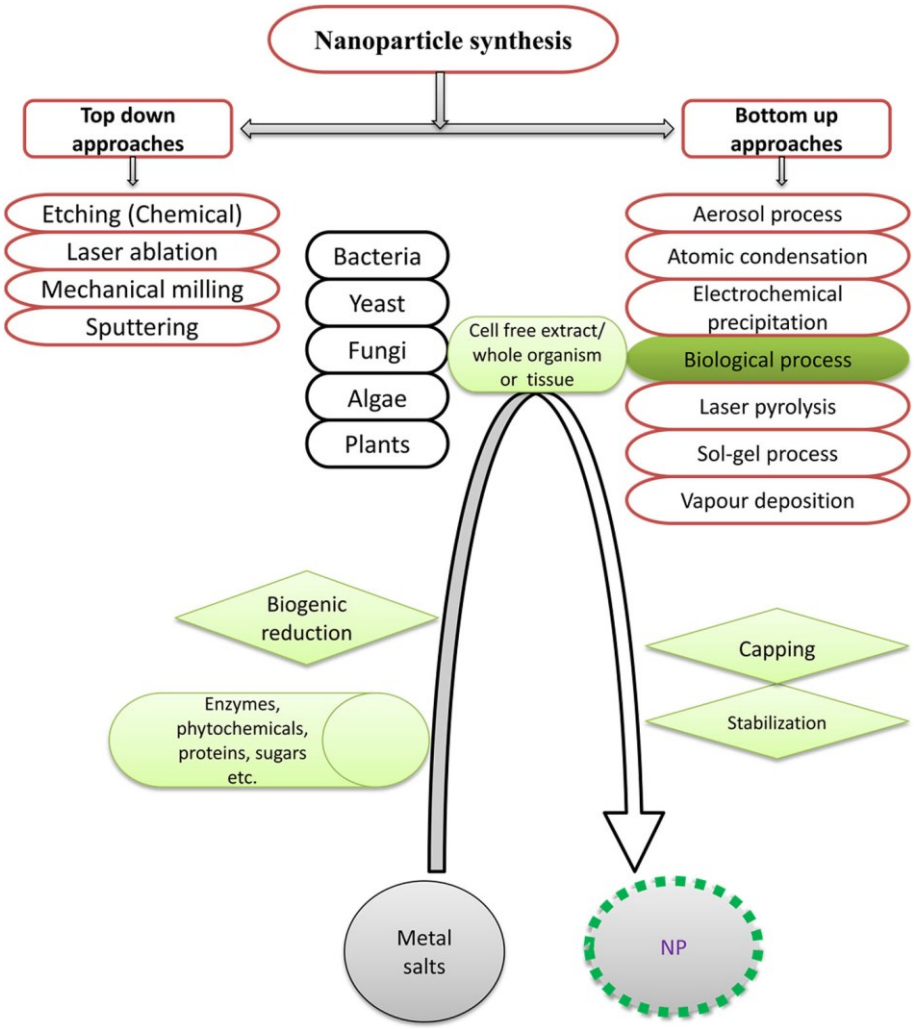


***Figure 2.*** Synthesis methods of NPs showing the Top-down and Bottom-up approaches. Figure adapted from (Hussain et al., 2016).

## 1.4 Classification of NMs

### *1.4.1 Inorganic NMs*

This group includes all inorganic elements based NMs (with few exceptions; **Fig. 3**). For metal-based NMs there are different ways of synthesis and almost all metal elements can be transformed at the nanoscale. This class of NMs can be manipulated to assume different tunable characteristics as: pore size, superficial charge, shape, surface/volume ratio and the hiring of an amorphous or crystalline structure. For these reasons metal-based NMs finds application in a lot of research areas. Another class is represented by metal oxide-based NMs, where the oxidized metal can be employed to offer superior reactivity and physio-chemical properties compared to the metal form (Ealia and Saravanakumar, 2017). In last times ceramic NPs are also getting attention, are synthesized in

different forms (e.g. crystalline, dense, amorphous, porous) (Sigmund et al., 2006), are chemically inert and demonstrate a great heat resistance, for these reasons are applied in the biomedical field (C Thomas et al., 2015). Important inorganic-based NMs are represented by semiconductors, the resistivities and energy gaps in the middle between insulators and conductors are distinctive for this NMs. These parameters are controlled changing the crystal lattice or adding some impurities to modify the conductivity (Terna et al., 2021). Quantum Dots (QDs), take part to the semiconductors NMs class, possess a zero-dimensional structure, then electrons are constrained, quantum states can be tuned during the synthesis to change their optical and emission properties. QDs are applied in electroluminescent devices but also in bio-imaging and solar panels (Bera et al., 2010).

### *1.4.2 Organic NMs*

In last years a strong interest raised on the development and application at the nanoscale for organic compounds as lipids, polymers or carbohydrates (**Fig. 3**). The biomedical field has a great interest on this NMs thanks to the dispersity, structural stability and the controlled release of substances useful for drug delivery applications (Virlan et al., 2016). Different NMs are classified as organic-based NMs (e.g. dendrimers, liposomes, micelles, vesicles and polymeric NPs). Different drug delivery systems can be based on this NMs, drugs can be loaded on or in the NMs by conjugation on the surface, in the core or by physical encapsulation. These attributes mixed with the excellent biocompatibility could be determinant in the development of innovative and more efficient delivery systems.

#### *1.4.2.1 Carbon-based NMs*

This class of specific NMs is based on different carbon structures and are also categorized as organic NMs. Some of the more important compounds representing carbon-based NMs are: fullerenes, carbon nanotubes (CNTs), graphene and nano-diamonds. Fullerenes have unique electric, optical and mechanical properties, thanks to these characteristics are one of the most utilized formulations of carbon-based NMs. In C60 fullerene, for example, carbon atoms are arranged in a globular cage composed of 20 hexagonal and 12 pentagonal rings. In CNTs, atoms are organized in a tubular form, in this shape NM assume different qualities as rigidity, field emission, electric conductivity, and elasticity therefore find application in many fields as promising NMs with excellent and versatile properties. Nano-diamonds are miniaturized diamonds at the nanoscale level, have characteristic of high stability and are utilized as abrasive, protective coatings and semiconductors. One of the last

carbon-based NM is represented by graphene, it exhibits similar properties to nanotubes, but the different morphology allows variations in the electric properties; furthermore, graphene is flexible and at the same time robust and can be used for the formulation of thin and flexible materials (Cha et al., 2013; Sudha et al., 2018).

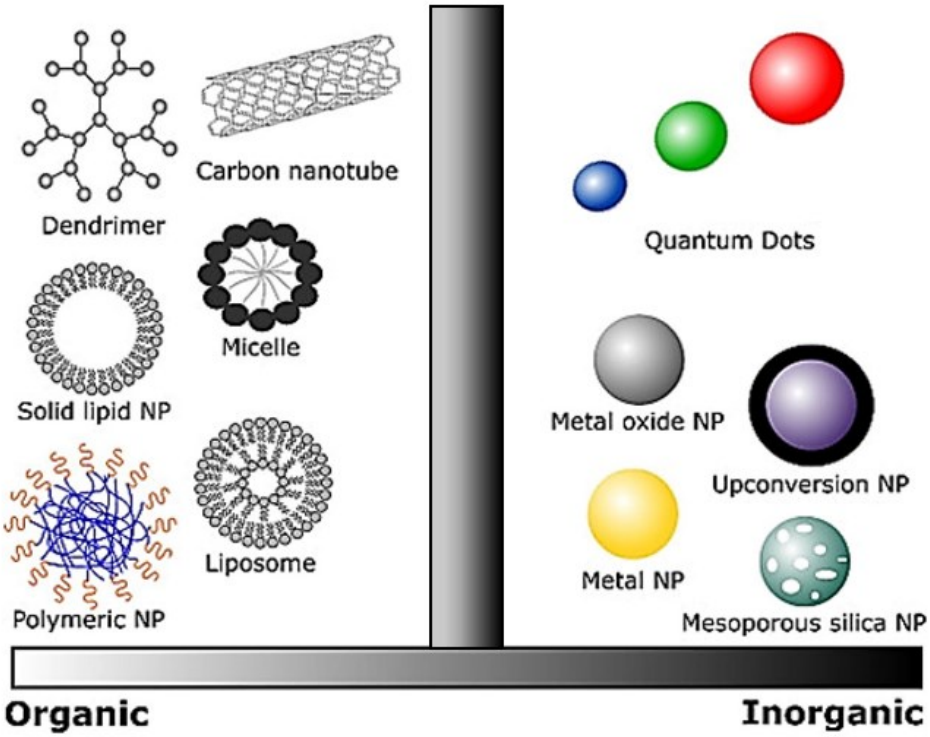


***Figure 3.*** Scheme representing different organic and inorganic NPs. Figure adapted from (Bodunde et al., 2021).

## 1.5 Synthetic silica nanoparticles

Silicon is the common name to identify the bulk material composed by units of silicon dioxide having chemical formula SiO2. It can be found in the environment in crystalline or amorphous form, the crystalline structures can be different depending on the spatial dispositions assumed by the atoms in the three dimensions and take also different names; the common α-quartz after heating is transformed for example into β-quartz, tridymite and cristobalite. The amorphous form is also present in nature as the ordinary glass or as opals. Silica NPs (SiNPs) can be synthesized artificially using different methods generally divided as wet or dry methods, the products show differences in the morphology and in the physio-chemical characteristics (**Fig. 4**). The crystalline forms of silica are characterized by ordered structured that are formed exploiting different synthesis strategies. Different quartz formulations are obtained heating the aqueous solution, obtaining different structures and particles dimensions varying parameters as pressure or temperature. When controlled crystallization occurs in presence of organic molecules, also called porogens, are obtained porosils (Napierska et al., 2010).

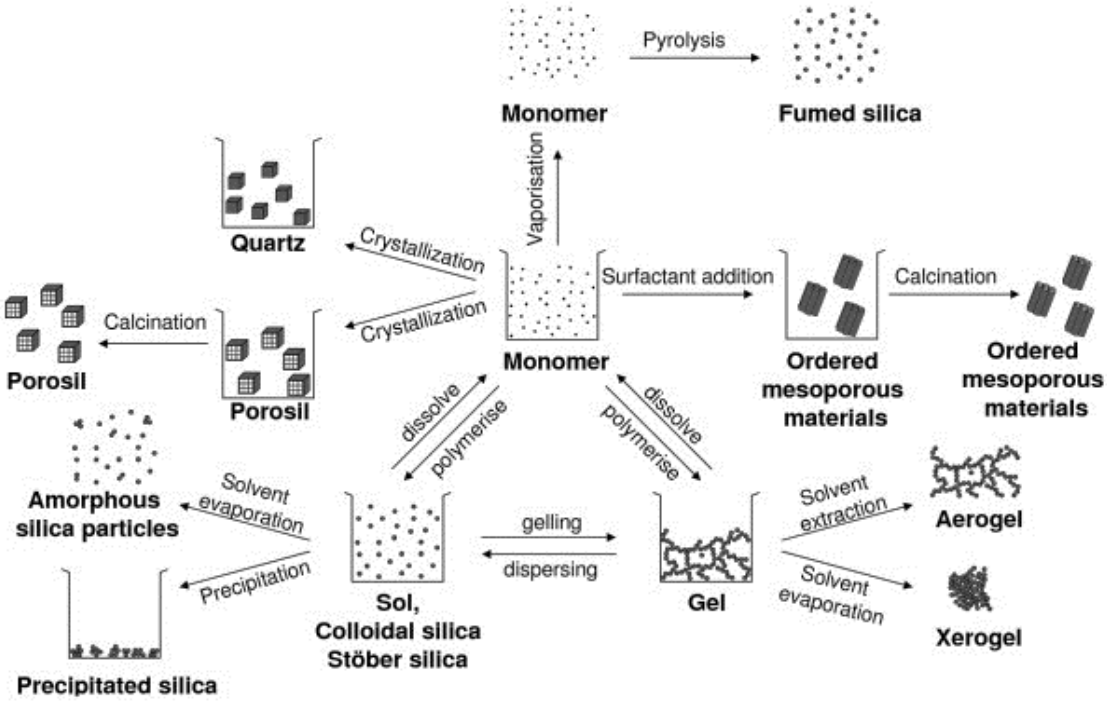


**Figure 4.** Different routes of synthesis of SiNPs. Figure adapted from (Napierska et al., 2010).

In wet approaches we can found different products as the colloidal silica, also named silica sol, composed by dispersion of particles in a liquid medium, in the case of colloidal silica this state can

be reached acidifying an anhydrous concentrated alkaline sodium silicate solution having chemical formula Na2SiO3, this process release $Si(OH)_4$ molecules that condensates, when the concentration is over $2*13^{-3}$M colloidal silica NPs start to forms. Even Stober's silica sol is prepared as a colloidal solution, the precursor utilized for this process is the tetraethylorthosilicate (TEOS), that in an alcoholic solution in presence of ammonia go through subsequent reactions of hydrolysis and polycondensation reactions producing non-porous SiNPs (**Fig. 5a**) (Napierska et al., 2010). This method was successively developed and optimized for the synthesis of different composites, for example during the synthesis process the addition of surfactants is used to synthesize mesoporous silica NPs (MSN) with pore sizes ranging between 2 and 50 nm. Another method is microemulsion, here are exploited oil in water or reverse micelles to create a tunable nano-environment where the reaction of hydrolysis and condensation of the precursor occurs, in this method other molecules can be easily added to drug the NPs for other uses e.g. drug delivery (**Fig. 5b**) (Selvarajan et al., 2020).

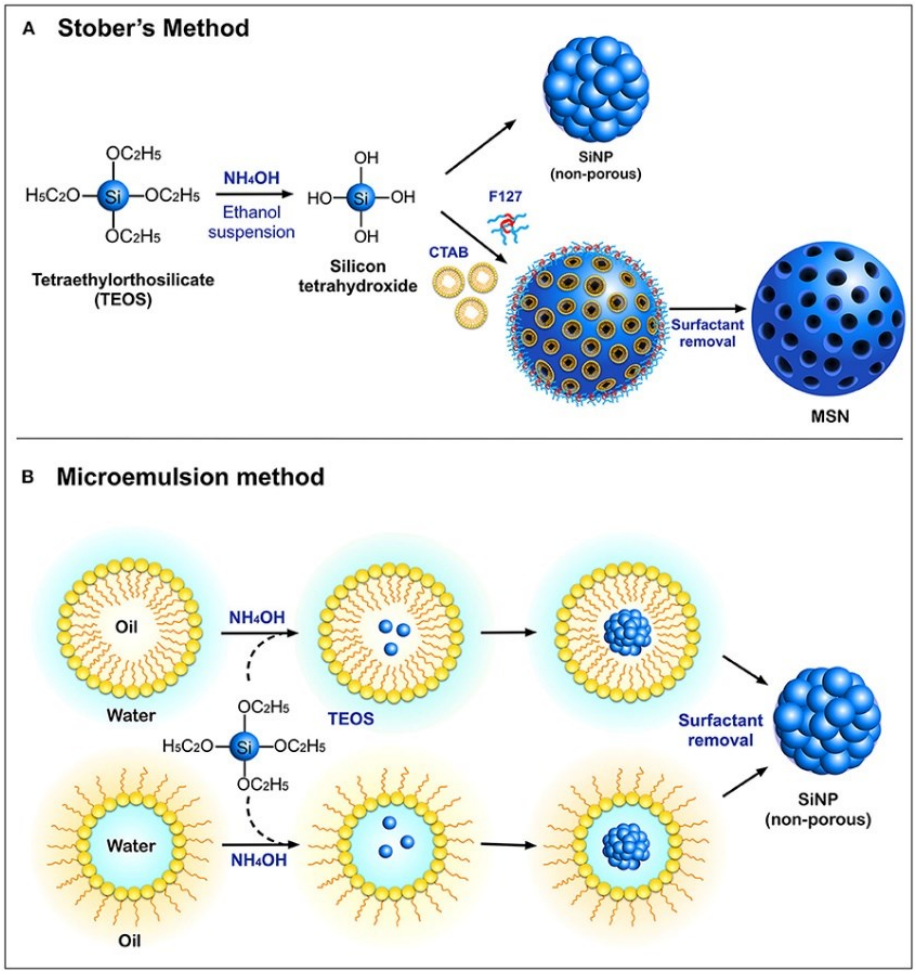


***Figure 5.*** Representation of Stober's and microemulsion methods. Figure adapted from (Selvarajan et al., 2020).

Other variations to the protocol are applied to control shape and dimension, adjusting some reaction parameters as ammonia concentration precursor addition or solution mixing.

When silica sol il destabilized can be obtained silica-gel where 3-D structures parameters of gel change basing on the dimensions of silica sol particles dimensions (**Fig. 4**).

### *1.5.1 Pyrogenic and precipitated silica amorphous silica used in this study*

SAS NPs are one of the most commercially utilized silica NPs, they found application in many fields such as: food additive, in pharmaceutical products or in cosmesis. This NPs are widely used as food additive under the name of E551 including two formulations, precipitated SAS NPs (NM-200) and pyrogenic SAS NPs (NM-203) (Additives et al., 2018). The synthesis of these two formulations is pretty different, NM-200 originates from the silica sol that is destabilized altering temperature or concentrations of the reagents and the times of reaction; the precipitated SAS NPs are then collected washed and desiccated obtaining an extremely pure powder. NM-203 also known as fumed silica come out from distinct synthesis steps, indeed the process start from a vapor phase of silicon tetrachloride (SiCl4), these vapors are oxidized through the exposition to a high temperature flame reaching from 1200°C to 1400°C (Zhang et al., 2012). From this process silicon tetrachloride is oxidized and produces gradually bigger aggregates until forming a fine and fluffy powder of amorphous silica. NM-203 final NPs in particular are characterized by an interesting surface/volume ratio oscillating between 200-300 $m^2/g$ (Napierska et al., 2010).

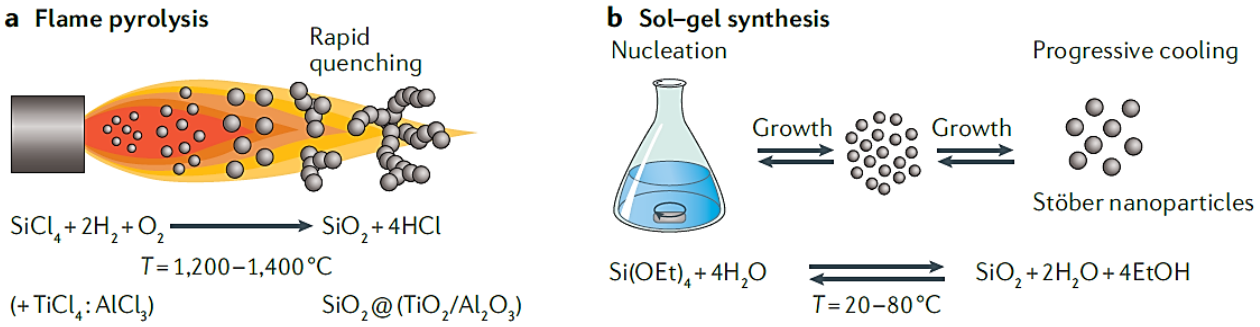


***Figure 6.*** Different synthesis processes characterizing NM-203 (a) and NM-200 or Stober's silica (b). Figure adapted from (Croissant et al., 2020).

### *1.5.2 NM-200 and NM-203, morphology and structural properties*

The synthesis process of these two forms determines important differences under the morphological aspect, NM-203 conditions of synthesis importantly affect the aggregates spatial disposition, characterized by spherical particles that are produced first during the high temperature synthesis, this particles merges to form a more disordered disposition of the aggregates in the 3-D space assuming a fractal dimension and are impossible to divide (**Fig. 7a**). NM-200 is instead characterized by rather ordered disposition (**Fig. 7b**) (De Temmerman et al., 2012). From the TEM images of **Figure 6** is also important to look at the completely amorphous structure of this two NMs.

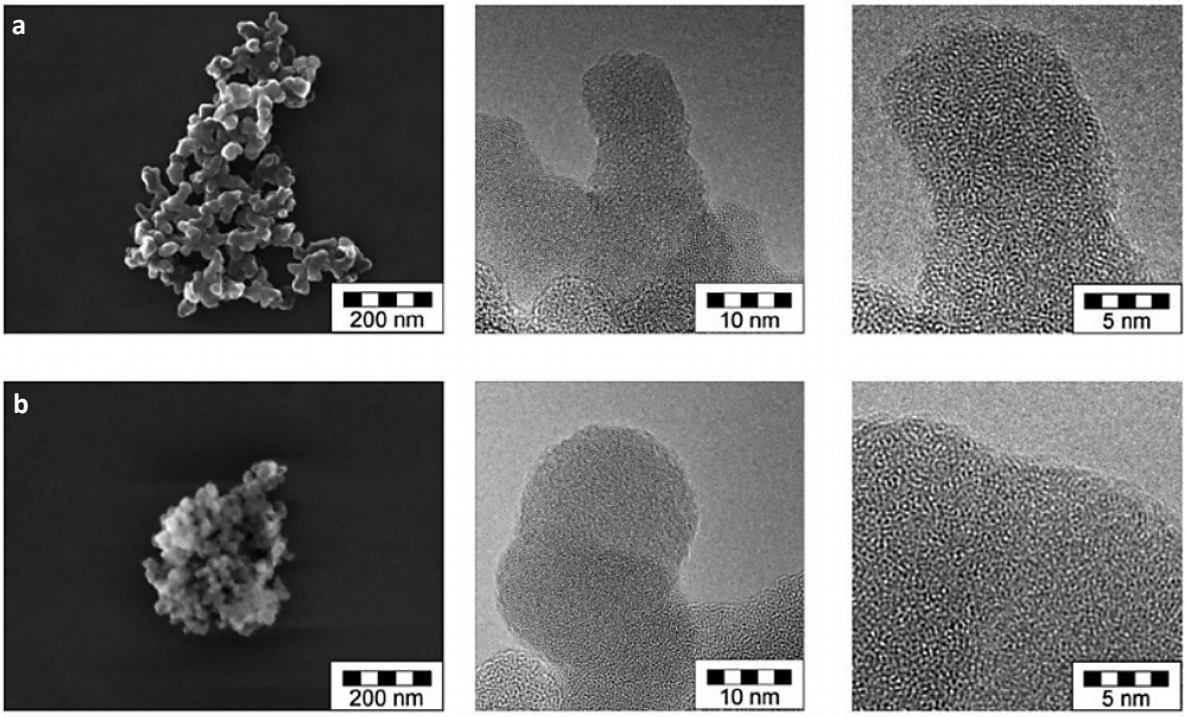


***Figure 7.*** SEM images of isolate aggregates (left) and TEM images with different magnifications (right) of NM-203 (a) and NM-200 (b). Figure adapted from (Albers et al., 2015).

Isolate aggregates are obtained in **Figure 7** by sonication, this process is crucial for NMs that have the natural tendency to form larger macro-aggregates that are difficult to study and analyze. Further details on the morphology can be obtained using other techniques, for example the PCA analysis made by De Temmerman et al. (2012), analyzed three important NMs parameters as mean diameter, sphericity and shape including also NM-200 and NM-202 respectively other two comparable forms of precipitated and pyrogenic silica NPs. The results of this investigation reported a clear similarity in all these three parameters within the precipitated NMs (NM-200 and NM-201)

and pyrogenic NMs (NM-202 and NM-203) groups, but an important divergence between these groups. Especially sphericity and shape factor resulted different between pyrogenic and precipitated SAS NPs (**Fig. 8**).

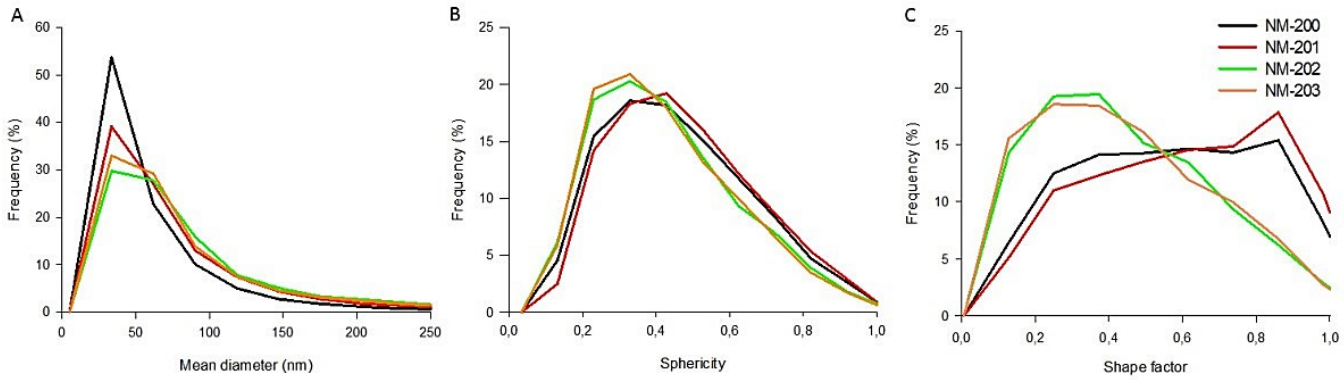


***Figure 8***. Number-based distributions of the mean diameter (A), sphericity (B) and shape factor (C) of agglomerates and aggregates of SAS NPs. Figure adapted from (De Temmerman et al., 2012).

These data together with other works reported important morphological differences between NM-200 and NM-203 where the pyrogenic form, because of the high temperature synthesis method, is characterized by a more disordered and variable structure (Boldridge, 2010). From these morphological distinctions there might be implications on the interaction among biological systems or human organism, that because of the massive deployment of these NPs could potentially enter in contact with this NMs every day.

### *1.5.3 Toxicological impact of the surface chemistry*

The diverse structural characteristics, due different synthesis methods, have also important reflections on the chemical groups exposed on the surface of the NPs. Basically SAS NPs are composed by siloxane bonds (Si-O-Si) in the core part of the particles, in the superficial part this siloxane chains stops forming silanol groups that are exposed outside. The chemistry of silanols variate basing on the quantity of the exposed groups, vicinal silanols groups can in fact interact each other through hydrogen bonds. There are also different typologies of silanols as geminal and isolated silanols groups that possess lower pKa thus aren't hydrogen bonded although vicinal (**Fig. 9a**). The siloxane network is structured in interlinked rings, these rings are classified in unstrained when composed by 4 or more atoms of Si and in strained when the atoms are 2 or 3. On the exterior

of the particles the exposing part of the rings also take the name of siloxane bridges, NM-203 during the high temperature synthesis process acquire a high quantity of 2 or 3 membered rings that in the wet methods are absent, these strained rings have a great propensity to homolytic cleavage, directly responsible in the generation of hydroxyl radicals (**Fig. 9b,d**). Also, other surface radical can be formed on the SAS NPs surface (**Fig. 9c**) and events as radical-transfer can take place on the surface of SAS NPs (**Fig. 9e**), where high surface volume ratio has an enhancing effect of these events. (Croissant et al., 2020; Zhang et al., 2012).

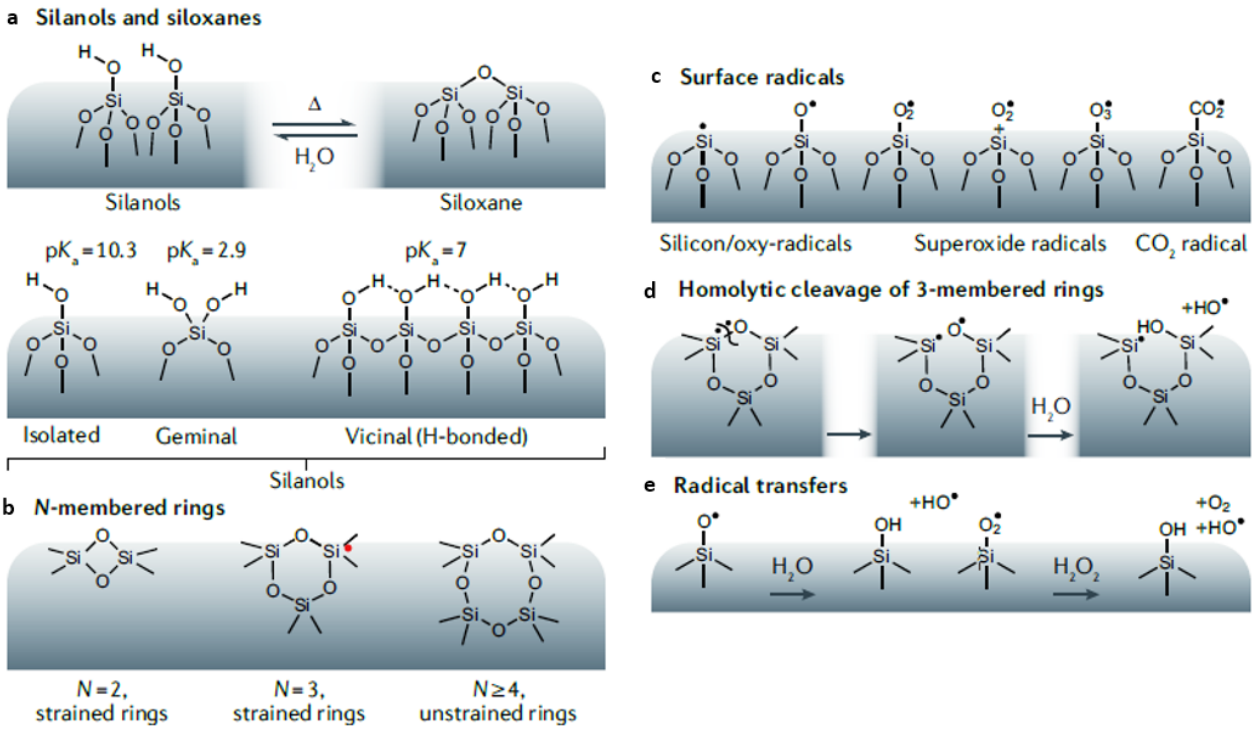


***Figure 9.*** Chemistry of the different groups present on SAS NPs and examples of radical species formation that can occur on the surface. Figure adapted from (Croissant et al., 2020).

Surface hydrophobicity and hydrophilicity represent another critical element that differentiate NM-200 and NM-203, these attributes are conferred by silanols superficial groups. As previously mentioned, silanols vicinal groups and other silanols species that are hydrogen bonded have a good propensity in hydrophilic interactions with water molecules. On the other hand, isolated silanols, geminals and siloxane bridges are hydrophobic because they can't form hydrogen bonds. In NM-203 the high temperatures synthesis has important repercussion on surface chemistry, reducing the overall silanols that are fused forming siloxane bonds, consequentially hydrogen bonding available

groups are drastically lowered. NM-200 not being exposed to high temperatures is rich in silanols and characterized by a higher hydrophilicity (Napierska et al., 2010). This differences could also have important repercussion on a differential toxicity and biological interaction of the two formulations.

### *1.5.4 Toxicity determinants of SAS NPs*

To assess the toxicity of NPs or drugs, one of the principal *in vitro* tests is represented by the hemolytic assay. NM-200 and NM-203 shows a different hemolytic activity in red blood cells (RBC), Zhang et al. (2012) tested both these two formulations finding a low hemolysis activity by precipitated Stober's silica and an important higher activity by the fumed silica at the same conditions of treatment (Zhang et al., 2012). These results are similar with those of Slowing et al. (2009) where an important difference caused by the two synthesis methods was found and fumed silica aggregates showed an important hemolytic effect (**Fig. 10a**). The main cause of those different effects can be found in silanols groups that establish interactions at physiological pH with secondary proteins amides and with the trimethyl-ammonium head groups of the membrane lipids. The membrane perturbation caused by these interactions could be a critical factor to differentiate the toxicology of precipitated or fumed NPs. On the other hand, fully hydroxylated forms of crystalline silicas showed a lower hemolytic effect. To confirm this theory, the functionalization of silanols groups with positive 3-aminopropyl groups drastically lowered the hemolytic activity of NM-203 and didn't alter the activity of MSN utilized in this work (**Fig. 10**). The electrostatic interactions are central to explain the different interactions within biological membranes, the functionalization in fact switched the z-potential from -49 to +27 mV. NM-203 resulted more hemolytic because have more geminal and isolated silanols and less hydroxyl groups that cause the electrostatic repulsion with RBC membrane. Thus NM-203 obtain a sensible higher interaction with the membrane, where at the same time more hydrophilic SAS NPs formulation are characterized by a superior membrane repulsion and less interactions with the membrane lipids and proteins (Gerashchenko et al., 2002; Slowing et al., 2009).

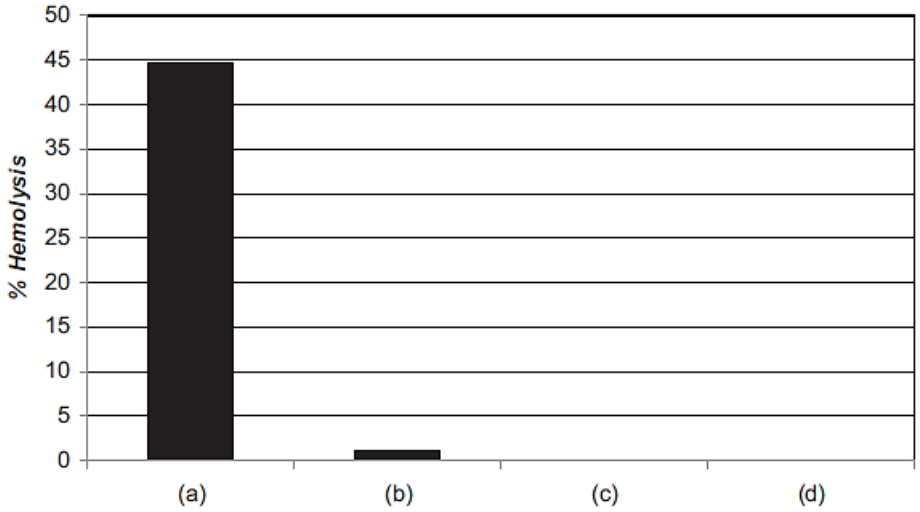


***Figure 10.*** The hemolytic effects on RBC of Fumed silica (a) versus MSN (b), after the functionalization with positive 3-aminopropyl groups the hemolytic activity of the fumed silica is suppressed (c) while for MSN the low activity remains unaffected (d). Figure adapted from (Slowing et al., 2009).

The stronger activity of NM-203 must be evaluated also considering the presence of the strained (2 or 3 membered) siloxane rings and the other chemical groups mentioned before, representing a source of radical species, the formation and the consequent reactivity of the radical species take to a peroxidation of the membrane lipids and a consequent lysis of the cells. *In vitro* cytotoxicity assays also demonstrate an important decrease of the viability in human lung epithelial BEAS-2B cells treated with different silica NP typologies, where NM-203 importantly decreased cell viability compared to other formulations (**Fig. 11**). Another important work made by Farcal et al. (2015) evaluated NM-200 ad NM-203 toxicity in human monocyte-derived macrophages (HMDM) cells, again the comparison between the two SAS NPs confirmed a major viability decrease from NM-203 exposition (**Fig. 12**). In this work another important screening has been made, treating different cell lines with this two SAS NPs forms and other typologies of oxide NMs. The results reported that NM-200 and NM-203 demonstrated important toxic effect in Murine alveolar macrophages (MH-S) cells. In this case was measured the IC50 index, a classical index that define the concentration of NM necessary to inhibit 50% of the growth of the cells under study. The IC50 for MH-S cells was <10 µg/ml for NM-203, indicating a higher toxicity compared with NM-200 with a IC50 comprised

between 25 and 60 µg/ml. Another cell that showed similar effects on viability was the mouse embryonic stem (mES) cell line where NM-203 showed a higher toxicity (**Fig. 13**) (Farcal et al., 2015).

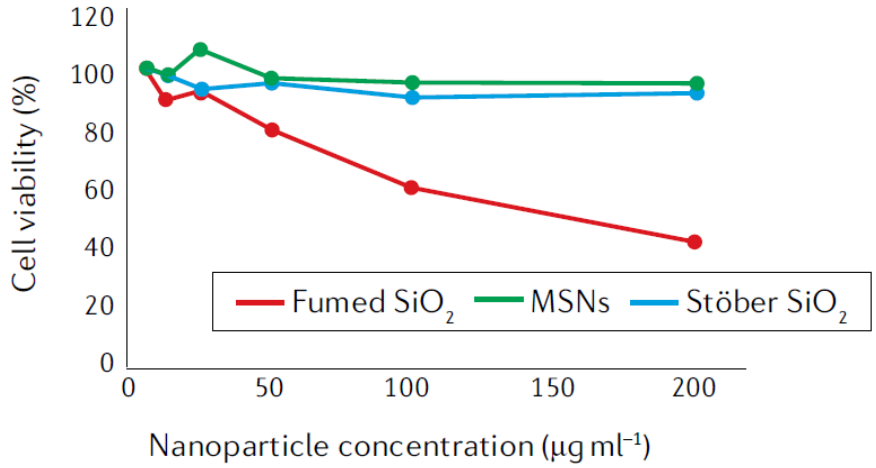


***Figure 11.*** BEAS-2B cells viability assay with different SAS NP formulations. Figure adapted from (Croissant et al., 2020).

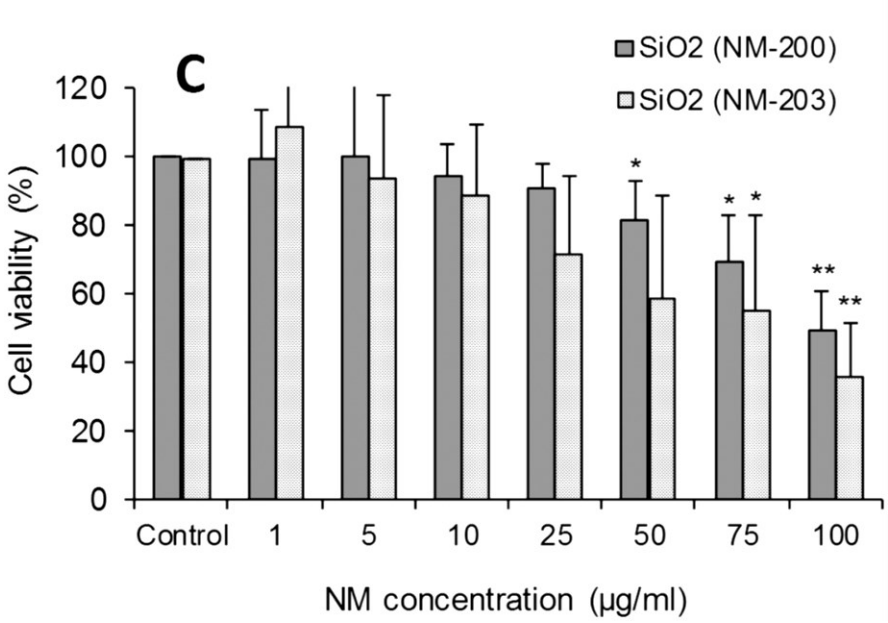


***Figure 12.*** HMDM cell viability after the treatment with NM-200 or NM-203. Figure adapted from (Farcal et al., 2015).

| System | Cells | Exposure time | $TiO_2$ | | ZnO | | $SiO_2$ | | Assay |
|---|---|---|---|---|---|---|---|---|---|
| | | | NM-103 | NM-104 | NM-110 | NM-111 | NM-200 | NM-203 | |
| Immune system | HMDM | 24h | >100 | >100 | >100 | >100 | ~100 | 75-100 | LDH |
| | Raw 264.7 | 24h | >100 | >100 | 12.48 | 12.75 | >100 | >100 | Resazurin |
| | | 48h | >100 | >100 | 12.16 | 14.88 | >100 | >100 | |
| | | 72h | >100 | >100 | 14.72 | 10.88 | >100 | 64.00 | |
| | | 24h | >100 | >100 | 18.40 | 15.68 | >100 | >100 | NRU |
| | | 48h | >100 | >100 | 25.48 | 19.64 | >100 | >100 | |
| | | 72h | >100 | >100 | 19.68 | 22.08 | >100 | 86.40 | |
| | | 24h | >100 | >100 | - | - | - | - | WST-8 |
| | | 24h | >100 | >100 | - | - | - | - | LDH |
| | MH-S | 24h | >100 | >100 | 22.08 | 24.64 | 59.36 | 8.96 | Resazurin |
| | | 48h | >100 | >100 | 17.44 | 19.68 | 26.56 | 6.24 | |
| | | 72h | >100 | >100 | 17.92 | 19.68 | 25.92 | 6.24 | |
| | | 24h | >100 | >100 | 19.68 | 20.16 | 54.08 | 5.44 | NRU |
| | | 48h | >100 | >100 | 21.44 | 13.28 | 30.4 | 7.04 | |
| | | 72h | >100 | >100 | 23.04 | 15.20 | 27.68 | 6.24 | |
| Respiratory system | Calu-3 | 24h | >100 | >100 | >100 | >100 | >100 | >100 | Resazurin |
| | | 48h | >100 | >100 | >100 | >100 | >100 | >100 | |
| | | 72h | >100 | >100 | 94.08 | >100 | >100 | >100 | |
| | | 24h | >100 | >100 | >100 | >100 | >100 | >100 | NRU |
| | | 48h | >100 | >100 | >100 | >100 | >100 | >100 | |
| | | 72h | >100 | >100 | >100 | >100 | >100 | >100 | |
| | RLE-6TN | 24h | >100 | >100 | - | - | - | - | WST-8 |
| | | 24h | >100 | >100 | - | - | - | - | LDH |
| | 16HBE | 24h | >100 | >100 | 17.79 | 56.46 | >100 | >100 | WST-8 |
| Male reproductive system | TM3 | 24h | >100 | >100 | 10.06 | 6.16 | >100 | >100 | WST-1 |
| | TM4 | 24h | >100 | >100 | 11.88 | 7.16 | >100 | >100 | WST-1 |
| Embryonic tissues | NIH/3T3 | 24h | >100 | >100 | - | - | - | - | LDH |
| | | 24h | >100 | >100 | - | - | - | - | WST-8 |
| | | 10d | 37.4 | >100 | 1.09 | 0.40 | 45.00 | 52.00 | WST-1 |
| | mES | 10d | 11.40 | 23.50 | 11.08 | 15.50 | >100 | 21.80 | WST-1 |
| Kidneys | NRK-52E | 24h | >100 | >100 | - | - | - | - | WST-8 |
| | | 24h | >100 | >100 | - | - | - | - | LDH |

| IC50 (µg/ml) | <10 | 10,1-30,0 | 30,1-50,0 | 50,1-70,0 | 70,1-100,0 | >100 |
|---|---|---|---|---|---|---|
| Code colour | | | | | | |

***Figure 13***. Evaluation of IC50 index of different NMs, in particular for SAS NPs NM-203 showed a higher toxicities compared to NM-200 especially in immune system cells. Figure adapted from (Farcal et al., 2015).

### *1.5.5 Uptake of SAS NPs by cells*

Different *in vitro* experiment on various cell lines evidenced cellular uptake of SAS NPs with various modalities. The three main ways of internalization of NPs are represented by endocytosis macropinocytosis and phagocytosis, basing of the typology SAS NP formulation different internalization methods are employed by cells resulting in different toxic outcomes (**Fig. 13a**) (Fatieiev et al., 2017) (Dong et al., 2020). In the study from Zhang et al. (2012) the treatment with Stober's colloidal SAS NPs in BEAS-2B cells showed that the internalization pathways involved were macropinocytosis and endocytosis. Instead for NM-203 was evident a membrane perturbation event caused by the treatment with the NPs, the membrane appeared ruffled, and the uptake toke place through filapodia formation and subsequent phagocytosis by the cells (Zhang et al., 2012)**.** As previously mentioned for NM-203, the higher electrostatic affinity for membranes it's also reflected in the interaction with cells (**Fig. 13b**) (Croissant et al., 2020). Thus NM-203 and NM-200 have different ways of interaction and could elicit different effects on cells.

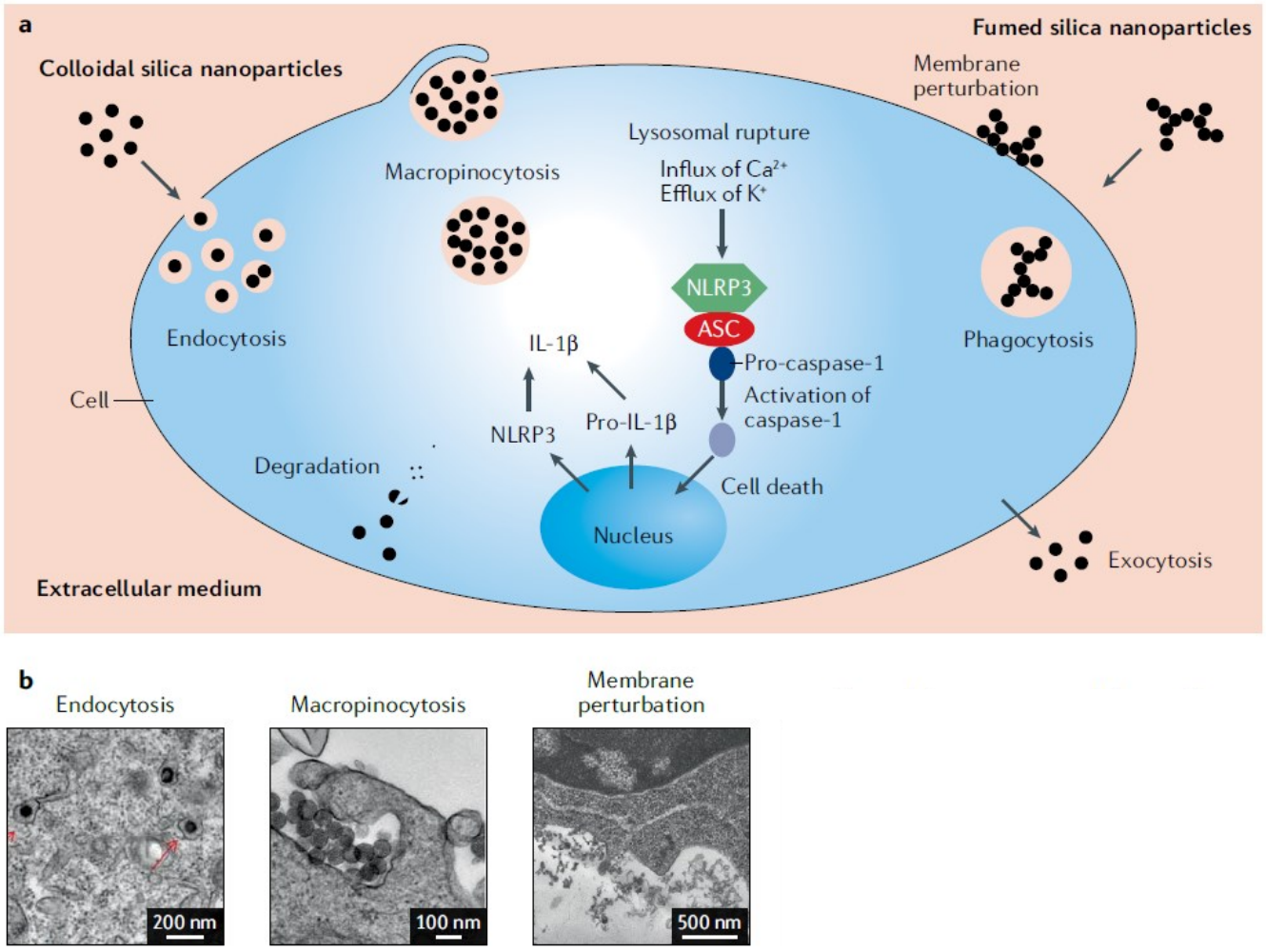

***Figure 13.*** (a) Different internalization pathways involved in the interaction between cells and SAS NPs, (b) TEM images showing the uptake events and membrane interaction of NM-203. Figure adapted from (Croissant et al., 2020).

Another important evidence of the different interactions was detected by Di Cristo et al. (2016) on MH-S cells and the murine macrophage cell line (RAW264.7) using He-ion microscopy (HIM), in this experiment cells were treated for 24 h with NM-200 or NM-203 SAS NPs 10 µg/cm$^2$ in **Figure 14** are clearly visible the different interactions modalities, NM-200 NPs are visible as agglomerates near the cells and the interactions seem to be weaker in comparison with NM-203 NPs that completely surrounded the cells that appears rough, MH-S cells interacted stronger with NM-200 than RAW264.7 cells (Di Cristo et al., 2016). These images confirmed the different interactions of the two SAS NP formulations with the cellular plasma membrane.

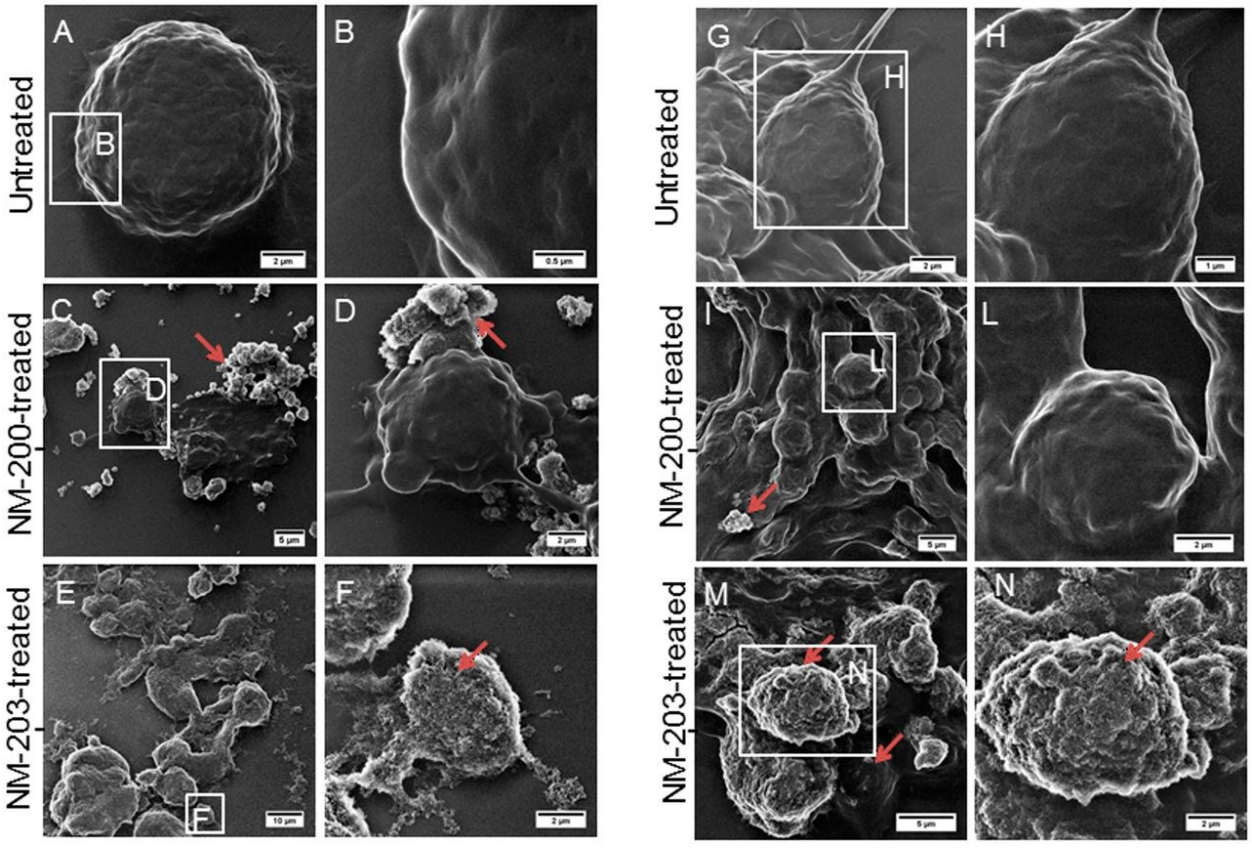


***Figure 14.*** Visualization of MH-S (A-F) and RAW264.7 (G-N) cells through HIM. Cells were treated or not with NM-200 or NM-203 SAS NPs. Figure adapted from (Di Cristo et al., 2016).

Other cells lines were examined demonstrating the NPs internalization, human non-small cell lung carcinoma cells (H1299) were also able to uptake 50 nm SAS NPs, in this case NPs were found incapsulated in organelle or free in the cytoplasm but never in the nucleus (Chu et al., 2011). Also, in human umbilical vein endothelial cells (HUVEC) the internalization of 15 nm, 30 nm and 100 nm SAS NPs has been proven, in this case cytotoxicity was size dependent, where 15 nm NPs demonstrated a higher cytotoxicity. HUVEC cells internalized the NPs that were found in the lysosome and also the cellular morphology was altered (Liu et al., 2021b). In another study performed using RAW264.7 cells were employed colloidal fluorescent 70 nm SAS NPs unmodified, or chemically modified with amine or carboxyl groups. The unmodified SAS NPs showed a higher cytotoxicity where at the same time modified NPs didn't show important cytotoxic effect, suggesting in this case that surface groups are crucial for the toxicity of the NPs. The uptake and the localization were also different, where unmodified NPs localized in the cytoplasm and also in the nucleus, amine modified NPs localized only in the plasma membrane and the carboxyl modified NPs localized in the cytoplasm in a modest concentration (**Fig. 15**) (Nabeshi et al., 2011).

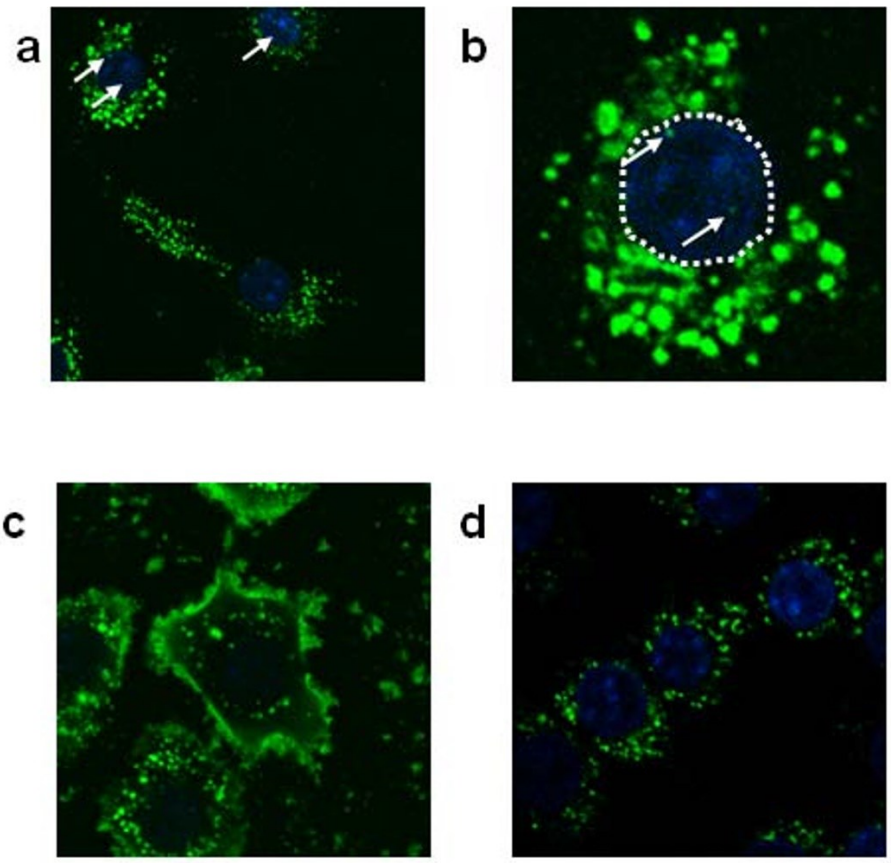


***Figure 15.*** Internalization of different types of fluorescent SAS NPs (70 nm) on RAW264.7 cells. (a,b) Unmodified NPs characterized by a high levels of internalization, (c) amine-modified SAS NPs

localized to the plasma membrane, (d) carboxyl-modified SAS NPs internalized in the cytoplasm at lower concentration. Nuclei (in blue) were stained with DAPI; white arrows indicates the NPs localized in the nuclear space. Figure adapted from (Nabeshi et al., 2011).

This work underlines the importance of the surface composition in the interaction between SAS NPs and cells, modifications of silanols groups could importantly affect the uptake pathways and the sub-cellular localization of the NPs.

### *1.5.6 In vitro cellular effects*

The internalization or the superficial interactions of SAN-NPs lead to significant cellular effects, different between NM-200 and NM-203. NM-203 is actually internalized by cells in a modest extent and the effects deriving from these interactions are hypothetically attributable to those observed with the asbestos fibers, called frustrated phagocytosis. In this process the cells can't conclude the phagocytic process and NLRP3 inflammasome is activated, leading to maturation of interleukin (IL)-1ß and the triggering the inflammation (Ishida et al., 2019). Similar effect were observed in human monocytic cell line derived from an acute monocytic leukemia (THP-1) cells, where NM-203 treatment activated Nalp3 inflammasome and (IL)-1ß, on the other hand NM-200 treatment modestly activated the (IL)-1ß production. Moreover, the inflammation triggering isn't directly dependent by the "classic" lysosomal damage and cathepsin b release associated with asbestos fibers, but supposedly by the strained rings present on NM-203 surface that producing radicals and triggers the inflammation response. Different effects are once again directly dependent by the physiochemical characteristics and different uptake pathways (Zhang et al., 2012). In MH-S and RAW 264.7 cells other inflammation markers were tested after NM-200 and NM-203 exposure and Nos2 induction, NO production, Hmox1 and TNF-α levels were importantly modulated after the treatment. Moreover, for NM-203 these effects were always higher than NM-200, demonstrating a pro-inflammatory effect by the SAS NPs where Hmox1 levels modulation confirm an oxidative stress basis (Di Cristo et al., 2016). In the last years all these evidences, especially in immune system related cells, raised the attention on SAS NPs but still are needed further validations. Anyway, radical oxygen species (ROS) are constantly a common cytotoxic factor in different SAS NP formulation and can explain a lot of the toxicity determinants. Genotoxic effects were also observed in different human tumor cell lines (lung, kidney, skin, and gastro-intestinal systems) but the literature is still poor and the protocols and the evaluations methods need to be standardized, in this case the genotoxic effects were found for Stober's and colloidal SAS NPs, the size of NPs had an important correlation

on the double strand break formation; genotoxicity could anyway be a secondary effect of ROS generation excluding a direct cause by NPs. Different parameters such as, cell type and exposure methodologies affect importantly the evaluation of these effects (Murugadoss et al., 2017). Autophagy represents an important defensive mechanism for cells, where damaged cellular components are degraded and recycled in different manners. Macro-autophagy is one of the principals and more important autophagic system, the process starts from structures called autophagosomes that are fused with lysosome where the content is processed (Kobayashi, 2015). SAS NPs blocked the autophagic flux on THP-1 cells activating principally on mTORC1 that is an important negative regulator of the autophagy in NM-203 treated cells and not significantly in NM-200 cells. The authors of this study supposed a mimicking effect of SAS NPs in correlation with those triggered by *Salmonella,* also the exposure to lipopolysaccharides (LPS), important stimulators of autophagy, did not triggered the pathway in NM-203 treated cells thus the blocking effects of the autophagic flux could enhance the toxicity exerted by LPS exposition related to bacterial infection weakening the immune response of the cells (Bianchi et al., 2020). SAS NPs also triggers apoptosis, as demonstrated in RAW264.7 cells using precipitated SAS NPs classical morphological hallmark of apoptosis (shrinkage and blebbing, nuclear condensation and fragmentation) are present after the treatment at different concentrations, and these data were confirmed by Annexin V/PI staining. In this study the main cause of the apoptosis triggering was the lysosomal rupture which proceeds parallel with the cell death and apoptosis, the interaction with the lysosomal membrane could be crucial to explain this effect (Hsiao et al., 2019). Also mitochondria could represent a target for the toxicity, Stober's SAS NPs in HUVEC cells had a perturbating effect on mitochondrial structure and morphology, disturbing also mitochondrial dynamics and biogenesis. In particular mitochondrial swelling and cristae rupture had an impact on mitochondrial membrane potential causing a depolarization mainly caused by the loss of physical integrity, also the inhibition of biogenesis markers as GC-1a, NRF1 and TFAM was observed. The dose effect response visible in the treatment was also correlated with ROS production, where the oxidative stress caused by SAS NPs enhanced the radical species produces by mitochondrial dysfunction inhibiting also the ATP production. Was also observed an important dysregulation in mitochondrial dynamics, in fact the expression of genes regulating these processes FIS1 and DRP1 increased (**Fig. 16**). The exaggerated expression of fission genes is a factor that boost the susceptibility to the apoptosis (Guo et al., 2018; Scaini et al., 2017).

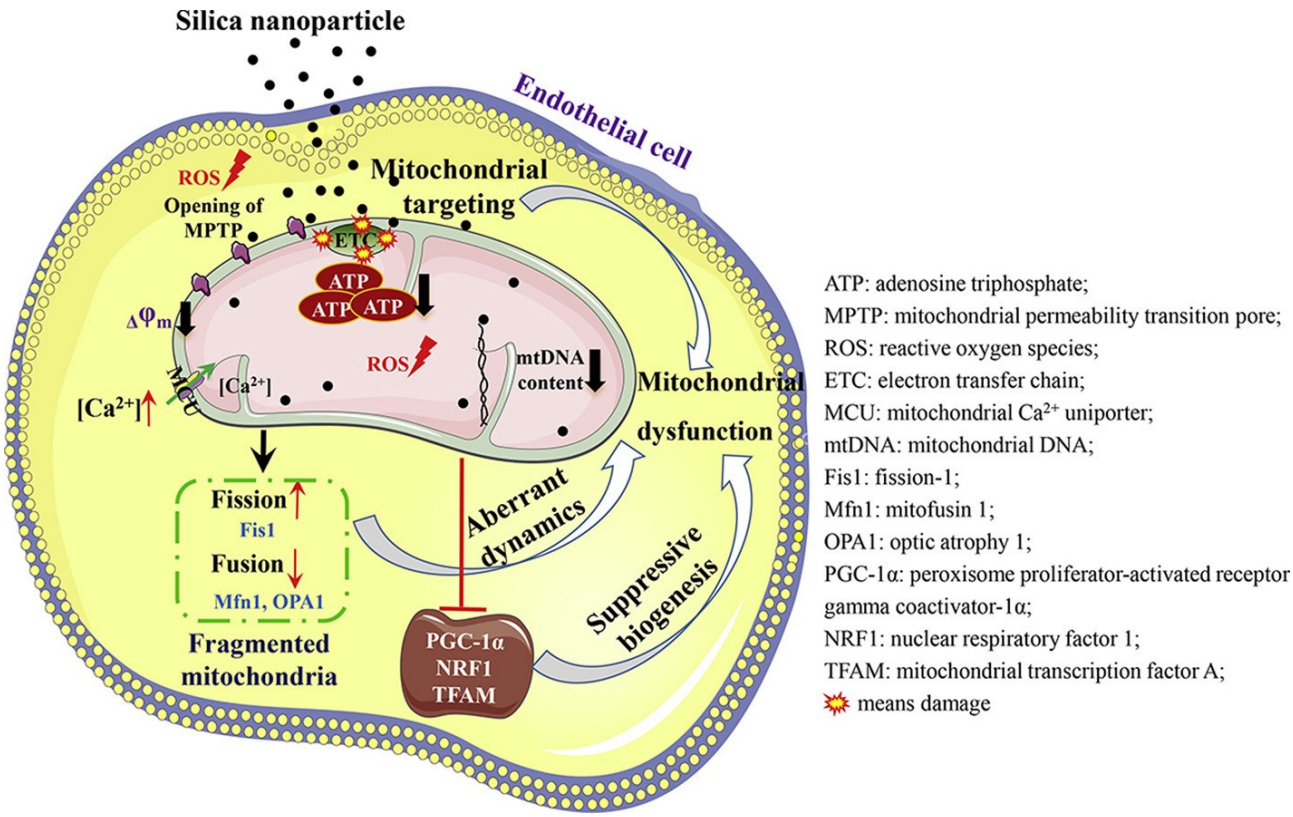


***Figure 16.*** Impairment of mitochondrial functions and pathways triggered by Stober's SAS NPs exposition. Figure adapted from (Guo et al., 2018).

Therefore, apoptosis is another process triggered by SAS NPs, Lu et al. (2011) observed an important stimulation of this process in human hepatoma (HepG2) cells using SAS NPs with dimension of 7 nm, 20 nm and 50 nm. On this cell line toxicity demonstrated to be higher from 20 nm NPs exposure. Different pathways of apoptosis were analyzed, and the results reported the activation of p53, upregulation of Bax/Bcl-2 ratio, and activation of procaspase-9 and caspase-3. The markers belong to the mitochondrial apoptosis pathway, once again the principal cause could be importantly linked with the oxidative stress (Lu et al., 2011).

### *1.5.7 In vivo cellular effects*

Toxicological effects aspects of crystalline $SiO_2$ have been well established in last decades, a rich literature is present on silicosis deriving from the inhalation of $SiO_2$ crystalline forms that are inserted into group 1 by IARC and thus considered carcinogenic to humans (Humans, 2012). On the other hand, SAS NP toxicological categorization is more controverse, in fact this NPs are placed into group 3 by IARC and considered as non-cancerogenic. As mentioned before the application in the

many industrial fields are various including the application as food additive under the acronym “E551”. In 2018 the former Panel on Additives and Nutrient Sources of the European Food Safety Authority (EFSA) opened a re-evaluation on E551 as food additive, concluding that currently there aren’t sufficient data in the literature to well establish the toxicological determinants, especially studies performed on long terms with sub-chronical administration in vivo. The re-evaluation concluded that at the moment the Acceptable Daily Intake (ADI) couldn’t be specified and suggest more investigations to well establish the safety of the additive (Additives et al., 2018). The actual studies, examining the *in vivo* toxicological risk are heterogenous for many parameters as, the dose or time of administration and a crucial factor like the typology of SAS NPs utilized is often not mentioned; this represent fundamental problem because NM-200 and NM-203, as discussed before, could elicit different effects and activate different toxicological pathways so is important to set the focus on the more recent and well characterized literature where the type of NM utilized is well-defined. SAS NPs exposition studies in humans derive principally from the oral intake deriving from the food additive utilization of the NPs, with a daily dietary intake estimated in the range between 5 and 25 mg/kg bw per day (Additives et al., 2018), and where is not comprised in this estimation the possible intake deriving for example from the utilize as abrasive in the toothpaste. However, the NPs assumed by oral ingestion pass through the gastrointestinal (GI) tract as a normal food resisting at the stomach acidic conditions and going in the intestinal tract (IT). In mice has been studied 70 nm SAS NPs adsorption, using inductively coupled plasma optical emission spectrometer (ICP-OE) and analyzing the intestinal tissue after 28 days, administering 2.5 mg/kg bw/day of SAS NPs by oral feeding. In this case SAS NPs were absorbed through the intestine (Yoshida et al., 2014). The potential impact of NPs adsorption could be different compared to other substances because of the high surface/volume ratio and the peculiar interaction with biological systems and with specific categories of cells. After passing over the GI barriers , NMs could distribute to tissues such as liver and spleen that are important for the presence of mononuclear phagocyte system cells, then the toxicokinetic and the potential distribution in tissues must be severely evaluated (Landsiedel et al., 2012). The adsorption via oral intake has been estimated in rat in other works. A study from Boudard et al. (2019) focused the attention on a long-temporal exposure administering low doses of NM-200 for 18 months using two different wild-type mouse lines, none of the previous studies administered for such a long time SAS NPs in a superior organism. The examination of distribution in tissues reported a presence of NM-200 in liver and spleen in both lines, where the quantity of NM in liver was higher (**Fig. 17**). Ther work from Boudard et al. (2019) determined that after the

exposition to SAS NPs liver and kidneys tissues reported lesions, these lesions were accompanied by inflammation states in both organs and vacuolization of tubular epithelial cell. Was also observed amyloidosis in kidney glomeruli and in perivascular regions in livers, moreover the NPs long exposure was related with lymphoid infiltrates and morphological modifications of the renal tubular cells, suggesting the triggering of a chronic inflammatory process. The 18 months long period of administration gave important information about the safety of NM-200 and the effects in humans by the way are required further evidence to fully understand the risks deriving from the oral assumption (Boudard et al., 2019).

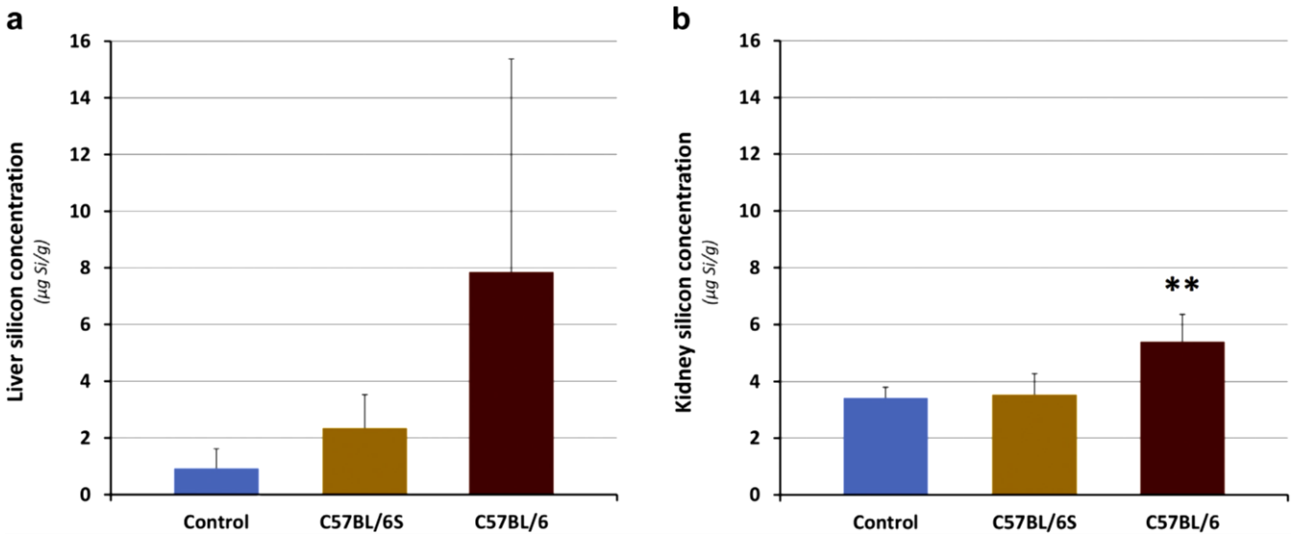


***Figure 17***. Accumulation of NM-200 after 9 months of water administration in an estimated dose of 2 mg mg/kg bw/day. Figure adapted from (Boudard et al., 2019).

The toxicity from NM-203 by oral ingestion has been also studied in rat models dispensing for 90 days different doses of the NPs starting from 1 to 50 mg/kg bw/day, the biodistribution of NM-203 was very limited, but the liver was an important toxicological target. In this organ was observed a marked vacuolization accompanied by steatosis and lymphoid infiltration, female rats appeared to be more vulnerable to the exposure. The immune reactivity of T cells in female rats was higher suggesting a sex dependent effect, other markers were analyzed as the count of white blood cells (WBC) and of the lymphocytes (LYMP) showing a reduction in the overall count of these cells (Tassinari et al., 2020). The low adsorption levels detected in a lot of studies could be considered in a wrong manner, this factor is in fact influenced by the toxico-kinetics of SAS NPs. Another important aspect is that previous studies, examining the SAS NPs effects by oral administration, utilized high

doses of treatment, where an agglomeration effect of the NPs caused by the high concentrations utilized decreased the adsorption and the interaction in the GI tract (van der Zande et al., 2014). The distribution of SAS NPs must be also related with the permanence in the organs, data from experiment carried out through venous injection reported an important permanence of the NMs in liver and spleen after 90 days after the administration, this in important evidence suggests that a low elimination rate could trigger in a chronical intake (comparable with the human ingestion deriving from food) an accumulation in target organs (De Jong et al., 2013). Finally, van Kesteren et al. (2015) tried to model the kinetic of the adsorption and excretion of SAS NPs designing a model based on the relation between the doses administered and the toxicological parameter linked to the internalization of the NPs, this model could be applied also for the risk assessment of NMs in general. All the parameters in the model are taken by toxicity studies that estimated the ADI, integrating these data whit *in vivo* toxicity studies and the estimated GI adsorption in humans, important to approximate the internal concentration of SAS NPs. In these models is crucial to consider that different formulation of NMs could have different GI adsorption and toxicological parameters (**Fig. 18**). Is obviously impossible to measure these aspects directly in humans maintaining a scientific approach, so researchers are often forced to make simulations applying this typology of models, where are exploited the toxicological *in vivo* experiment performed in superior organisms as mice or rats. In a first model calculated, where compared the results of van der Zande et.al and the model were based on the ADI and the liver accumulation of SAS NPs. The liver accumulation and toxicity effects were deduced from an intravenous injection study, is important to contemplate the limits of this approach, that considered the liver as only target of biodistribution in a sub-chronical time of exposure that don't correspond to a realistic intake scenario. However, the model employed described an estimated concentration of SAS NPs on human liver of 21–23 mg Si/kg that in rats is proven to cause liver fibrosis (**Fig. 19a**) (van der Zande et al., 2014; van Kesteren et al., 2015).

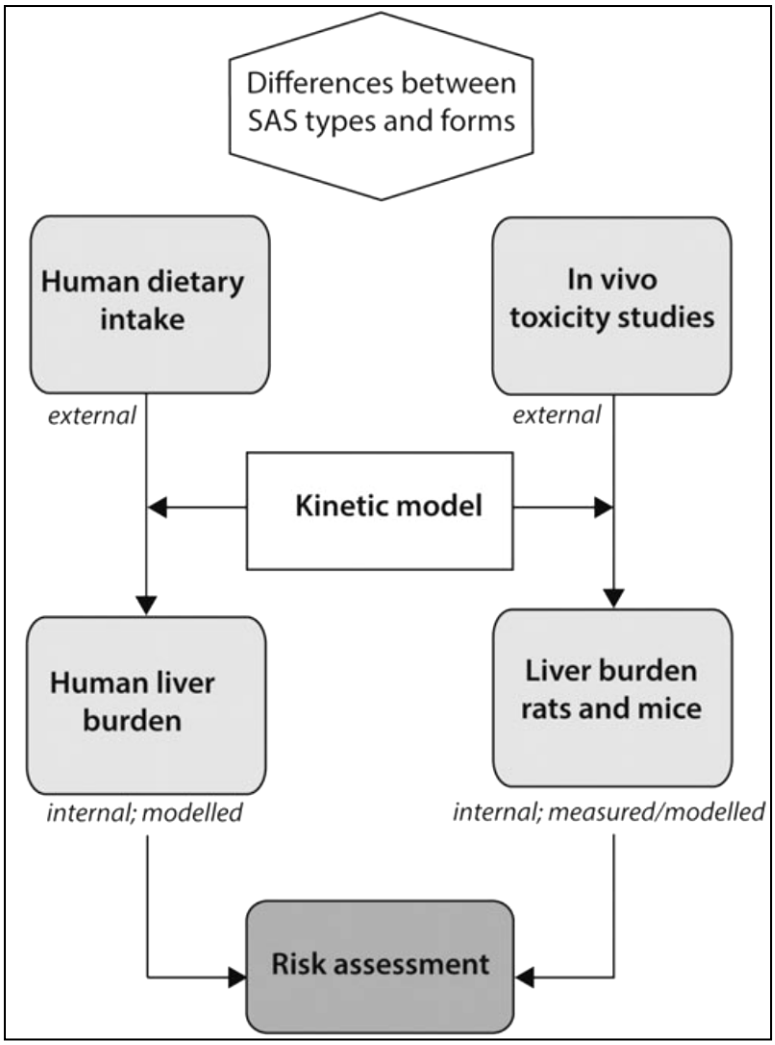


***Figure 18.*** Modelling approach for the estimation of toxicological determinants of SAS NPs in humans. Figure adapted from (van Kesteren et al., 2015).

A second approach was applied in this case the model was developed on studies made from the administration of SAS NPs by intravenous injection (**Fig. 19b**). The previously estimated internal dose of 21–23 mg Si/kg was not adequate to compare with certainty human and rats and the different administration methods from the considered studies were problematic to confidently make any conclusion. For these models application, data were insufficient to estimate realistically the lowest dose at which there was an observed toxic or adverse effect (LOAEL) or the highest dose at which there was not an observed toxic or adverse effect (NOAEL). For both approaches there are, by the way, important evidences, indicating possible toxicological effects of SAS NPs especially assuming the NPs chronically (van Kesteren et al., 2015).

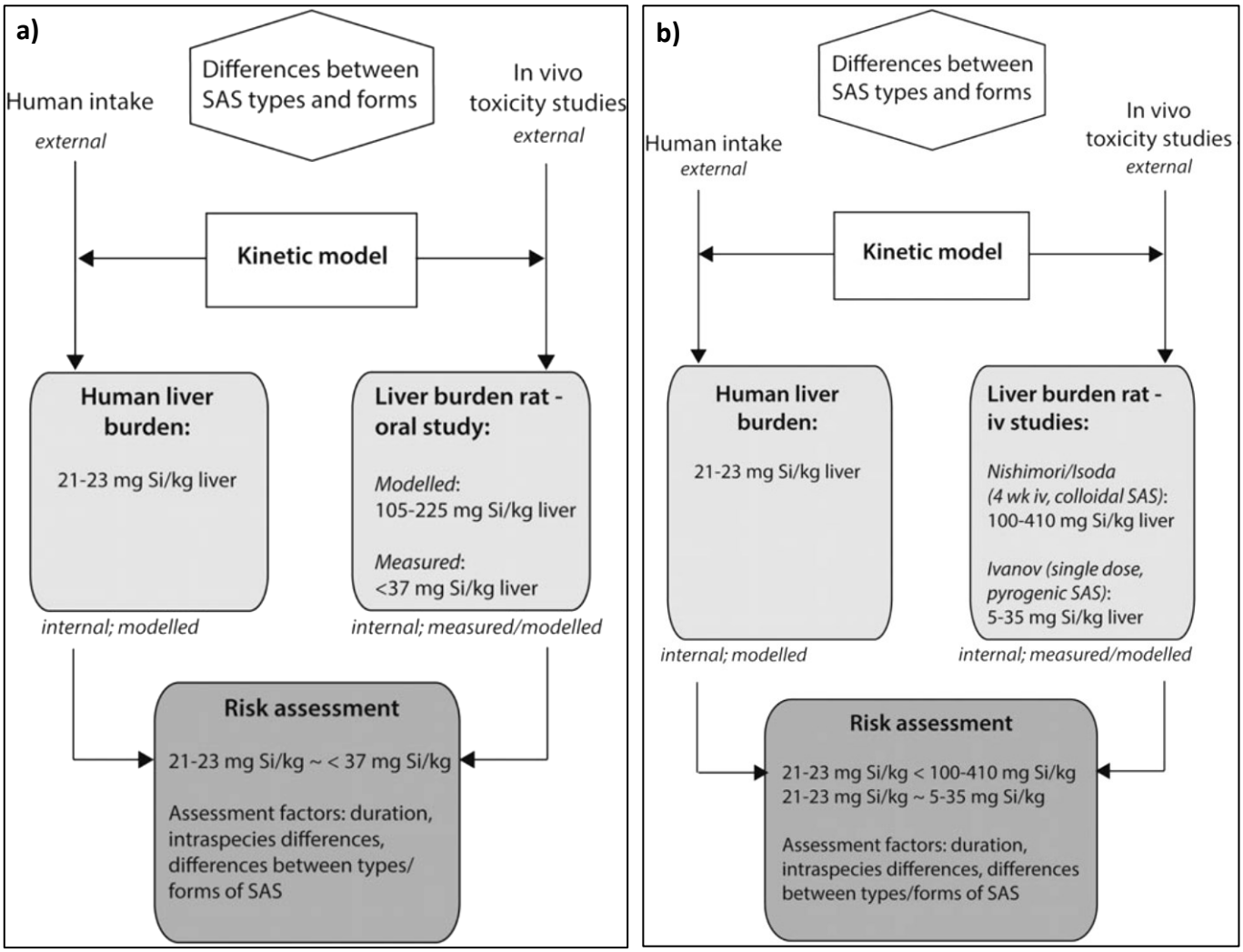


***Figure 19.*** Modelling applied in different scenarios of administration, (a) application on data deriving from oral exposure by (van der Zande et al., 2014) (b) application basing on different intravenous toxicity studies. Figure adapted from (van Kesteren et al., 2015).

All the *in vivo* findings are still under investigation by a lot of groups, but the major part of the results suggest that the application of SAS NPs as food additive is potentially harmful and as previously discussed might have for some implications, mostly regarding possible interaction with the immune system and also for the triggering of inflammatory episodes in spleen, liver and GI tract. From the last literature the observations of inflammatory response and liver damages are clear, adsorption and accumulation might have consequence that necessitate deeper analysis. The discrepancy in methods, as the time of administration and employed SAS NP formulations, certainly generate difficulties in the evaluation of the toxicity determinants and is also problematic to estimate the realistic internalization rate, affected by a great variability in the oral intake and adsorption. The

intestinal tract could represent a toxicological target of SAS NPs, in dextran sulfate sodium (DSS)-induced colitis mice models the oral administration of 10 nm SAS NPs intensified effects associated with the induction of the colitis. In particular, the intestinal inflammation was triggered by an inflammatory pathway dependent by the Apoptosis-associated speck-like protein containing a C-terminal caspase recruitment domain (ASC). The NRLP3/ASC inflammasome a pathway is characteristic of the immune cells and important for the immunological response in the intestinal epithelium, SAS NPs exposition induced the activation of this pathway. The potentiation of inflammation in the intestinal epithelium is then an effect of SAS NPs and inflammatory bowel disease (IBD), that include different conditions as ulcerative colitis and Crohn's disease could be hypothetically partially linked to a chronical exposition to this typology of NPs (Ogawa et al., 2021). The incidence of these pathologies is beginning to have an high-incidence, mostly in northern Europe and North America regions, accomunated by similar lifestyles and eating habits known as "western diet", characterized by the consumption raffinate foods often combined with additives including E551 (Loftus Jr, 2004; Hanauer, 2006). The impact on GI tract epithelium by SAS NPs is related to the ability to penetrate the epithelial barrier, albeit in minimal quantities, and trigger inflammatory processes activating macrophages (Hirai et al., 2012). In an already damaged mucosal barrier, the facilitation to pass over the barrier could have an enhancing effect on a previously present inflammatory processes (Lee et al., 2018). All the *in vivo* discussed evidence suggests that E551 employment, in both synthesis forms and especially for NM-203, must be better evaluated, more long-term studies and an improved homogeneity in the literature, with specifications on the manufacture process of the SAS NPs utilized, are however necessary to fully draw clear conclusions.

## 1.6 Cerium oxide nanoparticles

### *1.6.1 An overview*

Cerium is a metal appertaining at the lanthanides group, represent the most abundant element of the lanthanide's series. One of the typical traits of cerium is the particular electron state in the 4f orbital (Xe $4f^1 5d^1 6s^2$) directly responsible of a reduction/oxidation switching cycle between the ceric form $Ce^{4+}$ and the cerous form $Ce^{3+}$ (Kilbourn, 2000). In the bulk form is a highly reactive metal with strong affinity for oxygen and sulfur. The cerium dioxide (CeO2) is the most stable oxide form of cerium. When cerium is in form of Cerium oxide nanoparticles (CeO2 NPs) the oxidation states $Ce^{4+}$ and $Ce^{3+}$ are both present on the NPs surface conferring unique characteristic which will soon be discussed (Campbell and Peden, 2005; Esch et al., 2005; Reed et al., 2014). Generally, the applications of CeO2 are multiple for example as polishing agent (Hedrick and Sinha, 1994), in solar cells (Corma et al., 2004), as ultraviolet adsorber (Dao et al., 2011), in biosensors (Charbgoo et al., 2017), as catalyst (Wang and Lin, 2004) or as fuel additive (Cassee et al., 2011) with other possible bio-medical applications under examination for the near future (Saifi et al., 2021; Schlichtmann et al., 2021; Padmanabhan et al., 2020). The raising attention on the uses and properties of CeO2 are directly linked with the reactivity and physio-chemical characteristics showed by the elaboration into NPs.

### *1.6.2 $CeO_2$ NPs synthesis*

The synthesis methods of $CeO_2$ NPs are various. The chemical synthesis methods are several, the precursors used for the synthesis are often cerium salts reacting under basics conditions. The precipitation method is one of the most common and cheap techniques for the synthesis of $CeO_2$ NPs, this approach can be carried out at room or at high temperatures depending on the protocols (Farahmandjou et al., 2016; Zhang et al., 2009). Precipitation can be done also using surfactants as tween or CTAB to obtain NPs of different sizes with the possibilities to tune the superficial area (Terribile et al., 1998) (**Fig. 20a**). Another important method for the synthesis is represented by the hydrothermal method where the precursor solution is heated under pressure in a water solution, different precursors can be used and the change of reaction parameters yields to the production of NPs of different size, shape and with different superficial characteristics (**Fig. 20b**) (Sutradhar et al., 2011; Zhou et al., 2005; Zhou et al., 2007). Microwave synthesis is another efficient and cheap way to produce CeO2 NPs, in this case the thermal increase that initiate the reaction is the direct heat transfer from microwaves in the reaction mixture and the final product is produced rapidly and in

high quantities (**Fig. 20d**) (Lew et al., 2002; Wang et al., 2002). As for SAS NPs microemulsion method is employed for $CeO_2$ NPs synthesis. Two different types of microemulsions, oil-in-water (O/W) or water-in-oil (W/O), are utilized with the possibility to add surfactants (**Fig. 20e**). These microemulsions are actually colloidal solution that create a tunable nano-environment where the reaction occurs, $CeO_2$ NPs obtained using this methods have different size and characteristics depending on the setup of the reaction (Sathyamurthy et al., 2005; Huang et al., 2011). Oxidation method is another approach for CeO2 NPs production, in this case an oxidizing agent is used for the NPs production from the precursor and varying the concentration of oxidant is possible to optimize the size of the NPs (**Fig. 20f**) (Karakoti et al., 2007; Lee and Choi, 2004). Another important approach is represented by the sonochemical method, where high-intensity ultrasounds application to the reaction mixture triggers the growth and collapse of bubbles that locally increases the medium temperature starting the reaction, the size of the NPs can be tuned adding different types of molecules to the reaction mixture (**Fig. 20g**) (Yin et al., 2002). Finally, the most interesting approach is represented by green synthesis of $CeO_2$ NPs from different sources. Green synthesis products are important for their sustainability, safety in the production and low energetic impact. All the biological elements exploited for the green synthesis act as capping and stabilizing agents allowing the production of biocompatible NPs and the yield in the production of NPs is relatively higher compared to the chemical methods (**Fig. 20c**). *Gloriosa superba* leaf extract and cerium chloride salt had been used to synthesize spherical $CeO_2$ NPs with dimension of 5 nm (Arumugam et al., 2015). Also, other leaf extracts are efficient for the production of CeO2 NPs. Other methods are linked to the utilize of fungi mediated synthesis, where the addition of the precursor to *Curvularia lunata* fungal culture filtrate produced NPs with dimension ranging from 5 to 20 nm after a mixing step at 80 °C (Munusamy et al., 2014). Other biological compounds are utilized for the green synthesis as, egg whites, pectin or starch (Singh et al., 2020).

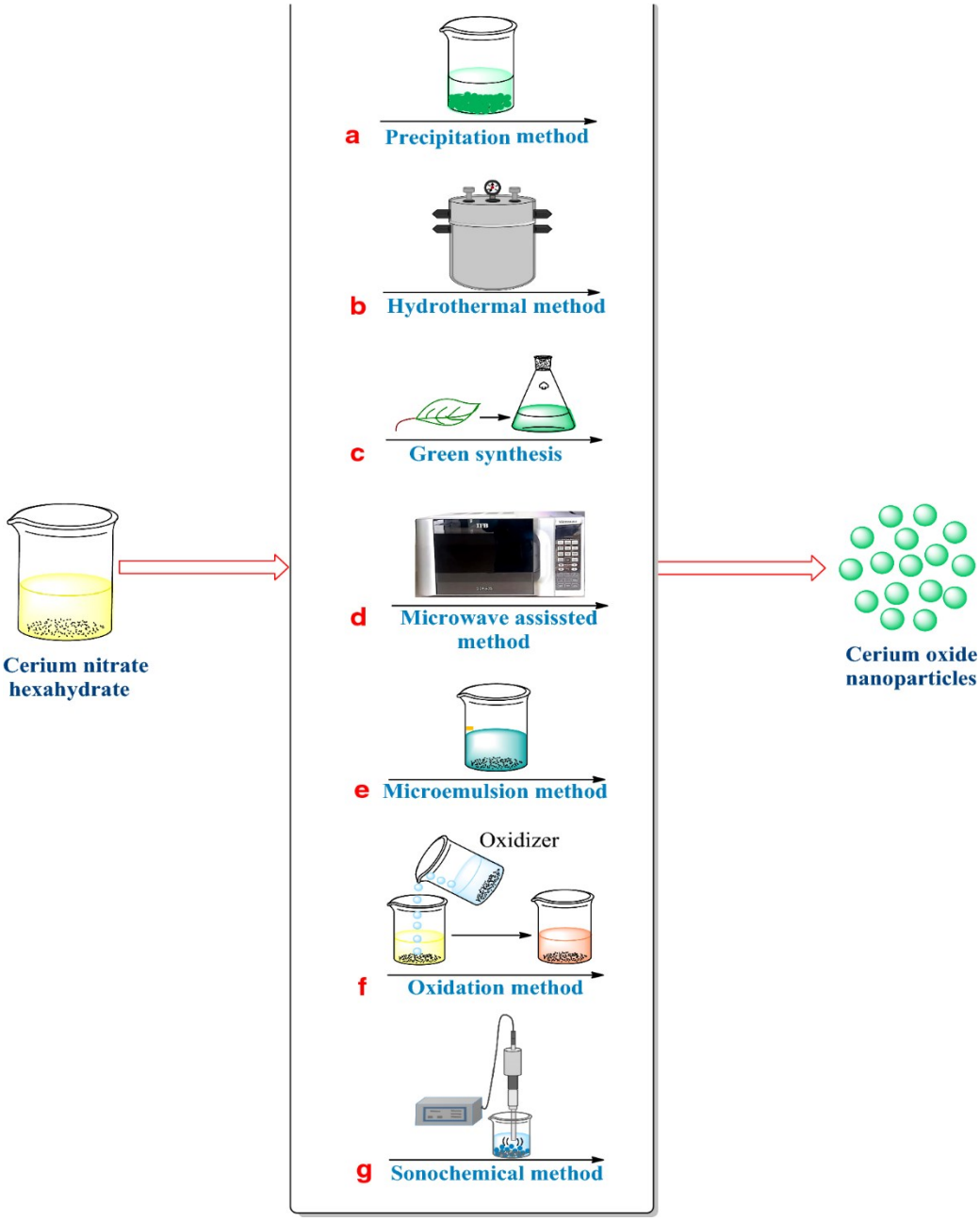


***Figure 20.*** Different synthesis methods for the production of $CeO_2$ NPs. Figure adapted from (Thakur et al., 2019).

### *1.6.3 $CeO_2$ NPs morphology and physiochemical properties*

The crystalline nature of $CeO_2$ is characterized by the coordination of one atom of cerium with eight oxygens, then each cerium is a 8-fold coordinated with an oxygen atom while each oxygen is 4-fold coordinated with a cerium atom (**Fig. 21a,b**). In $CeO_2$ NPs the complete unit cell ($Ce_4O_8$) is a face centered cubic fluorite lattice measuring 0.51 nm (5.1 Å) on an edge (**Fig. 21c**). Unit cells assembly

into crystallites and crystallites assembly in particles forming $CeO_2$ NPs, crystallite disposition can vary basing on the synthesis method utilized. For $CeO_2$ NPs the disposition of unit cells into a mono-crystalline composition is pretty rare, in fact $CeO_2$ NPs have almost always a polycrystalline composition (**Fig.22**) (Singh et al., 2020; Reed et al., 2014).

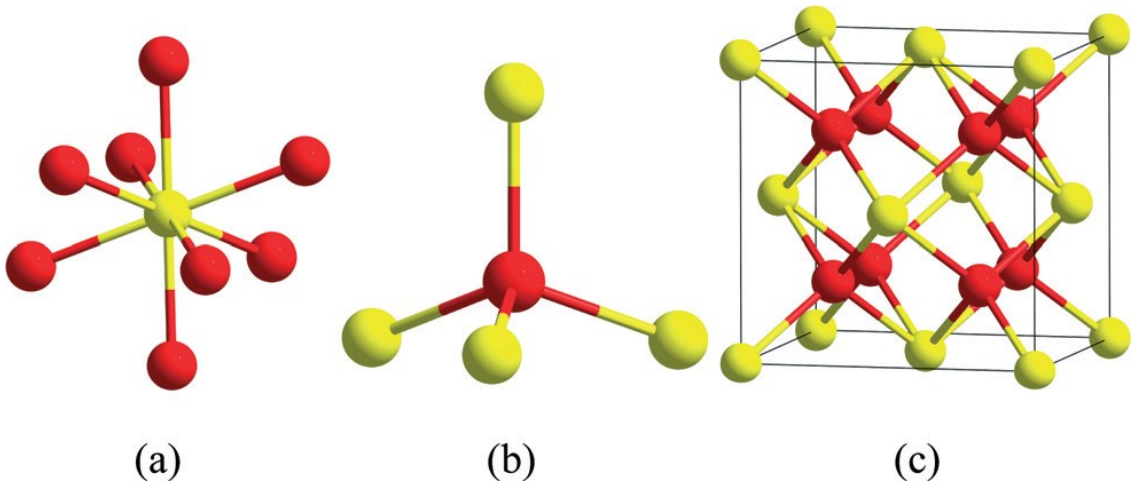


***Figure 21.*** Cerium crystal cerium in yellow and oxygen in red, (a) cerium 8-fold coordination with oxygen, (b) oxygen 4-fold coordination with cerium, (c) $Ce_4O_8$ primitive unit cell. Figure adapted from (Reed et al., 2014).

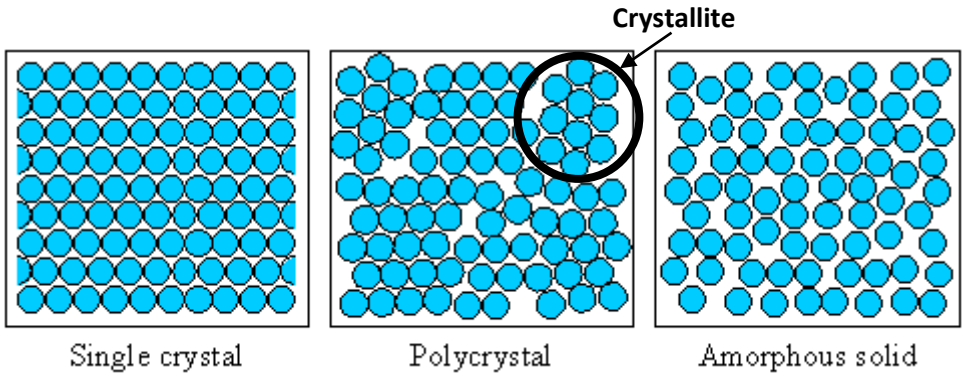


***Figure 22.*** Disposition of the unit cells into crystallites forming polycrystals, $CeO_2$ NPs are characterized by a crystallite nature. Figure adapted from *https://eng.libretexts.org/@go/page/780*

The presence of oxygen vacancies on the surface of the NPs is caused by the lack of a single or multiple oxygens (until 3 oxygen) in the unit cell. Different groups studied this event that represent the direct cause of the simultaneous presence of $Ce^{4+}$ and $Ce^{3+}$ species on the surface of $CeO_2$.

Deeply investigating about oxygen vacancies, Esch and co-workers analyzed the $CeO_2$ surface using high-resolution scanning tunneling microscopy (STM) detecting superficial defects especially after treatments at high temperatures, these defects are caused by subsurface oxygen vacancies triggering the formation superficial of oxygen vacancies spots that occasionally are organized into clusters (**Fig. 23**) (Esch et al., 2005).

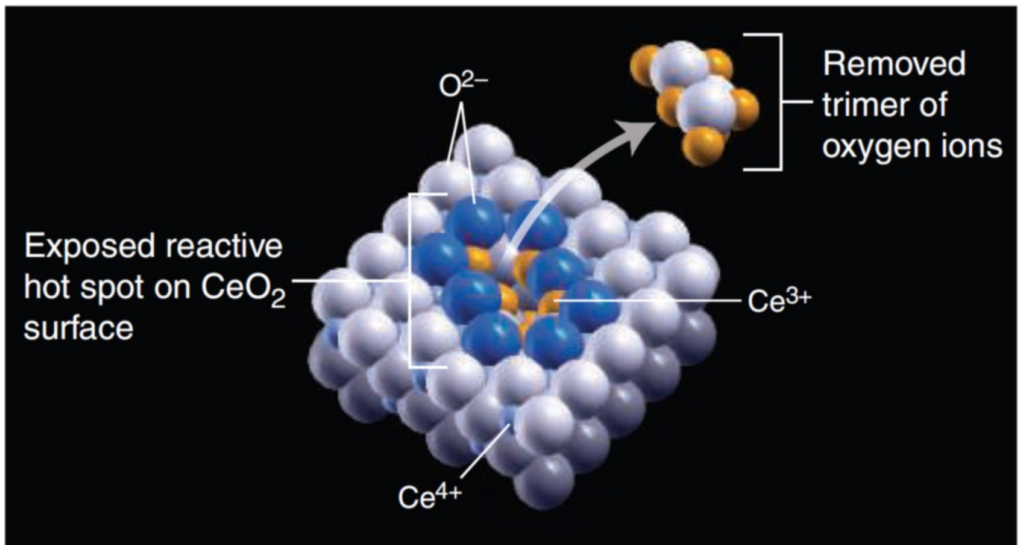


***Figure 23.*** A visual representation of the oxygen vacancies where the presence of superficial defects causes the creation of $Ce^{+3}$ clusters surrounded by stable $Ce^{+4}$ species. Figure adapted from (Campbell and Peden, 2005).

The catalytic effects and the other properties of $CeO_2$ are therefore attributable to these clusters of reduced $Ce^{+3}$, the presence of oxygen vacancies clusters can be importantly enhanced in the NP formulation of $CeO_2$ principally because of the high surface/volume ratio of the NPs, where a significant quantity of atoms is present on a the surface with a smaller area (Dutta et al., 2006; Tsunekawa et al., 2000). Another important factor to evaluate is the size of the NPs, in the nano-structured cerium the reduction on the size causes a lattice expansion and determines a decreased rate of adsorption/release of oxygen this event cause in smaller nanoparticle a higher abundance of reduced $Ce^{+3}$ (Hailstone et al., 2009).

### *1.6.4 Oxidative stress and $CeO_2$ NPs catalytic mechanism*

Oxidative stress is an important biological event where the imbalance between the scavenging and the production of ROS, as free radical or peroxides, cause the damage of different cellular components as lipid, proteins and DNA leading to different final consequences as alteration in the enzymes function, defects in gene expression and alteration of mitochondrial physiology (Birben et al., 2012; Pizzino et al., 2017). The pathogenesis of several chronic diseases as, diabetes, neurodegenerative diseases (ND), cancer or cardiovascular diseases is deeply linked with oxidative stress. The biological systems are prepared to fight against oxidative stress with radicals scavengers that can enzymatic: superoxide dismutase (SOD), catalase (CAT), ascorbate peroxidase (APX), guaiacol peroxidase (GPX), glutathione reductase (GR). Also, non-enzymatic anti-oxidants as ascorbic acid (AA), reduced glutathione (GSH), α-tocopherol, carotenoids, flavonoids are utilized to scavenge radicals (Das and Roychoudhury, 2014; Halliwell, 2007). Is then important a deep knowledge of these mechanism where $CeO_2$ NPs could represent a promising component for therapeutical applications as potential radical scavenger. On the other hand, $CeO_2$ NPs demonstrate a bivalent nature exhibiting pro or anti-oxidant activities depending on the environment. As mentioned before, size and morphology are crucial to determine oxygen vacancies and the cerium oxidation states, also other factors as pH play important roles to determine the oxidant and anti-oxidant characteristics. In fact, $CeO_2$ NPs can at acidic pH $CeO_2$ NPs exert an oxidase like activity and can oxidize different organic molecules (**Fig. 24a**) (Asati et al., 2009). We will first talk about the pro-oxidant nature of $CeO_2$ NPs to better comprehend the NPs safety in their potential applications. Peroxidase mimetic effect demonstrated where caused principally by the high presence of $Ce^{+3}$ combined with the high surface volume ratio of the NPs with a hypothetical mechanism where the adsorption of the oxygen on the NP surface lead to the creation of superoxide ($O_2^{\bullet -}$) species in acidic conditions, next $Ce^{+4}$ is reduced to $Ce^{+3}$ with concomitant oxidation of the substrate followed by the oxidation of $Ce^{+3}$ by $O_2^{\bullet -}$into $Ce^{+4}$ **(Fig. 24b**) (Lord et al., 2021). This effect could have important application in cancer detection, peroxidase-like activity could be applied to ELISA test technique to enhance the sensitivity of the immunoassay (Tian et al., 2015).

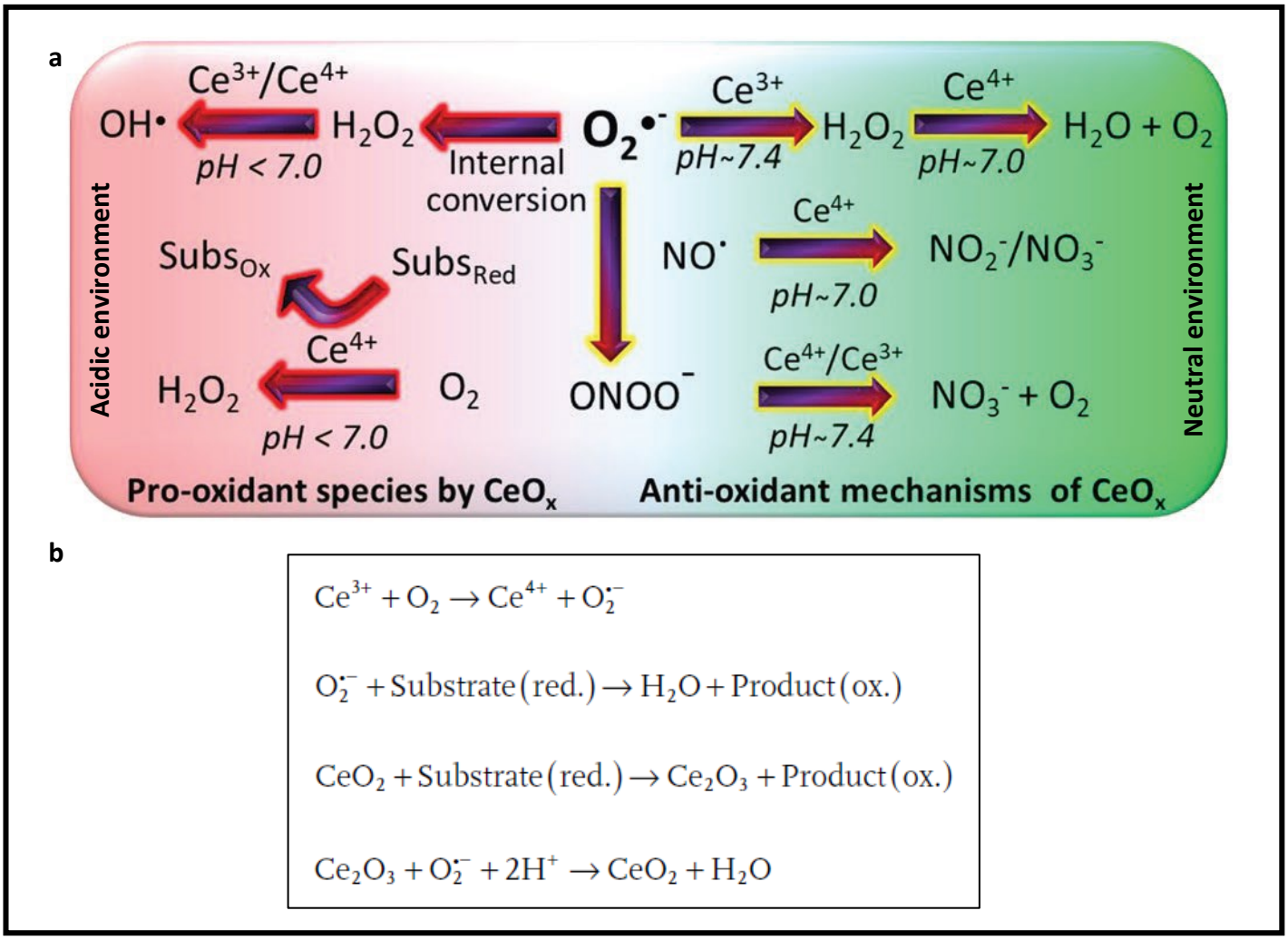


***Figure 24*.** Pro or anti-oxidant activity of $CeO_2$ depending on the environment pH (a),hypothetical mechanism of oxidase-like activity (b). Figure adapted from (Lord et al., 2021).

The shifting oxidant and anti-oxidant activity of $CeO_2$ NPs was examined to study possible application linked with the acidic environment of cancer cells, the treatment with the NPs exerted oxidase and peroxidase activities in tumor cells increasing oxidative stress in his characterizing acidic pH, causing ROS induced cytotoxicity (Saifi et al., 2021) (**Fig. 25**).

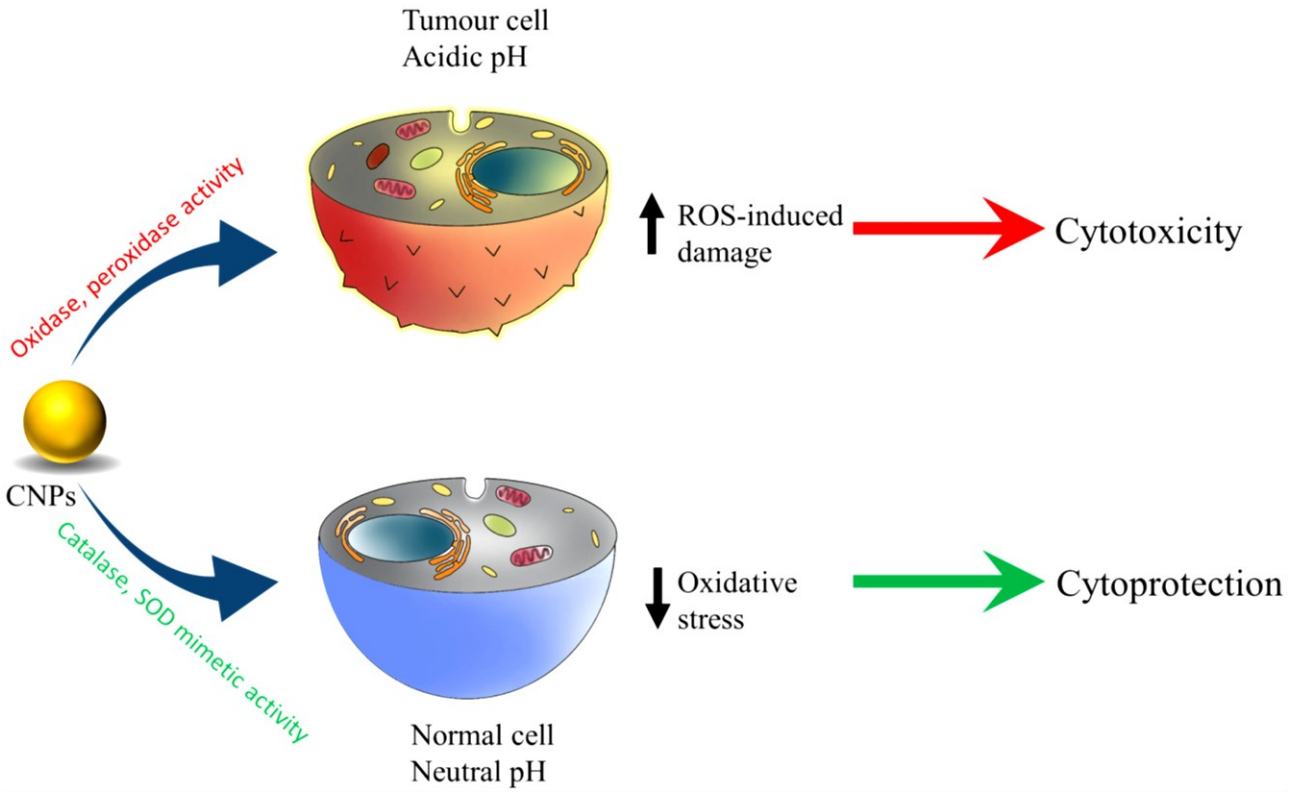


***Figure 25***. Schematic representation of $CeO_2$ NPs effect comparing the reduction of the oxidative stress in normal cells vs the cytotoxic effect in tumor cells with acidic pH. Figure adapted from (Saifi et al., 2021).

Although $CeO_2$ NPs exert an oxidizing effect in particular conditions, it shows a minimal global toxicity a work from Liu et al. (2013) analyzed the structure-activity relationships (SAR) of different metal oxides NPs on BEAS-2B and RAW 264.7 cells. Were evaluated different parameters using single parameter screening (SPS) and multi-parameter high-throughput screening (HTS) also including the ROS production, $CeO_2$ NPs in this study didn't show significant toxicity (Liu et al., 2013). Actually, other studies reported different results demonstrating in some case cytotoxicity, but essentially $CeO_2$ NPs behavior is different from other metal oxides. The displayed toxicity is dependent principally from particular micro-environmental situations difficult to find in physiological conditions where the NPs exhibits their oxidative potential, or by peculiar morphological aspects that cause physical cellular damage (sharp shaped NPs) (Lord et al., 2021). The other side of the bivalent nature of $CeO_2$ NPs is embodied by the catalytic anti-oxidant activity, well documented in the literature. The activity showed is similar to different biological enzymes as

SOD or CAT, the core of this scavenging action against ROS resides in the regenerative reaction mechanism of $CeO_2$ NPs. The particular activity of $CeO_2$ is due to the reduction of superoxide radicals species combined to the oxidation of peroxide ions to oxygen. This mechanism acts as radical and peroxides scavenger and proceeds in a cyclic manner. The sequential interaction with superoxide and peroxide species ($H_2O_2$) is cyclic, regenerating the oxidation state of the $CeO_2$ (**Fig. 26**) (Celardo et al., 2011; Lord et al., 2021).

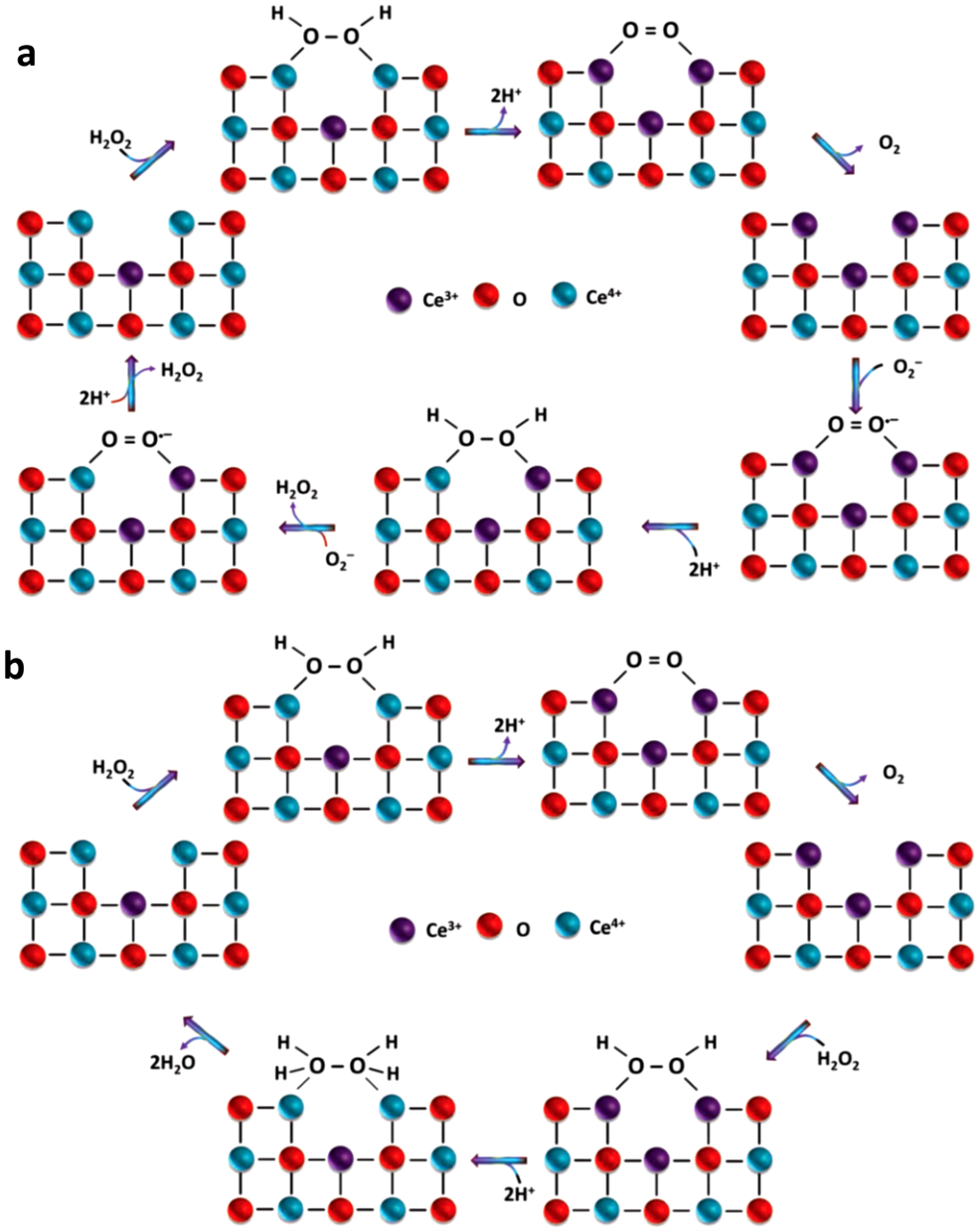


***Figure 26.*** Representation of the self-regenerating and ROS scavenging activity on the surface of $CeO_2$ NPs, dismutation of $O_2^{\bullet -}$ (a) and $H_2O_2$ (b). Figure adapted from (Lord et al., 2021).

SOD mimicking activity by CeO2 NPs resides into the switching between Ce4+ and Ce3+ oxidation states and a higher Ce3+/ Ce4+ ratio determines an higher catalytic activity against $O_2^{\bullet-}$, the catalytic rate was measured using a competitive SOD activity assay with cytochrome C and showed a catalytic rate of 3.60 x 109 M-1 s-1 higher than the catalytic rate of the natural SOD enzyme comprised between 1.3 and 2.8 x 109 M-1 s-1 (Korsvik et al., 2007). The enzyme mimicking activity showed by CeO2 NPs is also similar to the CAT, in particular the adsorption of $H_2O_2$ on the surface of the NPs is followed by several steps producing $H_2O$ and $O_2$, as showed in **Figure 26b** all these steps are coordinated by the changes in the oxidation states on the surface of the NPs and the cyclic regeneration that characterize the catalytic nature to the process (Baldim et al., 2018).

### *1.6.5 Biocompatibility and benefic effects of $CeO_2$ NPs*

Looking at the different benefic effects of $CeO_2$ NPs is although important the risk assessment for their potential applications. The literature is often conflicting and scarce due to the really recent discovering of the proprieties of these NPs and the correlation with a hypothetical application in nanomedicine. However, several studies on oral administration or intravenous injection in murine models demonstrated the liver and spleen as major accumulation organs. Intravenous administration in rats of $CeO_2$ NPs with different sizes (5 nm, 15 nm and 30 nm) dispensed at different doses resulted in liver accumulation, 5 nm sized NPs were detected in a higher amount respect to other sizes in liver 30 days after the administration, suggesting a size dependent accumulation of smaller NPs; 15 and 30 nm NPs accumulated in higher quantity in spleen (Yokel et al., 2014). Similar studies evaluating the accumulation after 1 and 20 h again confirmed the preferential accumulation in liver and spleen (Yokel et al., 2009). Other administration routes where also tested in murine models, intratracheal instillation of $CeO_2$ NPs resulted in liver accumulation and retention of the NPs detected up to 28 days. Oral administration determined a low adsorption by the Gastrointestinal (GI) tract accompanied with a rapid fecal elimination, inhalation of CeO2 NPs show a low adsorption rate where NPs were detected in feces and in lungs but in small amount in other organs (Molina et al., 2014; Casals et al., 2020; Schwotzer et al., 2017). From the majority of the results detected in the literature, the administration of $CeO_2$ NPs is well tolerated in murine models. Regarding at the long-term studies, data are yet scarce to make conclusions, one of the few studies on Wistars rat, after exposure to 40 nm $CeO_2$ NPs by inhalation for 3 or 6 months didn't show genotoxicity, $CeO_2$ exposition only NPs caused an slight increasing in oxidative stress and inflammation on respiratory tract (Cordelli et al., 2017). Results are however still poor to make

conclusion on the long-term toxicity. Another event to take into account is the potential dissolution of $CeO_2$ NPs in a complex biological environment, Graham et al. (2014) for example reported in Sprague–Dawley rats, the retention in liver and brain of the NPs for 90 days, after this period was detected the formation of a second group of NPs characterized by a smaller size and a higher redox activity (Graham et al., 2014). Those results suggest a process of bio transformation of $CeO_2$ NPs, that could in this case, enhance the biological redox activity. Other groups reported events of dissolution and bio-transformation by CeO2 NPs in the liver (Modrzynska et al., 2018), but the release of molecular $CeO_2$ did not increase the toxicity. Different benefic effects are linked with the administration of $CeO_2$ NPs, treatment in P23H-1 rat (autosomal dominant retinitis pigmentosa model) ameliorated the rod and cone function after the injection and reduced lipid peroxidation and apoptotic events in the retinal tissue, retarding the progression of the disease after a single administered dose. (Wong et al., 2015). The treatment with the NPs in rats obesity models didn't show toxicity and reduced the weight of the rats and the plasma levels of insulin, leptin, glucose, and triglycerides, in this case the NPs acted on the adipogenic pathway reducing the mRNA transcription of genes involved in adipogenesis, and by impeding the triglycerides accumulation (Rocca et al., 2015). One of the most important traits of those NPs is the ability to cross the BBB, treatment with NPs in a murine model of multiple sclerosis (MS) [experimental autoimmune encephalomyelitis (EAE)] resulted in accumulation and retention in brain tissues and ROS decrease without impairing the central nervous system (CNS) immune cells physiological role and trafficking. In MS the prolonged oxidative stress and inflammation, lead to the chronic form of the disease, $CeO_2$ NPs demonstrated to have a long half-life in brain tissues, ameliorating the symptoms, reducing the disease severity and improving the motor function (Heckman et al., 2013). Other neuroprotective effects have been detected in the principal ND as Alzheimer's diseases (AD), Parkinson's diseases (PD) and other debilitating conditions of the CNS as ischemic stroke (IS) and amyotrophic lateral sclerosis (ALS), these effects are probably linked to the ability to scavenge ROS mixed with the small size of the NPs that are able to penetrate the BBB residing with a long half time in the CNS ameliorating the oxidative stress that is a common factor of these diseases (**Fig. 27**) (Naz et al., 2017).

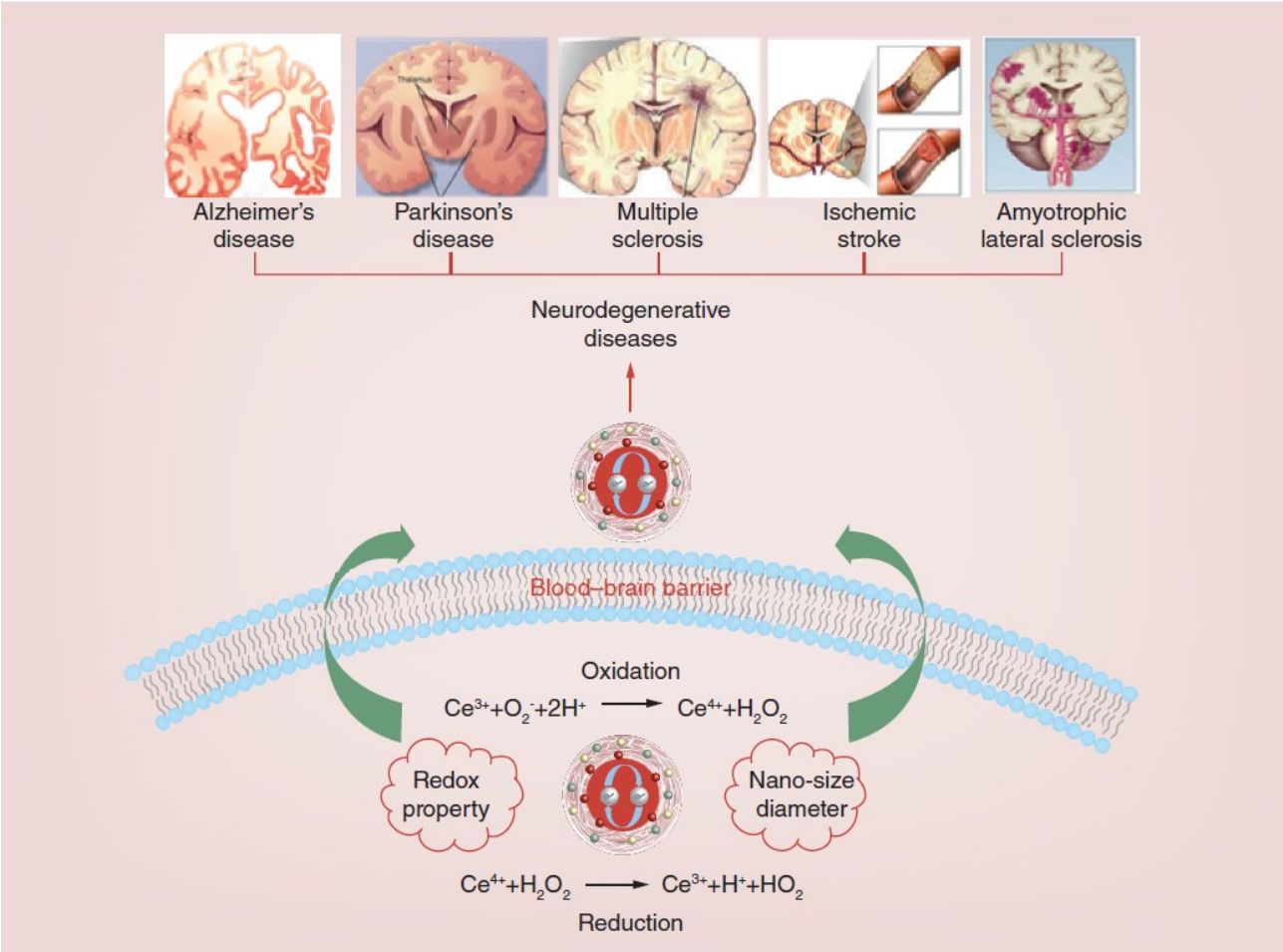


***Figure 27***. Schematic representation of protective effect showed by $CeO_2$ NPs on different ND. Figure adapted from (Naz et al., 2017).

All the described effect mixed with the low or non-toxic profile could make $CeO_2$ NPs as a potential long-term antioxidant, because is well tolerated by biological systems can also reside for long term in tissues acting as self-regenerative radical scavenger and thanks to the high surface volume ratio determining a high number of potential catalytic sites. Further studies are required to fully consider the toxicity especially on long-term exposure hypothetically lined with an application in nanomedicine.

## 1.7 Protein Corona

NPs growing application in last decades and the linked potential exposition require a deeper knowledge of the effects and mechanism originating from the interactions with biological systems. In particular when NPs enter in contact with a biological fluid, they find different macromolecules present in the medium (proteins, phospholipids, nucleic acids, carbohydrates) that dynamically interacts with the surface of the NPs. These physiochemical interactions are driven by different factors and forces, the principal class of macromolecules interacting with NPs is represented by proteins that surrounds the surface of the NPs forming the "so called" Protein Corona (PC). The PC composition defines the biological identity of a NP, his study is crucial for the comprehension of potential toxicological effects and fate of NPs in a biological environment and also for his potential exploiting and control that could be relevant for NPs applications. The first reference to the term PC was made in 2007 by Cedervall et al. (2007) in this study is reported the importance in the characterization of the PC and are proposed different techniques as isothermal titration calorimetry (ITC) for the characterization of the affinity binding between NP surface and proteins and surface plasmon resonance (SPR) for a perspective on association and dissociation rates between proteins and NPs; from this first report suggesting a systematic study of the PC, many works had been made and actually we could report a more complete perspective about the different factors characterizing and influencing the PC (Cedervall et al., 2007).

### *1.7.1 Factors influencing the protein corona formation*

There are many factors involved in the formation of the PC as NPs shape, solubility, size, superficial charge, and exposed chemical groups. It becomes fundamental to understand the interaction at the nano-bio interface because this modification on the NPs surface could have relevant effects in bio-medical application or in the potential toxicity modifying the cellular uptake or other factors as NPs dispersion, stability, circulation time or biocompatibility (Miceli et al., 2017). The triggering factor causing the formation of the PC is principally attributable to the high free energy present on NPs surface that when enter in contact with a biological fluid rapidly adsorbs proteins, these adsorbed proteins are in a dynamic equilibrium of continuous adsorption and desorption ($k_{ads}$ and $k_{des}$)

defining affinity of the proteins for the NPs surface. The binding between a protein (*P*) and the NP surface (*S*) is reversible and the kinetics of this process it can be summarized in this equation:

$$P + S \underset{k_{des}}{\overset{k_{ads}}{\leftrightarrows}} P_S$$

where $P_s$ represent the protein-NP complex. The equilibrium between $k_{ads}$ and $k_{des}$ defines the affinity for a protein for the NP and when $k_{des}$=0 this reaction become irreversible. Different forces participate to the protein adsorption as hydrogen bonds, van der Waals interaction, electrostatic interaction, **π- π** stacking, salt bridge formations or hydrophilic/hydrophobic interactions (**Fig. 28**) (Kopac, 2021; Ahsan et al., 2018; Tenzer et al., 2013; García-Álvarez and Vallet-Regí, 2021).

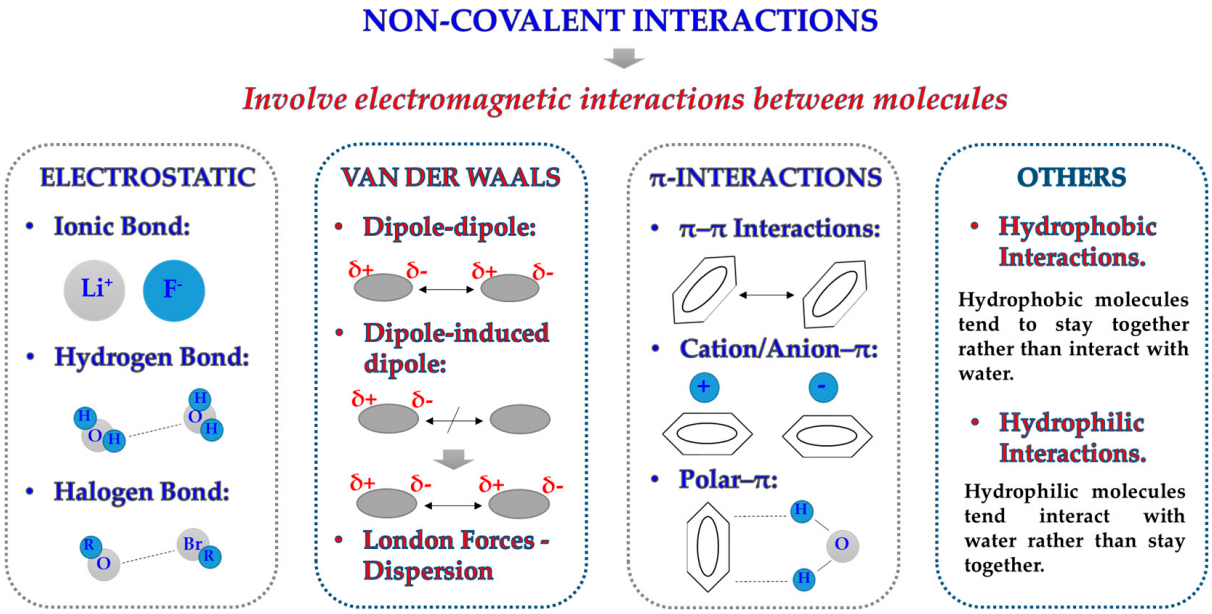


***Figure 28.*** Schematic representation of the different non-covalent interactions involved in the protein adsorption on NPs surface. Figure adapted from (García-Álvarez and Vallet-Regí, 2021).

The majority of the studies on PC had been made using the human plasma as biological media to simulate the corona formation easily detect the nature of the adsorbed protein on NPs surface. A study by Lundqvist et al. analyzed the PC formed exposing to human plasma differently charged polystyrene NPs (PS-NPs) plain, carboxyl-modified, and amine-modified, each of two sizes (50 and 100 nm). In this case electrostatic interactions had a high importance in the protein adsorption, for

example plain PS-NPs, possessing neutral superficial charge, adsorbed a lower variety of proteins on them surface compared to charged NPs. The PCs on the two different sized neutral NPs had a really high similarity in the composition, underlying the importance of the hydrophobic interactions. At the same time the two differently charged NPs of different size had different PC composition caused by the size variations of the NPs, thus the composition of the PC is affected by the combination of different factors as superficial charge, size, surface curvature, or different exposed chemical groups (Lundqvist et al., 2008). Surface curvature is dependent by the size of the NPs and variations on this parameters affect the surface/volume area of the NPs and the protein adsorption, a study by Tenzer et al. (2011) showed the importance on size variation in the plasmatic protein adsorption on the surface of three different sized $SiO_2$ NPs, in this case the variation didn't affect the quality of the protein adsorbed but had a quantitative effect on the 37% of 125 identified 'corona' proteins. Smaller proteins were preferentially bound in a higher amount on smaller $SiO_2$ NPs while larger proteins were highly represented in larger NPs (Tenzer et al., 2011). These molecular events, defining together affinity of the proteins for the NPs surface, are important also in the time dependent evolution of the corona composition, in fact Monopoli et al. (2011) showed that $SiO_2$ NPs and PS-NPs exposed to human plasma are readily covered by proteins even at low concentrations of plasma and more interestingly that at longer times of exposure was associated a displacement of the low binding affinity protein with those with a higher affinity for the NPs. From this work we have the important demonstration that the serum-NPs system that initially is characterized by the high free energy on the NPs surface is covered by a layer of protein that lower this energy, then some proteins are progressively exchanged selecting those with a high affinity (**Fig. 29a**). Moreover, the layer of protein that is generate on NPs is irreversibly bound on the NPs surface (Monopoli et al., 2011). The highly associated proteins to NPs surface are important for the characterization of the PC, for the cause that in a biological fluid we will observe the formation of an inner core layer of tightly associated protein on the surface, that defines hPC, and an external layer of loosely bound proteins that interacts with the hPC forming proteins and with a lower affinity with the NPs forming the so-called soft PC (sPC). The hPC have a more stable composition over the time of NPs persistence in a biological fluid while the composition of sPC is more variable and characterized by a higher exchange rate of the proteins. Also, in a biological system the time-scale evolution of PC is maintained, and hPC proteins maintain his composition when pass through different biological environments and have a fundamental role in the interaction between NPs and cells while sPC is importantly altered (**Fig 29b**). Is also important to underline that the order of exposure of the

proteins to the NPs represent a relevant factor, this because the first layer of protein that forms the hPC characterized by an extremely low exchange rate over time or by an irreversible binding, equipping the NPs of a unique fingerprint that could implicate diverse effects on biological systems (Milani et al., 2012; Ahsan et al., 2018; Lundqvist et al., 2011).

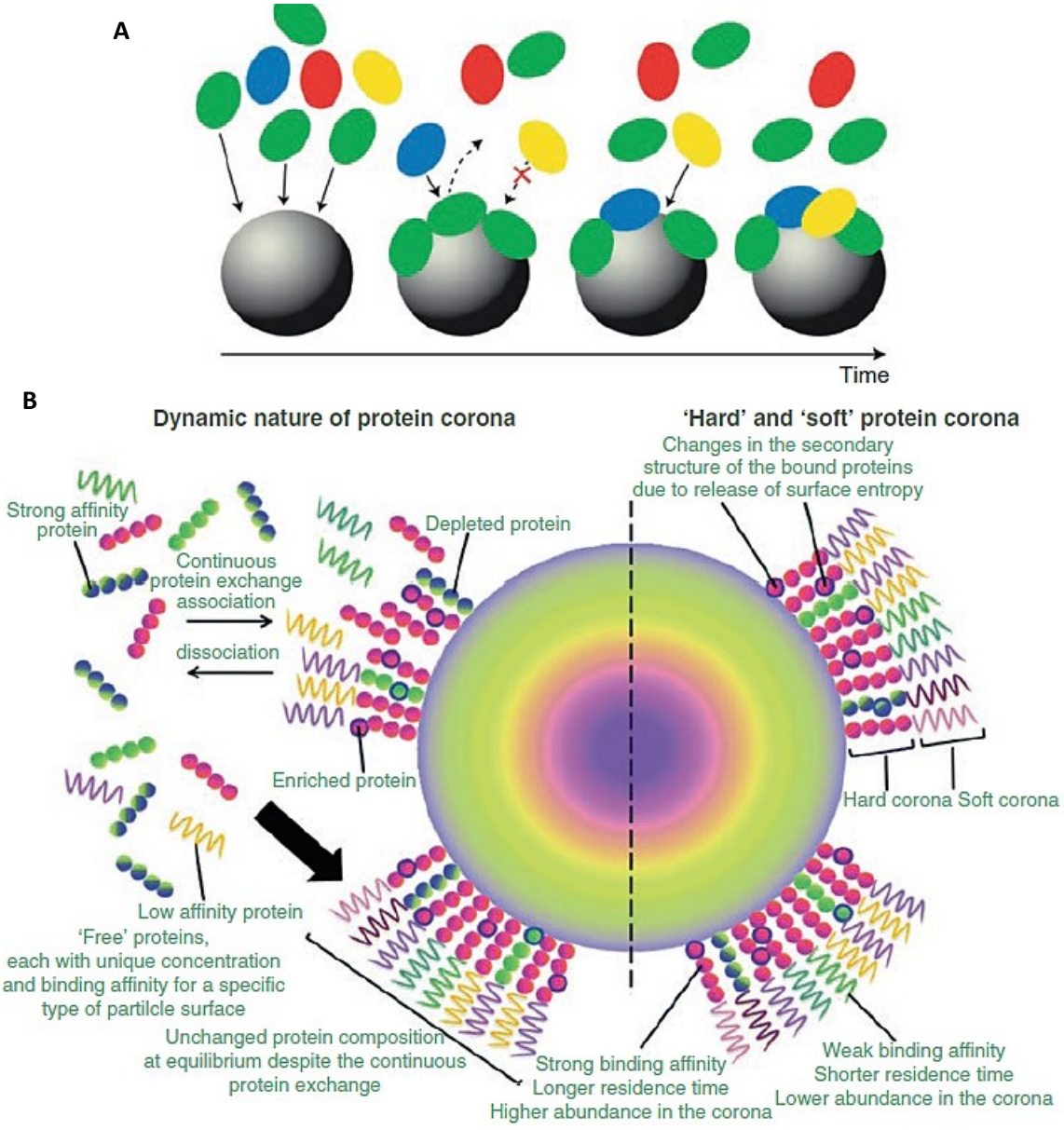


***Figure 29***. (A) Visualization of the rapid primary adsorption of a first layer of proteins (green) to NPs surface, followed by the time-dependent exchange of some these replaced with other with higher affinity (blue and yellow), this fingerprint is maintained overtime. (B) Schematic representation of the hPC and sPC were hPC layer is characterized by strong binding affinity and long residence time of the proteins while sPC have weaker affinity of the proteins and a shorter residence time, the

continuous association/dissociation of the protein is dependent by the equilibrium established between the NPs-protein complex and from this complex between the biological environment. Figure adapted from (Ahsan et al., 2018).

### *1.7.2 Protein corona composition and variability*

The biological identity from a NP exposed to a biological environment is principally furnished by the hPC because of the stability and the conserved protein fingerprint for these reasons of scientific relevance, hPC is the most studied also because of the simpler protocols linked to his isolation and identification. As mentioned before the set of physio-chemical feature of the NPs define the interaction with selected proteins, human plasma is composed approximately of 4000 proteins but only a dozen interacts with an extremely high affinity to different NPs forming the hPC although some aren't very abundant. For example a set of protein redundant in the identification in most of the NPs are: immunoglobulin kappa chain, different forms of light and heavy-chains of immunoglobulins, albumin, complement C3, complement C4, haptoglobin, alpha-1-antitrypsin, α-2-macroglobulin, apolipoprotein A-I, apolipoprotein A-III, apolipoprotein C-III, kininogen, plasminogen, keratin, vitronectin (Ahsan et al., 2018; Tenzer et al., 2011; Cedervall et al., 2007). Walkey et al. (2012) reported that from two to six proteins are common in the characterization of the PC on many NPs reported in the literature, where 3 of the most common proteins represent the 56% of the total amount of adsorbed proteins. They also imposed a threshold of 10% of the total present protein mass detected with a high abundance and in this case 21 of 125 proteins where present at least in one of the NPs examined. In particular histidine-rich glycoproteins, hemoglobin, histidine-rich glycoproteins, Ig gamma chain, Ig light chain, Ig mu chain, inter alpha trypsin inhibitor H1, mannose-binding protein C, paraoxonase-1, antithrombin-III, apolipoproteinA-1, apolipoprotein A-IV, apolipoproteinB-100, apolipoprotein C-II, apolipoprotein C-III, apolipoprotein E, clusterin and complement C3, albumin, transferrin, fibrinogen, haptoglobin, hemoglobin. The cause of the binding of all these proteins is conducible not at the physiological role but at the protein-NPs affinity due to the physio-chemical characteristics of the NPs and at the protein structural characteristics (Walkey and Chan, 2012). Another factor that potentially could influence the PC characterization in many studies is the medium utilized for the NPs incubation with cells, DMEM and RPMI are two of the most utilized culture. Was demonstrated on Au NPs that the PC formed in NPs incubated in these two media are different and dependent by the size of the NPs, especially for RPMI where PC had variations dependent NPs size, while for DMEM this effect wasn't detected. Another difference

were detected in the protein corona proteins amount, higher in DMEM compared to RPMI, that showed additionally an higher toxicity (Maiorano et al., 2010). Also, the differential use of serum or plasma can cause variation in PC composition. For example for Ag NPs or $SiO_2$ NPs were found that the total amount of protein was similar but with important variations in the composition. The PC formed in plasma had a higher variability compared to corona formed in serum, the influence of these variations had repercussion in cellular treatment where cells treated with NPs deriving from plasma incubation showed a superior viability and lower cellular uptake compared to the treatment with NPs incubated with serum. The explanation of this event was attributed to the presence of apolipoprotein j or clusterin, highly represented in NPs incubated with plasma (Aoyama et al., 2016). This is a clear demonstration of the PC importance in toxicological effects and in what manner one single protein adsorber on the NPs surface could determine different biological implications.

### *1.7.3 Protein corona influence in uptake and biological distribution*

The formation and composition of PC is a multi-factorial event, although other additional aspects are importantly involved in PC biological implications. Once PC is formed on NPs surface, the molecular interactions with biological systems could be drastically modulated by the presence of peculiar proteins that populates the *corona*, this aspect is crucial in NPs design that represents an important field of research where are studied different strategies to vehiculate NPs in a specific target, crucial for nanomedical applications. PC could drastically modify the fate of NPs distribution, a work made on $SiO_2$ NPs conjugated with transferrin (tf) demonstrated the influence of the PC on NP targeting. Were utilized adenocarcinomic human alveolar basal epithelial (A549) cells that easily uptaked $SiO_2$ NPs conjugated with tf, by the way when tf conjugated NPs were exposed to fetal bovine serum (FBS) the uptake was drastically reduced, the cause of the reduction is conducible to a “masking” effect by the PC formed after the exposition to FBS that avoided the interaction between tf and his cellular receptors (**Fig. 30**). PC could then interfere with the biological interaction of the NPs and determine some applications failure (Salvati et al., 2013).

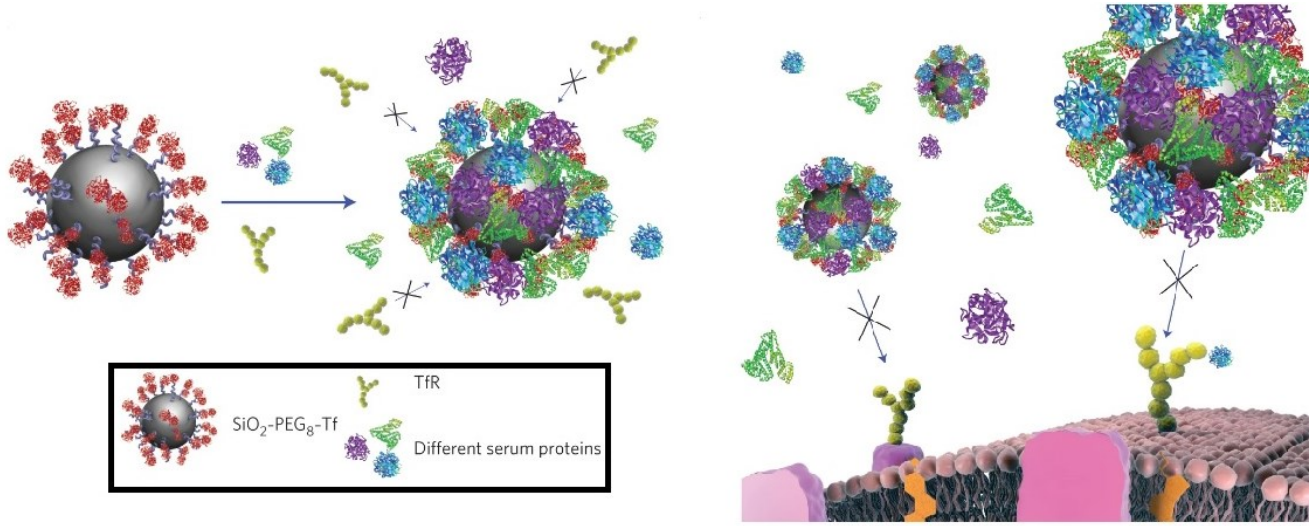


***Figure 30.*** "Masking" effect of the FBS PC generated on the surface of tf conjugated $SiO_2$ NPs interfering with the interaction between tf and his receptor and avoiding in that manner the uptake of the NPs. Figure adapted from (Salvati et al., 2013).

PC could regulate the NPs uptake also in other typologies of NPs, enhancing or reducing the internalization depending on variation in composition or in different cellular lines treated. PS-NPs functionalized with different chemical groups (PS-COOH, PS-$PO_3$, PS-$NH_2$, PS-$SO_3$) and previously treated with human serum showed different uptake in HeLa cells. In this case the authors showed a clear correlation between the uptake and the presence of apolipoprotein H (ApoH) that was highly represented in the most uptaked NPs (PS-COOH, PS-$PO_3$) while was poorly represented in PS-$NH_2$ and PS-$SO_3$ NPs that showed a low uptake rate. ApoH protein have different biological roles including the capacity to bind negatively charged compounds and as well phospholipids, this characteristic could in this case act as uptake enhancer when complexed on NPs surface (Ritz et al., 2015; Sheng et al., 1996). Another study by Lesniak et al. (2012) on A549 cells treated with naked $SiO_2$ NPs or $SiO_2$ NPs previously exposed to human serum in order to pre-form a PC, showed that the NPs with a preformed PC had a low internalization compared to bare NPs that demonstrated a high membrane adherence accompanied with a great uptake by the cells. The hPC formed from the bare NPs was recovered from the cellular surface and characterized. The detected proteins were cytoskeletal proteins, membrane proteins and were also found membrane lipids. Also the hPC from the preformed corona NPs was analyzed after the treatement, and the comparison between this two types of NPs utilized resulted in an high variability in PC composition from bare NPs (≃800

proteins) compared to the serum preformed PC NPs (≃300 proteins). In this case the cellular damage provoked by the naked $SiO_2$ NPs surely contributed to the higher variability. Also, the uptake pathways were different, naked NPs were found in the cytosol and in the lysosomes while le preformed PC NPs only in the lysosomes. Even in this case PC importantly altered the uptake, intracellular distribution, and toxicological parameters of the NPs (Lesniak et al., 2012). Another aspect of the PC concerns the bio-distribution of the NPs that can be potentially altered by peculiar proteins present in the PC, a study on the PC composition in superparamagnetic iron oxide nanoparticles (SPIONs) with different sizes and charges demonstrated the importance of the NPs size in the adsorption of smaller proteins on smaller NPs and the other way around. The charge was also important, NPs with negative charge had a higher protein variability followed by positively charged NPs and at last by plain NPs that presented modest variability. Finally, the more interesting observation was that the smaller and negative SPIONs had a high propensity to cross the BBB in a mouse model, this was explained by the high PC representation of the apolipoprotein ApoA-I that is normally transported through the BBB thanks to a saturable transport mechanism. In this case the important quantity of ApoA-I adsorbed on smaller and negative SPIONs, acted as a carrier enabling the BBB crossing while at the same time small positively charged SPIONs did not cross the BBB. This work furnishes another important scientific evidence underlining how PC could influence the NPs distribution and potentially produce accumulation in specific tissues (Mahmoudi et al., 2015).

### *1.7.4 Controlling the protein corona*

The uptake and distribution parameters of the NPs could be controlled functionalizing the NPs surface and consequentially modifying the PC composition, these surface modifications are important to confer a shield on the NPs surface in order to avoid the interaction with undesired proteins that potentially could wrongly vehiculate the NPs or influence the uptake. The immune system has the biological role to detect remove the extraneous objects ,as in this case NPs, the opsonization of the NPs surface act as recognition system for the immune cells that are triggered and active the phagocytic pathway for the NPs elimination, this process could be activated at the same manner by PC thanks to the exposition of proteins specific epitopes that are recognized by the immune system (Goodridge et al., 2012; Owens III and Peppas, 2006). In some cases, is important to control or avoid the PC formation. The NPs surface decoration with polyethylene glycol (PEG) is a utilized strategy to avoid the interaction between the proteins and the NPs forming a steric shield around the NPs, basing on the PEG density this method could be more or less effective where, the

dense disposition of PEG on NPs surface is one of the more effective methods to avoid the interaction with proteins (Schipper et al., 2009; Bartucci et al., 2002). However, there are some issues, because immune system could develop specific antibodies against PEG and stimulate in this manner a paradoxical rapid elimination of the functionalized NPs (Knop et al., 2010). By the way PEGylation is one of the most common modification together with other polymers as poly(2-oxazoline) (POx), and poly(zwitterions) potentially more efficient for the design of long-circulating NPs useful for nanomedical applications (Tarannum and Singh, 2013; Chapman et al., 2000). In last years were developed other efficient surface functionalization methods exploiting biological peptides or membranes. For example, the NPs decoration with the CD47 transmembrane peptide, that interacts with the signal regulatory protein alpha (SIRPα) present on the macrophages surface, act as powerful inhibitor of the phagocytic pathway (Murata et al., 2014). One other interesting method to make NPs stealth, is the surface functionalization with biological membrane for example the RBC membrane functionalization on Au NPs efficiently masked the NPs from the uptake by macrophages (Hu et al., 2011). In a similar manner cancer cellular membranes can be used, in fact these cells are specialized to evade the immune system control. Sun et al. applied this technique, for the functionalization of doxorubicin loaded gold nanocages with 4T1 cancer cell membranes (**Fig. 31**), this NPs efficiently targeted and accumulated on tumor site of an *in vivo* orthotopic breast tumor murine model (Sun et al., 2017).

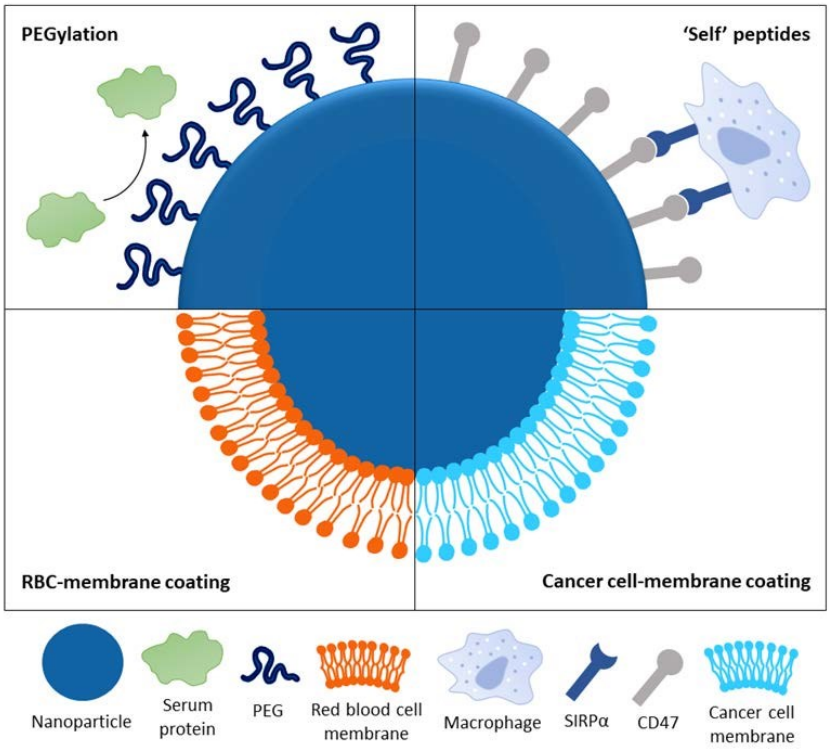

***Figure 31.*** Different functionalization methods that could limit the protein interaction controlling or avoiding the PC formation or produce stealth NPs through different bio-camouflaging modification on the surface. Figure adapted from (Fam et al., 2020).

### *1.7.5 Protein corona: toxicological aspects*

The adsorption of protein on NPs surface influence various factors as uptake, distribution, circulating time and biological fate of the NPs. Actually, there's another important factor that that could influence the toxicity of the NPs and regards the possible protein structural modification on the NPs surface. When proteins are adsorbed on NPs forming the PC, they can undergo structural changes that can alter their biological role in different manners. As previously mentioned, the exposition of epitopes, triggered by structural changes, could improve the recognition by the immune system and start the phagocytic pathway in order to eliminate the NPs (**Fig. 32**). But other molecular events can be triggered by distortions in the protein structure, in fact the structural distortion could cause the protein functional inactivation (Ghosh et al., 2014; Assarsson et al., 2014; Shang et al., 2007; Zoungrana et al., 1997). For example in a study on the adsorption of lysozyme on $SiO_2$ NPs, was observed that the unfolding of a critical α-helix of the lysozyme disrupted the catalytic activity of the enzyme (Vertegel et al., 2004) (**Fig. 32**). The protein unfolding caused by the structural distortion on the NPs surface, is then an important event that could potentially have different effects. One of this could be the creation of favorable condition for unfolded proteins aggregation and fibrillation, events that are related to different ND (**Fig. 32**) (Stefani and Dobson, 2003; Nel et al., 2009). The reasons of the protein unfolding on the NPs may be due to a structural adaptative conformational change of the protein, in this case the size and related surface curvature of the NP become important, supporting this hypothesis a correlation between NPs size and protein unfolding has been observed. Larger NPs cause a higher protein conformational change, hypothetically the protein elongates his structure to reach a higher contact with the NPs energetically favorable, this event could cause as consequence a high protein unfolding propension (Teichroeb et al., 2008). On the other hand, also the high surface energy characteristic of the NPs could influence the unfolding after the adsorption. Nel et al. hypothesized that a change of contact forces and the consequent release of free surface energy, through surface reconstruction, may enhance the unfolding process (Nel et al., 2009). An possible explanation linked to the superficial energy is compatible to an electron confinement or the formation of electron–hole pairs on the NPs, leading to a cleavage of

structural bonds or covalent crosslinking of protein SH domains, destabilizing in that manner the protein structure (**Fig. 32**) (Nel et al., 2009).

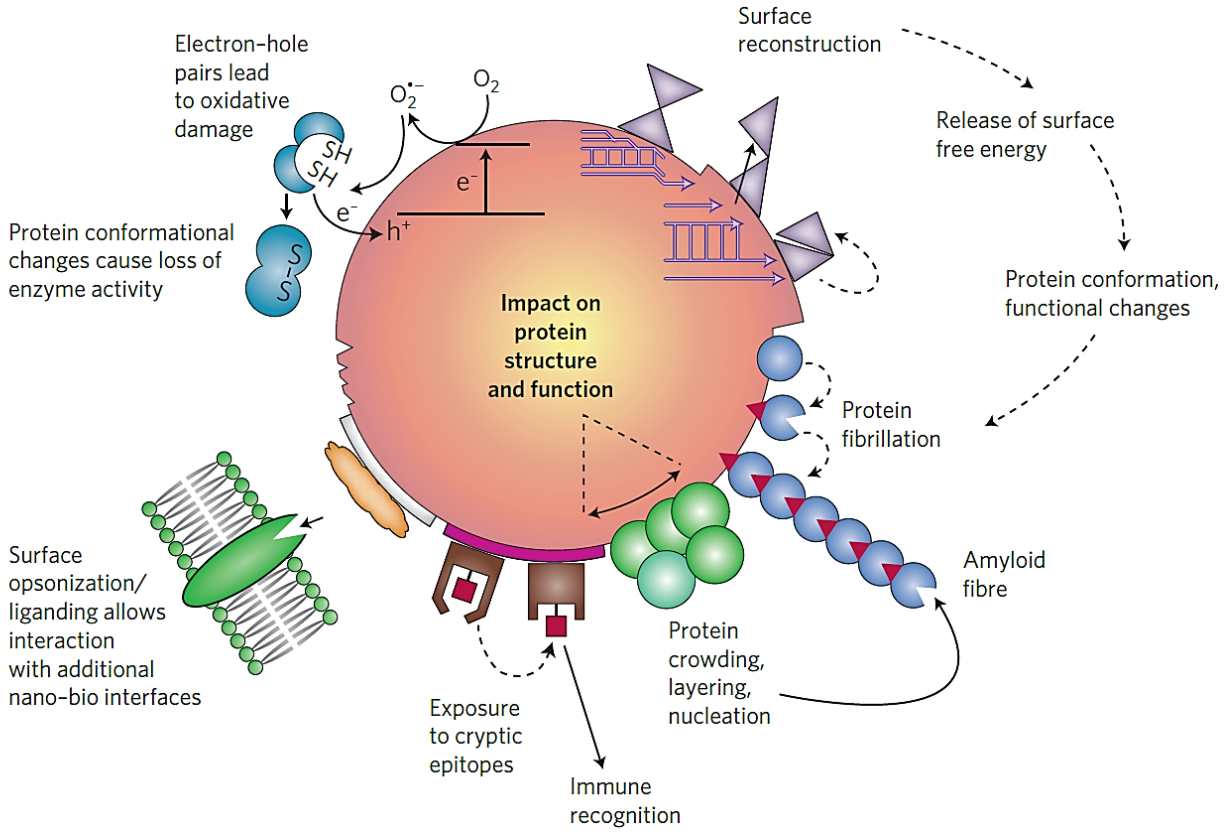


***Figure 32.*** Representation of the possible protein unfolding mechanisms that may occur on the NPs surface, leading to a potential different biological outcome. Figure adapted from (Nel et al., 2009).

Other toxicological aspects are related to the protein "sequestration" by NPs, the adsorbed proteins can be important for cellular functioning for their cellular physiology role recovered. The consequent cellular reaction to the sequestration of these proteins is characterized by an up-regulation of the related genes in order to replace the lacking proteins. Ruotolo et al. (2018) using a yeast model treated with QDs NPs (associated with toxic effects) observed that the adsorbed hPC proteins caused the lowering the "free" proteins amount, this effect was compensated by a modulation in the expression of the related genes. This effect can be associated by the physical sequestration by the NPs together with the previously discussed inactivation of the protein after the

adsorption also in this case hypothesized (Ruotolo et al., 2018). All this factor may contribute to the cellular toxicity. Recently Liu et al. (2021) analyzed RAW264.7 PC composition using RAW264.7 cells extracts on 5 different potential toxic NPs: iron-cobalt-nickel alloy NPs (FeCoNi NPs), iron oxide NPs ($Fe_3O_4$ NPs), carbon NPs (CNPs), $SiO_2$ NPs, and AuNPs. The analysis of the PC reported an enrichment of pathway related to the unfolded protein response (UPR) pathway, linked to different ND. The presence of unfolded proteins also caused recruitment of UPR related chaperones and in particular

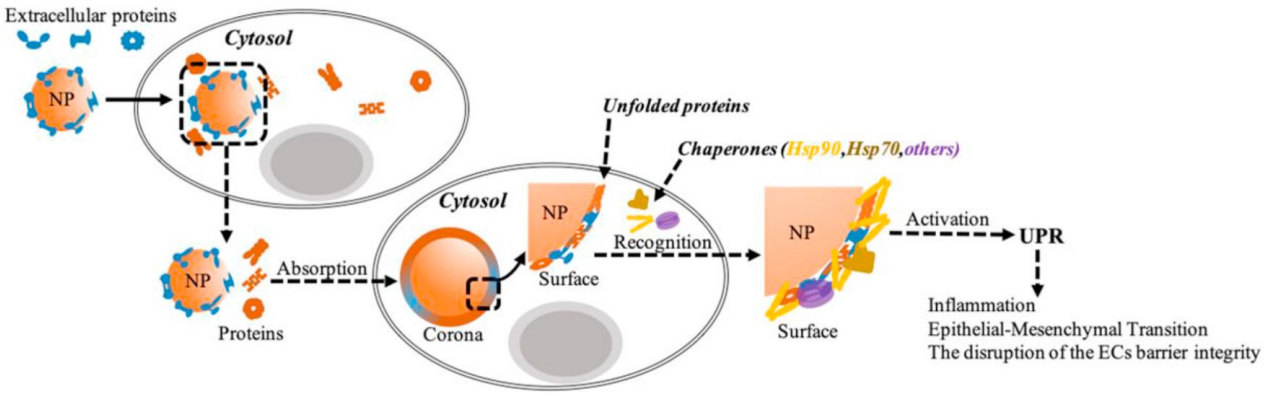


triggered the activation of Hsp90ab1, this protein induces a set of cellular reactions, comprising the UPR pathway activation, that when is chronically switched-on lead to pathological outcomes strongly linked with different ND (**Fig. 33**) (Liu et al., 2021a). Definitively, the toxicological implications related with PC could be multi-factorial, potentially impacting on different biological processes, for these reasons the understanding and characterization of the PC become relevant.

***Figure 33***. Hypothetical mechanism of action of the activation of the UPR triggered by the unfolded proteins originated on the PC. Figure adapted from (Liu et al., 2021a).

From the various aspects discussed PC interaction with biological system are various a complex, is important also to underline the possible positive implication that can origin from a deep knowledge of the PC. We discussed about important parameters of NPs uptake and distribution, strictly dependents from the PC composition with the possibility to exploit those results in the nanomedical field. PC could also directly play beneficial role, for example mitigating the toxicity of some classes of NPs, limiting the interaction with the cell membrane and shielding from direct NP-membrane interaction that might be disruptive (Lesniak et al., 2012; Ge et al., 2011). PC could also furnish

important information to comprehend toxicological aspects of NPs but also with other implication for the comprehension of molecular aspects in some diseases (Liu et al., 2021a). Recently, also the concept of Personalized PC (PPC) was quoted as promising future field of application, PPC take advantage of the PC characterization and the analysis PC of the composition in a healthy patient could reveal differences compared to an ill patient; the presence of detectable biomarkers on the PC possibly will be useful for the detection of different diseases. In the same manner the different plasmatic proteome between different peoples might affect the NPs biodistribution for nanomedical application, then the PPC in future could represent an important way to detect diseases or personalize the treatments with relevant clinical perspectives (Corbo et al., 2017).

### *1.7.6 Protein Corona: formation and methods of characterization*

The PC formation is a phenomenon driven by different factors, the PC formation in biological fluids is a spontaneous event but different parameters can affect the composition. The majority of studies are performed *in vitro* for the reason that is easier to obtain the corona, recover the NPs and go ahead with the characterization steps, on the other hand the PC obtained could importantly differs from a PC formed *in vivo*. *In vivo* PC formation and characterization is more difficult because of the difficulty to recover the NPs once injected in the animal models. Factors as, serum concentration, pH, temperature, time of exposure together with the physiochemical properties of the NPs are important for obtaining a realistic final result and at the same time difficult to be replicated *in vitro*, different *in vivo* parameters are dynamic and quite difficult to be reproduced *in vitro* (**Fig. 34**) (Singh et al., 2021).

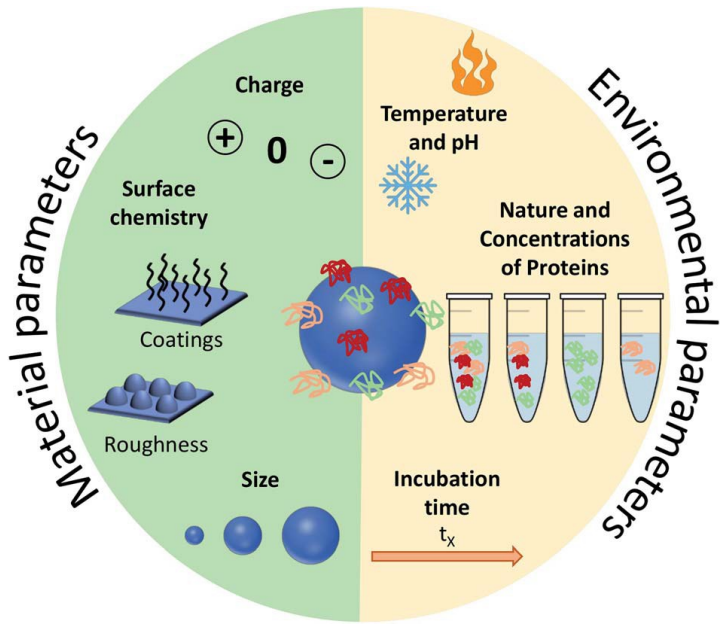

***Figure 34.*** Representation in the parameters involved in the *in vitro* PC formation.

Monopoli et al. introduced in 2011 the variations that can occur in PC at different plasma concentrations in order to evaluate PC evolution, in this first report a simple change in plasma concentration determined different PC profiles suggesting that in a more complex biological context PC evolution could have deeper implications underlining how *in vitro vs in vivo* evaluation of the PC might importantly differs. Another *in vivo* variable is represented by the fluid dynamicity that can alter the PC, Palchetti et. compared the PC formed on liposomes incubated in FBS in static vs a dynamic incubation mimicking the aortic flow speed. PC composition importantly changed between the two incubation methods demonstrating that a dynamic environment represents another element that alters the PC formation (Palchetti et al., 2016). All the parameters to consider for an accurate *in vivo* prediction of the PC are summarized in **Figure 35**. The difficulties for the *in vivo* PC characterization are linked principally with the recovery of the NPs of that can also influence the PC composition, the NPs must be recovered from the biological environment once PC is formed, and the recovery step represents the most problematic part of the process. Moreover, the study of PC formed on NPs internalized by the cells and the recovery from tissues or organs NPs require other isolation steps, a solution can be represented by the utilize of SPIONs doped NPs that allow the isolation from the internalized NPs (Bertoli et al., 2014) at the same time the physiochemical characteristics of the NPs might variate after the doping processes. A possible solution for the mimicking the internalization without alter the NPs nature is the use of cellular extracts, followed by an *in vitro* PC formation that then could be characterized (Liu et al., 2021a; Ruotolo et al., 2018; Klein et al., 2016). By the way after the *in vivo* or *in vitro* formation of the PC for the NPs recovery are commonly utilized several techniques as centrifugation, differential centrifugation sedimentation, size exclusion chromatography, and magnetic separation. Where the centrifugation represents the most simple and versatile method (García-Álvarez and Vallet-Regí, 2021). There are two principal ways to characterize the PC proteins, divided into *in situ* and *ex situ* techniques. For the *ex situ* characterization, the recovered NPs are washed and the hPC selected, washing steps are executed in order to remove the weakly bound proteins, indeed sPC is yet altered after the removal from the biological medium and by the centrifugation steps, for this reason is convenient to fully remove sPC protein in order to reduce the variability and avoid inaccurate analysis. The PC characterization the validated techniques, after the NPs recovery and selection, are several and

applied for *in vitro* PC and similarly for *ex situ* PC characterization. The morphological visualization of the PC can be made using TEM (Mahmoudi et al., 2011) or atomic force microscopy (AFM) (Guan et al., 2015) while for the ion quantitative/qualitative PC protein composition identification the most utilized technology is represented by SDS-polyacrylamide gel electrophoresis (SDS-PAGE) and liquid chromatography tandem mass spectrometry (LCMS/MS) (Walkey et al., 2014) (Pinals et al., 2020). To evaluate the adsorption kinetics of the proteins-NPs interaction is utilized the ITC (Fleischer and Payne, 2014; Cedervall et al., 2007). To estimate the proteins structural variations are employed: circular dichroism (CD) spectroscopy (Fleischer and Payne, 2014; Yan et al., 2013), fourier transform infrared spectroscopy (FTIR) (Wang et al., 2012), nuclear magnetic resonance (NRM) (Brancolini et al., 2012) and the evaluation of the enzymatic activity (Gagner et al., 2011; Ruotolo et al., 2018). For the *in situ* technique is not essential to separate NPs from the biological medium, because it directly gives information about PC directly when the NPs are dispersed into the biological environment, *in situ* characterization represent and emerging method born thanks to the development of new detection techniques. One significant feature of the *in situ* PC characterization is related to the information which are provided on the *soft corona* that is normally lost in traditional techniques, due to the selection and washing steps of the NPs which cause the loss of the sPC. One of the last *in situ* characterization methods employed the cryoTEM and synchrotron-radiation CD permitted to analyze the weakly bound proteins and reveal molecular basis of sPC in situ. In this recent work the sPC composition was discovered to be altered by the protein unfolding states shifting at physiological temperatures (Sanchez-Guzman et al., 2020). Another sPC characterization technique was recently validated utilizing the *in situ* click-chemistry reaction (Mohammad-Beigi et al., 2020).

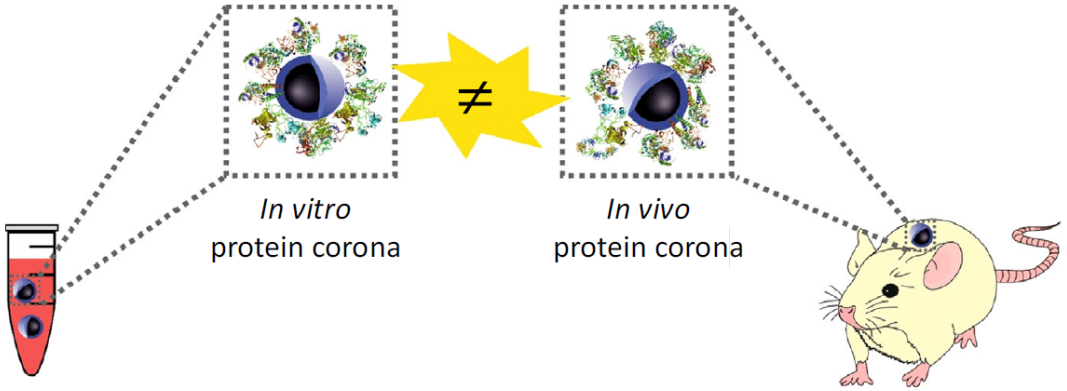


| ***In vitro* protein corona** | ***In vivo* protein corona** |
|---|---|
| • Comprises the same amount of protein as *in vivo* corona | • Comprises a wider variety of biomolecular species |
| • Does not have a role in fasting, diet body tempeature, etc. | • Has a role as a fasting, diet, body temperature, etc. |
| • Does not have a role in personlized corona | • Has a role as a personalized corona |
| • Cannot mimic the dynamic and fluidic variations protein as *in vivo* corona | • Effects of dynamic and fluidic variations are considered |

***Figure 35.*** Different parameters that define the differences between *in vivo* or *in vitro* PC. Literature on *in vivo* PC is still poor and certainly need more results to define a full panoramic of the molecular events involved in the biological identity of the PC. Is also reported the importance of a dynamic environment, that might be crucial for to create shear stress on NPs providing a continual source of new biomolecules. Figure adapted from (Caracciolo et al., 2017).

## 1.8 Parkinson's disease

Parkinson's disease represents the second most common ND affecting 2-3% of the population over 65 years old. Is a long-term central nervous system neurodegenerative disease. Different factors are involved in the genesis of the disease, the cause of the development of PD is still unknown, familiar or environmental factors could play an important role in the set-up of the illness. The motor symptoms detected in the disease are due to the death of cells in the substantia nigra, a region of the midbrain, leading to a dopamine deficit. The most evident early symptoms are tremor, rigidity, slowness of movement, and difficulty with walking. Cognitive and behavioral problems may also occur with depression, anxiety, and apathy occurring in many people with PD (Poewe et al., 2017). The real cause of the neuronal cell death is still poorly understood, but a common trait present in PD patient brains is the accumulation of misfolded proteins into Lewy bodies, composed principally of α-synuclein associated with other proteins. α-Synuclein is a typical intrinsically disordered protein (IDP) that can adopt a number of different conformational states. In physiological conditions, α-syn exists in a tightly-regulated equilibrium between cytoplasmic monomeric (unstructured) proteins and membrane-bound α-syn with a broken α-helix conformation. Normally α-syn associates with membranes interacting the first 100 amino acids of its N-terminal region thus his physiological role is involved in the in the modulation of neurotransmitter release (Davidson et al., 1998); in pathological conditions, α-syn undergo a series of lipid-dependent conformational changes leading to the formation of β-sheet-rich aggregates (α-syn oligomers), considered the most neurotoxic forms of α-syn. In the traditional models it was thought that was the α-syn direct fibrillization leading to the formation of Lewy bodies that represent the pathological hallmark of synucleinopathies (Longhena et al., 2020; Bartels, 2019). α-Syn toxic oligomers are synergic with the alteration of others different cellular pathways: alterations in autophagy, synaptic vesicles trafficking defects, alteration in lysosomal degradation, alteration in ER functions, mitochondrial and Golgi apparatus dysfunction and disruptions of nuclear processes (Vijiaratnam et al., 2021). Another problem regarding α-syn is the spreading of toxic species through exosomal secretion followed by an endocytic uptake, this prion-like spread of α-syn species could overwhelm the endosomal trafficking and transit the toxic form of α-syn in healthy neurons. The α-syn release together the formation of insoluble aggregated species, accompanied with fibrillation events could deprive the synapsis of the regulatory action of α-syn (Longhena et al., 2017). Recently, it has been highlighted that the Lewy bodies in PD patients consist of lipid vesicle clusters and fragmented organelles, including mitochondria, with high local concentrations of α-syn molecules

in oligomeric form (**Fig. 36**) (Fanning et al., 2021; Shahmoradian et al., 2019a). Still, there's no known cure for PD and the most common treatment utilized, is the levodopa administration that provides a symptoms control in the early stage of the disease but don't act on the neurodegeneration, moreover at late stage of PD, classic levodopa-resistance symptoms causes a disability increase in patients (Balestrino and Schapira, 2020). One of the last approaches for reducing α-syn toxicity is represented by the direct targeting different sites of the protein using anti-α-syn antibodies, the finality of antibodies applications is to enhance the protein immune mediate clearance and counteract the toxicity and spreading of toxic species (Sanchez-Guajardo et al., 2013). Also, the induction of the α-syn autophagy using Nilotinib, a non-receptor tyrosine kinase (ABL1) inhibitor, is potentially a powerful α-syn autophagy inductor (Hebron et al., 2013). Other potential therapeutic agents are based on the LRRK2 activity inhibition, the cause of some genetic PD forms is directly attributable to mutations on LRRK2 gene that cause an increase of the kinase protein activity leading to autophagic disruption and α-syn spreading (Cresto et al., 2019). Inhibitors or antisense oligonucleotides of LRKK2 were demonstrated to have a neuroprotective activities probably enhancing the autophagy (Manzoni et al., 2013; Korecka et al., 2020). However, this typology of approach is restricted only to LRKK2 mutations triggered PD forms. Another event detected PD post-mortem brain analysis is the over-presence of iron in *substantia nigra*, this disproportionate iron presence might be directly involved in neuronal death events by mitochondrial oxidative stress events, contribution in the formation of α-syn toxic aggregates and leading to apoptotic events (Dexter et al., 1987). The utilize of iron chelators as deferiprone have beneficial effects on PD progression and is well tolerated, a phase 2 clinical trial will readily validate the therapeutic potential of deferiprone in PD (Mahoney-Sánchez et al., 2021; Martin-Bastida et al., 2017). Another important hallmark of PD is represented by inflammation, neuroinflammations events characterizes PD in all the phases of the disease and are directly linked with neurodegeneration, the accumulation on α-syn aggregates trigger the production of inflammatory cytokines and chemokines (Lee et al., 2010). Also, different transcription factors of Nuclear factorκB (NF-κB), are involved in pathogenesis of PD. NF-Kb is a crucial regulator of inflammation and apoptosis and a dysregulation of NF-Kb caused by and over-abundance of one of his factors as RelA was detected in neurons and glial cells of PD patients, whereas an inhibition of RelA was associated with neuroprotective effects. Then the relationship between NF-Kb an PD is another important event to take into account to fully understand the mechanisms of PD (Bellucci et al., 2020). Gu et al. (2010) observed in mice models that the production of pro-inflammatory messengers caused a microglial activation associated with

neurodegenerative events, the suppression microglial activity was associated with an enhanced mice survival, suggesting a direct involvement of inflammation and microglial activation with the progression of the disease (Gu et al., 2010). Different inhibitors of microglial activation were tested, demonstrating a direct correlation with neuroprotective effects, for example. AZD3241, an inhibitor of microglial activation protects dopaminergic neurons, and was well tolerated in phase 1/2 trials (Jucaite et al., 2015). α-Syn pathogenic species also triggers the activation of the peripheral immune system in PD and this process is related with neurodegeneration and neuroinflammation (Gao et al., 2011; Williams-Gray et al., 2016). The use of Azathioprine, one of the most known and studied immunosuppressant drugs, was proposed for PD and the set-up of one clinical trial will assess if the treatment with this compound will exert positive effects with the ongoing of the disease (Broen and van Laar, 2020; Greenland et al., 2020). Mitochondrial physiological function and morphology is compromised in PD and mitochondrial dysfunction have a primary role in the pathogenesis of PD (Federico et al., 2012). α-Syn accumulation in mitochondria was assessed, and this is the main event that can lead to mitochondrial dysfunction and finally to cell death. The affinity of α-syn for membranes and the switch in pathological conformations leading to aggregation events, have effects on membrane fusion, this can explain causes ER/Golgi vesicle trafficking defects and mitochondrial fragmentation, the study of α-syn effects on mitochondria is then one of the most interesting fields for the comprehension of PD (Exner et al., 2012). Different promising compounds directly acting on mitochondria as pioglitazone urate or Q10 co-enzyme didn't show significant effects in trials (Vijiaratnam et al., 2021). Actually, the most promising molecule able to rescue the mitochondrial potential is represented by ursodeoxycholic acid, this compound licensed for use in human. Was yet demonstrated a mitochondrial protective potential in peripheral tissue of sporadic PD, ursodeoxycholic acid demonstrates a good CNS penetration and neuroprotection also in other ND, two trials started to the efficacy in PD (Carling et al., 2020; Keene et al., 2002; Sathe et al., 2020). Also polyphenols shows important inhibition effects in α-syn fibrillation, epigallocatechin gallate (EGCG) promotes the formation of non-toxic α-syn oligomers efficiently binding to the native unfolded polypeptides and preventing the formation of toxic aggregates (Ehrnhoefer et al., 2008; Jha et al., 2017). The complexity of cellular pathways and structure involved in the pathogenesis of PD is a problem for the identification of beneficial compounds effective for the different stage and typologies of PD.

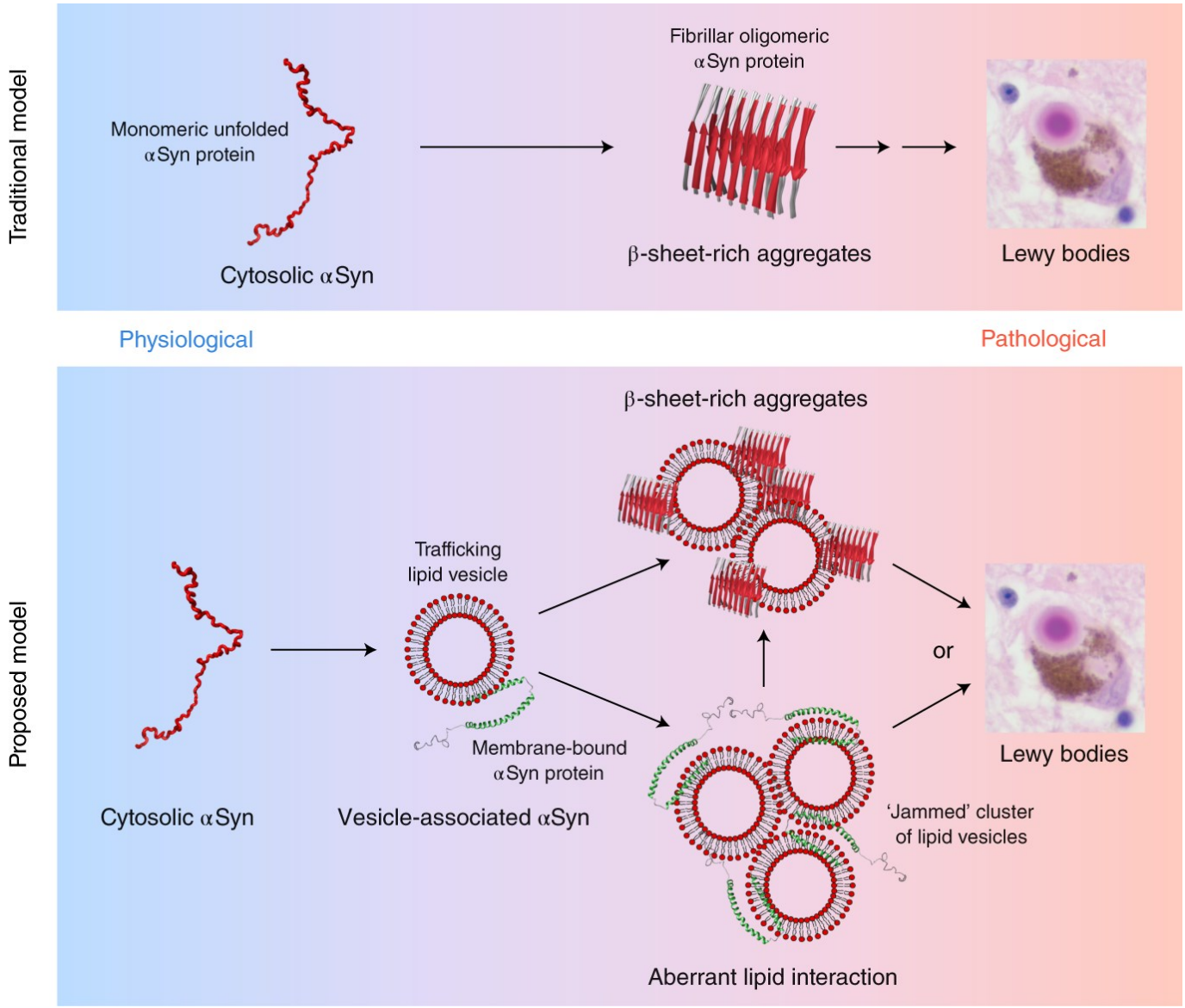


***Figure 37***. Comparison between the traditional model of Lewy bodies formation vs the modern model where the most toxic species are represented by β-sheet-rich aggregates (α-syn oligomers), Lewy bodies amyloid fibrils formation are associated in the new model with a late stage progression of the disease. Figure adapted from (Bartels, 2019).

## 1.9 The yeast *Saccharomyces cerevisiae*: a versatile model system

### *1.9.1 An overview*

Budding yeast *Saccharomyces cerevisiae* is playing a pivotal role for the study and comprehension of the eukaryotic biology. Thanks to the short cellular cycle, the non-pathogenicity and the simple genome engineering. Yeast possesses an efficient homologous recombination system that enable to easily delete or replace genes (Winzeler et al., 1999). Yeast also shares different cellular pathways and structures with other eukaryotes as, protein targeting and secretion, nucleic acid metabolism, organelle biogenesis, cell cycle progression and cytoskeletal structures (Smith and Snyder, 2006). Yeast was also the first eukaryote with a fully sequenced genome deserving as basis for the other genetic studies, yeast genome (≃6000 genes) is 100 times smaller than human genome, but about the 30% yeast of the genes have orthologs in the human genome and nearly 2/3 of the yeast genes share at minimum one conserved domain with human genes (Goffeau et al., 1996; Botstein et al., 1997). Another important attribute of yeast reside is the possibility of application in high-throughput analysis, through the creation of DNA and protein micro-arrays (Zhu et al., 2001; Spellman et al., 1998), were also made systematic deletion mutant arrays (Tong et al., 2001) and large scale two-hybrid screenings In order to identify the protein-protein interactions (Uetz et al., 2000), all together these works made yeast the first eukaryotic organism to be analyzed in a whole genome scale. The set of information on yeast, made it a powerful tool for the study of human disease and in various application in biochemistry and molecular biology.

### *1.9.2 Yeast as model for neurodegenerative diseases*

All the conserved yeast genes are important for the study of the molecular basis of many diseases, over 1000 genes present in yeast are correlated with human diseases from genetic diseases to cancer and ND (Heinicke et al., 2007). ND are actually a public health challenge, the correlation with the ageing of the population in the modern and developed countries make ND a public health problem. The most common diseases are represented by: AD, PD, ALS, Huntington's disease (HD) and Multiple system atrophy (MSA). The incidence of these diseases dramatically increases with age, the factor contributing to the onset of ND are multiple, where genetic and environmental factors are importantly involved together with sporadic events still poorly understood, almost for all these ND there aren't still valid cures (Checkoway et al., 2011). In last decades we had many insights from research that gave us information on the molecular basis of ND. Proteinaceous oligomeric or amyloid aggregation represents frequently the most common hallmark of many ND

where the effect-cause relationship remains is still under debate (Lansbury and Lashuel, 2006; Ross and Poirier, 2004). The observation that the aggregation of misfolded proteins of the same genre was a common trait in sporadic and familial forms of some ND, allowed researchers to create different animal models which assume a great importance for the study of these disease. In this scenario a simple unicellular fungus as yeast became an excellent model for the study of ND. Modelization of yeast for different ND demonstrated different salient feature of the diseases, protein aggregation represents a salient trait of this typology of diseases, if these aggregates formed by damaged or misfolded proteins are not readily removed can increase in number and dimensions impairing several cellular functions and leading finally to cell death (Stefani and Dobson, 2003). Yeast models of different ND were obtained transforming yeast cells with the protein-related diseases. For PD, α-syn aggregates can be detected in most case of the disease, the transformation and overexpression with α-syn in yeast result in a dose dependent toxicity with the formation of cytoplasmic aggregates (Auluck et al., 2010). Similar aggregation events are detectable in yeast AD models, AD is characterized by the aggregation and fibrilization of the Aβ peptide that is the principal component of soluble toxic oligomeric species in AD and also of the amyloid plaques (Treusch et al., 2011). Protein aggregation in present also in other yeast ND models of HTT and ALS [**Fig. 37**; (1)] (Tardiff et al., 2012). The yeast mentioned models also shares other important biological features, nucleocytoplasmic transport is another process importantly impaired in ND and also this pathway is impaired in yeast ND models (Bitetto and Di Fonzo, 2020; Jovičić et al., 2015) [**Fig. 37**; (2)]. Mitochondrial physiological function could be importantly impaired in ND and mitochondrial dysfunction have a primary role in the pathogenesis of PD, AD and ALS (Federico et al., 2012) also in yeast models there are important dysfunction in mitochondrial activity and morphology, especially in PD models (Ruotolo et al., 2020; Outeiro and Lindquist, 2003; Strain et al., 1998; Babcock et al., 1997; Tardiff et al., 2012) [**Fig. 37**; (3)]. Vesicular trafficking is crucial for neuronal cells functioning and for neurotransmitters release, a lot of scientific studies underlined that the impairment in synaptic vesicle regulation, endocytic trafficking, and lysosome-mediated autophagy are importantly related with many ND. Protein related with ND as for example α-syn and huntingtin are in fact important regulator of vesicles trafficking and a dysregulation of these proteins structure and functioning directly impact on these processes and in neurodegeneration progression (Caviston and Holzbaur, 2009; Wang et al., 2014). In yeast PD HTT and AD ND models also vesicular trafficking pathway is importantly dysregulated representing another compromised biological pathway comparable to the human ND (D'Angelo et al., 2013)}(Tardiff et al., 2012) [**Fig. 37**; (4)]. Finally,

another process dysregulated by protein aggregation in ND corresponds to the impairment of the cellular protein quality control machineries, corresponding to ubiquitin-proteasome system and autophagic processes. These two pathways are fundamental for cells, in order to remove damaged and misfolded proteins, the activity of these pathways have an important decline related to the aging and is dysregulated in ND leading to the accumulation of damaged and misfolded proteinaceous species which leads to neuronal death (Nedelsky et al., 2008). These pathway are conserved in yeast and also in ND models these quality control pathways are compromised (Braun, 2015; Petroi et al., 2012; Sharma et al., 2006; Kraft et al., 2009) [**Fig. 37**; (5)]. As discussed, the sharing of different important pathways between yeast and human cells accompanied with many assimilable cellular and structural functions governed by equivalent genetic instructions was precious for the creation of "humanized" yeast models in order to study in a simple and effective way ND caused by different factors. The large-scale set of the experiment and the direct information on growth and viability are also important features compared to other models (**Fig. 37**). One clear example of the implications of the yeast modelization for human ND was the study by Babcock et al. (1997) on the Friedreich's ataxia, a rare and fatal ND disorder that induce neurodegeneration and cardiomyopathy. Friedreich's ataxia is caused by the mutation of the gene FXN codifying for fratraxin. Frataxin have a putative homologous in yeast the Yfh1p and thanks to the different techniques appliable to the yeast model, growth and biochemical assays accompanied to genome editing, Babcock and co-workers demonstrated that mutations on FXN gene and subsequently on fratraxin protein cause a fatal mitochondrial damage. Thanks to these findings was identified the therapeutic target that enabled the design of two drugs that improve the symptoms of the disease, currently in a clinical trial phase (Babcock et al., 1997; Zesiewicz et al., 2018).

**CULTIVATION**
- Non-hazardous organism (GRAS)
- Rapid growth (90-120 min per cell division)
- Low cost medium for growth
- Controllable switch between glycolysis and oxidative fermentation

**GENETIC MANIPULATION**
- Stable haploid and diploid states
- Extensively annotated genome
- Ease of gene engineering
- Well characterised mutant collections

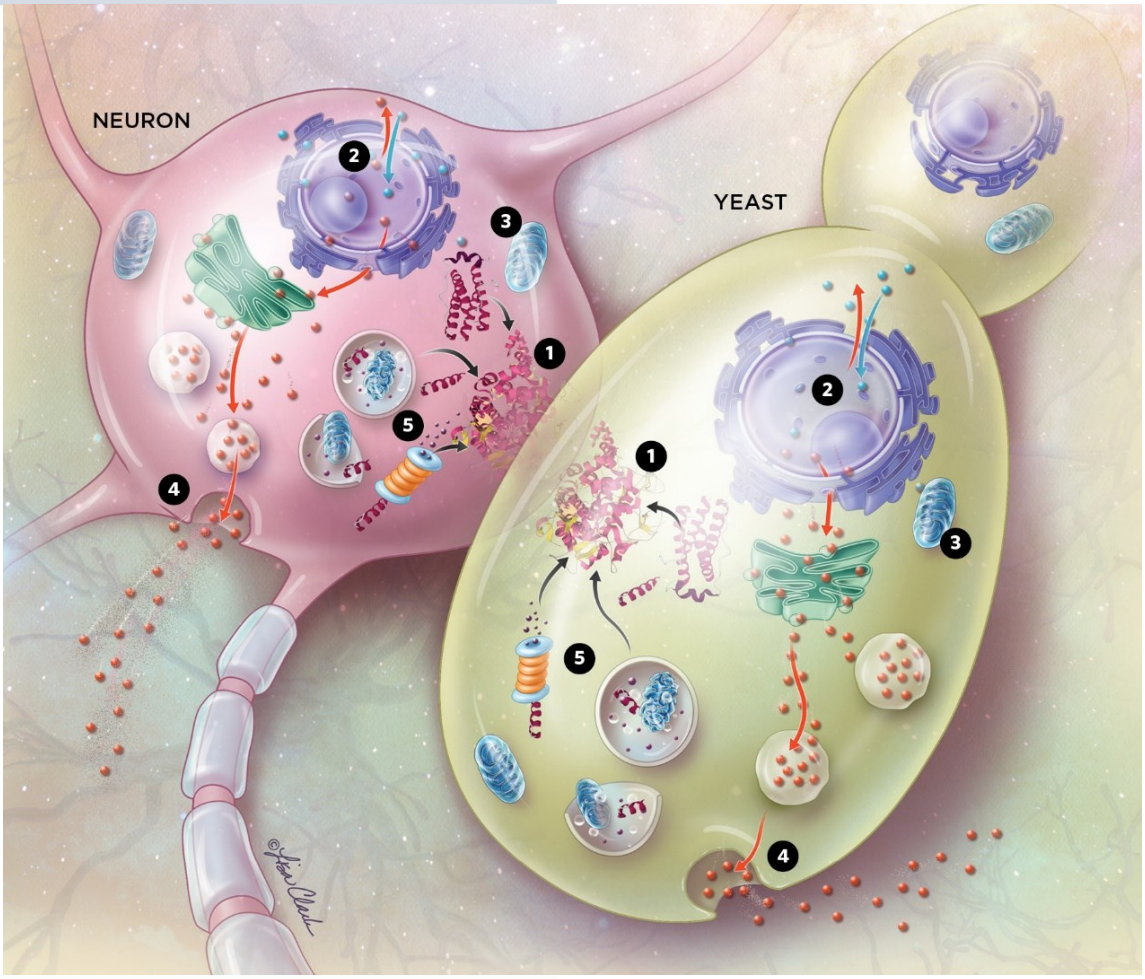


**HUMAN CHARACTERISTICS**
- Cellular organisation; nucleus, mitochondria etc
- Conserved cellular processes
- Many human orthologues
- Ease of 'humanisation'

**ENDOGENOUS AMYLOIDS**
- Endogenous amyloids
- Expression of mammalian amyloids
- Readily screenable phenotypes
- High throughput screen (HTS) friendly

***Figure 37.*** Salient features of yeast deployment as model for ND. Yeast and neurons share of many similar cellular processes as **(1)** protein aggregation, **(2)** nucleocytoplasmic transport, **(3)** mitochondrial functioning **(4)** vesicle trafficking, **(5)** quality control machineries. These pathways are equivalently impaired in neurons and in yeast. The citated similarities together with the simple

cultivation, hi-throughput analysis possibilities and efficient genetic manipulation of yeast made this simple unicellular fungus an excellent model for the study of ND. Figure adapted from (Tuite, 2019) and *https://www.the-scientist.com/features/yeast-models-provide-new-insights-into-ND-diseases-69204.*

### *1.9.3 Yeast model of PD utilized in this work*

The first modelization and characterization of PD in yeast was made in 2003 by Outiero et al.; in this pioneering work were assessed the toxicity determinants linked with different α-syn expression dosages (Outeiro and Lindquist, 2003). The transformation of yeast strains was performed fusing the green fluorescent protein (GFP) at the carboxy terminal of the human SNCA gene codifying for α-syn with a linker composed by 4 amino acids (**Fig. 38**). This construct is controlled by a GAL1 galactose-regulated promoter that is repressed in presence of glucose and activated in presence of galactose, avoiding a selective pressure determined by continuous α-syn expression and having the advantage to induce a synchronous α-syn expression only by changing the sugar carbonium source in the culture medium.

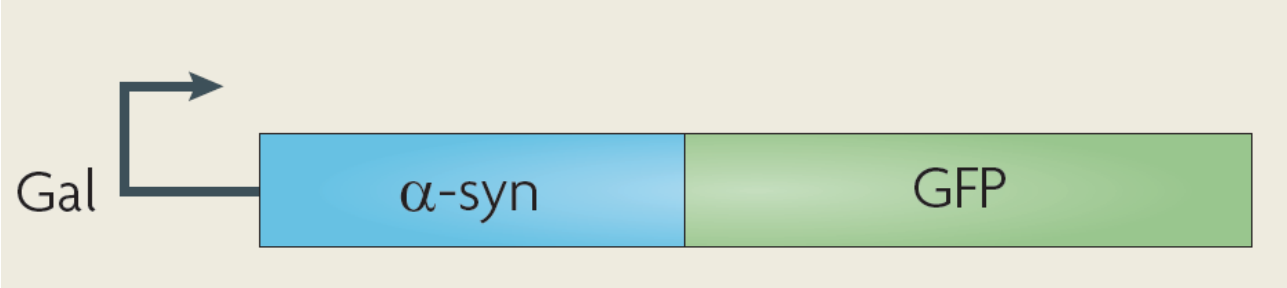


***Figure 38***. Construct utilized to transform PD model yeast strain. Figure adapted from (Khurana and Lindquist, 2010).

Thanks to the efficient homologous recombination of yeast this cassette was integrated directly into the yeast genome with single or double integrations in different genetic loci. The integration of GFP allow the direct analysis of the α-syn expression directly by fluorescence microscopy, a simple and useful way to visualize the protein expression and localization. Moreover, the presence of GFP don't alter the α -syn functioning and distribution, in fact the strain without the α-syn-GFP fusion exhibits comparable biological effects. When α-syn is expressed in the single copy strain, also called NoTox, from the fluorescence microscopy is possible to detect a clear α-syn plasma membrane localization and from TEM images are visible slight vesicles trafficking defects (Gitler et al., 2008), plasma

membrane localization derives from α-syn trafficking from the ER to Golgi with a final delivering through vesicles that fuses on the plasma membrane (**Fig. 39**) (Allendoerfer et al., 2008). This fusion process is constitutive in yeast and comparable in neurons synaptic region in an extremely regulated equilibrium (Dixon et al., 2005). NoTox strain don't show alteration in growth rate or defects in others cellular district. The situation is different when the α-syn dosage increases, the IntTox strain was obtained from a plasmid transformation carrying the DNA construct, when α-syn is expressed from a high-copy (2μ) plasmid the resultant dosage is higher than the HiTox strain (**Fig. 39**). The consequences of this dosage increase are different, there is a reduction in the growth rate and the presence of α-syn both in plasma membrane and in vesicle clusters cytoplasmic inclusions, are also detected different cellular disfunctions as, ER stress, activation of the heat-shock response, and mitochondrial dysfunction (Cooper et al., 2006; Su et al., 2010). Finally, the genomic integration of two copies of the construct result in a high dosage of α-syn expression (HiTox) this strain is characterized by a block of the cellular division accompanied with a drastic change in the α-syn localization, that is visible in large cytoplasmic vesicles clusters inclusions. This α-syn foci don't derive, as conceivable, by the excess of the protein that isn't able to find space in the plasma membrane, but by a first accumulation step in plasma membrane where are readily formed small foci, this foci later accumulates in large cytoplasmic inclusions (**Fig. 39**) (Gitler et al., 2008). In HiTox strain is present a global cellular disfunction dictated by the complete engulfment of the ubiquitin-proteasome system, together with an important impairment in vesicle trafficking and is visible an accumulation of lipid droplets, mitochondrial morphology and functioning is significantly compromised (**Fig. 39**). In HiTox strain ER-stress increase is another effect of the α-syn overexpression (Cooper et al., 2006; Auluck et al., 2010). ROS accumulation and increase in oxidative and nitrosative stress are other effects clearly linked with the α-syn overexpression in this model, and crucially involved in the pathogenesis of almost all ND including PD (Su et al., 2010). The α-syn dosage, correlated growing disfunctions and increasing toxicity recapitulate several parallelisms between of the human PD and yeast PD models, for example in familiar PD cases caused by SNCA gene duplication or triplication is evident a similar correlation between α-syn dosage and related toxicity and α-syn foci detection (Ibáñez et al., 2009). In conclusion this model represents a powerful tool to expand the knowledges on ND human disease and a potential discovery platform to find the genetic factors involved in the genesis and progression of PD or potential compounds able to prevent or lower the α-syn toxicity in PD.

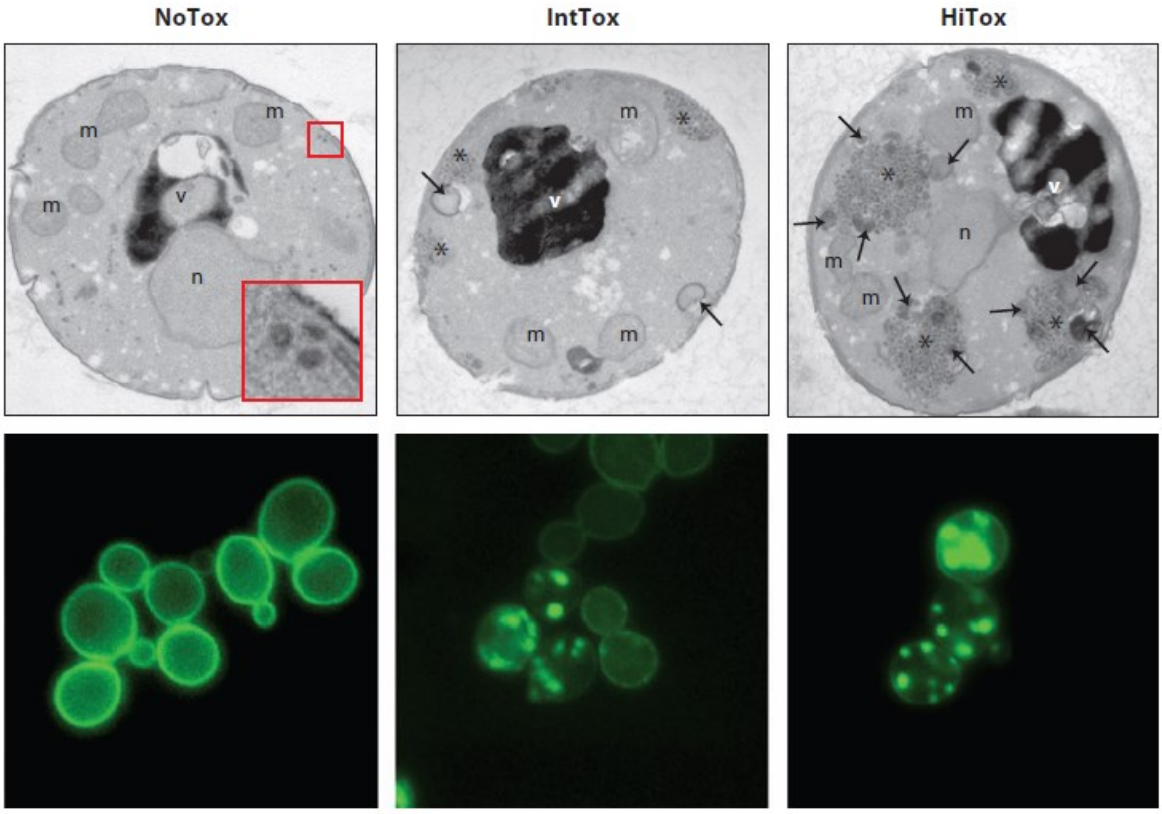


| | NoTox | IntTox | HiTox |
|---|---|---|---|
| **α-Syn localization** | Membraneous | Membraneous<br>Small foci | Large foci |
| **Growth rate** | Normal | Decreased | No growth |
| **Vesicle accumulation** | Mild | Moderate | High |
| **ER-to-Golgi complex trafficking defect** | Absent | Present | Present |
| **Mitochondrial defects** | None | Low | High |
| **Lipid droplet accumulation** | Absent | Rare | Present |

***Figure 39.*** TEM and Fluorescence microscopy images of NoTox IntTox and HiTox strains (m, mitochondria; n, nucleus; v, vacuole and asterisk denotes the vesicle clusters). In the table is reported a classification of the different α-syn dosages related cellular dysfunctions in different cellular compartments or pathways. Figure adapted from (Auluck et al., 2010; Su et al., 2010).

### *1.9.4 Nanoparticles for the treatment of Parkinson's disease*

Nanotechnology products like NPs could provide to some innovative solution for the treatment of PD, NPs thanks to their dimension an superficial characteristics might be applied for a targeted CNS drug delivery or for a direct interaction with α-syn (Singh and Lillard Jr, 2009; Mohammad-Beigi et al., 2019). As we discussed the peculiar superficial characteristics of NPs, the small dimensions and the important surface/volume ratio might be important for the interactions with α-syn and α-syn toxic species. Generally different typologies of NPs had been studied and depending on their surface chemistry or superficial modification are able to inhibit or retard α-syn the aggregation or fibrillation, on the other hand some typologies of NPs could enhance these processes (Nel et al., 2009; Kim et al., 2018; Yang et al., 2013; Vitali et al., 2018). NPs represent an interesting platform for the study of new strategies useful for the treatment and understanding of PD also thanks to their simple tunability. In this scenario the adsorption of α-syn on the NPs and then the PC could have important implications for NPs application in PD (Tira et al., 2020)}(Mohammad-Beigi et al., 2019). Different NPs had been tested and the results in some cases are encouraging, for example gold nanoclusters prevented α-syn aggregation and fibrillation and improved cell viability in mice MPP+ lesioned cell PD model (Gao et al., 2019). Amphiphilic fullerenols showed anti-aggregative effects on α-syn amyloid species formation inhibition, interacting with the NAC (non-amyloid-β component) region of the protein, a critical component for α-syn fibrillation (Sun et al., 2019). Viologen-phosphorus dendrimers are able to inhibit the fibrillation of α-syn *in vitro* (Milowska et al., 2013). NPs interacting with lipids are also able to protect from the formation of α-syn toxic species, zwitterionic nanoliposomes loaded with cholesterol or functionalized with PEG are able to interact with the N-terminal region of α-syn increasing the cell viability of different dopaminergic cell lines (PC12, SHSY5Y, and SHSY5Y over-expressing α-syn) tested, reducing neurotoxicity and ROS levels (Aliakbari et al., 2018). Zhu et al. (2003) showed the *in vitro* α-Syn interaction with vesicles composed by different phospholipids and was hypothesized a strong correlation between the capability of α-Syn to assume the α-helix conformation with an inhibition of aggregation and fibrillation, suggesting the importance of the protein conformation in a biological context with his propension to aggregate into toxic species (Zhu and Fink, 2003). From all the listed recent updates on NPs application for PD, one of the most relevant is represented by gold nanocrystals under the name of CNM-Au8®, able to restore the metabolic energy in the CNS, and showing neuroregenerative and neuroprotective effects, CNM-Au8 is currently in evaluation for a phase 3 trial for the treatment of ALS and a phase 2 for MS and is in a pilot phase 2 trials also PD yet

demonstrating good results (Jagaran and Singh, 2021) (Vucic et al., 2021) https://parkinsonsnewstoday.com/2021/09/24/cnm-au8-improve-brain-energetic-profile-parkinsons-disease-patients-repair-pd-trial/. All this findings suggest how NPs could potentially contribute to the treatment of PD and ND thanks to their versatility, small dimensions and the easy tunability. Future research on NPs are required to assess their safety and find and optimize new and more effective NPs helpful for biological application.

# 2. MATERIALS AND METHODS

## *2.1 Materials and Methods Section relative to the I part of PhD thesis*

### *2.1.1 Preparation and characterization of SAS NPs*

Precipitated (NM-200) and pyrogenic (NM-203) SAS NPs with a surface/volume ratio respectively of 183.16 and 203.92 $m^2/g$ (Centre et al., 2013) were provided by the JRC Nanomaterials Repository (Ispra, Varese, Italy). Before the experiments, SAS NPs powders were heated at 250 °C for 4 h to obtain sterile and LPS-free preparations. NPs were dispersed in pure water (milliQ) supplemented with 0.05% bovine serum albumin (BSA, Sigma-Aldrich, Milan, Italy) to obtain stock suspensions following the NANOGENOTOX dispersion protocol (Jensen et al., 2011). Zeta potentials and particle size distribution of the NPs dispersions were measured by dynamic light scattering (DLS) using Zetasizer Nano ZSP (Malvern Instruments Ltd., Malvern, UK) and revealed a hydrodynamic diameter of 284 nm in aqueous media and a zeta potential of -43 mV.

Prior to use, both formulations of SAS NPs were sonicated for 16 min at room temperature (RT) using a water bath sonicator (Transsonic 460, ElmaTM) and subsequently vortexed for 2 min to reduce agglomeration of the SAS NPs.

### *2.1.2 Human cell lines*

In collaboration with Prof. Bussolati (Department of Medicine and Surgery, University of Parma), several human cell lines were used in the present work. The human acute monocytic leukemia (THP-1) cell line was originally provided by the Cell Bank of the 'Istituto Zooprofilattico Sperimentale della Lombardia ed Emilia-Romagna' (Brescia, Italy). THP-1 cells were cultured in high-glucose (4.5 g/L) Dulbecco's Modified Eagle's Medium (DMEM; Euroclone, Milan, Italy) and supplemented with 2 mM glutamine (Sigma-Aldrich), antibiotics (100 U/mL penicillin and 100 µg/mL streptomycin) and 10% FBS (Fetal Bovine Serum, Gibco, Thermo Fisher, Milan, Italy). Monocyte differentiation to macrophage was induced by the treatment with phorbol 12-myristate 13-acetate (PMA, 100 nM) for 72 h (Bianchi et al., 2020). After differentiation, THP-1 cells were gently washed three times with FBS-free culture medium, prior to exposure to SAS NPs for 48 h.

Calu-3 lung cancer cell line was cultured in Eagle's Minimal Essential Medium (EMEM) supplemented with 2 mM L-glutamine, 10% fetal bovine serum and 1% penicillin/streptomycin.

A549 adenocarcinomic human alveolar basal epithelial cells were cultured in Ham's F-12 supplemented with 1 mM L-glutamine, 10% FBS, 1% penicillin/streptomycin.

Caco-2 human colorectal adenocarcinoma cell line was cultured in RPMI medium, supplemented with 1% L-glutamine, 20% FBS, and 1% penicillin/streptomycin (100 U/100 μg/mL).
Human cell lines were maintained in a humidified atmosphere of 5% $CO_2$ in air at 37 °C.

### *2.1.3 Viability Assay*

For the viability assay, human cell lines cultured in their respective complete growth media were seeded in 96-well plates After 24 h, growth media were replaced with fresh media supplemented with increasing doses (2.5-80 μg/cm$^2$) of NM-200 or NM-203 (Bianchi et al., 2015; Farcal et al., 2015; Di Cristo et al., 2016). After 48 h of SAS NP treatment, cell viability was assessed with the resazurin assay kit (O'Brien et al., 2000). Resazurin is a non-fluorescent, cell-permeable indicator dye that can be reduced by viable cells to highly fluorescent resorufin. Cell viability was tested replacing the cellular media with fresh ones containing in addition a solution of resazurin (44 μM, Sigma-Aldrich). After 3h, fluorescence was measured (λex = 515 nm; λem = 586 nm) with the multimode plate reader Perkin Elmer Enspire (Waltham, MA, USA). The possible interference of SAS NPs with viability test was assessed pre-incubating the resazurin dye with the highest dose of SAS NPs used (80 μg/cm$^2$) (Bianchi et al., 2015).

### *2.1.4 Cell extracts*

Differentiated THP-1 cells grown in 24 well plates were gently washed with ice cold PBS. Using a cell scraper, THP-1 cells were detached from the plates, transferred into a 1.5 ml microtube, frozen in liquid nitrogen and stored at -80 °C. Human cells were then thawed in ice and resuspended in a cold extraction buffer (20 mM Tris-HCl, pH 7.5, 150 mM NaCl, 1 mM EDTA, 1 mM EGTA, 1% Triton, 2.5 mM sodium pyrophosphate, 1 mM β-glycerophosphate, 1 mM $Na_3VO_4$, 1 mM NaF, 2 mM imidazole), supplemented with a protease inhibitor cocktail (Complete, Mini, EDTA-free, Roche, Monza, Italy). Cellular lysis was performed by two rounds of sonication (15 sec pulse) followed by 5 min incubation on ice to minimize the sample heating using Sonicator Ultrasonic Processor XL (Misonix, New Highway Farmingdale, NY, USA). Cells lysates were transferred into fresh tubes and insoluble fraction of lysates was removed by centrifugation (for 30 min at 14000 rpm, 4 °C). Supernatant (soluble fraction of lysates) was collected, and the protein concentration was determined using Bradford assay (Bio-Rad, Hercules, CA, USA).

### *2.1.5 In vitro NP-binding assay*

Prior to the NP-binding assay, cellular extracts (soluble fraction) were previously centrifuged (for 15 min at 14000 rpm, 4 °C) to remove all proteins able to precipitate in absence of NPs.

Cell extracts (7 g/L, final concentration) obtained from THP-1 cells were incubated at 4°C for 24 h with gentle agitation in the binding buffer (200 mM Tris-HCl pH 8.0, 150 mM ammonium sulfate, 10% glycerol) with the addition of NM-200 or NM-203 (0.5 g/L, final concentration), as previously described (Ruotolo et al., 2018). After incubation, 'corona' proteins adsorbed on the NP-surface were recovered by centrifugation (at 14000 rpm g for 5 min, 4 °C); unbound proteins (flow-through fraction) were collected in a fresh tube and loosely bound proteins (forming the 'soft corona') were removed by washing the protein-NP pellets five times with phosphate-buffered saline (PBS, pH 7.4). After each wash, protein-NP pellets were gently vortexed, centrifuged (at 14,000 rpm for 5 min, 4 °C) and supernatants collected in fresh tubes. Furthermore, the presence of proteins in these supernatant fractions were evaluated using Bradford assay (BioRad). After washing, hard corona proteins were removed from SAS NPs by incubation in agitation for 60 min at RT in hot solubilization buffer (60 mM Tris-HCl pH 6.8, 2% SDS, 10% glycerol), followed by denaturation at 100 °C for five minutes. Aliquots of each wash and hard corona proteins were dissolved in SDS-sample buffer (62.5 mM Tris-HCl pH 6.8, 2.5% SDS, 0.02% Bromophenol Blue, 2% β-mercaptoethanol, 10% glycerol), denatured at 95°C for 5 min and analyzed in 11% SDS-polyacrylamide gel electrophoresis (SDS-PAGE).

### *2.1.6 Hard corona protein identification by liquid chromatography analysis coupled with mass spectrometry*

For the characterization of hPC of SAS NPs, samples of hard corona proteins were incubated with 6 M urea and 25 mM ammonium bicarbonate at RT for 1h to completely denature proteins and reduce cysteine residues. Reduced cysteine residues were alkylated by adding iodoacetamide (32 mM) for 1 hour at RT in the dark, and disulfide bonds were reduced by adding dithiothreitol (35 mM, final concentration). Afterwards, the urea concentration was lowered to 0.6 M by adding 25 mM ammonium bicarbonate, trypsin (Sigma-Aldrich) was added (in a 1:30 ratio, w/w) and protein samples were incubated overnight (O/N) at 37°C. The samples were then acidified with formic acid (0.5%, final concentration) to stop the trypsin digestion, incubated with gentle agitation at 37°C for 15 min and lyophilized for 3h (Speedvac, Savant). Lyophilized samples were resuspended in 0.1% formic acid and analyzed with a liquid chromatography-mass spectrometry (LC-MS/MS) using a

Dionex Ultimate 3000 micro HPLC device coupled to an LTQ-Orbitrap XL mass spectrometer (Thermo Fisher Scientific) according to (Ruotolo et al., 2018). UniProt database (www.uniprot.org/) and ProtParam tool (web.expasy.org/protparam/) were employed for the analysis of the detected proteins.

### *2.1.7 Binding assay between SAS NPs and BSA*

To evaluate if the protein adsorption on the SAS NP surface was increased by hydrophobic interactions, different samples of BSA (7 g/L, final concentration) were prepared and subjected to various denaturation steps varying the temperature (from 75°C to 95°C) and the incubation time (1, 2 or 10 min) (Borzova et al., 2016). After the heating steps, BSA samples were placed on ice for 5 min. NM-200 or NM-203 (0.5 g/L, final concentration) were then added to different BSA samples and incubated at 4°C for 24 h with gentle agitation in the same conditions of the *in vitro* NP-binding assay. Samples were centrifuged (for 30 min at 14000 rpm, 4 °C), the supernatant were discarded, and the BSA-NP pellets were resuspended in PBS, prior to protein concentration determination using Pierce™ BCA Protein Assay Kit (Thermo Fisher Scientific).

### *2.1.8 Western blot analysis*

Aliquots of cell extracts (25 μg, total concentration of proteins) obtained as previously described from different samples of THP-1 cells treated or not with SAS NPs (5-20 μg/cm2) were separated on a 10% SDS-polyacrylamide gel and then blotted on PVDF membranes (Immobilon-P, Millipore Merck Corporation, MA, USA). After 1h of incubation in the presence of 10% of blocking solution (Western Blocking Reagent, Roche) in Tris-buffered saline (TBS; 20 mM Tris-HCl pH 7.5, 0.8% NaCl), membranes were incubated O/N at 4°C with anti-hnRNP K (Cell Signaling Technology, Danvers, MA, USA; 1:1000 dilution) or anti-tubulin (Merck, Sigma-Aldrich; 1:4000 dilution) antibody in TTBS (TBS supplemented with 0.1% Tween 20). Following washing with TTBS, membranes were incubated for 1 h at RT with IRDye-labeled goat anti-rabbit (for anti-hnRNP K; 1:10000 dilution in blocking solution) or goat anti-mouse (for anti-tubulin; 1:10000 dilution in blocking solution) antibody for 1h at RT. Membranes were then washed with TTBS, dried and visualized with a Chemidoc MP Imaging System (Bio-Rad). Bands density of the target protein hnRNP K were analyzed with the iBrigth™ Analysis software (Thermo Fisher) and normalized with that of the loading control tubulin.

### *2.1.9 Immunocytochemistry and confocal microscopy*

After 48h of exposure to NM-200 and NM-203, THP-1 cells were rinsed in ice-cold PBS and fixed in 3.7% paraformaldehyde (PFA) in PBS for 15 min at RT. The monolayers were than blocked for 1h in PBS with 2% BSA (w/v) and 2% (v/v) of normal goat serum (Merck, Sigma-Aldrich, Milan IT), and then incubated O/N with anti-human hnRNP K primary antibody (1:100 dilution) in PBS-2% BSA. After three washes in PBS, cells were then incubated for 1h with Alexa Fluor 488-conjugated goat anti-rabbit IgG (H+L) cross-adsorbed secondary antibody (Invitrogen, Milan, IT; 1:400 dilution) in PBS supplemented with 2% BSA. Cell nuclei and actin cytoskeleton were stained, respectively, with propidium iodide (1 µg/mL) and Alexa Fluor 633-conjugated phalloidin (3U/mL; Invitrogen). Slides were then mounted with a coverslip, using a glycerol-based anti-fade mounting medium (Millipore Merck), and observed with an inverted LSM510 Meta confocal system (Carl Zeiss, Germany). Single-section confocal images were taken with excitation at 543 nm and emission recorded through a 580- to 630-nm band pass barrier filter to visualize cell nuclei; excitation at 488 nm and emission through a 515- to 540-nm band pass filter for hnRNP K detection; excitation at 633 nm and emission recorded through a 650-nm long pass filter for actin cytoskeleton detection.

### *2.1.10 Phagocytosis assay*

THP-1 cells were exposed for 48h to 5, 10 or 20 µg/cm$^2$ of NM-200 or NM-203. In the last 24h of incubation, 10 x 10$^3$ fluorescent latex beads/cm$^2$ (Latex beads, carboxylate-modified polystyrene, fluorescent yellow-green; Merck, Sigma-Aldrich) were added to the incubation medium. Thereafter, THP-1 cells were washed 3 times with pre-warmed medium, incubated for 20 min with DRAQ5 (5µM; Thermo Fisher) in FBS-free medium for nuclei staining and then observed at the confocal microscope. Differential interference contrast (DIC) method was used for cell body visualization in transmitted light, while cell nuclei (in blue) were rendered exciting with a 543 nm laser line and using for emission a LP 650 nm filter. Latex beads (in green) were visualized exciting at 488 nm and acquiring through a BP 505-530 emission filter. Four single sections of each experimental condition were acquired using a 40X Planapo (1.4 NA) oil objective. Images were analyzed and internalized beads were counted in twenty cells for condition. Phagocytic activity was expressed as number of latex beads/cell.

### *2.1.11 Statistical analysis*

Data are reported as means ± SD and analyzed using Prism 5™ (GraphPad, La Jolla, CA; USA). For each endpoint, three independent experiments have been performed with a number of replicates, specified in each legend. Differences between the groups were evaluated with either t-test or 1-way ANOVA, as specified and considered significant when $p<0.05$.

# 2. MATERIALS AND METHODS

## *2.2 Materials and Methods Section relative to the II part of PhD thesis*

### *2.2.1 Cerium oxide nanoparticle characterization*

Cerium oxide nanoparticles ($CeO_2$ NPs) (Sigma-Aldrich; <25 nm, particle size) were previously characterized in other works (Hegazy et al., 2017; Ciofani et al., 2013). Prior to their use, NPs were sonicated for 16 min using a water bath sonicator (Transsonic 460, ElmaTM) and subsequently vortexed for 2 min to reduce agglomeration of the $CeO_2$ NPs. Zeta potentials and particle size distribution of the NP solutions were measured by dynamic light scattering (DLS) using Zetasizer Nano ZSP (Malvern Instruments Ltd., Malvern, UK), and revealed a hydrodynamic diameter of 130 nm in aqueous media, indicating NP aggregation, and a zeta potential of 41 mV suggesting that $CeO_2$ NPs possess a net superficial positive charge in suspension (Ruotolo et al., 2020).

### *2.2.2 Yeast strains and growth conditions*

As wild-type reference strain (WT) strain was utilized a low-efflux mutant (W303 *pdr*Δ1*pdr*Δ3; MATα *can*1–100, *his*3–11,15, *leu*2–3,112, *trp*1-1, *ura*3-1, *ade*2-1, *pdr*1::*kan*MX, *pdr*3::*kan*MX) containing two copies of the gene coding for the green fluorescent protein (GFP) integrated into *URA3* and *TRP1* loci was used as reference. As yeast model of PD was utilized the HiTox strain (W303 *pdr*Δ1*pdr*Δ3 genetic background) containing two copies of the α-syn-GFP gene integrated into the URA3 and TRP1 loci. The expression of *GFP* and *α-syn-GFP* genes in these two strains was under the control of the galactose-inducible *GAL1* promoter. These strains were provided by the laboratory of Susan Lindquist (Outeiro and Lindquist, 2003; Gitler et al., 2008; Su et al., 2010). WT and HiTox strains were grown at 28 °C in synthetic defined minimal medium (SD) containing 0.67% (w/v) of yeast nitrogen base deprived of amino acids and with the addition of: adenine (20 μg/mL), histidine (20 μg /mL), leucine (30 μg/mL). As carbon source were utilized 2% (w/v) glucose (for SD 'repressing' condition) or galactose (for SGal 'inducing' condition). For mitochondrial morphology visualization, the two strains were transformed with a pYX142 plasmid (*LEU* selectable marker) expressing a mitochondrial-localized red fluorescent protein (mtRFP) supplied by the laboratory of Dr. Winderickx (KU Leuven, Leuven, Belgium).

### *2.2.3 Viability assays*

For serial dilution assays (spot assays), yeast cells were pre-grown for 24 h at 28 °C in SD medium and collected by centrifugation, washed two times with sterile milliQ water, and corrected to an

$OD_{600}$ (optical density at 600 nm) value of 1.0. Yeast cells were serially diluted in ten-fold increments previous to spotting (4 µL aliquots for each dilution) in selective agar plates containing respectively SD or SGal media. After the incubation at 28 °C for 48 h, yeast growth was evaluated by a visual examination and images were acquired. For the clonogenic assays (Ruotolo et al., 2018), yeast pre-cultures in SD medium were collected, washed and diluted to an $OD_{600}$ value of 0.05 in SGal medium. Cultures were then aliquoted to 96-well plates with different concentrations of NPs (10–100 ng/µL) and incubated for 48 h at 28 °C without agitation, with parallel untreated controls (without NPs). Cultures were then diluted 500-fold with sterile milliQ water, and each dilution was seeded in SD agar plates incubated for 72 h in order to allow colonies formation. After the incubation step, colony-forming units (CFU) were recorded.

### *2.2.4 Cell wall degradation assay*

To test the interaction between NPs and plasma membranes, yeast cells pre- grown in SD medium were collected, washed and diluted to an $OD_{600}$ value of 0.2 in SGal medium. Cells were grown in SGal medium for 1.5 h at 28 °C and then treated for 30 min at 28 °C with lyticase (500 U/$OD_{600}$ unit of cells; Merck, Sigma-Aldrich) to degrade cell walls. Spheroplasts obtained after the lyticase treatment were centrifuged, resuspended in SGal medium and incubated at 28 °C for 4 h with or without $CeO_2$ NPs (50 ng/µL). Treated and untreated spheroplast were then analyzed by optical microscopy.

### *2.2.5 Fluorescence microscopy analysis*

For the fluorescence microscopy analysis of yeast samples and images acquisition was utilized a Zeiss Axio Imager.Z2 fluorescence microscope (Carl Zeiss Microscopy GmbH, Jena, Germany). All images were acquired with the same settings to guarantee the reproducibility among all the experiments. For the visualization of the α-syn-GFP localization, cells were cultivated following the same conditions utilized in the clonogenic assays. During the image analysis, cells were scored evaluating at least 150 cells from three independent experiments and the fraction of 'positive' cells was estimated in relationship to the total cells present in the considered fields.

For cell wall staining, yeast cells were collected, washed and then stained for 30 min at 28 °C in the dark with 25 µM calcofluor white M2R (excitation/emission at 365 nm and 435 nm; Thermo Fisher Scientific,Waltham, MA, United States).

For the mitochondrial morphology analysis, mtRFP-transformed yeast cells were pre-grown for 24 h at 28 °C in SD medium and collected by centrifugation, washed two times with sterile milliQ water, and incubated in SGal medium in agitation for 24 h at 28 °C with or without of $CeO_2$ NPs (50 ng/µL). After the treatment, yeast cells were analyzed using fluorescence microscopy (TRITC filter).

For the detection of oxidative stress, yeast cells were incubated in agitation in SGal medium for 4 h at 28 °C in presence or not of $CeO_2$ NPs (50 ng/µL). Staining with CellROX® Orange Reagent (5 µM, final concentration; Thermo Fisher Scientific) allowed the detection of different types of ROS species; in particular, this cellular permeable dye is non-fluorescent in a reduced state, while displays a bright orange fluorescence (with excitation/emission at 545/565 nm) upon oxidation mediated by ROS species. After the exposure to NPs, cells were then stained for 30 min at 37 °C with CellROX® (5 µM, final concentration) according to manufacturer's instructions and then visualized by fluorescence microscopy.

### *2.2.6 Flow cytometry analysis*

For the flow cytometry (FC) analysis was utilized a NovoCyte® flow cytometer (ACEA Biosciences Inc., San Diego, CA, USA) and the recorded data were elaborated using the Novocyte® Express software. For each analysis, at least 20000 cells (events) were collected in each specimen and analysis was conducted on viable α-syn-expressing cells (FITC-positive). For the side scatter (SSC) measurement, yeast cells were incubated at 28 °C in SGal medium for 24 h or 48 h with or without $CeO_2$ NPs (50 ng/µL) or SAS NPs (100 ng/µL) prior to FC analysis. To evaluate the mitochondrial activity using FC analysis, we used MitoTracker Deep Red (MTDR; Thermo Fisher Scientific), a far red-fluorescent dye (with excitation/emission at 644/665 nm) that is able to stain active and unharmed mitochondria in living cells (Xiao et al., 2016). For MTDR staining, yeast cells were cultivated in SGal medium for 4 h at 28 °C in the presence (or not) of $CeO_2$ NPs (50 ng/µL). After the treatment cells were harvested and resuspended in milliQ water and thus stained for 30 min at 28 °C with MTDR (0.5 nM) according to the manufacturer's instructions (Thermo Fisher Scientific) (Ruotolo et al., 2020). To determine cellular autofluorescence, unstained sample controls were utilized.

### *2.2.7 Identification of the yeast proteins adsorbed on the surface of $CeO_2$ NPs (hPC assay)*

WT (not expressing α-syn) and HiTox strains were grown in inducing conditions for 24 h. Yeast cells were harvested by centrifugation, resuspended in ice-cold lysis buffer (25 mM Tris-HCl pH 7.5, 50

mM KCl, 1 mM $MgCl_2$, 1 mM EDTA, 1% Triton X-100, 10% glycerol, supplemented with protease inhibitors) and an equal volume of glass beads (0.5 mm diameter) was added to the sample tubes for the mechanical lysis process performed by five rounds of strong vortexing (1 min stroke followed by 5 min incubation on ice to avoid samples overheating) using a Mini-Beadbeater-16 (BioSpec Products Inc., Bartlesville, OK, USA). Cell lysates were centrifuged (at 14000 rpm for 30 min, 4 °C) and supernatants (soluble fractions) were transferred to new microcentrifuge tubes; protein concentration of these samples was determined by Bradford assay (Bio-Rad). Aliquots of each sample were dissolved in SDS-sample buffer (62.5 mM Tris-HCl pH 6.8, 2.5 % SDS, 0.02 % Bromophenol Blue, 2% β-mercaptoethanol, 10% glycerol), denatured at 95°C for 5 min and analyzed in 11% SDS-PAGE to verify the cell extract quality.

For the *in vitro* NP-binding assay, WT or HiTox cell extracts (7 g/L protein, final concentration) were incubated in the presence of $CeO_2$ NPs (0.5 g/L, final concentration) in PBS at 4 °C for 16 h with gentle agitation. $CeO_2$ NPs, along with their adsorbed yeast proteins, were recovered by ultracentrifugation (at 40000 rpm for 20 min, 4 °C), and unbound proteins were removed by rinsing the protein-NP pellets five times in PBS. After each rinse, the pellets were gently vortexed, re-centrifuged (at 40000 rpm for 20 min, 4 °C) and supernatants were discarded. Adsorbed 'corona' proteins were eluted from the NP surface after 1 h incubation at RT in PBS and denatured at 100 °C for 5 min. Aliquots of these hPC samples were utilized for: 1) the immunological detection of α-syn protein in hPC of $CeO_2$ NPs using dot blot assay; 2) the identification of yeast 'corona' proteins using LC-MS/MS analysis using the same procedure previously described (see 2.1.6 paragraph, "Materials and Methods" Section).

### *2.2.8 Protein extracts for immunological assays*

For the preparation of whole cell extracts (WCE), yeast cultures (HiTox strain) were incubated in SGal medium ($OD_{600}$ value of 0.3) for 6 h or 24 h at 28 °C with or without $CeO_2$ NP treatment (25 ng/µL, 35 ng/µL or 50 ng/µL), as indicated in the "Results and Discussion" Section.

After the treatment, yeast cells were harvested by centrifugation and resuspended in ice-cold lysis buffer (25 mM Tris-HCl pH 7.5, 50 mM KCl, 1 mM $MgCl_2$, 1 mM EDTA, 1% Triton X-100, 10% glycerol, and protease inhibitors); an equal volume of acid-washed glass beads (0.5 mm diameter) was added to the test tubes for the mechanical lysis process performed by five rounds of strong vortexing (1 min stroke followed by 5 min incubation on ice to avoid samples overheating) with a Mini-Beadbeater-16 (BioSpec Products Inc., Bartlesville, OK, USA). A brief centrifugation (at 1,000 rpm

for 10 sec, 4 °C) was made to eliminate the foam formed during the lysis process, samples were resuspended by pipetting and transferred to new microcentrifuge tubes. The WCEs were utilized for the detection of α-syn oligomers or Kar2 protein performed by dot blot analyses.

As indicated in the "Results and Discussion" Section, WCEs were also further processed through a fractionation step. WCE samples were centrifuged (at 14,000 rpm for 15 min, 4 °C) and the supernatant (soluble portion) was transferred to a new microcentrifuge tube. Pellets were resuspended in a solubilization buffer (50 mM Tris-HCl, 5 mM $MgCl_2$, 50 mM NaCl, 143 mM β-mercaptoethanol, 2% SDS, 1% Triton X-100, 2.5 mM EDTA and protease inhibitors), centrifuged at 14,000 rpm for 10 min (4 °C) and the supernatant (insoluble fraction of lysate) was transferred to a new microcentrifuge tube.

### *2.2.9 Dot Blot analysis*

Different protein samples (WCEs, samples and soluble and insoluble fractions of protein extracts; see previously Section) were analysed with dot blot. BSA (500 ng, 1 μg) was added as negative control for the immunoassays.

Dot blot analysis was performed using a Bio-Dot® microfiltration apparatus (Bio-Rad) with a 96-well plate format for vacuum-transfer of the protein samples (100 μL, final volume) on nitrocellulose membranes (0.2 μm pore-size; Bio-Rad) prewetted with TBS. Sample-loaded membranes were then blocked by incubation for 2 h at RT in TTBS containing 5% (w/v) BSA as blocking agent. After the blocking step, membranes were incubated O/N at 4°C with the primary antibody required: anti-α-synuclein (Santa Cruz Biotechnology Inc., Dallas, TX, USA; 1:200 dilution), anti-α-synuclein oligomers (MJFR-14-6-4-2, Conformation-Specific; Abcam, Cambridge, MA, USA; 1:20000 dilution), anti-Kar2 (Invitrogen, Carlsbad, CA, USA; 1:2000 dilution) or anti-Pgk1 antibody (Abcam; 1:2000 dilution). Following washing with TTBS, membranes were incubated for 1 h at RT with IRDye-labeled goat anti-rabbit (for anti-α-syn and anti-α-syn-oligomers) or goat anti-mouse (for anti-Kar2 and anti-Pgk1) secondary antibodies (LI-COR Biosciences; 1:10000 dilution). Membranes were then washed with TTBS, dried and visualized with a Chemidoc MP Imaging System (Bio-Rad).

### *2.2.10 Statistical analysis*

Statistical analysis was performed using GraphPad Prism v6.0. For each experiment, three biological replicates and at least three technical replicates were performed. Statistical analysis was performed using one-way ANOVA, followed by Dunnett's multiple comparisons test (*, $p < 0.05$; **, $p < 0.01$; ***, $p < 0.001$; ****, $p < 0.0001$).

# 3. RESULTS AND DISCUSSION

## PART I: POTENTIAL HEALTH RISKS OF SAS NPs

### *3.1 Viability assay*

To evaluated the potential toxicity of both formulations of SAS NPs used as food additives (NM-200 and NM-203), we have tested several human cell lines representing main known routes of internalization of NPs from different sources of exposition. In particular, we have utilized four different cell lines representing the immune cell system (THP-1 cell line), the respiratory tract (Calu-3 and A549 cell lines) and the intestinal mucosa (Caco-2 cell line). This approach is in line with the application of an intelligent testing strategy (ITS), useful for the detection of the potential toxicity of NPs (Farcal et al., 2015). SAS NPs were tested in a range of concentrations between 0 to 80 μg/cm$^2$ and the cell viability was evaluated after 48 h of exposition using the resazurin assay kit (see "Materials and Methods" Section).

As shown in **Figure 40**, different responses were observed in human cell lines exposed to SAS NPs. Human bronchial epithelial cells (Calu-3) were the most resistant to the treatment with both SAS NPs, while the NP exposure decreased the viability of human alveolar cell line (A549) by 40% compared to untreated cells. Caco-2 cells, a cellular model for the intestinal epithelial barrier, showed very low sensitivity to SAS NP treatment. Human monocytic cell line THP-1 were differentiated into adherent macrophage-like cells and exhibited greater toxicity when exposed to both formulations of SAS NPs (**Fig. 40**). $IC_{50}$ values, that represent the concentration at which a substance exerts half of its maximal inhibitory effect, were 9.5 μg/cm$^2$ for NM-200 and 5.4 μg/cm$^2$ for NM-203, respectively, highlighting a greater toxicity for the pyrogenic form of SAS NPs in THP-1 cells (**Fig. 40**).

These results are in line with those of Farcal et al. (2015) and Di Cristo et al. (2016) in which NM-203 showed greater toxicity than NM-200 in murine macrophagic cell lines (MH-S and RAW264.7 cells, respectively). THP-1 cells are widely used in many toxicological studies (Chanput et al., 2014; Ozleyen et al., 2021; Brzicova et al., 2019) and will be used in the present work for the further characterization of molecular determinants of SAS NP toxicity.

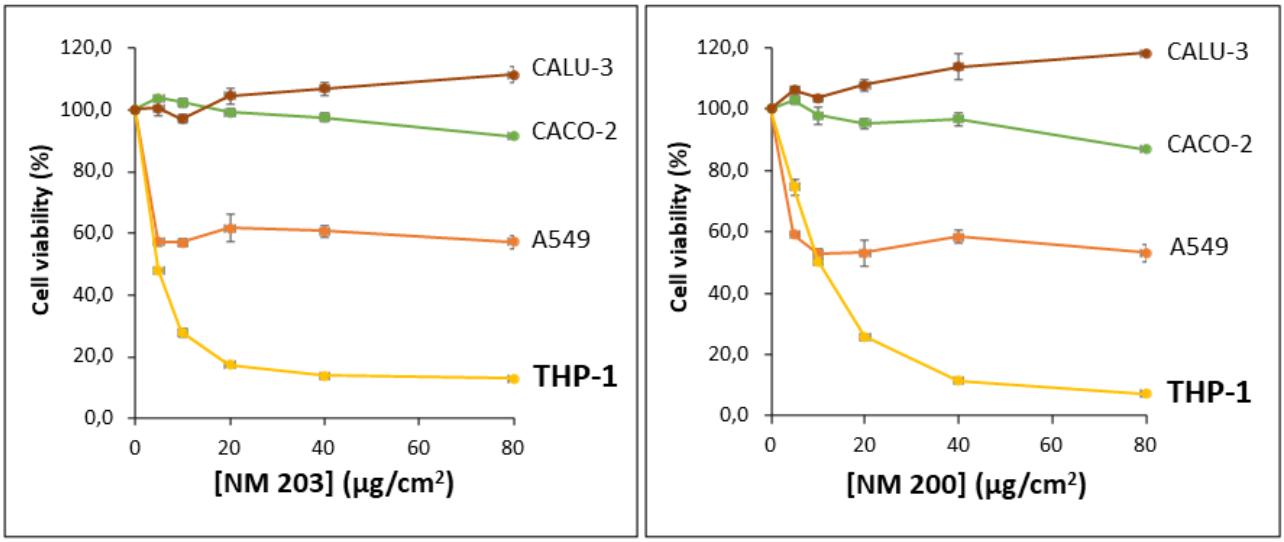


***Figure 40***. Viability assays in different cell lines exposed to NM-203 (*left*) or NM-200 (*right*) for 48 h. Cell viability of SAS NP-treated cells was reported as percentage (%) calculated respect to untreated cells (100%).

### *3.2 Characterization of hPC of SAS NPs in THP-1 cellular extracts*

To understand the molecular basis of the increased toxicity of NM-200 and NM-203 in THP-1 cells, we have isolated and characterized the entire set of proteins, which are adsorbed with high affinity to the SAS NP surface. These proteins form the so-called "hard corona" (hPC), the composition of which defines the biological identity of NPs. The characterization of the hPC is fundamental to better define the molecular determinants that potentially contributes to the toxicological impact of SAS NPs (Liu et al., 2021a). In most cases, the proteins which absorb on the surface of NPs and contribute to the hPC composition undergo a conformational change (misfolding) or an inhibition of their activity mediated by NP binding (Zoungrana et al., 1997; Klein et al., 2016; Ruotolo et al., 2018).

hPC is characterized by an extremely low exchange rate of the proteins over time and by an almost irreversible binding on the NPs surface, and acts as a unique 'fingerprint' that interacts with biological systems in a different way from that of 'naked' NPs (Milani et al., 2012; Ahsan et al., 2018). The limits of these investigations are due to the difficulties to track and recover the NPs *in vivo* without modifying their physico-chemical characteristics (e.g., with the addition of tags to facilitate their purification or fluorescent groups to determine their cellular localization), that could modify the molecular interactions *in vivo*. In our work to address this problem, we have decided to develop an *in vitro* NP-binding assay using THP-1 cellular extracts without altering the physico-chemical characteristics of the NPs, but exploiting the ability of the NPs to aggregate in solution and to be

easily recovered by centrifugation, together with the proteins adsorbed on their surface (Liu et al., 2021a; Ruotolo et al., 2018; Klein et al., 2016).

Protein extracts obtained by THP-1 cells (after their differentiation in macrophage-like cells) were incubated for 24 h with gentle agitation at 4 °C in the presence of NM-200 or NM-203. Hard 'corona' proteins adsorbed to SAS NPs were recovered by centrifugation and multiple centrifugation steps and extensive washes were used to release almost all non-bound and soft corona proteins (see "Materials and Methods" for details; **Fig. 41a**). Hard 'corona' proteins were then detached from the NP surface using a solubilization protocol followed by denaturation (see "Materials and Methods" for details), a necessary step because proteins are strongly bound to NPs. Protein quantification of hPC isolated from the surface of SAS NPs was conducted using Pierce™ BCA Protein Assay and showed that NM-203 adsorbs on their surface more proteins than NM-200 (two-fold increment). SDS-PAGE analysis of hPC samples shows similar protein profiles, but a different abundance of specific proteins that form the hPC of NM-200 and NM-203 (**Fig. 41b**).

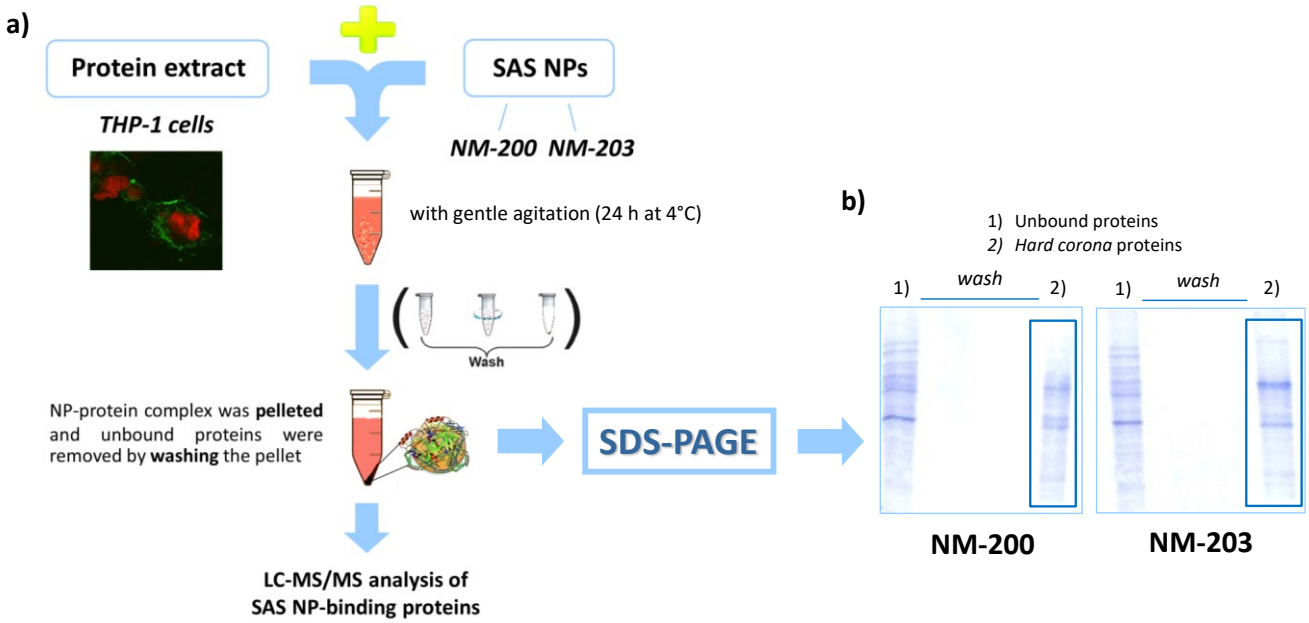


***Figure 41.*** Schematic representation of the strategy of the isolation of hPC of SAS NPs. a) After the incubation of NM-200 or NM-203 with THP-1 cellular extracts for 24 h at 4°C, hPC proteins were isolated using different washing and centrifugation steps, important for the removal of unbound proteins and soft corona proteins. The 'corona' proteins can further be subjected to in-solution tryptic digestion and subsequently identified using LC-M /MS analysis. b) 'Corona' proteins isolated by hPC can thus be visualized using SDS-PAGE. Aliquots of unbound proteins, the washing solutions and proteins forming the hPC were visualized by 11% SDS-PAGE.

Hard 'corona' proteins isolated from SAS NP surface were further identified (after tryptic digestion) using LC-MS/MS analysis (**Fig. 41a**; see "Materials and Methods" for details). Unexpectedly, mass spectrometry analysis showed that the hPC composition of both SAS NPs does not change and id composed by the presence of the same 15 proteins in both cases (**Fig. 42**). These proteins probably interact with both SAS NPs with different binding affinity, as evidenced by the greater amount of proteins bound by NM-203 and by the different relative abundances of individual proteins in the hPCs of SAS NPs showed by the SDS-PAGE analysis (**Fig. 41b**).

| Protein | UniProt ID | p.I. | I.I. | Protein function | Biological process |
|---|---|---|---|---|---|
| **SRSF3** | P84103 | 11.6 | 113.3 | *splicing factor arginine/serine-rich 3* | *RNA metabolism* |
| **SRSF6** | Q13247 | 11.4 | 103.8 | *Serine/arginine-rich splicing factor 6 (SRSF6)* | *RNA metabolism* |
| **ALYREF** | Q86V81 | 11.2 | 43.0 | *Aly/REF export factor* | *RNA metabolism* |
| **RBMX** | P38159 | 10.1 | 63.9 | *Heterogeneous nuclear ribonucleoprotein G* | *RNA metabolism* |
| **SNRPE** | P62304 | 9.5 | 52.3 | *Small nuclear ribonucleoprotein E* | *RNA metabolism* |
| **SFPQ** | P23246 | 9.5 | 66.2 | *Splicing factor, proline- and glutamine-rich* | *RNA metabolism* |
| **NONO** | Q15233 | 9.0 | 65.8 | *Non-POU domain-containing octamer-binding protein* | *RNA metabolism* |
| **KHSRP** | M0R0I5 | 6.8 | 55.3 | *KH-type splicing regulatory protein (KHRSP)* | *RNA metabolism* |
| **HNRNP U** | Q00839 | 5.8 | 45.8 | *Heterogeneous nuclear ribonucleoprotein U (hnRNP U)* | *RNA metabolism* |
| **HNRNP K** | P61978 | 5.4 | 59.8 | *Heterogeneous nuclear ribonucleoprotein K (hnRNP K)* | *RNA metabolism* |
| **RPL23A** | P62750 | 10.4 | 53.3 | *60S ribosomal protein L23a* | *Translation* |
| **EEF1A1** | P68104 | 9.1 | 27.1 | *Elongation factor 1-alpha 1* | *Translation* |
| **HSPD1** | P10809 | 5.2 | 28.4 | *heat shock 60kDa protein 1 (chaperonin), mitochondrial protein* | *Translation* |
| **MYH9** | Q92945 | 5.5 | 51.2 | *myosin heavy chain 9* | *Cytoskeleton organization* |
| **ACTB** | P60709 | 5.3 | 35.3 | *Actin* | *Cytoskeleton organization* |

| |
|---|
| p.I. (Isoelectric point) > 7 |
| I.I (Instability index) > 40 |

| |
|---|
| p.I. (mean value) = 8.38 |
| I.I. (mean value) = 57.63 |

***Figure 42.*** Proteins identified in the hPCs of NM-200 and NM-203 through the LC-MS/MS analysis. The hPC composition of SAS NPs was qualitatively the same; most of the proteins identified are positively charged (p.I. mean > 7) and have high values of instability index (I.I.; mean value > 40).

These 'corona' proteins belong to three functional classes (**Fig. 42**): RNA metabolism, translation and cytoskeleton organization.

Among the proteins identified, most are proteins involved in RNA metabolism. Between these, ALYREF (THO complex subunit 4) is a component of THO complex, a key factor involved in nuclear export of spliced and unspliced mRNA (Masuda et al., 2005; Peña et al., 2012).

SRSF3 and SRSF6 (Serine/arginine-rich splicing factor 3-6) are part of the serine/arginine (SR)-rich protein family. SR proteins are involved in the recruitment of the splicing machinery (Black, 2003; Graveley, 2000).

HnRNP K (heterogeneous nuclear ribonucleoprotein K) represents one of the major pre-mRNA binding proteins, and plays an important role in p53/TP53 response to DNA damage. This protein could also be involved in the autophagy processes and was recently found, with a still not well defined role, as important component in podosomes, actin-rich structures important for the functionality of macrophagic cell lines (Cervero et al., 2012; Bomsztyk et al., 2004; Heinrich et al., 2009; Li et al., 2018). RBMX (RNA-binding motif protein, X chromosome), also known as hnRNP G, is a RNA-binding protein with several roles in pre- and post-transcriptional processes regulation and in splicing site selection (Heinrich et al., 2009; Kanhoush et al., 2010).

HnRNP U (heterogeneous nuclear ribonucleoprotein U) is a DNA- and RNA- binding protein important in RNA splicing and in the transcription process; it's known that HNRP U binds also the actin in the transcription cooperation processes (Xiao et al., 2012; Kukalev et al., 2005).

SNRPE (small nuclear ribonucleoprotein E) have a role in pre-mRNA splicing acting as core component of the SMN complex, which mediates the formation of the spliceosome (Grimm et al., 2013).

KHSPRP (KH type-splicing regulatory protein) is also a component of the splicing machinery and is involved in degradation of unstable mRNAs; KHSPRP can bind single stranded DNA and activate gene expression (Min et al., 1997; Davis-Smyth et al., 1996).

SFPQ (Splicing factor, proline- and glutamine-rich) is a RNA- and DNA-binding protein involved in a multitude of nuclear processes, it is also involved in spliceosome formation and functioning (Cosker et al., 2016; Knott et al., 2016).

NONO (non-POU domain-containing octamer-binding protein) is a DNA- and RNA-binding protein involved in several nuclear processes like double-strand break response and splicing process; this protein acts often as a heterodimer with SFPQ in many processes (Li et al., 2017; Passon et al., 2012; Salton et al., 2010). The strong molecular interaction of the complex SFPQ/NONO could determine the co-absorption of both on SAS NP surface; it is possible that one of the two proteins could interact directly with the NPs and bring its molecular interactor to the surface of the NPs.

In line with Klein et al. (2016) which identifies yeast proteins forming the hPC of SAS NPs, most of the proteins identified are RNA-binding proteins (RBPs), with a high structural disorder and with a

positive charge, indicating that electrostatic interactions can stabilize the binding of these proteins with negatively charged SAS NPs (Z-potential values: -47.5 mV for NM-200 and -46.1 mV for NM-203, respectively). Electrostatic interactions are important for NP-proteins interaction together with different other non-covalent interactions involved in the protein adsorption on NPs surface (García-Álvarez and Vallet-Regí, 2021; Kopac, 2021). Since RNA is a negatively-charged macromolecule, it is possible that NPs can bind in the RNA binding pocket present in these proteins, disrupting their cellular function. Given the crucial biological roles of these proteins identified in hPC, the toxicological impact of their binding with SAS NPs could be significant.

Were also found in the hPCs of SAS NPs three proteins involved in the translation process (**Fig. 42**), including RPL23A (60S ribosomal protein L23a), a component of the 60s subunit of the ribosome (Klinge et al., 2011), and EEF1A1 (Elongation factor 1-alpha 1), an elongation factor involved in the protein synthesis (Vera et al., 2014). Translation factors have already been identified in the hPC of other NPs (Klein et al., 2016; Ruotolo et al., 2018). Klein et al. (2016) demonstrates that SAS NPs inhibit the translation process through the formation of hPC.
HSPD1 (60 kDa heat shock protein), a molecular chaperone acting also in the mitochondrial protein import (Viitanen et al., 1992; Levy-Rimler et al., 2001). Curiously, HSPD1 is the only protein of the hPCs of SAS NPs with isolectric point (p.I) and instability index (I.I.) values that deviate from those of others. It is therefore possible that HSPD1 may have been isolated in hPC due to the fact that, being a chaperone, can strongly interact with misfolded proteins present on the surface of SAS NPs. Since most of the proteins presents very high instability index values [greater than 40, typical of intrinsically disordered proteins (IDP)] it is possible to hypothesize that many of the proteins can bind to the NPs through hydrophobic interactions mediated by the misfolding of the protein, as observed for other NPs (Zoungrana et al., 1997; Klein et al., 2016; Ruotolo et al., 2018).

Other proteins identified in hPCs are MYH9 (myosin-9) and ACTB (actin), proteins involved in the cellular structure and motility (Clarke and Spudich, 1977). The alteration of structures in which these proteins are involved could strongly alter the functionality of macrophage cells.

### *3.3 The hydrophobic interactions are crucial involved in the protein binding to NM-200 and NM-203*

Hydrophobic interactions are an important element in the protein adsorption on NPs and can determine differences in the composition and abundance of adsorbed proteins (Lundqvist et al., 2008). NM-200 and NM-203 surface hydrophobicity and hydrophilicity importantly differs because of the distinct synthesis processes. For NM-203 the thermal synthesis have important physiochemical repercussions, reducing the overall silanols groups that fuses between them forming siloxane bridges. Consequently, the hydrogen bonding available groups are drastically lowered resulting in a more hydrophobic nature of NM-203 compared to NM-200, that not being exposed to high temperatures is remains rich in silanols groups and is characterized by a higher hydrophilicity (Napierska et al., 2010).

For these reasons to better understand the importance of the hydrophobic interactions for the protein adsorption on SAS NPs surface, was performed an *in vitro* SAS NP-binding assay using different preparations of BSA subjected to denaturation for different times (1 min to 10 min) and temperatures (75-95 °C) (Borzova et al., 2016; Nikolaidis and Moschakis, 2017). BSA is known for his low binding affinity for SAS NPs (Yadav et al., 2016) and the denaturation steps were made in order to gradually expose the hydrophobic core and detect how the adsorption is dependent from hydrophobic interactions. An *in vitro* SAS NP-binding assay was performed in the presence of (partially) denatured BSA in the same condition used for the hPC isolation (see “Materials and Methods” for details). BSA (thermal-treated or not) bound to NPs was recovered with centrifugation/wash procedure and the protein amount bound on NP surface was quantified using Pierce™ BCA Protein Assay Kit (**Fig. 43**).

Control reactions (made in parallel) without SAS NPs, exclude that the heat treatment destabilizes BSA protein, causing it to precipitate. We observed that the thermal treatment of BSA progressively increases its binding with both SAS NPs, in particular with NM-203 (**Fig. 43**). Of note, a mild heat treatment (for 2 min at 75 °C) increases by two times the protein amount bound to NM-203. This result is reminiscent of the fact that a two-fold increase was observed for the protein amount bound by NM-203 compared to NM-200 in the hPC; taking into account that the isolated ‘corona’ proteins are for the most part proteins with a high structural flexibility which expose their hydrophobic core more easily than proteins with a more stable conformation (Radivojac et al., 2004), it is possible that this type of interactions can stabilize their binding to the pyrogenic SAS NPs.

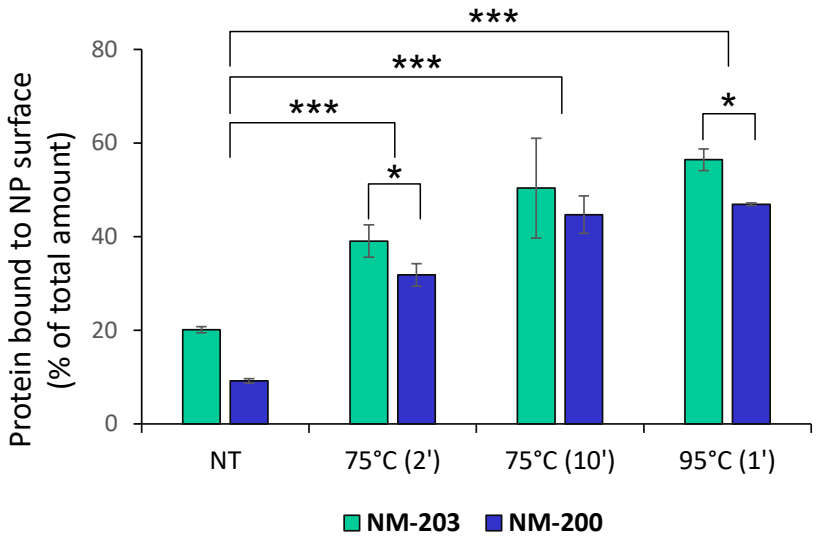


***Figure 43.*** The partial denaturation of BSA determines a higher binding predisposition on both SAS NP forms, in particular for NM-203. In this histogram is reported the amount of protein (BSA) bound to SAS NP surface respect to total amount of BSA (100%) utilized in these assays; a prolonged heat treatment [greater denaturation of BSA (Borzova et al., 2016; Nikolaidis and Moschakis, 2017)] is linked with greater quantity of this protein adsorbed on SAS NPs. Significance was determined by one-way ANOVA with Dunnett's multiple comparisons test (*, $p < 0.05$; ***, $p < 0.001$). NT, untreated sample (not subjected to heat treatment).

### *3.4 The potential role of HNRNP K protein in SAS NP toxicity*

RBPs are the main constituent of the hPC of both formulations of SAS NPs. Among these proteins, heterogeneous nuclear ribonucleoprotein K (hnRNP K) attracted our attention. hnRNP K doesn't represent only an essential protein for vertebrates and nematodes (Bomsztyk et al., 2004) but recently has been detected in the extra-nuclear space in human peripheral blood monocytes in particular as part of peculiar structures fundamental for adherence and motility of macrophages named podosomes (Cervero et al., 2012), these structures are actin rich and have roles in mechanosensing and cellular remodeling and are also important in cells migration and adhesion (Linder et al., 2000; Veillat et al., 2015; Schachtner et al., 2013). hnRNP K doesn't represent only an essential nuclear protein for vertebrates and nematodes (Bomsztyk et al., 2004) but recently has been identified as an important component of peculiar actin-rich structures fundamental for adherence and motility of macrophages named podosomes (Cervero et al., 2012; Linder et al., 2000; Veillat et al., 2015; Schachtner et al., 2013). Comparing our data with those of Cervero et al. (2012),

which study the proteomic composition of podosomes, we have observed that not only hnRNP K, but the most of the proteins we have identified in the hPCs of SAS NPs are constituents of podosomes (**Fig. 44**). hnRNP K is highly represented in podosomes and it has been demonstrated to localize in a ring structure around the actin core in osteoclast podosomes (Cervero et al., 2012; Fan et al., 2015) (**Fig. 44**; *bottom image*). Osteoclasts are direct descendant of the monocyte-macrophage lineage and in these cells hnRNP K seems to play an important role in the their differentiation processes (Fan et al., 2015). hnRNP K also possesses a KI domain (a.a. 240–337) involved in the interactions with numerous kinases and could also have roles in the regulation of cell signaling (Bomsztyk et al., 2004). We then performed an immunofluorescence experiment, tracking two podosome proteins (F-actin and hnRNP K) with fluorescent-labeled antibodies. The results, reported in **Figure 45**, show that, although mainly expressed in cell nuclei, hnRNP K is localized also in the cytoplasm of THP-1 cells. The exposure to 10 μg/cm2 for 48h of both NM-200 and NM-203, lowered the signal corresponding to hnRNP K and induced a cellular re-organization of hnRNP K, that delocalized from the extracellular space into the nucleus. Moreover, SAS NPs exposure also affected cytoskeleton integrity and cell morphology causing a ruffling of the F-actin filaments associated with cell rounding. Such effect was more evident in NM-203 treated cells, where NM-203 caused the disorganization of cortical actin bundles. This effect on actin, induced in that case by the exposition to Stober's SAS NPs, was also observed in HUVEC cells with cytoskeletal destructuration effects after the exposure to SAS NPs (Duan et al., 2014).

To evaluate if the treatment with SAS NPs alters the total amount of hnRNP K protein expressed *in vivo*, we performed a Western blot analysis using proteins extracted from THP-1 cells treated at different concentration of both formulation of SAS NPs. We have observed that exposure to NM-200 determine a dose-dependent reduction of hnRNP K levels in THP-1 cells, while the effect was already significant at the lowest dose used (5 μg/cm2) for the treatment with NM-203 (**Fig. 45**; *bottom panel*).

Therefore, THP-1 exposure to SAS NPs seems to cause an alteration of the cytoskeleton organization confirmed by immunofluorescence and Western blot experiments. Additionally, these results highlight an unexpected role of hnRNP K, whose alteration could be a important deterinat of SAS NP toxicity, also looking at his potential involvement in many cellular pathways.

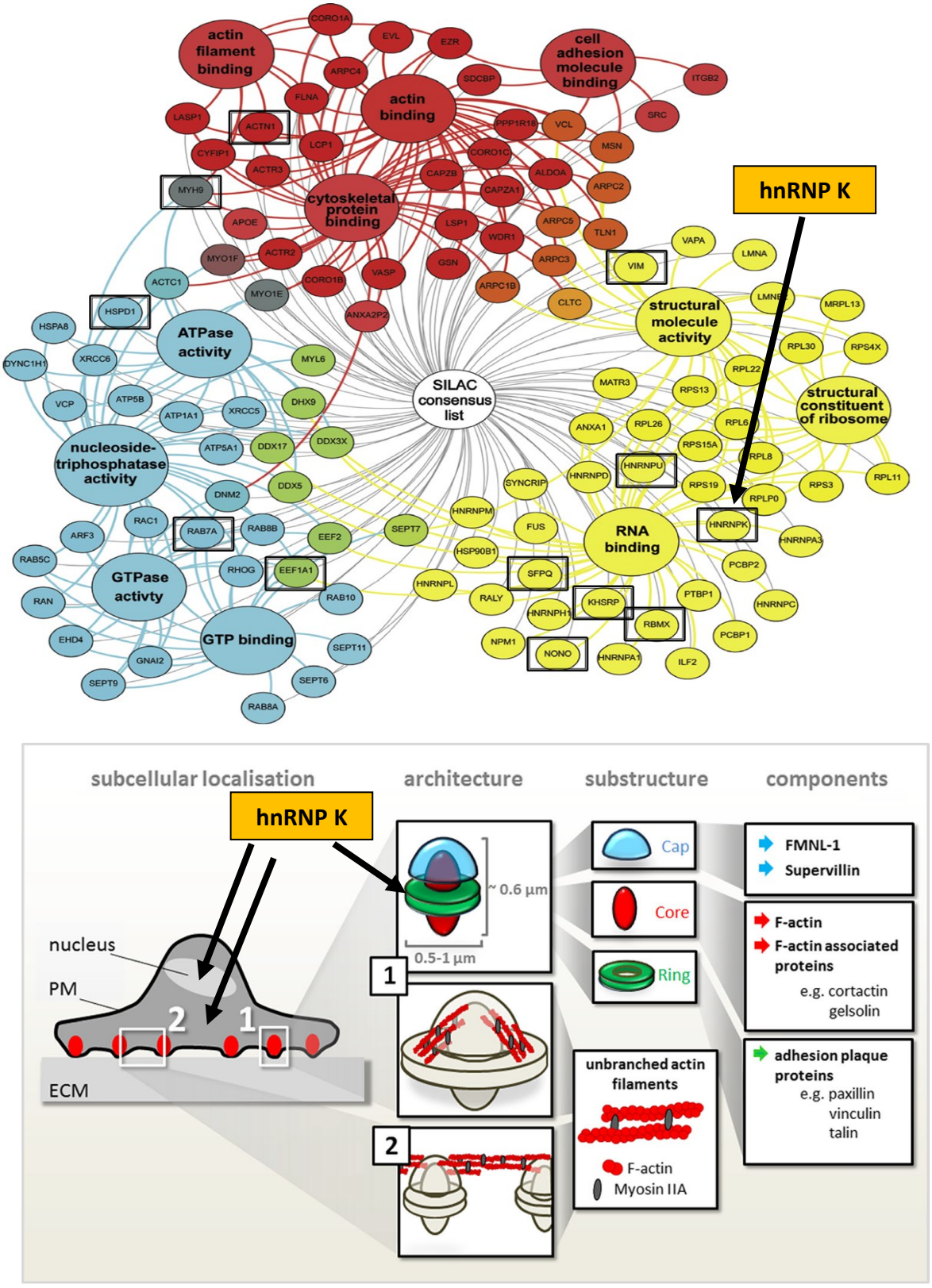


**Figure 44.** Many 'corona' proteins identified (80%) are structural components of podosomes. In the upper image [figure adapted from (Cervero et al., 2012)] is reported the interactomic organization of podosomal proteome. Proteins identified in hPCs are indicated with black boxes. In the lower

image [figure adapted from (Linder and Wiesner, 2015)], it is possible to observe the structural organization of the podosomes. These actin-rich structures are characterized by an actin core and a by a ring structure where hnRNP K localizes, in addition to its nuclear location.

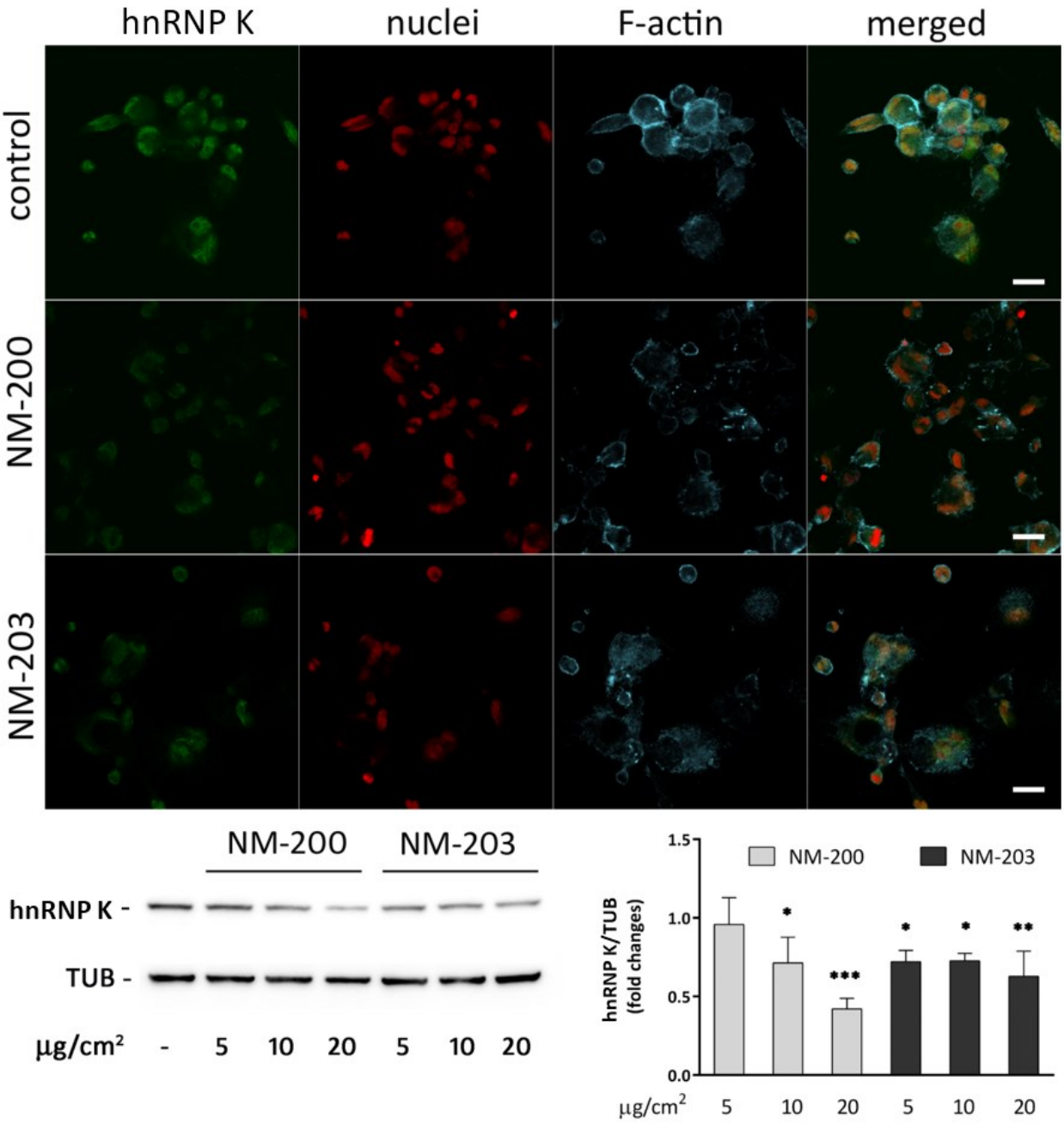


***Figure 45.*** SAS NP exposure negatively affects the cellular localization and the expression of hnRNP K and Actin in THP-1 cells. (*Upper panel*) THP-1 cells were exposed to 10µg/cm$^2$ of NM-200 or NM-203. After 48 h, cell were fixed and stained for hnNRP K (green), F-actin (blue) or for cell nuclei (red). Single confocal sections of representative fields are shown. Scale bar, 20 µm. (*Bottom panel*). Cells were exposed to increasing doses of SAS NP for 48 h and then processed for Western Blot as described in "Materials and Methods". *Left*, a representative Western Blot. *Right*, fold changes of

band densities representing the mean of tree independent experiments ± SD. Significance was determined by one-way ANOVA with Bonferroni post-hoc test (*, $p<0.05$; **, $p<0.01$; ***, $p<0.001$).

### *3.5 Effects of SAS NPs on phagocytosis*

We described how the treatment (even at low dosage for NM-203) importantly compromised cytoskeletal structures and hnRNP K abundance and distribution. For macrophages these events are crucially linked with phagocytosis. Phagocytosis is a vital process for macrophages biological role and is guided by the actin filaments that during the first steps of the phagocytosis are organized in a dense lattice below the plasma membrane forming the phagocytic cup, that guided by the actin cytoskeleton, progressively evolves his structure leading to the closing of the phagosome membrane. After the phagosome formation this process go on with the fusion of endosome and lysosome in order to form phagolysosomes (Uribe-Querol and Rosales, 2020). Podosomes are linked with phagocytosis, in fact the phagocytic cup is extremely similar to podosomes-like structures and share many structural and functional traits with podosomes, these structures were proposed to mediate the particle internalization by macrophages and involved in the closing process of the phagosome (Ostrowski et al., 2019; Allen and Aderem, 1996). For this reason we tested the phagocytic activity of fluorescent latex beads (FLB) in lipopolysaccharide (LPS) activated THP-1 cells exposed to SAS NPs. FLB phagocitation was evaluated after the treatment with 10 $\mu g/cm^2$ of NM-200 or NM-203. From **Figure 46** is clearly visible a drastic lowering of FLB internalized into the cytoplasm after the treatment with both formulations indicating that SAS NPs importantly impact on the phagocytosis in macrophages. In particular for NM-203 this process was importantly inhibited. In conclusion the evaluation and analysis of hPC protein detected on SAS NPs surface allowed to identify the hypotheticals perturbed pathway after the THP-1 exposure to SAS NPs especially from the NM-203 (pyrogenic form) a protein like hnRNP K could be crucially involved in the toxicity mechanism and an important cytoskeletal destructuration was also detected. In this scenario peculiar macrophagic structures like podosomes that mediates different processes like, cell–matrix adhesion, extracellular matrix degradation, migration, infiltration and also probably phagocytosis might be involved in the SAS NP toxicity mechanism. Further analyses are required to fully understand hnRNP K and podosomes involvement in SAS NPs mediated toxicity.

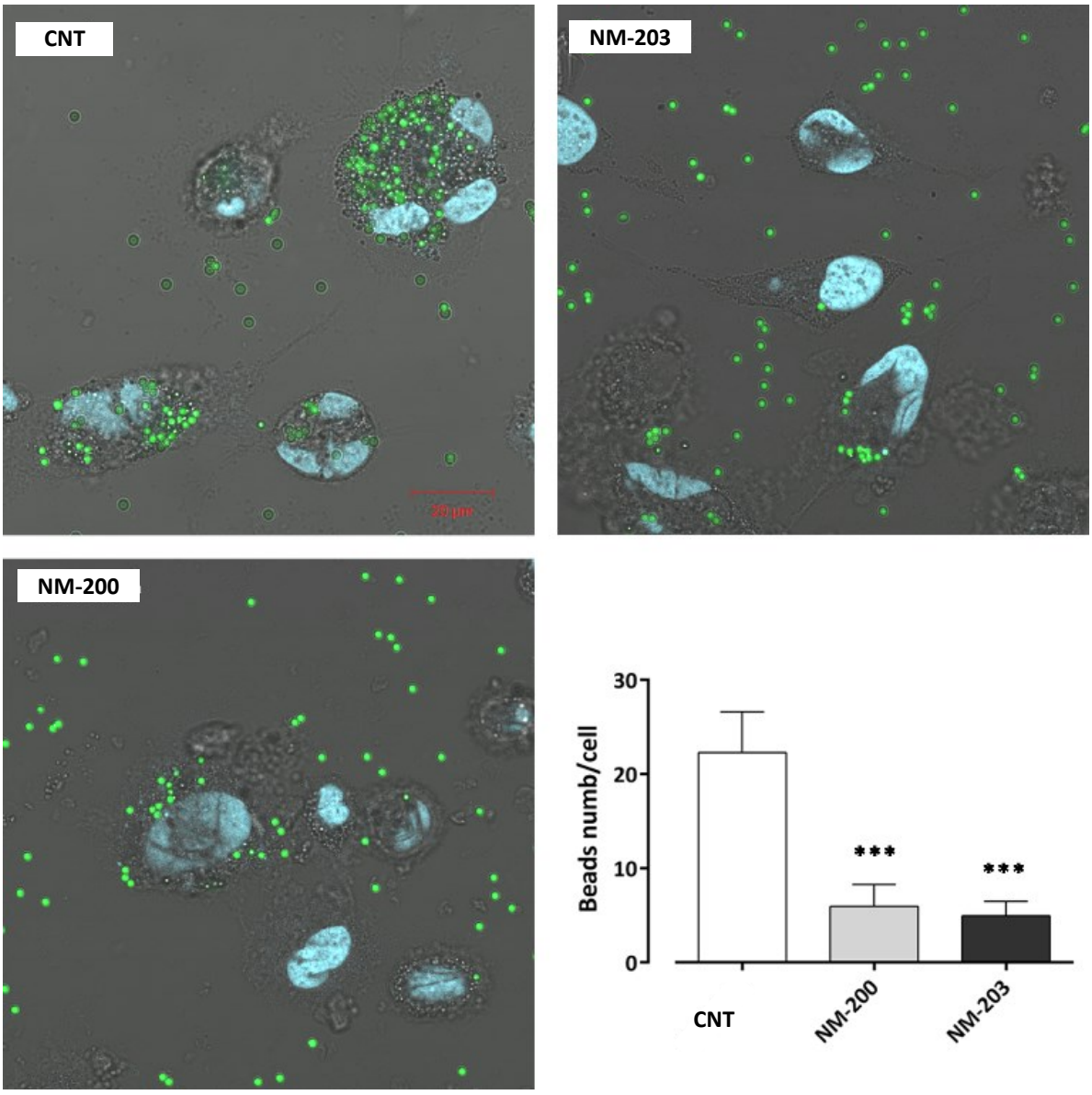


***Figure 46.*** THP-1 cells, pre-exposed to SAS NPs for 24 h, were incubated with LPS (100ng/ml) for further 24 h in the presence of fluorescent latex beads. Representative single confocal sections of untreated (control) or SAS NPs treated (NM-200 or NM-203; 10µg/cm$^2$) cells are reported, as indicated. Nuclei were stained with DRAQ5 (blue). The phagocytic activity of THP-1 cells compared to control were drastically reduced in both treatments with a higher perturbation visualized in NM-203 treatment. Bottom right, the number of internalized beads, derived from means ± SEM of at least 20 cells in five independent fields. Significance was determined by one-way ANOVA with Bonferroni post-hoc test (***, $p < 0.001$ vs control).

# 3. RESULTS AND DISCUSSION

## PART II: BIOMEDICAL APPLICATIONS OF ENGINEERED INORGANIC NANOPARTICLES

Parkinson's disease (PD) is an age-related neurodegenerative disorder (ND) affecting more than 10 million people worldwide (Dorsey et al., 2018), with incidence rising exponentially above 60 years (Bloem et al., 2021). As a result of the progressive population ageing and of environmental factors (Bloem et al., 2021), PD is considered the fastest growing neurological disorder in the world thus determining one of the major socio-economic burdens on citizens and health systems.

PD is characterized by loss of dopaminergic neurons in the substantia nigra pars compacta, producing a decline in striatal dopamine levels with the loss of motor functions. The neuropathological hallmark of PD is the presence of intraneuronal inclusions called Lewy bodies, composed by mistrafficked lipid vesicles and oligomeric aggregates of the α-syn protein (Spillantini et al., 1997; Shahmoradian et al., 2019b). In addition to PD, other synucleinopathies, such as Lewy body dementia and multiple system atrophy, are characterized by the accumulation of misfolded syn in Lewy bodies. Under physiological conditions, α-syn seems to be involved in the regulation of vesicle trafficking network at the synapses of dopaminergic neurons (Lashuel et al., 2013) and its dysfunction appears to be a critical determinant for the development of PD (Lee and Trojanowski, 2006). In support of this, genetic mutations, as well as duplications or triplications of the syn locus, cause rare familial autosomal-dominant forms of PD (Polymeropoulos et al., 1997; Singleton et al., 2003; Chartier-Harlin et al., 2004). α-Syn is an intrinsically disordered protein with an N-terminal domain which presents five conserved lysine-rich repeats and adopts an amphipathic broken-helix conformation when associated with biological membranes (Killinger et al., 2019), while the C-terminal acidic domain remains unstructured. The central hydrophobic region of α-syn (residues 61–95), known as the nonamyloid component (NAC), has a crucial role in syn misfolding. In physiological condition, this aggregation-prone region is shielded from the solvent by transient intramolecular contacts, but during pathogenesis triggers the formation of oligomeric species, considered the most neurotoxic forms of α-syn, which can further mature into amyloid fibrils.

α-Syn is a typical intrinsically disordered protein (IDP), which in pathological conditions, α-syn undergo a series of lipid-dependent conformational changes leading to the formation of α-syn oligomers (Bartels, 2019). The link between NPs, hPC and IDPs and has been discussed formerly, in fact SAS NPs showed a strong interaction with IDPs and the high structural flexibility that characterizes this typology of proteins might importantly contribute to the high affinity binding on

NP surface allowing a better surrounding on the surface and increasing the contact sites (Klein et al., 2016). Moreover, also for SAS NPs the interaction with α-syn *in vitro* is accompanied by enhanced aggregation propensity, modulating the amyloidogenic potential of the protein (Vitali et al., 2018). An interesting work from Kaushik et al. (2018) reported an important link between different NPs and potential applications for ND. NPs (that are able to cross the BBB) can directly target the CNS and this aspect could be crucial for applications in ND. Kaushik et al. (2018) applied a computational approach to define the contact sites between NPs and α-syn; these molecular docking simulations reported that $CeO_2$ NPs best fit to the active site of α-syn. $CeO_2$ NPs also shows anti-oxidant regenerative properties (Korsvik et al., 2007; Baldim et al., 2018), neuroprotective effects and are able to cross the BBB (Celardo et al., 2011; Lord et al., 2021; Heckman et al., 2013; Naz et al., 2017), and those qualities have a higher importance if we also consider the high biocompatibility of these NPs (Cordelli et al., 2017; Graham et al., 2014; Modrzynska et al., 2018).
All these characteristics potentially configure $CeO_2$ NPs as a potential long-term antioxidant, tolerated by biological systems with a self-regenerative and radical scavenger activity, supplemented by the high surface volume ratio and consequent ability to catalyze a high quantity of reaction on his surface.
For those reasons we decided to evaluate the effects of $CeO_2$ NPs in a validated yeast model of PD (HiTox strain) (Outeiro and Lindquist, 2003; Auluck et al., 2010; Su et al., 2010), which is known to recapitulate a number of crucial cellular features of syn oligomer-induced cytotoxicity. In this model, overexpression of human syn (fused to GFP) under the control of a galactose-inducible promoter results in dose-dependent toxicity and global cellular dysfunction. This model, using as readout the cell growth inhibition caused by the formation of oligomeric forms of human syn, provides a rapid and inexpensive tool for discovering novel inhibitors effective in reversing the oligomer-induced toxicity. Moreover, this model, focusing on oligomers as promising target for PD in an *in vivo* context in which no amyloid fibrils are produced, allows to evaluate not only if the selected molecules affect the formation, accumulation and cellular localization of syn oligomers *in vivo*, but also possible indirect mode-of-actions of these molecules using systems biology approaches.

### *3.6 Viability assay in HiTox strain*

In order to test if the treatment with $CeO_2$ NPs have effect on HiTox strain viability we performed a clonogenic assay; α-syn expression in controlled by a galactose inducible promoter, and the induction of the two copies of the gene present integrated in the genome of HiTox strain was

obtained growing the cells in inducing conditions (SGal medium). The induction of α-syn overexpression determine a strong inhibition of the yeast cell growth compared with wild type (WT) (**Fig. 47a**). The clonogenic assay was made exposing cells to different concentrations of $CeO_2$ NPs (from 10 up to 100 ng/µL) for 48h at 28 °C in SGal medium, then diluted aliquots of the cells were seeded in SD (containing glucose, repressing condition) agar plates. After 72 h of incubation, colony-forming unit (CFU) were counted. As shown in **Figure 47b**, the exposure to $CeO_2$ NPs strongly increased the viability of the yeast model of PD and a dose-response curve is clearly visible. Considering the probability of negative effects from SAS NPs on α-syn aggregation and toxicity (Vitali et al., 2018) we also treated the HiTox strain in inducing condition upon treatment with SAS NPs (from 10 up to 100 ng/µL). In this case weren't detected variations on viability compared to untreated cells, but at the highest dosage (100 ng/µL) was detected an additional toxic effect estimated in 50% the reduction of viability compared to the control (untreated HiTox cells).

Yeast cells were also evaluated in their morphology through optical microscopy after 48h of induction and simultaneous exposition to $CeO_2$ NPs or SAS NPs (**Fig. 47c**). In the untreated cells or in cells exposed to SAS NP treatment are clearly visible morphological alterations with irregular cells with aberrant bud. These detected morphological alterations resemble the classical phenotype observed in cellular senescence (Lee et al., 2012; Kakolyri et al., 2016). On the other hand, $CeO_2$ NP treatment completely restored the oval-shaped physiological yeast morphology suggesting a recover of the cellular division process. The exposition of cells to $CeO_2$ NPs resulted in an important protective effect from these NPs. We subsequently decided to monitor the first phases of exposition, in order to comprehend the interaction mechanism of $CeO_2$ NPs and additionally to evaluate the internalization events associated with the benefic effects detected. Yeast cells were exposed to SAS NPs or $CeO_2$ NPs in inducing condition for 4 h. As observed at the optical microscope (**Fig. 48a**), $CeO_2$ NPs have a 'caging' effect on the cellular surface, whereas for SAS NPs exposed cells was not detectable any evident interaction between cells and NPs. This $CeO_2$ NP cage was formed after an early exposition and completely disappeared after 48 h of treatment (**Fig. 47c**), suggesting a time-dependent internalization of $CeO_2$ NPs in yeast cells, probably mediated by this first (strong) interaction with the cell surface. Therefore, the internalization of $CeO_2$ NPs was evaluated through flow cytometry analysis; yeast cells in inducing condition were treated with $CeO_2$ NPs at a concentration of 50 ng/µL (maximum effective dose; **Fig. 47**). Using a gating strategy that eliminated dead cells, cellular debris and smaller-sized particulates, we analyzed viable α-syn-expressing cells to generate histogram plots for side scatter (SSC) signals. SSC data provide information about the

internal complexity (i.e., granularity) of the cell, and previous reports have shown a correlation between increasing SSC signals and cellular uptake of NPs (Suzuki et al., 2007; Friedrich et al., 2015; Njoroge et al., 2018). Analyzing the SSC signals from the plot in comparison between $CeO_2$ NP treated cells and control cells (untreated), was detected a time-dependent increase of SSC signal indicating an internalization of the NPs from the yeast cells (**Fig. 48b**).

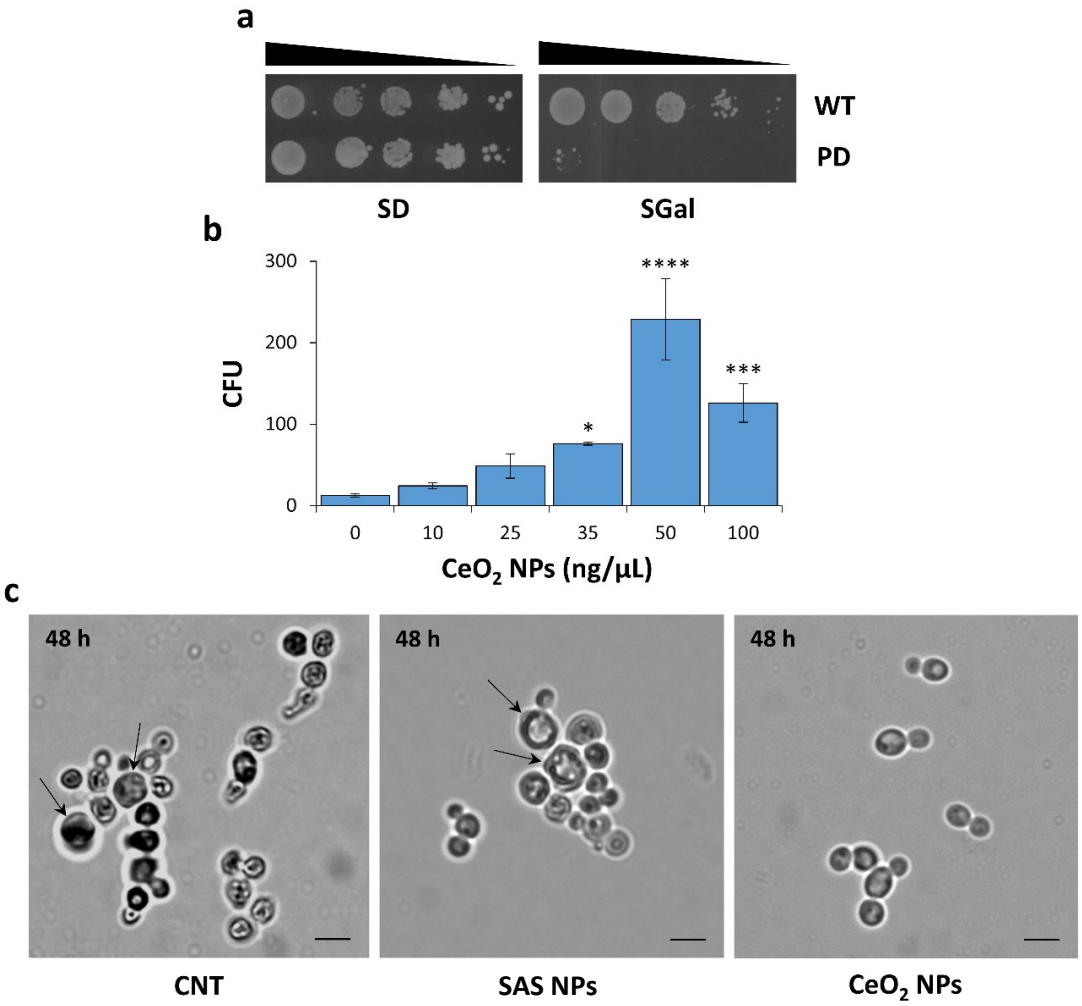


***Figure 47***. CeO2 NPs strongly increase the viability of yeast cells expressing human α-syn. In the upper part of the figure **(a)** is reported a serial dilution spot assay (10-fold input cell dilutions ranging from $10^1$ to $10^4$) made on WT and HiTox strains. Cells were spotted on agar plates containing glucose (repressing conditions) or galactose (inducing conditions), and growth was assessed after 48 h at 28 °C. In the right panel is clearly visible the toxicity that derives from the induction of α-syn expression when galactose-inducible promoter switched on. In the middle part of the figure **(b)** is reported the protective effect of $CeO_2$ NP treatment at different concentrations. The number of colony-forming units (CFU) developed on agar plates at 28 °C for 72 h were recorded and counted manually. Data are the mean ± SD of three independent experiments performed at least in triplicate. Significance

was determined by one-way ANOVA with Dunnett's multiple comparisons test (*, $p < 0.05$; ***, $p < 0.001$; ****, $p < 0.0001$). In the lower part of the Figure **(c)** are reported the imaged acquired by optical microscopy (phase contrast). α-Syn-expressing cells were grown in inducing conditions with or without SAS NPs (50 ng/µL) or $CeO_2$ NPs (50 ng/µL) for 48 h at 28 °C prior to observation. Cells after the exposure to $CeO_2$ NPs shows a physiological phenotype while in CNT (untreated) or SAS NPs exposed cells is visible a senescence-like phenotype with small irregular shaped cells and large mother cells (indicated with black arrows). Scale bars were set at 5 µm.

### *3.7 Interaction of NPs with yeast cells*

The confirmation of internalization was an important element explaining the protective effects of $CeO_2$ NPs. To evaluate if yeast plasma membrane directly mediates the interaction and the adsorption of $CeO_2$ NPs, yeast cells were subjected to cell wall digestion through a lyticase treatment. Lyticase is a hydrolytic enzyme that selectively degrades the cellular wall of vegetative yeast cells generating living spheroplast. Cell wall degradation was assessed utilizing calcofluor white, a selective chitin/chitosan fluorescent dye that permits the detection of the cell wall using fluorescence microscopy. In **Figure 48c** is reported the result of cell wall degradation of yeast cells treated with $CeO_2$ NPs; cells treated with lyticase presented a degraded cell wall and an strong interaction with the NPs compared with untreated (with lyticase) cells that interacted to a lesser extent with NPs. This result underlined the importance of interaction between NPs and plasma membrane as possible mediation of cellular uptake. Considering the zeta potential of $CeO_2$ NPs (41 mV; see 'Materials and Methods' for details), it is possible that an electrostatic interaction with negatively-charged plasma membranes can favour the adsorption of these NPs. Of note, no interaction with the cell surface was observed with negatively-charged SAS NPs (zeta potential, −43 mV) even at the highest concentration tested (100 ng/µL). SAS NPs appeared to be internalized in yeast to a lesser extent respect to $CeO_2$ NPs and a different mechanism may be responsible for the uptake of these negatively-charged NPs (Foroozandeh and Aziz, 2018). The electrostatic interactions between $CeO_2$ NPs and plasma membrane could be crucial, where positive NPs and negative phospholipids headgroups are the principal primary uptake mediators, subsequently NPs internalization can follow mechanisms like endocytosis, where an endocytic process could be favored by a membrane bending caused from the first electrostatic interactions (Zhang et al., 2015).

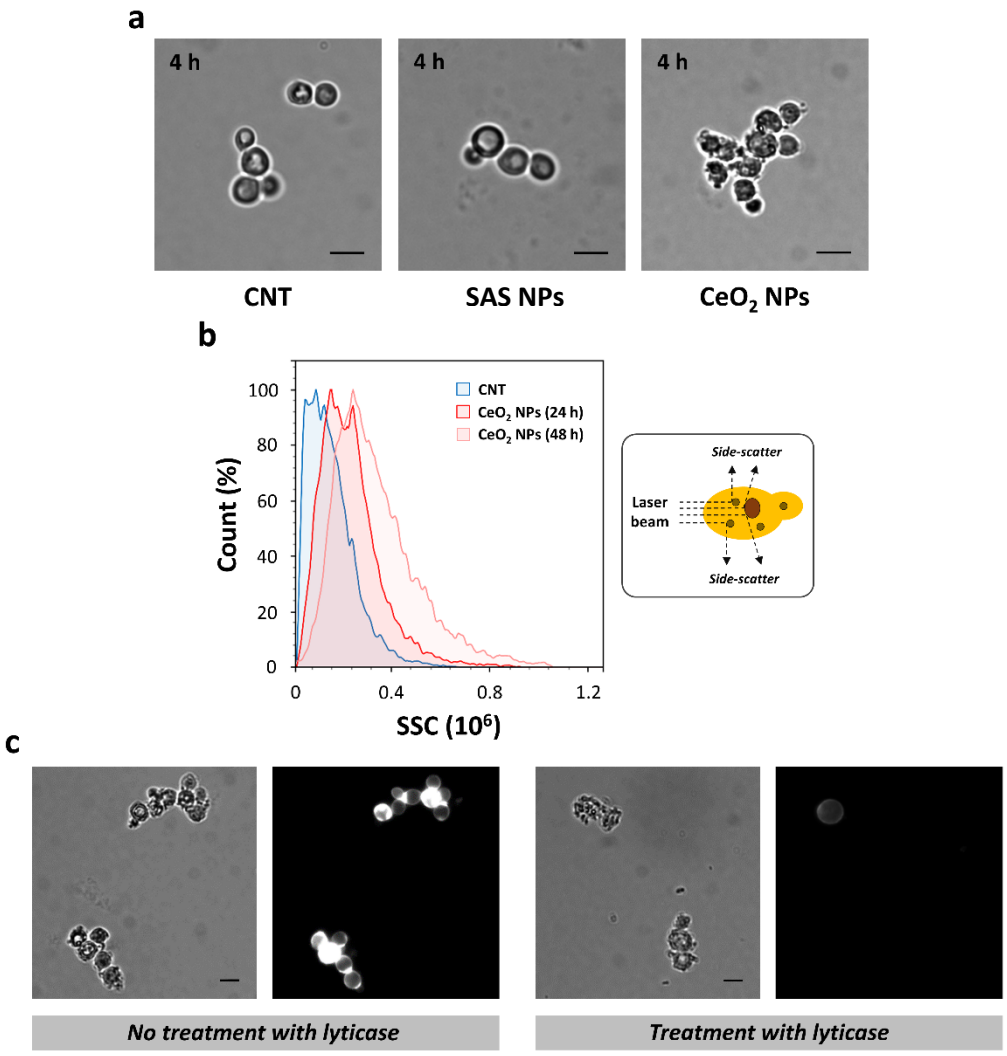


***Figure 48.*** α-Syn-expressing cells were grown with or without SAS NPs (100 ng/µL) or $CeO_2$ NPs (50 ng/µL) for 4 h at 28 °C prior to microscopy observations **(a)**. CNT indicates the control (untreated sample), the cellular surface adsorption of $CeO_2$ NPs importantly differed respect to SAS NPs that didn't show adsorption on cells, scale bars were set at 5 µm. **(b)** Flow cytometry analysis of α-syn-expressing cells grown on SGal medium with or without $CeO_2$ NPs for different times of incubation (24–48 h). A schematic representation of SSC signal detection by flow cytometry was illustrated (right panel) in which an optical detector measures light scatter at a ninety-degree angle relative to the laser beam of flow cytometer. A progressive internalization from $CeO_2$ NPs was detected by the increase of SSC signal. **(c)** Fluorescence microscopy images of yeast cells untreated (left) or treated (right) with lyticase, exposed to $CeO_2$ NPs (50 ng/µL) for 4 h at 28 °C and then stained with calcofluor white, phase contrast (left-side) and fluorescence (right-side). The cell walls degradation was

associated with a higher amount of NPs adsorbed on plasma membrane, this typology of interaction might be decisive for NPs uptake. Scale bars, 5 µm.

### *3.8 $CeO_2$ NPs effects on α-syn oligomeric toxic species*

When expressed in yeast, α-syn first accumulates at the plasma membrane in a highly selective manner before forming cytoplasmic inclusions (intracellular foci; **Figure 49a**, upper panel) that cause cellular toxicity (Cooper et al., 2006; Su et al., 2010; Outeiro and Lindquist, 2003). Intracellular foci containing monomeric or oligomeric aggregates of α-syn, but not amyloid fibrils.

The global cellular dysfunction is dictated by the complete engulfment of the ubiquitin-proteasome system together with an important impairment in vesicle trafficking, ER stress, an accumulation of lipid droplets, mitochondrial dysfunction and reactive oxidative species (ROS) production (Cooper et al., 2006; Auluck et al., 2010; Gitler et al., 2008; Allendoerfer et al., 2008). α-Syn is integrated is fused with GFP at the C-terminal allowing the direct analysis of the α-syn expression directly by fluorescence microscopy; the presence of GFP don't alter the α-syn functionality and cellular localization (Outeiro and Lindquist, 2003).

We have therefore investigated about the effects of the exposure to $CeO_2$ NPs on α-syn cytoplasmic inclusions localization and accumulation using fluorescence microscopy analysis. Yeast cells that induced α-syn-GFP expression (SGal medium) were treated or not with $CeO_2$ NPs (50 ng/µL) for 48 h. In **Figure 49a** are reported the image acquired by fluorescence microscopy; the treatment with $CeO_2$ NPs drastically reduced the presence of fluorescent cytoplasmic inclusions of α-syn and decreased (in parallel) the toxicity deriving from α-syn-GFP expression (**Figure 47b**). Furthermore, the $CeO_2$ NP treatment changed the α-syn localization that were almost completely present in the plasma membrane region, while in the untreated cells (without $CeO_2$ NP) was detectable in cytoplasmic foci (**Fig. 49b,c**). The treatment with $CeO_2$ NPs reduced the formation of fluorescent cytoplasmic inclusions of α-syn in a dose-dependent manner and this trend is analogous to a plasma membrane localization that increases inversely to the reduction of the cytoplasmic foci.

To exclude any direct effect from $CeO_2$ NPs on the α-syn gene expression, we then performed a dot blot analysis using an anti-α-syn antibody to evaluate the expression levels of the α-syn protein, using as housekeeping/loading control an anti-Pgk1 antibody (**Fig. 49d**). Dot blot analysis does not show any significant reduction of α-syn protein abundance, suggesting that the reported results probably come from a direct interaction between the NPs and α-syn in his oligomeric or monomeric conformation.

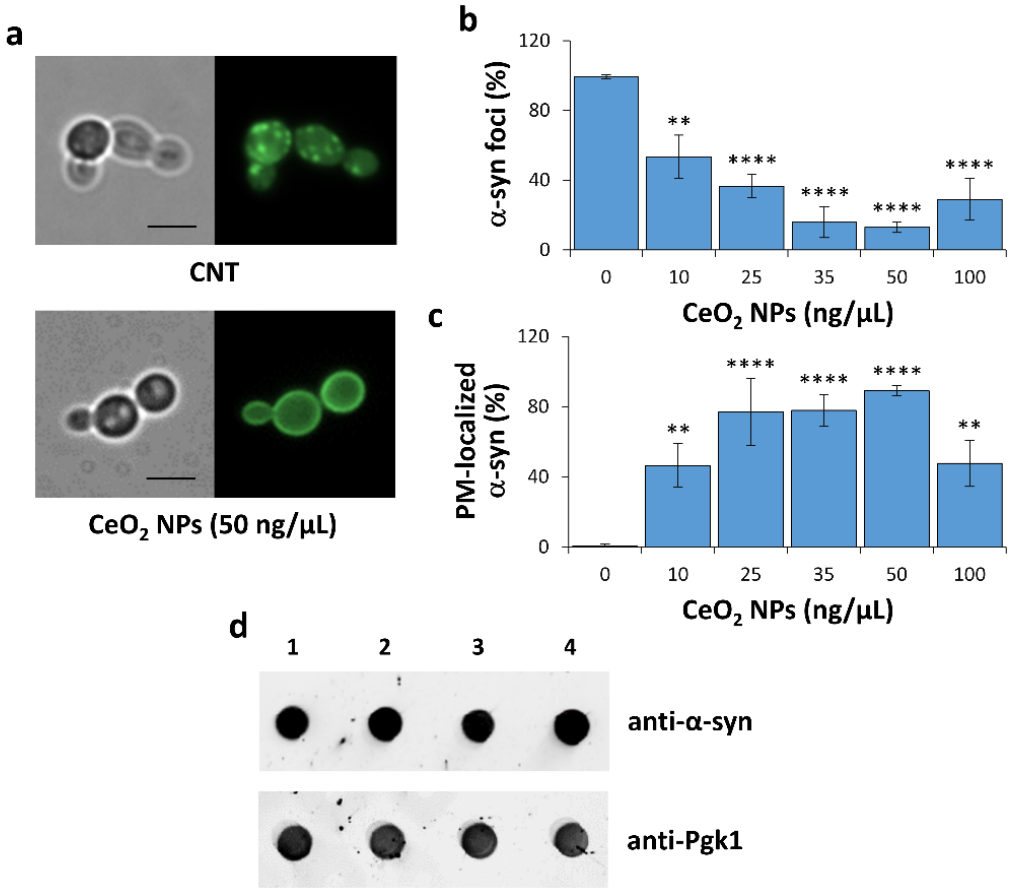


***Figure 49***. Fluorescence microscopy images observation of α-syn-GFP-expressing cells (HiTox strain) grown with or without $CeO_2$ NPs (50 ng/µL) for 48 h at 28 °C **(a)**. For each sample, phase contrast (left) and fluorescence (right) CNT indicates the control (untreated sample). $CeO_2$ NPs importantly reduced the presence of α-syn cytoplasmic inclusion and determined a localization of the protein on the plasma membrane. Scale bars, 5 µm. **(b)** Yeast cells were treated with different concentrations of $CeO_2$ NPs (10-100 ng/µL) for 48 h at 28 °C and the percentages of cells with α-syn cytoplasmic foci were quantified relative to the total number of cells. Significance was determined by one-way ANOVA with Dunnett's multiple comparisons test (**, $p < 0.01$; ****, $p < 0.0001$). It was detected a dose-response effect of $CeO_2$ NPs concentration in the reduction of α-syn foci inverse proportionally to the plasma membrane localization of the protein. **(c)** Yeast cells were treated as indicated in **(b)** and the percentages of cells with α-syn associated to the plasma membrane were quantified relative to the total number of cells. **(d)** Results from the dot blot analysis performed with an anti-α-syn antibody on whole cell extract samples (10 µg total protein each) derived from untreated (1) or NP-treated samples for 6 h [CeO2 NP concentrations: 25 ng/µL (2); 35 ng/µL (3); 50

ng/µL (4)]. Immunoreactivity was compared with the constitutively expressed phosphoglycerate kinase enzyme (Pgk1) served as a housekeeping/loading control.

### *3.9 Direct interaction between α-syn and $CeO_2$ NPs*

The binding between plasma membrane and $CeO_2$ NPs could importantly promote the physical interaction with the α-syn that preferentially localize in this region (Gitler et al., 2008). Supporting this hypothesis, SAS NPs that didn't show interaction with plasma membrane, don't display protective effects on α-syn induced toxicity, conversely could contribute to aggregation and at high concentrations of treatment produce additional toxic effects, similarly to other NPs (Vitali et al., 2018; Álvarez et al., 2013; Wu and Xie, 2016). The direct interaction between $CeO_2$ NPs and α-syn could then be important to explain the benefic effects on viability and α-syn foci formation. To test if the NPs physically interacts whit α-syn, the protein adsorbed on $CeO_2$ NPs where isolated utilizing a similar approach to that employed for the hPC isolation for SAS NPs. The protein extracts from WT and HiTox strains were incubated in agitation with $CeO_2$ NPs, in order to allow the proteins adsorption on the NP surface, simulating a hPC formation. After 24 h of incubation absorbed proteins were recovered by centrifugation and loosely bound or unbound proteins were eliminated with different washes, the selected high affinity bound proteins were detached from the NPs surface and analyzed through dot blot analysis with an anti-α-syn antibody (see "Materials and Methods" for details) (**Fig. 50**). The dot blot analysis confirmed a direct interaction between α-syn and $CeO_2$ NPs, thus α-syn is directly adsorbed on the NP surface with a high affinity. This result is in line with the *in-silico* study from Kaushik et al. (2018) that reported a best fitting between $CeO_2$ NPs and the active site of α-syn (Kaushik et al., 2018).

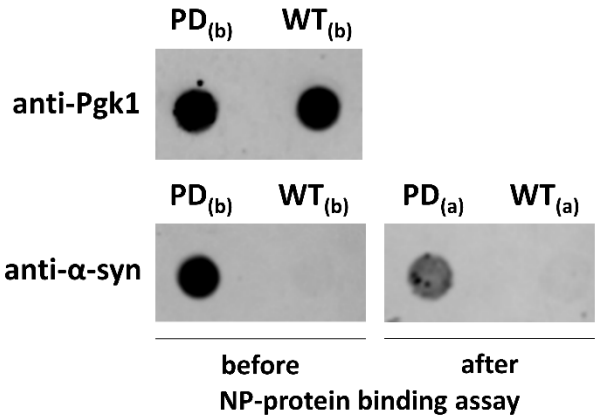


***Figure 50.*** Protein extracts obtained from HiTox and WT strains were used for an *in vitro* NP-protein binding assay. The adsorbed proteins from HiTox and WT strains (*PD(a)* and *WT(a)*) were recovered

from $CeO_2$ NP surface by a centrifugation and different washings steps and then analyzed by dot blot using an anti-α-syn antibody. Aliquots (5 µg) of HiTox and WT protein extracts ($PD_{(b)}$ and $WT_{(b)}$) were used as controls for immunodetection, and anti-Pgk1 antibody as loading control for protein extracts. The dot blot visualization reported a high affinity α-syn protein adsorption directly on the NPs surface. $PD_{(b)}$, HiTox protein extract (5 µg); $WT_{(b)}$, WT protein extract (5 µg); $PD_{(a)}$, absorbed proteins from the *in vitro* binding assay made with HiTox protein extracts; $WT_{(a)}$, absorbed proteins from the *in vitro* binding assay made with WT protein extract.

We also confirmed that $CeO_2$ NPs have an anti-aggregative effect utilizing a specific anti-α-syn oligomers antibody and dot blot analysis. Yeast cells grown in inducing conditions were treated with $CeO_2$ NPs at the most effective concentration (50 ng/µL) for 6 or 24 h. In order to preserve the α-syn oligomeric species after the treatment, we extracted the protein in non-denaturing conditions and without separating the insoluble phase from the soluble (whole cell extracts). Subsequently whole cell extracts were analyzed using dot blot analysis (**Fig. 51**). An important increase of α-syn oligomer abundance was observed after 24 h of induction in untreated cells, while the treatment with $CeO_2$ NPs strongly reduce the abundance of these species confirming an anti-aggregative effect on α-syn oligomer formation (**Fig. 51**).

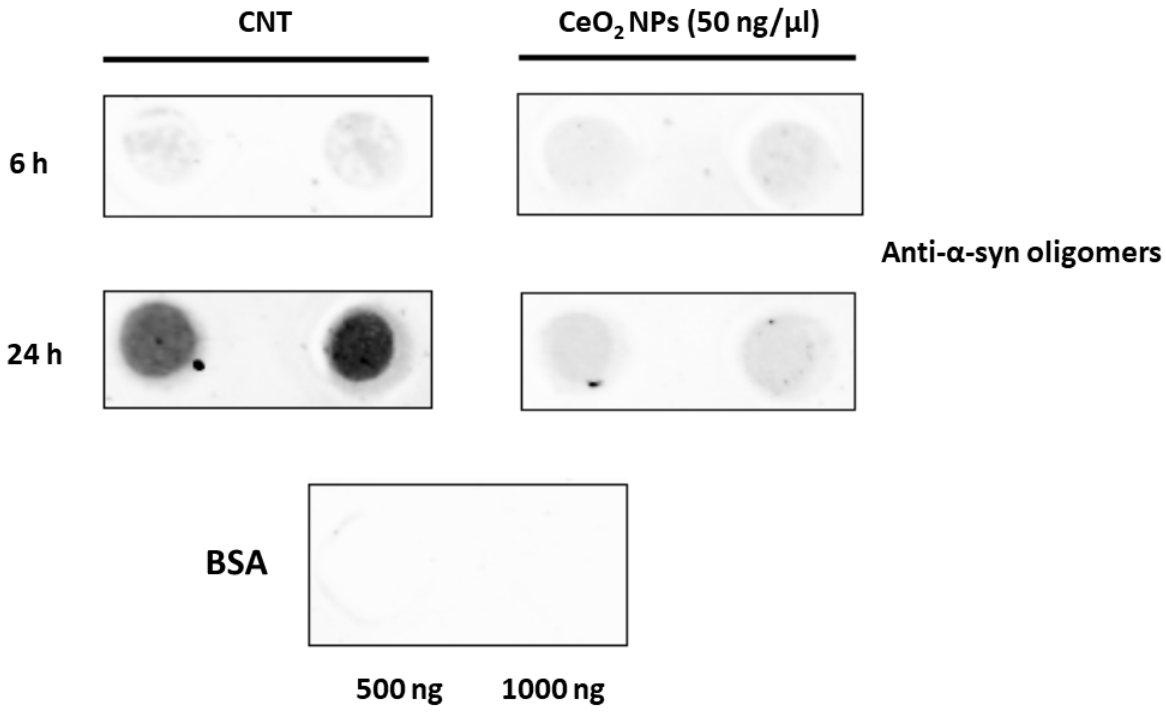


***Figure 51***. Dot blot analysis show a drastic reduction of oligomeric aggregates after $CeO_2$ NP treatment. α-Syn-expressing cells were grown with or without $CeO_2$ NPs (50 ng/µL) for 6 h or 24 h

at 28 °C. After the treatments, whole cell extracts were obtained in non-denaturing conditions and a dot blot has been set up. BSA was utilized as negative control for the primary antibody reactivity. CNT, untreated sample.

The result of dot blot significantly revealed a reduction of α-syn aggregation after $CeO_2$ NP treatment in line with the disappearance of the intracellular foci formed by syn observed with the fluorescence microscope (**Fig. 49**). NAC region in α-syn protein is critical for α-syn aggregation (Sun et al., 2019) and the interaction between α-syn and $CeO_2$ NP could occur at the level of this region, inhibiting the lipid-dependent conformational changes that lead to the formation of β-sheet-rich aggregates (α-syn oligomers), considered the most neurotoxic forms of α-syn (Longhena et al., 2020; Bartels, 2019). This typology of interaction might be comparable with different molecules that are able to directly stabilize the physiological α-helical lipid-bound conformation state of α-syn, avoiding the development of pathological conformations (Fonseca-Ornelas et al., 2014). The mechanism of action by $CeO_2$ NPs could also partially be explained by an α-syn physiological α-helical conformation stabilization mediated by the adsorption on NP surface.

### *3.10 $CeO_2$ NP treatment reduced the aggresome formations*

Aggresomes represents another important hallmark common in different ND, including PD (Ardley et al., 2003). Aggresomes are dynamic structures, formed in misfolded proteins overload conditions, containing ubiquitylated proteins as result of the ubiquitin/proteasome system (UPS) impairment and other abnormal or misfolded potentially toxic proteins. Aggresomes can reflecting a failed attempt by the cell to remove this harmful species (Corboy et al., 2005; García-Mata et al., 1999). These particulars cellular inclusion had also been related with Lewy bodies, sharing many components of the UPS that are similarly recruited in both typologies of cellular inclusions to facilitate proteolysis (McNaught et al., 2002). Some originals hypothesis proposed that Lewy bodies in PD actually originates from expanded aggresomes, developed in response to proteolytic stress, that the proteasomal machinery failed to clear (Olanow et al., 2004). However, these structures represent a protective response to cellular stress triggered by misfolded proteins. In PD are an important hallmark of a global proteolytic cellular stress accompanied by an engulfment of proteasomal machinery and UPS (Kopito, 2000). Yeast aggresomes are highly similar to mammalian aggresomes; aggresome system was therefore conserved in evolution, and yeast could provide a valid model for elucidating mechanisms of aggresome formation and the relationship with ND

(Wang et al., 2009). To evaluate if $CeO_2$ NP treatment is able to reduce aggresome formation, yeast cells were treated or not (CNT) with the $CeO_2$ NPs (at a concentration of 50 ng/µL) for 6 h in inducing condition (SGal medium); subsequently, cells were stained with a specific fluorescent aggresome dye (ProteoStat®). ProteoStat dye specifically interacts with the misfolded proteins presents in the aggresomes, in particular interacting with the β-sheets structures typical of aggregated proteins (Shen et al., 2011). ProteoStat binding to the aggresomes increases its fluorescence, allowing the visualization of the aggresomes using a fluorescence microscope. In **Figure 52a**, it is possible to observe the formation of aggresomes in untreated cells (CNT). The treatment with $CeO_2$ NPs drastically reduced the aggresome formation in HiTox strain (**Fig. 52b**)**.** These results confirmed that $CeO_2$ NPs are able to reduce the aggresome cellular presence, suggesting a restore of the impaired cellular pathways leading to their formation and crucial for the clearance of toxic species deriving from α-syn oligomerization.

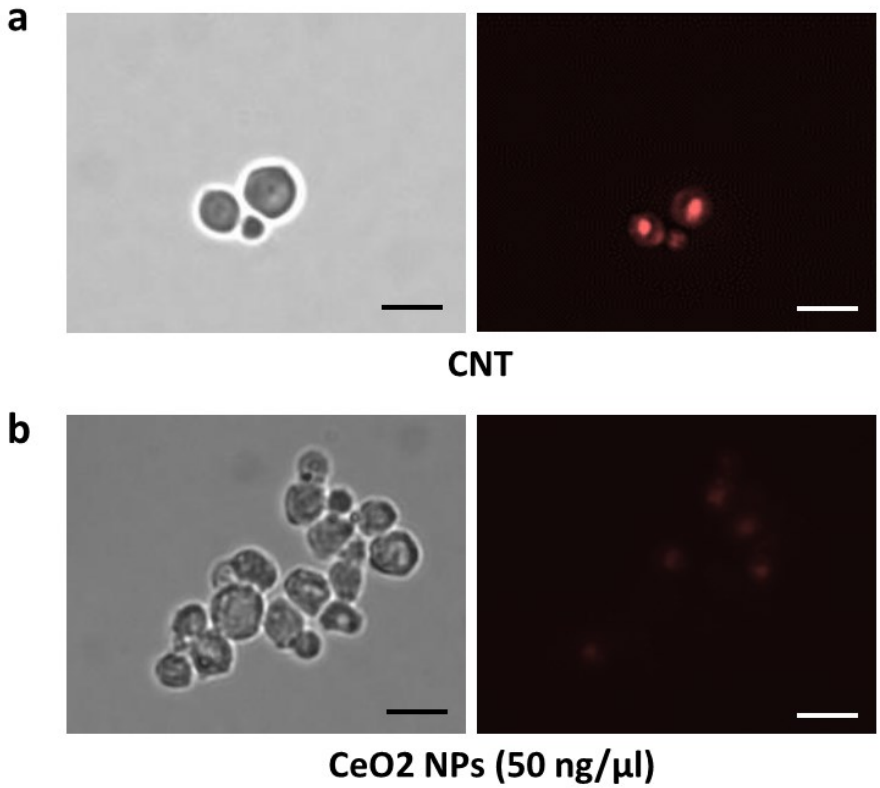


***Figure 52***. α-Syn-expressing cells were grown with or without $CeO_2$ NPs (50 ng/µL) for 6 h at 28 °C and subsequently stained with ProteoStat® prior to fluorescence microscopy images acquisition (see "Materials and Methods" for more details). **(a)** Untreated samples (CNT) where is clearly visible the aggresome formation. **(b)** The treatment with $CeO_2$ NPs drastically reduced the aggresome formation. Scale bars were shown at 5 µm.

### *3.11 $CeO_2$ NPs strongly counteract the mitochondrial damage and ROS production*

Mitochondrial dysfunctions represent another classic hallmark of PD and have a central role in PD pathogenesis (Federico et al., 2012). α-Syn toxic species can accumulate in mitochondria leading to mitochondrial dysfunction and cell death; when these toxic oligomeric species are present, the affinity of α-syn for membranes induce membrane fusion triggering ER/Golgi vesicle trafficking defects and mitochondrial fragmentation (Exner et al., 2012). Also in our model of PD (HiTox), the mitochondrial morphology and functioning is significantly compromised (Cooper et al., 2006; Auluck et al., 2010; Gitler et al., 2008; Allendoerfer et al., 2008). To analyze mitochondrial morphology, HiTox strain was transformed with a plasmid expressing a mitochondrial-localized red fluorescent protein (mtRFP). The import of mtRFP into the mitochondrial compartment doesn't appear to be hindered in respiratory-deficient mutants with reduced membrane potential; this allowed the application of mtRFP also in a probable reduced membrane potential state from the HiTox strain. Moreover, mtRFP transformation gave us the advantage to directly analyze the mitochondrial morphology by fluorescence microscope observations, thanks to the stable fluorescence of mtRFP, without needing others staining steps. In WT cells (not expressing α-syn) mitochondria are normally organized in an extensive tubular reticulum, this morphology is maintained by a dynamic equilibrium between mitochondrial fission and fusion events. When this dynamic equilibrium is disturbed by cellular stress events, this mitochondrial pattern is disrupted leading to the formation of smaller and punctuated mitochondria (Shaw and Nunnari, 2002; Suen et al., 2008). We tested the effects of $CeO_2$ NP exposition (50 ng/µL) in mtRFP transformed α-syn-expressing cells after 24 h of induction (**Fig. 53**). We have observed in untreated cells (CNT) a mitochondrial fragmentation caused by α-syn overexpression (**Fig. 53a**); the treatment with $CeO_2$ NPs completely restored the normal tubular mitochondrial morphology of WT cells (**Fig. 53a**).

To confirm the preserving effect mediated by $CeO_2$ NPs on normal mitochondrial morphology and functionality, the yeast cells were grown for 4 h in inducing condition and stained using MitoTracker Deep Red (MTDR), a specific dye that selectively stains undamaged mitochondria in living cells. MTDR passively diffuses across the plasma membrane and accumulates only in active mitochondria; once targeted the mitochondria, MTDR covalently binds the thiol groups of the cysteine residues of mitochondrial proteins (Xiao et al., 2016), increasing his fluorescence and allowing to visualize the "active" mitochondria. Yeast cells grown in inducing condition were treated with $CeO_2$ NPs (50 ng/µL) for 4 h; cells were recovered and stained with MTDR and the rate of active mitochondria was evaluated through flow cytometry analysis. The fluorescence of MTDR was detected using the flow

cytometer APC channel. The results showed in **Figure 53b** reported an interesting higher amount of respiring mitochondria (evaluated in a 50% of increment) by the cells already after 4 h of $CeO_2$ NP treatment compared to the untreated sample (CNT).

We also evaluated the generation of ROS in yeast cells after the treatment with $CeO_2$ NPs. In order to detect the ROS we used a dye (CellROX®) which allows to detect several types of ROS *in vivo* (Kwon et al., 2016); this dye is weakly fluorescent in a reduced state, while exhibits a photostable fluorescence upon oxidation by ROS. Induced cells were treated with $CeO_2$ NPs (25 or 50 ng/µL) for 4 h and cells were recovered and stained with CellROX®. CellROX® fluorescence was evaluated through fluorescence microscopy observations. In untreated cells (CNT), we have observed that an importantly detected fluorescence deriving from the dye oxidation by ROS; in cells treated with CeO2 NPs, the number of cells CellROX®-positive drastically decreased in a dose-dependent manner demonstrating a decrease of the free radical pool (**Fig. 53c**).

$CeO_2$ NPs demonstrated to have protective effects from ROS-induced damage in different models of ND, including PD, AS, MS, IS and ALS (Naz et al., 2017). Those protective effects have been attributed to the prevention of ROS generation, reduction of mitochondrial fragmentation, attenuation of apoptosis, and regulation of signal transduction pathways involved in neuroprotection (Dowding et al., 2014; Heckman et al., 2013; D'Angelo et al., 2009; Kwon et al., 2016). In our yeast model the protective effects mediated by $CeO_2$ NPs are not only attributable to rescue from the cytotoxicity due to a lowered formation of α-syn toxic species, but additionally to a prevention of the mitochondrial fragmentation caused by α-syn overexpression and a lowering the ROS levels. Our results also indicated that the protective effect from $CeO_2$ NPs on mitochondria is already present after few hours of the α-syn expression induction. Mitochondrial dysfunctions are importantly linked with the production of ROS in PD and the mitochondrial damage caused by α-syn is an important trigger for ROS generation (Büttner et al., 2008; Su et al., 2010). In a vicious circle, the mitochondrial dysfunction generates oxidative stress that could in turn contribute to the formation of α-syn toxic aggregates leading to apoptotic events (Dexter et al., 1987). $CeO_2$ NPs can act on different phases of this 'vicious circle': directly acting on α-syn stabilization, lowering ROS levels, and maintaining mitochondrial morphology and other physiological functions.

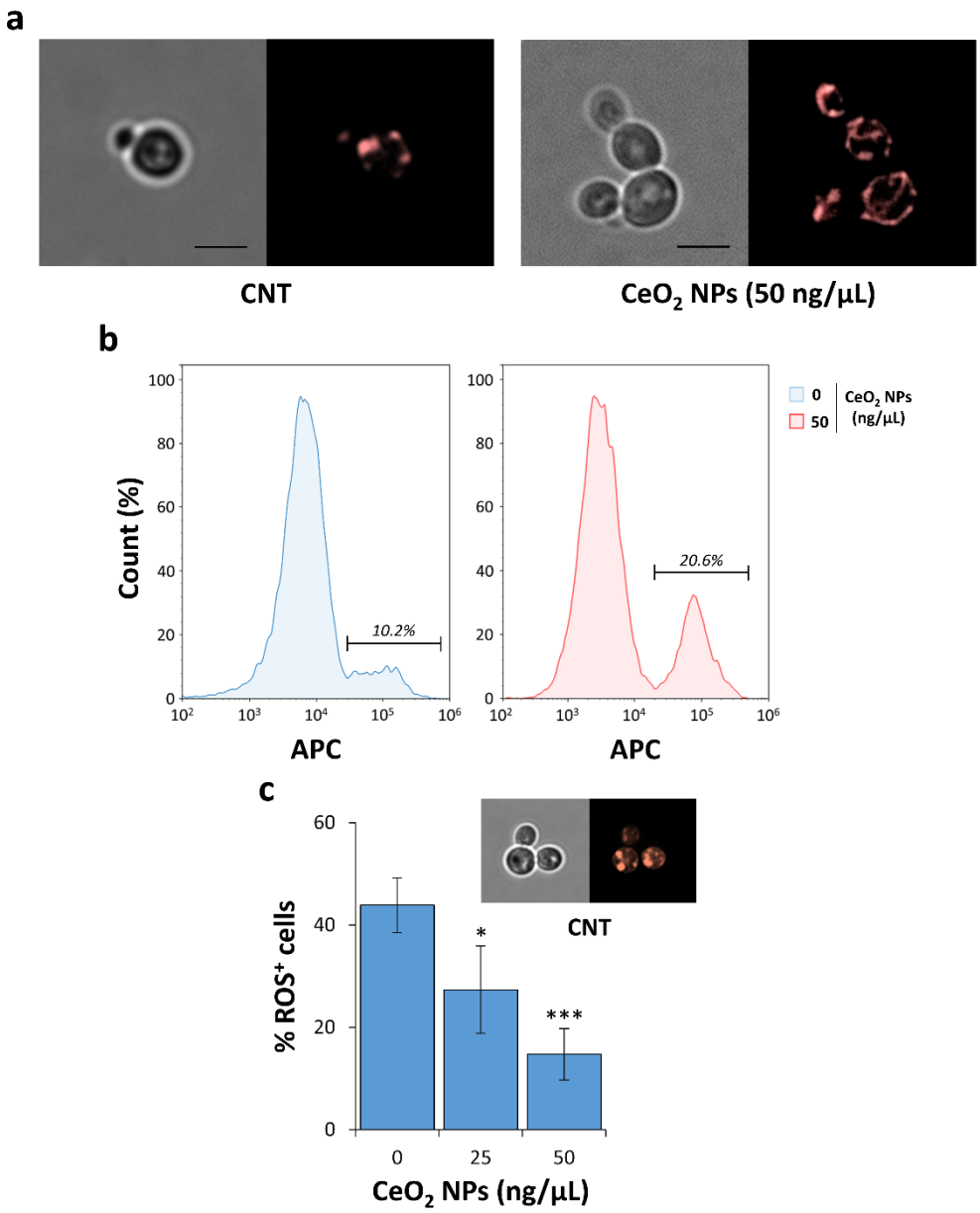


***Figure 53.*** **(a)** The treatment with $CeO_2$ NPs restored yeast the tubular mitochondrial morphology. HiTox strain was transformed with a construct for the expression of mtRFP and grown in inducing conditions (SGal) for 24 h with or without $CeO_2$ NPs (50 ng/µL). For each sample, phase contrast (*left-side*) and fluorescence (*right-side*) microscopy images were shown. *CNT*, control (untreated) sample; scale bars, 5 µm. **(b)** Yeast cells were grown in SGal medium for 4 h with or without $CeO_2$ NPs (50 ng/µL). Active mitochondria in α-syn-expressing (GFP-positive) cells were monitored by MTDR fluorescence using flow cytometer analysis in APC channel. Representative histogram plots were shown, and the percentages of MTDR-positive mitochondria in α-syn-expressing cells were indicated for each sample. **(c)** Yeast cells were stained with CellROX® Orange Reagent and visualized with fluorescence microscopy. CellROX-positive cells were scored. A representative microscope

image is shown above the graph. A dose dependent reduction of ROS positive cells was detected after the exposition to $CeO_2$ NPs. Significance was determined using one-way ANOVA with Dunnett's multiple comparisons test (*, $p < 0.05$; ***, $p < 0.001$).

### *3.12 Identification and characterization of the hPC of $CeO_2$ NPs*

Although we defined different mechanisms potentially explaining the protective effects of $CeO_2$ NPs, the adsorption and identification on the NPs surface of others molecular interactors in addition to α-syn could contribute to the protective effects exhibited. As previously discussed, NPs biological identity is principally provided by the hPC because of the extremely low exchange rate of the proteins over time and by an almost irreversible binding on the NPs surface (Milani et al., 2012; Ahsan et al., 2018). For these reasons, it was important to identify the hPC of $CeO_2$ NPs. We formerly demonstrated that α-syn is adsorbed on the NPs surface according with the study from Kaushik et al. (2018) that reported a best fitting between $CeO_2$ NPs and the active site of α-syn (Kaushik et al., 2018). A similar approach to that employed for the hPC isolation for SAS NPs was utilized for $CeO_2$ NPs . Protein extracts from WT strain and α-syn expressing HiTox strain were incubated in gentle agitation with $CeO_2$ NPs in order to allow the proteins adsorption on the NPs surface, simulating a hPC formation. After 24 h of incubation, absorbed proteins were recovered by centrifugation and loosely bound or unbound proteins were eliminated with different washes selecting the hPC. Subsequently, proteins were detached from the NPs surface, solubilized, denatured, alkylated and trypsin digested in order to be analyzed through LC-MS/MS (see "Materials and Methods" for more details). In **Figure 54** the proteins identified in the hPC of $CeO_2$ NPs were reported. Many proteins involved in translation have been identified.

In this case an interesting factor is the high p.I. of these proteins indicating that are positively charged which might suggest that electrostatic interactions with these proteins may not be as crucial as NPs are negatively charged.

The implication of the adsorption of protein involved in translation on the surface of $CeO_2$ NPs could be very important. As suggested above, the adsorption process might in fact cause proteins structural distortion and their functional inactivation (Ghosh et al., 2014; Assarsson et al., 2014; Shang et al., 2007; Zoungrana et al., 1997). The reduction of translation in the contest of HiTox strain could an attenuation of protein synthesis reducing α-syn aggregation and thus lighten its toxicity. Additionally, the lacking of 60S and 40S ribosomal subunits pools might promote the expression of the Gcn4 transcription factor, that induces the expression of genes related to autophagy and ER

stress response that are crucial in PD pathogenesis (Postnikoff et al., 2017; Caviston and Holzbaur, 2009; Wang et al., 2014). The other proteins identified in the hPC are involved in different cellular pathways and diverse biological processes. An example is the outer membrane protein porin 1 (Por1), a mitochondrial protein important for ionic stability and mitochondrial integrity in Saccharomyces cerevisiae (Sánchez et al., 2001). The adsorption of mitochondrial proteins could suppose an interaction of $CeO_2$ NPs for mitochondrial membranes that could mediate benefic effects on mitochondrial morphology, functioning and ROS production. Another interesting protein detected was Pma1, a plasma membrane ATPase having important roles for the regulation of peculiar yeast structure called eisosomes (Ferreira et al., 2001). Eisosomes have been suggested to function as organizing sites for endocytosis, and have roles in the regulation of sphingolipid synthesis and in the response to plasma membrane stress acting as sensor of plasma membrane stress (Berchtold et al., 2012; Fröhlich et al., 2009; Kamble et al., 2011). Plasma membrane and membrane-associated eisosome complexes are altered in PD models, reflecting a perturbation of membrane architecture upon formation of early α-syn inclusions (Melnik et al., 2020; Reynolds et al., 2011). The adsorption of Pma1 with $CeO_2$ NP confirmed the strong interaction with cellular membranes by $CeO_2$ NPs. Hypothetically the maintenance from the NPs of the plasma membrane architecture concomitant with α-syn stabilization in non-toxic conformations can contribute to the protective effects.

An accumulation of unfolded proteins in the ER triggers a direct interaction between Kar2 and these misfolded proteins, causing the dissociation of Kar 2 from Ire1. The dissociation of Kar2 from Ire1 permits his dimerization leading to his trans-autophosphorylation and to the activation of the RNase domain. When Ire1 is in this activated, state starts the mRNA splicing of Hac1, that activates the transcription of a subset of UPR-related genes linked to protein folding, secretion, ERAD, and lipid synthesis (Wu et al., 2014; Hwang and Qi, 2018). This pathway is extremely conserved and in human cells this pathway is regulated by Grp78, a Kar2 homolog (Wu et al., 2014; Rose et al., 1989). Different studies demonstrated that the dysregulation of the UPR pathway is directly linked with the onset of different ND including PD; a chronical UPR pathway activation (Hoozemans et al., 2007; Liu et al., 2021a) and the accumulation of unfolded species of α-syn is a crucial factor for the etiopathogenesis of the disease (Mercado et al., 2018; Selvaraj et al., 2012). From the analysis of post-mortem PD patients brain tissues, emerged a strong de-regulation of the Grp78 mRNA levels underlining the link between a UPR pathway dysregulation and PD insurgence that was also associated with a co-localization of Grp78 and α-syn (Baek et al., 2016). All this data irrevocably

suggested that the molecular interaction between $CeO_2$ NP and Kar2 in the hPC might represent a crucial element for $CeO_2$ NP protective effects in HiTox strain.

In a comparative proteomic study performed by Melnik et al. (2020) in different yeast models of ND emerged that the abundance of different proteins identified in the hPC of $CeO_2$ NPs (e.g., Kar2, Tdh3, Rpl2B, Pma1 and Cox2) was increased in the HiTox strain highlighting that $CeO_2$ NPs appear to bind important interactors that mediate the cellular response in syn-induced cells.

Moreover, in this study was made an immunoprecipitation assay in order to detect the protein that physically interacted with α-sin among these, there is the Kar2 protein. This experiment further emphasized the important involvement of Kar2 in PD (Melnik et al., 2020).

| Protein | Biological process | I.I. | p.I. |
|---|---|---|---|
| 40S ribosomal protein S14-A | RNA metabolism | 40.26 | 10.73 |
| 60S ribosomal protein L31-A | RNA metabolism | 42.44 | 9.99 |
| 60S ribosomal protein L35-B | RNA metabolism | 41.37 | 10.58 |
| 60S ribosomal protein L35-A | RNA metabolism | 41.37 | 10.58 |
| 40S ribosomal protein S17-B | RNA metabolism | 47.07 | 10.51 |
| 40S ribosomal protein S24-A | RNA metabolism | 15.06 | 10.51 |
| 60S ribosomal protein L29 | RNA metabolism | 16.46 | 11.32 |
| 60S ribosomal protein L30 | RNA metabolism | 25.57 | 9.8 |
| 60S ribosomal protein L24-A | RNA metabolism | 37.17 | 11.28 |
| 60S ribosomal protein L26-B | RNA metabolism | 28.5 | 10.47 |
| 60S ribosomal protein L34-B | RNA metabolism | 49.45 | 10.84 |
| 40S ribosomal protein S24-B | RNA metabolism | 15.06 | 10.51 |
| 40S ribosomal protein S14-B | RNA metabolism | 40.72 | 10.54 |
| 60S ribosomal protein L43-B | RNA metabolism | 37.93 | 10.43 |
| 60S ribosomal protein L22-A | RNA metabolism | 36.58 | 5.9 |
| 60S ribosomal protein L26-A | RNA metabolism | 28.5 | 10.57 |
| 40S ribosomal protein S17-A | RNA metabolism | 46.16 | 10.51 |
| 60S acidic ribosomal protein P2-alpha | RNA metabolism | 43.13 | 3.94 |
| RPL25 | RNA metabolism | 25.6 | 10.11 |
| 60S ribosomal protein L5 | RNA metabolism | 36.71 | 6.39 |
| 60S ribosomal protein L43-A | RNA metabolism | 36.88 | 10.43 |
| 40S ribosomal protein S8-A | RNA metabolism | 52.55 | 10.67 |
| 60S ribosomal protein L32 | RNA metabolism | 42.79 | 11.17 |
| 60S ribosomal protein L4-A | RNA metabolism | 31.96 | 10.64 |
| 40S ribosomal protein S11-B | RNA metabolism | 51.03 | 10.79 |
| 60S ribosomal protein L19-A | RNA metabolism | 41.15 | 11.35 |
| 40S ribosomal protein S6-B | RNA metabolism | 37.36 | 10.44 |
| 40S ribosomal protein S11-A | RNA metabolism | 51.03 | 10.79 |
| 40S ribosomal protein S8-B | RNA metabolism | 52.55 | 10.67 |
| 40S ribosomal protein S26-B | RNA metabolism | 55.89 | 10.9 |
| 40S ribosomal protein S26-A | RNA metabolism | 55.17 | 10.76 |
| RPL24B | RNA metabolism | 33.47 | 11.37 |
| 40S ribosomal protein S30-A | RNA metabolism | 29.74 | 11.68 |
| RPL38 | RNA metabolism | 31.86 | 10.93 |
| 40S ribosomal protein S30-B | RNA metabolism | 29.74 | 11.68 |
| GAPDH 3 | Glycolitic process | 27.13 | 6.49 |
| GAPDH 2 | Glycolitic process | 29 | 6.49 |
| Pyruvate kinase 1 | Glycolitic process | 22.38 | 7.54 |
| Cytochrome c oxidase subunit 2 | Respiratory chain component | 36.2 | 4.43 |
| Cytochrome c1, heme protein | Respiratory chain component | 34.19 | 6.25 |
| Cytochrome c oxidase subunit 4 | Respiratory chain component | 29.72 | 5.1 |
| Outer membrane protein porin 1 | Mitochondrial porin | 32.77 | 7.68 |
| Plasma membrane ATPase 1 | ATP binding/ proton export | 33.9 | 4.96 |
| V-ATPase a 1 subunit | ATP binding/ proton export | 30.64 | 5.28 |
| eEF1A | Traslation Elongation factor | 30.47 | 9.14 |
| Yef3/Elongation factor 3A | Traslation Elongation factor | 31.26 | 5.73 |
| eIF-5B | Translation initiation factor | 48.89 | 5.61 |
| Kar2 | Endoplasmic reticulum chaperone | 26.45 | 4.71 |
| Non-classical export protein 2 | Protein transport | 37.42 | 9.55 |
| ADY2 | Acetate/ ammonium transport | 33.04 | 5.01 |

| | |
|---|---|
| **I.I.** > 40 | **I.I.**=Instability Index > 40 for unstable protein |
| **p.I.**> 7 | **p.I.**=Isoelectric point > 7 for positive charge |

***Figure 54.*** Proteins identified in the hPC of $CeO_2$ NPs through LC-MS/MS analysis (see "Materials and Methods" for more details).

### *3.12.1 The relationship between CeO2 NP effects and Kar2 regulation*

To analyze the effects of $CeO_2$ NP treatment on Kar2 abundance in the HiTox strain, cells grown in inducing conditions for 6 or 24 h were treated with $CeO_2$ NPs (50 ng/µL); the whole cell extracts were isolated and analyzed using dot blot analysis (**Fig. 55**). Dot blot analysis shows that the expression of Kar2 protein is strongly increased already after 6 hours of treatment with $CeO_2$ NPs in HiTox strain. After 24 h of induction, in untreated samples was detected a slightly higher amount of Kar2 protein respect to the samples treated with $CeO_2$ NPs, indicating probably that the cell is trying to regulate the UPR pathway, in a context where the cells are dying due to a higher cellular proteotoxic stress.

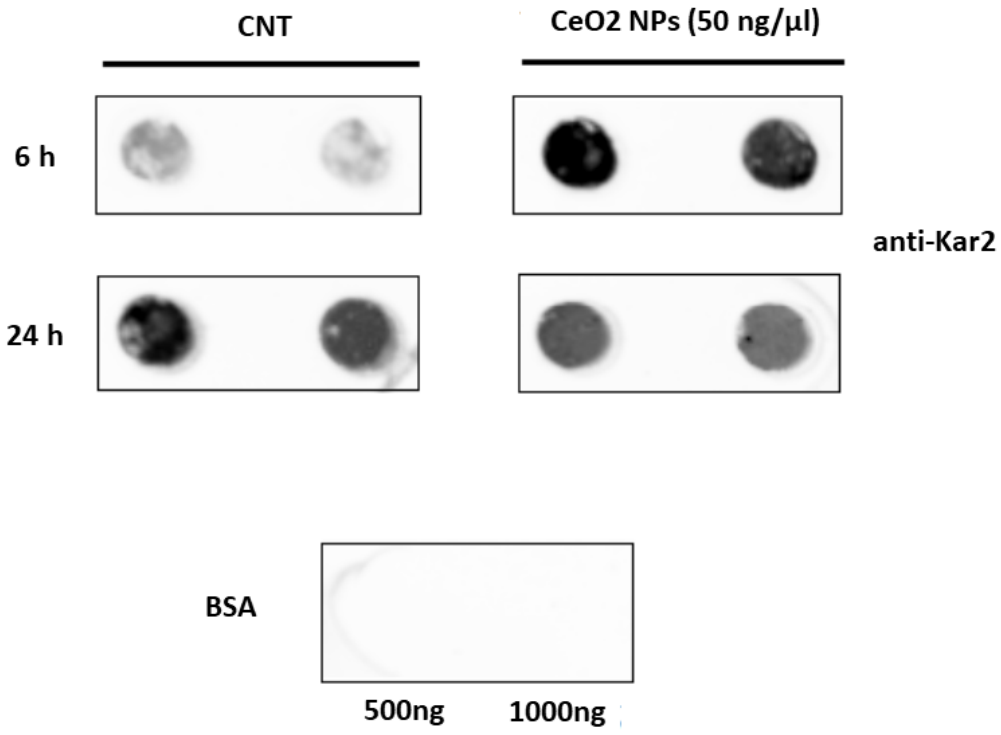


***Figure 55.*** α-Syn-expressing cells were grown with or without $CeO_2$ NPs (50 ng/µL) for 6 h or 24 h at 28 °C, after the treatments whole cell extracts were analyzed using an anti-Kar2 antibody. CNT indicates the control (untreated sample). BSA was utilized as negative control of the primary antibody reactivity.

In untreated cells a chronic activation of UPR pathway is related to pathological outcomes and finally leading to death from apoptosis (Hoozemans et al., 2007; Liu et al., 2021a). According to this

hypothesis in a work from Gorbatyuk et al. (2012) the over-expression of Grp78, the Kar homolog, in murine models reduced neuronal apoptotic events and resulted in an increase of dopaminergic neuron viability (Gorbatyuk et al., 2012).

We can finally hypothesize that the physical sequestration of Kar2 on the NPs surface early activates the UPR pathway allowing a more efficient management of the global cellular stress induced by α-syn aggregation and reducing the ER stress. This mechanism could be clarified by the results from Ruotolo et al. (2018) where the protein adsorption on QDs, another type of NPs, determined an up-regulation of the genes encoding 'corona' proteins as cellular attempt to replace the lack of proteins caused by the protein adsorption (Ruotolo et al., 2018).

### *3.13 $CeO_2$ NPs: a potential multi-target drug?*

In PD, α-syn aggregation affect an extremely complex set of pathways and cellular structures representing a central problem for the identification of beneficial compounds effective for the different stages and typologies of the disease. Other studies underlined the potential efficacy of different PD protective compounds able to target several dysregulated cellular pathways (Gitler et al., 2009; Kritzer et al., 2009; Su et al., 2010). In line with these considerations, it is possible to hypothesize a multi-target mechanism for $CeO_2$ NPs which makes these materials particularly promising for potential application in PD (Fig, 56). In the present work we have demonstrated that $CeO_2$ NPs can directly impact on α-syn aggregation, avoiding the formation of toxic oligomers, probably preserving the protein non-toxic physiological conformation. Another effect shown by $CeO_2$ NPs is the preservation of the mitochondrial morphology and activity that could prevent the ROS production. Also, the antioxidant autoregenerative activity of these NPs might be important to maintain cellular homeostasis, avoiding the vicious circle where the ROS generated by the mitochondrial dysfunction or by other proteotoxic events (as the protein aggregation) could in turn contribute to the formation of α-syn toxic aggregates. We can also theorize that the high membrane affinity of $CeO_2$ NPs could additionally facilitate the maintenance of the plasma membrane architecture and stabilize the α-syn in non-toxic conformation, subsequently reducing the plasma membrane stress. Finally, the interaction with Kar2 and the restoration and support of a correct UPR activation state could be an essential element to clarify the positive effects in viability and maintenance of the proper physiological status of the cells. The influence on UPR might avoid the engulfment of different pathways triggered by an unfolded proteins overwhelming, where a chronical UPR activation is related with apoptotic outcomes.

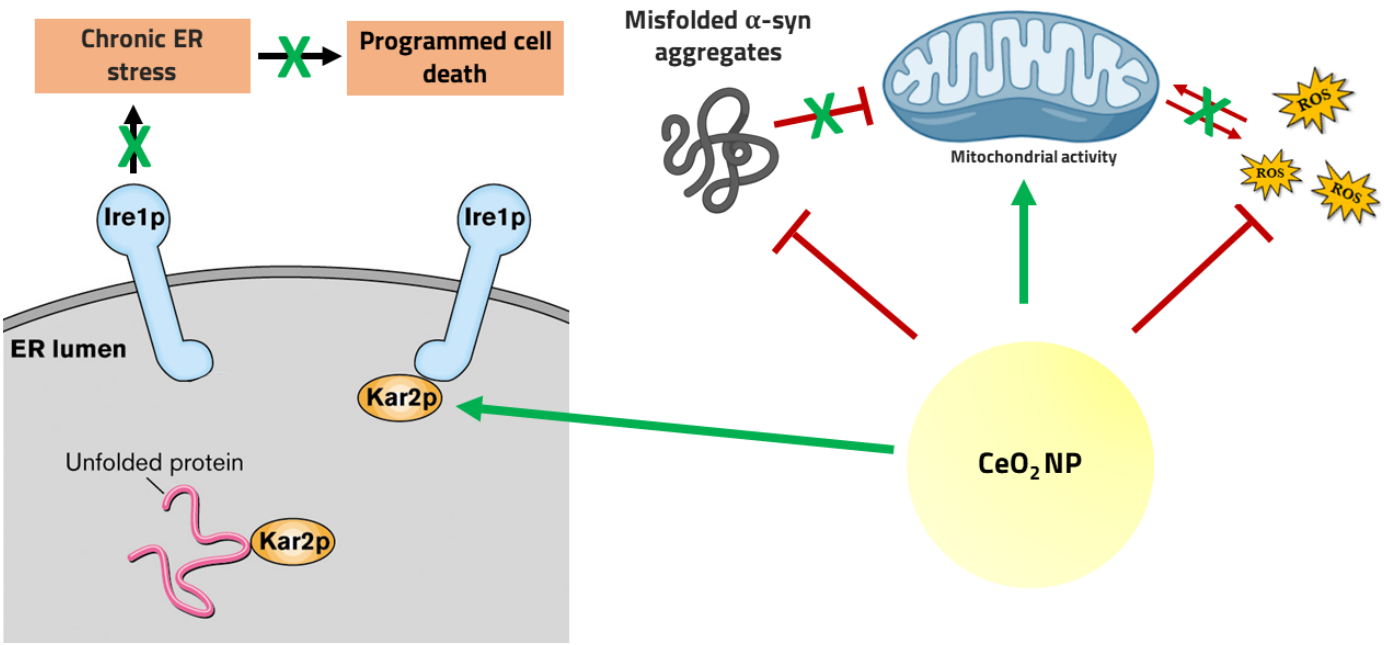


***Figure 56.*** Multi-target effects of $CeO_2$ NPs in yeast model of PD.

# CONCLUSIONS

NPs growing application in last decades and the linked increased potential exposition require a deeper knowledge of the effects and mechanism originating from the interactions with biological systems. In the first part of this work, we focused our attention on SAS NPs widely used in different fields and utilized as food additive under the acronym 'E551'. SAS NPs are made by two manufacturing methods resulting in the pyrogenic form (NM-203) produced by the thermal route or the hydrated products (precipitated silica, NM-200) produced by the wet route. These manufacturing processes lead to the production of small SAS nanoparticles (NPs) that interact to form larger agglomerates and aggregates normally greater than 100 nm. However, depending on starting material and synthesis method, it cannot be excluded that some aggregates of primary particles could be smaller than 100 nm in size (Additives et al., 2018). NM-200 and NM-203 toxicity was evaluated in different human cell lines. Especially in THP-1 cells, a human monocytic cell line differentiated into macrophages, NM-203 exhibited greater cytotoxicity than NM-200. In order to better comprehend the toxicity mechanism exerted by SAS NPs we have analyzed the composition of hPC of SAS NPs. The identification of SAS NPs hPC composition was conducted by an *in vitro* binding assay using protein extracts obtained from THP-1 cells. We have observed that NM-203 quantitatively adsorbs on their surface more proteins than NM-200 (two-fold increment), although the corona protein composition is the same for both SAS NPs. The proteins of hPC identified by mass spectrometry were RNA-binding proteins, proteins involved in translation and chaperoning processes and structural proteins implicated in cell shape and motility. These 'corona' proteins show an isoelectric point higher than 7, thus a positive charge at physiological pH, highlighting that the protein adsorption on the surface of negatively charged NM-200 and NM-203 is driven by electrostatic interactions. In addition, many of the identified proteins exhibited a high frequency of intrinsically disordered regions that could mediate the protein adsorption to SAS NPs by hydrophobic interactions, especially for NM-203 which has a more hydrophobic surface due to the presence of siloxane bridges created during the thermal synthesis method. The high structural flexibility that characterizes this typology of proteins might importantly contribute to the high affinity binding on NPs allowing a better surrounding on the surface. A deeper analysis showed that most of the proteins identified are constituents of specialized actin-rich structures of the macrophages called 'podosomes' that are involved in many roles, as phagocytosis, migration, and adhesion to the extracellular matrix (Linder et al., 2000; Veillat et al., 2015; Schachtner et al., 2013).

Among these proteins we found hnRNP K, an RNA-binding protein playing a role in the nuclear metabolism of RNAs but also highly represented in the podosomes (Cervero et al., 2012). We conducted confocal microscope and western blot analysis to evaluate the effects of SAS NP treatment on the abundance of two representative podosome-related proteins, as actin and hnRNP K. We have observed a reduction of the levels of both proteins and a de-localization and de-structuration of actin filaments, with the formation of punctuate structures. To evaluate the effects of SAS NPs on macrophage functionality we assayed the phagocytosis by measuring the internalization of fluorescent latex beads by the THP-1 cells after the treatment with SAS NPs. The confocal microscopy analysis showed a nearly complete block of the phagocytic process also at low dosage of both silica NPs. In conclusion, we have observed an increased cytotoxicity and protein binding of NM-203 compared to NM-200 that could be attributed to a higher surface reactivity of NM-203. Hydrophilic and hydrophobic interactions promote the tight adsorption on the surface of SAS NPs of proteins involved in crucial metabolic pathways for the macrophage functionality. In this scenario peculiar macrophagic structures like podosomes that mediates different processes like, cell–matrix adhesion, extracellular matrix degradation, migration, infiltration and also probably phagocytosis might be involved in the SAS NP toxicity mechanism.

The relationship between NPs, PC and intrinsically disordered proteins (IDP) might be important for NP applications in the biomedical field. α-Syn is one of the most known IDP representing the major component of Lewy bodies (LB), a histological hallmark of Parkinson's Disease (PD). This typical IDP in pathological conditions, undergo a series of lipid-dependent conformational changes leading to the formation of β-sheet-rich aggregates (α-syn oligomers), considered the most neurotoxic forms of α-syn. (Longhena et al., 2020; Bartels, 2019). SAS NPs interaction with α-syn *in vitro* is accompanied by enhanced aggregation propensity (Vitali et al., 2018). On the other hand, a recent work applying molecular docking simulations reported that $CeO_2$ NPs best fit with the active site of α-syn (Kaushik et al., 2018).

The second part of this work was then focused to study the potential biomedical application of $CeO_2$ NPs. These NPs show anti-oxidant properties and neuroprotective effects and are able to cross the BBB (Celardo et al., 2011; Lord et al., 2021; Heckman et al., 2013; Naz et al., 2017), and also highly biocompatible (Cordelli et al., 2017; Graham et al., 2014; Modrzynska et al., 2018). Another important trait of $CeO_2$ NPs is their self-regenerating antioxidant activity (Celardo et al., 2011; Lord et al., 2021), thanks to the cyclic redox switch between $Ce^{3+}$ and $Ce^{4+}$ state that occur on the NPs surface (Korsvik et al., 2007; Baldim et al., 2018). All these characteristics potentially configure $CeO_2$

NPs as a potential long-term antioxidant, tolerated by biological systems with a self-regenerative and radical scavenger activity, supplemented by the high surface volume ratio and consequent ability to catalyze a high quantity of reaction on his surface. We decided to test $CeO_2$ NPs in the HiTox yeast PD model (Outeiro and Lindquist, 2003; Auluck et al., 2010; Su et al., 2010) in order to comprehend in a molecular robust PD model the biological effects, interactions, and mechanisms that in future might be important for PD potential applications and comprehension. In our HiTox strain the treatment with SAS NPs did not ameliorate the viability and at high doses were observed further toxic effects. Conversely, $CeO_2$ NPs strongly counteracted α-syn-induced toxicity restoring oval-shaped budding morphology and cellular division after 48 h from the induction of α-syn expression (and NP treatment). After a few hours of exposure (4 h) in 'inducing' conditions, we observed that cells were 'caged' by $CeO_2$ NPs, firmly bound to the outside of the cells. This effect disappeared after 48 h treatment indicating that CeO2 NPs can be internalized in a time-dependent manner, as conformed by flow-cytometry analysis. Fluorescence microscopy analysis showed that the treatment with $CeO_2$ NPs re-localized α-syn at the plasma membrane level and strongly counteracted α-syn foci formation. In line with these results, dot blot analysis revealed that $CeO_2$ NP treatment did not affect the total protein expression levels, but drastically reduced the amounts of toxic oligomeric forms of α-syn. In human neurons, α-syn toxicity is associated to mitochondrial dysfunction and reactive oxygen species (ROS) overproduction. In our PD model, α-syn overexpression disrupts the tubular mitochondrial morphology and alters his functionality. Using a yeast PD model transformed with a plasmid expressing a mitochondrial-targeted Red fluorescent protein (mtRFP) we have observed that the treatment with $CeO_2$ NPs NP restored the mitochondrial morphology. Using a specific dye detecting different radical oxygen species, we have also observed that NP treatment decreased ROS accumulation in our PD model. Aggresomes are proteinaceous cytoplasmic inclusions formed when the protein degradation system of the cell is overwhelmed. Persistence or aberrant aggresome formation contributes to neurodegenerative disease. Using an aggresome-specific dye (Proteostat) we have observed that aggresomes were drastically reduced after the NP treatment suggesting the reestablishment of the protein engulfment state. We also analyzed the composition of hPC formed on the surface of $CeO_2$ NPs. Dot blot analysis with an anti-α-syn antibody detected the presence of α-syn in hPC, demonstrating a direct interaction between $CeO_2$ NPs and α-syn. In addition to α-syn, mass spectrometry analysis of hPC identified yeast proteins involved in translation, energetic (fermentative and respiratory) metabolism or the Unfolded Protein Response (UPR) pathway. UPR is a stress response pathway induced by

accumulation of misfolded proteins in the endoplasmic reticulum (ER). This pathway is highly triggered in many neurodegenerative diseases and a chronic ER stress can lead to programmed cell death. In particular, in the hPC of CeO2 NPs was detected the presence of Kar2, an important negative regulator of the UPR pathway. Dot Blot analysis showed an increased abundance of Kar2, after few hours of the treatment with $CeO_2$ NPs and a regulation of his abundance after long time of exposition. These results are in line with the observations where the upregulation of Grp78 (the human homolog of Kar2) significantly prevented loss of dopaminergic neurons (Gorbatyuk et al., 2012). We can thus hypothesize an important effect of $CeO_2$ NPs on the UPR pathway regulation that avoid a chronical activation of UPR. In conclusion, it is therefore possible that the $CeO_2$ NPs may have a multi-target mode-of-action. In fact, $CeO_2$ NPs play their role on different levels acting directly on the aggregation of synuclein, avoiding the formation of his toxic oligomers, preserving the mitochondrial activity, and preventing the generation of ROS. Finally, the interaction with KAR2 and the recovery of the correct UPR activation state could be crucial to explain the positive effects in viability avoiding apoptosis triggers and maintaining a correct physiological state of the cells.

# BIBLIOGRAPHY


Additives, E.P.o.F., Food, N.S.a.t., Younes, M., Aggett, P., Aguilar, F., Crebelli, R., Dusemund, B., Filipič, M., Frutos, M.J., Galtier, P., et al. (2018). Re-evaluation of silicon dioxide (E 551) as a food additive. EFSA Journal *16*, e05088.

Ahsan, S.M., Rao, C.M., Ahmad, M.F. (2018). Nanoparticle-Protein Interaction: The Significance and Role of Protein Corona. Adv Exp Med Biol *1048*, 175-198.

Albers, P., Maier, M., Reisinger, M., Hannebauer, B., Weinand, R. (2015). Physical boundaries within aggregates–differences between amorphous, para-crystalline, and crystalline Structures. Crystal Research and Technology *50*, 846-865.

Aliakbari, F., Mohammad-Beigi, H., Rezaei-Ghaleh, N., Becker, S., Dehghani Esmatabad, F., Eslampanah Seyedi, H.A., Bardania, H., Tayaranian Marvian, A., Collingwood, J.F., Christiansen, G., et al. (2018). The potential of zwitterionic nanoliposomes against neurotoxic alpha-synuclein aggregates in Parkinson's Disease. Nanoscale *10*, 9174-9185.

Allen, L.A., Aderem, A. (1996). Molecular definition of distinct cytoskeletal structures involved in complement- and Fc receptor-mediated phagocytosis in macrophages. J Exp Med *184*, 627-637.

Allendoerfer, K.L., Su, L.J., Lindquist, S. 2008. Yeast Cells as a Discovery Platform for Parkinson's Disease and other Protein Misfolding Diseases. *Parkinson's Disease.* Elsevier.

Álvarez, Y.D., Fauerbach, J.A., Pellegrotti, J.s.V., Jovin, T.M., Jares-Erijman, E.A., Stefani, F.D. (2013). Influence of gold nanoparticles on the kinetics of α-synuclein aggregation. Nano letters *13*, 6156-6163.

Aoyama, M., Hata, K., Higashisaka, K., Nagano, K., Yoshioka, Y., Tsutsumi, Y. (2016). Clusterin in the protein corona plays a key role in the stealth effect of nanoparticles against phagocytes. Biochem Biophys Res Commun *480*, 690-695.

Ardley, H.C., Scott, G.B., Rose, S.A., Tan, N.G., Markham, A.F., Robinson, P.A. (2003). Inhibition of proteasomal activity causes inclusion formation in neuronal and non-neuronal cells overexpressing Parkin. Mol Biol Cell *14*, 4541-4556.

Arumugam, A., Karthikeyan, C., Hameed, A.S.H., Gopinath, K., Gowri, S., Karthika, V. (2015). Synthesis of cerium oxide nanoparticles using Gloriosa superba L. leaf extract and their structural, optical and antibacterial properties. Materials Science & Engineering C-Materials for Biological Applications *49*, 408-415.

Asati, A., Santra, S., Kaittanis, C., Nath, S., Perez, J.e.M. (2009). Oxidase-Like Activity of Polymer-Coated Cerium Oxide Nanoparticles The authors acknowledge funding by the National Institutes of Health (CA101781) and an UCF-NSTC Start Up Fund, all to JMP. Angewandte Chemie-German Edition *121*, 2344.

Assarsson, A., Pastoriza-Santos, I., Cabaleiro-Lago, C. (2014). Inactivation and adsorption of human carbonic anhydrase II by nanoparticles. Langmuir *30*, 9448-9456.

Auluck, P.K., Caraveo, G., Lindquist, S. (2010). α-Synuclein: membrane interactions and toxicity in Parkinson's disease. Annual review of cell and developmental biology *26*, 211-233.

Babcock, M., de Silva, D., Oaks, R., Davis-Kaplan, S., Jiralerspong, S., Montermini, L., Pandolfo, M., Kaplan, J. (1997). Regulation of mitochondrial iron accumulation by Yfh1p, a putative homolog of frataxin. Science *276*, 1709-1712.

Baek, J.H., Whitfield, D., Howlett, D., Francis, P., Bereczki, E., Ballard, C., Hortobágyi, T., Attems, J., Aarsland, D. (2016). Unfolded protein response is activated in L ewy body dementias. Neuropathology and applied neurobiology *42*, 352-365.

Baldim, V., Bedioui, F., Mignet, N., Margaill, I., Berret, J.-F. (2018). The enzyme-like catalytic activity of cerium oxide nanoparticles and its dependency on Ce 3+ surface area concentration. Nanoscale *10*, 6971-6980.

Balestrino, R., Schapira, A.H.V. (2020). Parkinson disease. Eur J Neurol *27*, 27-42.

Bartels, T. (2019). A traffic jam leads to Lewy bodies. Nat Neurosci *22*, 1043-1045.

Bartucci, R., Pantusa, M., Marsh, D., Sportelli, L. (2002). Interaction of human serum albumin with membranes containing polymer-grafted lipids: spin-label ESR studies in the mushroom and brush regimes. Biochim Biophys Acta *1564*, 237-242.

Bellucci, A., Bubacco, L., Longhena, F., Parrella, E., Faustini, G., Porrini, V., Bono, F., Missale, C., Pizzi, M. (2020). Nuclear factor-κB dysregulation and α-synuclein pathology: critical interplay in the pathogenesis of Parkinson's disease. Frontiers in aging neuroscience *12*, 68.

Bera, D., Qian, L., Tseng, T.-K., Holloway, P.H. (2010). Quantum dots and their multimodal applications: a review. Materials *3*, 2260-2345.

Bertoli, F., Davies, G.L., Monopoli, M.P., Moloney, M., Gun'ko, Y.K., Salvati, A., Dawson, K.A. (2014). Magnetic nanoparticles to recover cellular organelles and study the time resolved nanoparticle-cell interactome throughout uptake. Small *10*, 3307-3315.

Bianchi, M.G., Allegri, M., Costa, A.L., Blosi, M., Gardini, D., Del Pivo, C., Prina-Mello, A., Di Cristo, L., Bussolati, O., Bergamaschi, E. (2015). Titanium dioxide nanoparticles enhance macrophage activation by LPS through a TLR4-dependent intracellular pathway. Toxicology Research *4*, 385-398.

Bianchi, M.G., Chiu, M., Taurino, G., Ruotolo, R., Marmiroli, N., Bergamaschi, E., Cubadda, F., Bussolati, O. (2020). Pyrogenic and Precipitated Amorphous Silica Nanoparticles Differentially Affect Cell Responses to LPS in Human Macrophages. Nanomaterials *10*, 1395.

Birben, E., Sahiner, U.M., Sackesen, C., Erzurum, S., Kalayci, O. (2012). Oxidative stress and antioxidant defense. World Allergy Organ J *5*, 9-19.

Bitetto, G., Di Fonzo, A. (2020). Nucleo–cytoplasmic transport defects and protein aggregates in neurodegeneration. Translational Neurodegeneration *9*, 1-16.

Black, D.L. (2003). Mechanisms of alternative pre-messenger RNA splicing. Annu Rev Biochem *72*, 291-336.

Bloem, B.R., Okun, M.S., Klein, C. (2021). Parkinson's disease. Lancet *397*, 2284-2303.

Bodunde, O.P., Ikumapayi, O.M., Akinlabi, E.T., Oladapo, B.I., Adeoye, A.O., Fatoba, S.O. (2021). A futuristic insight into a "nano-doctor": A clinical review on medical diagnosis and devices using nanotechnology. Materials Today: Proceedings *44*, 1144-1153.

Boldridge, D. (2010). Morphological characterization of fumed silica aggregates. Aerosol Science and Technology *44*, 182-186.

Bomsztyk, K., Denisenko, O., Ostrowski, J. (2004). hnRNP K: one protein multiple processes. Bioessays *26*, 629-638.

Borzova, V.A., Markossian, K.A., Chebotareva, N.A., Kleymenov, S.Y., Poliansky, N.B., Muranov, K.O., Stein-Margolina, V.A., Shubin, V.V., Markov, D.I., Kurganov, B.I. (2016). Kinetics of Thermal Denaturation and Aggregation of Bovine Serum Albumin. PloS one *11*, e0153495.

Botstein, D., Chervitz, S.A., Cherry, M. (1997). Yeast as a model organism. Science *277*, 1259-1260.

Boudard, D., Aureli, F., Laurent, B., Sturm, N., Raggi, A., Antier, E., Lakhdar, L., Marche, P.N., Cottier, M., Cubadda, F., et al. (2019). Chronic Oral Exposure to Synthetic Amorphous Silica (NM-200) Results in Renal and Liver Lesions in Mice. Kidney Int Rep *4*, 1463-1471.

Brancolini, G., Kokh, D.B., Calzolai, L., Wade, R.C., Corni, S. (2012). Docking of ubiquitin to gold nanoparticles. ACS nano *6*, 9863-9878.

Braun, R.J. (2015). Ubiquitin-dependent proteolysis in yeast cells expressing neurotoxic proteins. Frontiers in molecular neuroscience *8*, 8.

Broen, J.C.A., van Laar, J.M. (2020). Mycophenolate mofetil, azathioprine and tacrolimus: mechanisms in rheumatology. Nat Rev Rheumatol *16*, 167-178.

Brzicova, T., Javorkova, E., Vrbova, K., Zajicova, A., Holan, V., Pinkas, D., Philimonenko, V., Sikorova, J., Klema, J., Topinka, J., et al. (2019). Molecular Responses in THP-1 Macrophage-Like Cells Exposed to Diverse Nanoparticles. Nanomaterials (Basel) *9*, 687.

Büttner, S., Bitto, A., Ring, J., Augsten, M., Zabrocki, P., Eisenberg, T., Jungwirth, H., Hutter, S., Carmona-Gutierrez, D., Kroemer, G. (2008). Functional mitochondria are required for α-synuclein toxicity in aging yeast. Journal of Biological Chemistry *283*, 7554-7560.

Buzea, C., Pacheco, II, Robbie, K. (2007). Nanomaterials and nanoparticles: sources and toxicity. Biointerphases *2*, MR17-71.

C Thomas, S., Kumar Mishra, P., Talegaonkar, S. (2015). Ceramic nanoparticles: fabrication methods and applications in drug delivery. Current pharmaceutical design *21*, 6165-6188.

Campbell, C.T., Peden, C.H. (2005). Chemistry. Oxygen vacancies and catalysis on ceria surfaces. Science *309*, 713-714.

Caracciolo, G., Farokhzad, O.C., Mahmoudi, M. (2017). Biological Identity of Nanoparticles In Vivo: Clinical Implications of the Protein Corona. Trends Biotechnol *35*, 257-264.

Carling, P.J., Mortiboys, H., Green, C., Mihaylov, S., Sandor, C., Schwartzentruber, A., Taylor, R., Wei, W., Hastings, C., Wong, S. (2020). Deep phenotyping of peripheral tissue facilitates mechanistic disease stratification in sporadic Parkinson's disease. Progress in neurobiology *187*, 101772.

Casals, E., Zeng, M., Parra-Robert, M., Fernandez-Varo, G., Morales-Ruiz, M., Jimenez, W., Puntes, V., Casals, G. (2020). Cerium Oxide Nanoparticles: Advances in Biodistribution, Toxicity, and Preclinical Exploration. Small *16*, e1907322.

Cassee, F.R., van Balen, E.C., Singh, C., Green, D., Muijser, H., Weinstein, J., Dreher, K. (2011). Exposure, Health and Ecological Effects Review of Engineered Nanoscale Cerium and Cerium Oxide Associated with its Use as a Fuel Additive. Critical reviews in toxicology *41*, 213-229.

Caviston, J.P., Holzbaur, E.L. (2009). Huntingtin as an essential integrator of intracellular vesicular trafficking. Trends in cell biology *19*, 147-155.

Cedervall, T., Lynch, I., Lindman, S., Berggard, T., Thulin, E., Nilsson, H., Dawson, K.A., Linse, S. (2007). Understanding the nanoparticle-protein corona using methods to quantify exchange rates and affinities of proteins for nanoparticles. Proceedings of the National Academy of Sciences of the United States of America *104*, 2050-2055.

Celardo, I., Pedersen, J.Z., Traversa, E., Ghibelli, L. (2011). Pharmacological potential of cerium oxide nanoparticles. Nanoscale *3*, 1411-1420.

Centre, J.R., Health, I.f., Protection, C., 2013. *Synthetic amorphous silicon dioxide (NM-200, NM-201, NM-202, NM-203, NM-204) : characterisation and physico-chemical properties : JRC repository : NM-series of representative manufactured nanomaterials*, Publications Office.

Cervero, P., Himmel, M., Kruger, M., Linder, S. (2012). Proteomic analysis of podosome fractions from macrophages reveals similarities to spreading initiation centres. Eur J Cell Biol *91*, 908-922.

Cha, C., Shin, S.R., Annabi, N., Dokmeci, M.R., Khademhosseini, A. (2013). Carbon-based nanomaterials: multifunctional materials for biomedical engineering. ACS nano *7*, 2891-2897.

Chanput, W., Mes, J.J., Wichers, H.J. (2014). THP-1 cell line: an in vitro cell model for immune modulation approach. Int Immunopharmacol *23*, 37-45.

Chapman, R.G., Ostuni, E., Takayama, S., Holmlin, R.E., Yan, L., Whitesides, G.M. (2000). Surveying for surfaces that resist the adsorption of proteins. Journal of the American Chemical Society *122*, 8303-8304.

Charbgoo, F., Ramezani, M., Darroudi, M. (2017). Bio-sensing applications of cerium oxide nanoparticles: Advantages and disadvantages. Biosens Bioelectron *96*, 33-43.

Chartier-Harlin, M.C., Kachergus, J., Roumier, C., Mouroux, V., Douay, X., Lincoln, S., Levecque, C., Larvor, L., Andrieux, J., Hulihan, M., et al. (2004). Alpha-synuclein locus duplication as a cause of familial Parkinson's disease. Lancet *364*, 1167-1169.

Checkoway, H., Lundin, J.I., Kelada, S.N. (2011). Neurodegenerative diseases. IARC scientific publications, 407-419.

Chu, Z., Huang, Y., Tao, Q., Li, Q. (2011). Cellular uptake, evolution, and excretion of silica nanoparticles in human cells. Nanoscale *3*, 3291-3299.

Ciofani, G., Genchi, G.G., Liakos, I., Cappello, V., Gemmi, M., Athanassiou, A., Mazzolai, B., Mattoli, V. (2013). Effects of cerium oxide nanoparticles on PC12 neuronal-like cells: proliferation, differentiation, and dopamine secretion. Pharm Res *30*, 2133-2145.

Clarke, M., Spudich, J.A. (1977). Nonmuscle contractile proteins: the role of actin and myosin in cell motility and shape determination. Annu Rev Biochem *46*, 797-822.

Cooper, A.A., Gitler, A.D., Cashikar, A., Haynes, C.M., Hill, K.J., Bhullar, B., Liu, K., Xu, K., Strathearn, K.E., Liu, F. (2006). α-Synuclein blocks ER-Golgi traffic and Rab1 rescues neuron loss in Parkinson's models. Science *313*, 324-328.

Corbo, C., Molinaro, R., Tabatabaei, M., Farokhzad, O.C., Mahmoudi, M. (2017). Personalized protein corona on nanoparticles and its clinical implications. Biomater Sci *5*, 378-387.

Corboy, M.J., Thomas, P.J., Wigley, W.C. 2005. Aggresome formation. *Ubiquitin-Proteasome Protocols.* Springer.

Cordelli, E., Keller, J., Eleuteri, P., Villani, P., Ma-Hock, L., Schulz, M., Landsiedel, R., Pacchierotti, F. (2017). No genotoxicity in rat blood cells upon 3-or 6-month inhalation exposure to CeO2 or BaSO4 nanomaterials. Mutagenesis *32*, 13-22.

Corma, A., Atienzar, P., Garcia, H., Chane-Ching, J.-Y. (2004). Hierarchically mesostructured doped CeO 2 with potential for solar-cell use. Nature materials *3*, 394-397.

Cosker, K.E., Fenstermacher, S.J., Pazyra-Murphy, M.F., Elliott, H.L., Segal, R.A. (2016). The RNA-binding protein SFPQ orchestrates an RNA regulon to promote axon viability. Nat Neurosci *19*, 690-696.

Cresto, N., Gardier, C., Gubinelli, F., Gaillard, M.C., Liot, G., West, A.B., Brouillet, E. (2019). The unlikely partnership between LRRK 2 and α-synuclein in Parkinson's disease. European Journal of Neuroscience *49*, 339-363.

Croissant, J.G., Butler, K.S., Zink, J.I., Brinker, C.J. (2020). Synthetic amorphous silica nanoparticles: toxicity, biomedical and environmental implications. Nature Reviews Materials *5*, 886-909.

D'Angelo, B., Santucci, S., Benedetti, E., Di Loreto, S., Phani, R., Falone, S., Amicarelli, F., Ceru, M.P., Cimini, A. (2009). Cerium oxide nanoparticles trigger neuronal survival in a human Alzheimer disease model by modulating BDNF pathway. Current Nanoscience *5*, 167-176.

D'Angelo, F., Vignaud, H., Di Martino, J., Salin, B., Devin, A., Cullin, C., Marchal, C. (2013). A yeast model for amyloid-β aggregation exemplifies the role of membrane trafficking and PICALM in cytotoxicity. Disease models & mechanisms *6*, 206-216.

Dao, N.N., Dai Luu, M., Nguyen, Q.K., Kim, B.S. (2011). UV absorption by cerium oxide nanoparticles/epoxy composite thin films. Advances in Natural Sciences: Nanoscience and Nanotechnology *2*, 045013.

Das, K., Roychoudhury, A. (2014). Reactive oxygen species (ROS) and response of antioxidants as ROS-scavengers during environmental stress in plants. Frontiers in environmental science *2*, 53.

Davidson, W.S., Jonas, A., Clayton, D.F., George, J.M. (1998). Stabilization of α-synuclein secondary structure upon binding to synthetic membranes. Journal of Biological Chemistry *273*, 9443-9449.

Davis-Smyth, T., Duncan, R.C., Zheng, T., Michelotti, G., Levens, D. (1996). The far upstream element-binding proteins comprise an ancient family of single-strand DNA-binding transactivators. J Biol Chem *271*, 31679-31687.

De Jong, W., Jacobsen, N., Wallin, H., Oomen, A., Brandon, E., Krystek, P., Apostolova, M., Karadjova, I., Cubadda, F., Aureli, F. (2013). NANOGENOTOX, deliverable 7: identification of target organs and biodistribution including ADME parameters, Final Report. National Institute for Public Health and Environment (RIVM), Bilthoven, The Netherlands.

De Temmerman, P.J., Van Doren, E., Verleysen, E., Van der Stede, Y., Francisco, M.A., Mast, J. (2012). Quantitative characterization of agglomerates and aggregates of pyrogenic and precipitated amorphous silica nanomaterials by transmission electron microscopy. J Nanobiotechnology *10*, 24.

Dexter, D.T., Wells, F.R., Agid, F., Agid, Y., Lees, A.J., Jenner, P., Marsden, C.D. (1987). Increased nigral iron content in postmortem parkinsonian brain. Lancet *2*, 1219-1220.

Di Cristo, L., Movia, D., Bianchi, M.G., Allegri, M., Mohamed, B.M., Bell, A.P., Moore, C., Pinelli, S., Rasmussen, K., Riego-Sintes, J. (2016). Proinflammatory effects of pyrogenic and precipitated amorphous silica nanoparticles in innate immunity cells. Toxicological Sciences *150*, 40-53.

Dixon, C., Mathias, N., Zweig, R.M., Davis, D.A., Gross, D.S. (2005). α-Synuclein targets the plasma membrane via the secretory pathway and induces toxicity in yeast. Genetics *170*, 47-59.

Dong, X., Wu, Z., Li, X., Xiao, L., Yang, M., Li, Y., Duan, J., Sun, Z. (2020). The Size-dependent Cytotoxicity of Amorphous Silica Nanoparticles: A Systematic Review of in vitro Studies. Int J Nanomedicine *15*, 9089-9113.

Dorsey, E.R., Sherer, T., Okun, M.S., Bloem, B.R. (2018). The Emerging Evidence of the Parkinson Pandemic. J. Parkinsons Dis. *8*, S3-S8.

Dowding, J., Song, W., Bossy, K., Karakoti, A., Kumar, A., Kim, A., Bossy, B., Seal, S., Ellisman, M., Perkins, G. (2014). Cerium oxide nanoparticles protect against A β-induced mitochondrial fragmentation and neuronal cell death. Cell Death & Differentiation *21*, 1622-1632.

Duan, J., Yu, Y., Li, Y., Huang, P., Zhou, X., Peng, S., Sun, Z. (2014). Silica nanoparticles enhance autophagic activity, disturb endothelial cell homeostasis and impair angiogenesis. Part Fibre Toxicol *11*, 50.

Dutta, P., Pal, S., Seehra, M., Shi, Y., Eyring, E., Ernst, R. (2006). Concentration of Ce3+ and oxygen vacancies in cerium oxide nanoparticles. Chemistry of Materials *18*, 5144-5146.

Ealia, S.A.M., Saravanakumar, M. A review on the classification, characterisation, synthesis of nanoparticles and their application. IOP Conference Series: Materials Science and Engineering, 2017. IOP Publishing, 032019.

Ehrnhoefer, D.E., Bieschke, J., Boeddrich, A., Herbst, M., Masino, L., Lurz, R., Engemann, S., Pastore, A., Wanker, E.E. (2008). EGCG redirects amyloidogenic polypeptides into unstructured, off-pathway oligomers. Nature structural & molecular biology *15*, 558-566.

Esch, F., Fabris, S., Zhou, L., Montini, T., Africh, C., Fornasiero, P., Comelli, G., Rosei, R. (2005). Electron localization determines defect formation on ceria substrates. Science *309*, 752-755.

Exner, N., Lutz, A.K., Haass, C., Winklhofer, K.F. (2012). Mitochondrial dysfunction in Parkinson's disease: molecular mechanisms and pathophysiological consequences. EMBO J *31*, 3038-3062.

Fam, S.Y., Chee, C.F., Yong, C.Y., Ho, K.L., Mariatulqabtiah, A.R., Tan, W.S. (2020). Stealth Coating of Nanoparticles in Drug-Delivery Systems. Nanomaterials (Basel) *10*, 787.

Fan, X., Xiong, H., Wei, J., Gao, X., Feng, Y., Liu, X., Zhang, G., He, Q.-Y., Xu, J., Liu, L. (2015). Cytoplasmic hnRNPK interacts with GSK3β and is essential for the osteoclast differentiation. Scientific reports *5*, 1-17.

Fanning, S., Selkoe, D., Dettmer, U. (2021). Vesicle trafficking and lipid metabolism in synucleinopathy. Acta Neuropathol *141*, 491-510.

Farahmandjou, M., Zarinkamar, M., Firoozabadi, T.P. (2016). Synthesis of Cerium Oxide (CeO2) nanoparticles using simple CO-precipitation method. Revista mexicana de física *62*, 496-499.

Farcal, L., Torres Andon, F., Di Cristo, L., Rotoli, B.M., Bussolati, O., Bergamaschi, E., Mech, A., Hartmann, N.B., Rasmussen, K., Riego-Sintes, J., et al. (2015). Comprehensive In Vitro Toxicity Testing of a Panel of Representative Oxide Nanomaterials: First Steps towards an Intelligent Testing Strategy. PloS one *10*, e0127174.

Fatieiev, Y., Croissant, J.G., Alamoudi, K., Khashab, N.M. (2017). Cellular Internalization and Biocompatibility of Periodic Mesoporous Organosilica Nanoparticles with Tunable Morphologies: From Nanospheres to Nanowires. ChemPlusChem *82*, 631-637.

Federico, A., Cardaioli, E., Da Pozzo, P., Formichi, P., Gallus, G.N., Radi, E. (2012). Mitochondria, oxidative stress and neurodegeneration. J Neurol Sci *322*, 254-262.

Fleischer, C.C., Payne, C.K. (2014). Secondary structure of corona proteins determines the cell surface receptors used by nanoparticles. The Journal of Physical Chemistry B *118*, 14017-14026.

Fonseca-Ornelas, L., Eisbach, S.E., Paulat, M., Giller, K., Fernández, C.O., Outeiro, T.F., Becker, S., Zweckstetter, M. (2014). Small molecule-mediated stabilization of vesicle-associated helical α-synuclein inhibits pathogenic misfolding and aggregation. Nature communications *5*, 1-11.

Foroozandeh, P., Aziz, A.A. (2018). Insight into cellular uptake and intracellular trafficking of nanoparticles. Nanoscale research letters *13*, 1-12.

Friedrich, R.P., Janko, C., Poettler, M., Tripal, P., Zaloga, J., Cicha, I., Durr, S., Nowak, J., Odenbach, S., Slabu, I., et al. (2015). Flow cytometry for intracellular SPION quantification: specificity and sensitivity in comparison with spectroscopic methods. Int J Nanomedicine *10*, 4185-4201.

Gagner, J.E., Lopez, M.D., Dordick, J.S., Siegel, R.W. (2011). Effect of gold nanoparticle morphology on adsorbed protein structure and function. Biomaterials *32*, 7241-7252.

Gao, G., Chen, R., He, M., Li, J., Wang, L., Sun, T. (2019). Gold nanoclusters for Parkinson's disease treatment. Biomaterials *194*, 36-46.

Gao, H.-M., Zhang, F., Zhou, H., Kam, W., Wilson, B., Hong, J.-S. (2011). Neuroinflammation and α-synuclein dysfunction potentiate each other, driving chronic progression of neurodegeneration in a mouse model of Parkinson's disease. Environmental health perspectives *119*, 807-814.

García-Álvarez, R., Vallet-Regí, M. (2021). Hard and Soft Protein Corona of Nanomaterials: Analysis and Relevance. Nanomaterials *11*, 888.

García-Mata, R., Bebök, Z., Sorscher, E.J., Sztul, E.S. (1999). Characterization and Dynamics of Aggresome Formation by a Cytosolic Gfp-Chimera✪. Journal of Cell Biology *146*, 1239-1254.

Ge, C., Du, J., Zhao, L., Wang, L., Liu, Y., Li, D., Yang, Y., Zhou, R., Zhao, Y., Chai, Z., et al. (2011). Binding of blood proteins to carbon nanotubes reduces cytotoxicity. Proc Natl Acad Sci U S A *108*, 16968-16973.

Gerashchenko, B.I., Gun'ko, V.M., Gerashchenko, II, Mironyuk, I.F., Leboda, R., Hosoya, H. (2002). Probing the silica surfaces by red blood cells. Cytometry *49*, 56-61.

Ghosh, S., Ray, M., Das, M.R., Chakrabarti, A., Khan, A.H., Sarma, D.D., Acharya, S. (2014). Modulation of glyceraldehyde-3-phosphate dehydrogenase activity by surface functionalized quantum dots. Phys Chem Chem Phys *16*, 5276-5283.

Gitler, A.D., Bevis, B.J., Shorter, J., Strathearn, K.E., Hamamichi, S., Su, L.J., Caldwell, K.A., Caldwell, G.A., Rochet, J.-C., McCaffery, J.M. (2008). The Parkinson's disease protein α-synuclein disrupts cellular Rab homeostasis. Proceedings of the National Academy of Sciences *105*, 145-150.

Gitler, A.D., Chesi, A., Geddie, M.L., Strathearn, K.E., Hamamichi, S., Hill, K.J., Caldwell, K.A., Caldwell, G.A., Cooper, A.A., Rochet, J.-C. (2009). α-Synuclein is part of a diverse and highly conserved interaction network that includes PARK9 and manganese toxicity. Nature genetics *41*, 308-315.

Goffeau, A., Barrell, B.G., Bussey, H., Davis, R.W., Dujon, B., Feldmann, H., Galibert, F., Hoheisel, J.D., Jacq, C., Johnston, M. (1996). Life with 6000 genes. Science *274*, 546-567.

Goodridge, H.S., Underhill, D.M., Touret, N. (2012). Mechanisms of Fc Receptor and Dectin-1 Activation for Phagocytosis. Traffic *13*, 1062-1071.

Gorbatyuk, M.S., Shabashvili, A., Chen, W., Meyers, C., Sullivan, L.F., Salganik, M., Lin, J.H., Lewin, A.S., Muzyczka, N., Gorbatyuk, O.S. (2012). Glucose regulated protein 78 diminishes α-synuclein neurotoxicity in a rat model of Parkinson disease. Molecular Therapy *20*, 1327-1337.

Graham, U.M., Tseng, M.T., Jasinski, J.B., Yokel, R.A., Unrine, J.M., Davis, B.H., Dozier, A.K., Hardas, S.S., Sultana, R., Grulke, E.A., et al. (2014). In Vivo Processing of Ceria Nanoparticles inside Liver: Impact on Free-Radical Scavenging Activity and Oxidative Stress. ChemPlusChem *79*, 1083-1088.

Graveley, B.R. (2000). Sorting out the complexity of SR protein functions. Rna *6*, 1197-1211.

Greenland, J.C., Cutting, E., Kadyan, S., Bond, S., Chhabra, A., Williams-Gray, C.H. (2020). Azathioprine immunosuppression and disease modification in Parkinson's disease (AZA-PD): a randomised double-blind placebo-controlled phase II trial protocol. BMJ open *10*, e040527.

Grimm, C., Chari, A., Pelz, J.P., Kuper, J., Kisker, C., Diederichs, K., Stark, H., Schindelin, H., Fischer, U. (2013). Structural basis of assembly chaperone- mediated snRNP formation. Mol Cell *49*, 692-703.

Gu, X.-L., Long, C.-X., Sun, L., Xie, C., Lin, X., Cai, H. (2010). Astrocytic expression of Parkinson's disease-related A53T α-synuclein causes neurodegeneration in mice. Molecular brain *3*, 1-16.

Guan, G., Zhang, S., Liu, S., Cai, Y., Low, M., Teng, C.P., Phang, I.Y., Cheng, Y., Duei, K.L., Srinivasan, B.M., et al. (2015). Protein Induces Layer-by-Layer Exfoliation of Transition Metal Dichalcogenides. J Am Chem Soc *137*, 6152-6155.

Guo, C., Wang, J., Jing, L., Ma, R., Liu, X., Gao, L., Cao, L., Duan, J., Zhou, X., Li, Y., et al. (2018). Mitochondrial dysfunction, perturbations of mitochondrial dynamics and biogenesis involved in endothelial injury induced by silica nanoparticles. Environ Pollut *236*, 926-936.

Hailstone, R.K., DiFrancesco, A.G., Leong, J.G., Allston, T.D., Reed, K.J. (2009). A Study of Lattice Expansion in CeO2 Nanoparticles by Transmission Electron Microscopy. Journal of Physical Chemistry C *113*, 15155-15159.

Halliwell, B. (2007). Biochemistry of oxidative stress. Biochem Soc Trans *35*, 1147-1150.

Hanauer, S.B. (2006). Inflammatory bowel disease: epidemiology, pathogenesis, and therapeutic opportunities. Inflammatory bowel diseases *12*, S3-S9.

Hebron, M.L., Lonskaya, I., Moussa, C.E.-H. (2013). Nilotinib reverses loss of dopamine neurons and improves motor behavior via autophagic degradation of α-synuclein in Parkinson's disease models. Human molecular genetics *22*, 3315-3328.

Heckman, K.L., DeCoteau, W., Estevez, A., Reed, K.J., Costanzo, W., Sanford, D., Leiter, J.C., Clauss, J., Knapp, K., Gomez, C., et al. (2013). Custom cerium oxide nanoparticles protect against a free radical mediated autoimmune degenerative disease in the brain. ACS nano *7*, 10582-10596.

Hedrick, J.B., Sinha, S.P. (1994). Cerium-Based Polishing Compounds - Discovery to Manufacture. Journal of alloys and compounds *207*, 377-382.

Hegazy, M.A., Maklad, H.M., Samy, D.M., Abdelmonsif, D.A., El Sabaa, B.M., Elnozahy, F.Y. (2017). Cerium oxide nanoparticles could ameliorate behavioral and neurochemical impairments in 6-hydroxydopamine induced Parkinson's disease in rats. Neurochemistry international *108*, 361-371.

Heinicke, S., Livstone, M.S., Lu, C., Oughtred, R., Kang, F., Angiuoli, S.V., White, O., Botstein, D., Dolinski, K. (2007). The Princeton Protein Orthology Database (P-POD): a comparative genomics analysis tool for biologists. PloS one *2*, e766.

Heinrich, B., Zhang, Z., Raitskin, O., Hiller, M., Benderska, N., Hartmann, A.M., Bracco, L., Elliott, D., Ben-Ari, S., Soreq, H., et al. (2009). Heterogeneous nuclear ribonucleoprotein G regulates splice site selection by binding to CC(A/C)-rich regions in pre-mRNA. J Biol Chem *284*, 14303-14315.

Hirai, T., Yoshikawa, T., Nabeshi, H., Yoshida, T., Tochigi, S., Ichihashi, K.-i., Uji, M., Akase, T., Nagano, K., Abe, Y. (2012). Amorphous silica nanoparticles size-dependently aggravate atopic dermatitis-like skin lesions following an intradermal injection. Particle and fibre toxicology *9*, 1-11.

Hoozemans, J., Van Haastert, E., Eikelenboom, P., De Vos, R., Rozemuller, J., Scheper, W. (2007). Activation of the unfolded protein response in Parkinson's disease. Biochemical and Biophysical Research Communications *354*, 707-711.

Hsiao, I.L., Fritsch-Decker, S., Leidner, A., Al-Rawi, M., Hug, V., Diabaté, S., Grage, S.L., Meffert, M., Stoeger, T., Gerthsen, D. (2019). Biocompatibility of Amine-Functionalized Silica Nanoparticles: The Role of Surface Coverage. Small *15*, 1805400.

Hu, C.M.J., Zhang, L., Aryal, S., Cheung, C., Fang, R.H., Zhang, L.F. (2011). Erythrocyte membrane-camouflaged polymeric nanoparticles as a biomimetic delivery platform. Proceedings of the National Academy of Sciences of the United States of America *108*, 10980-10985.

Huang, Y.F., Cai, Y.B., Qiao, D.K., Liu, H. (2011). Morphology-controllable synthesis and characterization of CeO2 nanocrystals. Particuology *9*, 170-173.

Hulla, J.E., Sahu, S.C., Hayes, A.W. (2015). Nanotechnology: History and future. Hum Exp Toxicol *34*, 1318-1321.

Humans, I.W.G.o.t.E.o.C.R.t. (2012). Arsenic, metals, fibres, and dusts. IARC monographs on the evaluation of carcinogenic risks to humans *100*, 11.

Hussain, I., Singh, N.B., Singh, A., Singh, H., Singh, S.C. (2016). Green synthesis of nanoparticles and its potential application. Biotechnol Lett *38*, 545-560.

Hwang, J., Qi, L. (2018). Quality control in the endoplasmic reticulum: crosstalk between ERAD and UPR pathways. Trends in biochemical sciences *43*, 593-605.

Ibáñez, P., Lesage, S., Janin, S., Lohmann, E., Durif, F., Destée, A., Bonnet, A.-M., Brefel-Courbon, C., Heath, S., Zelenika, D. (2009). α-Synuclein gene rearrangements in dominantly inherited parkinsonism: frequency, phenotype, and mechanisms. Archives of neurology *66*, 102-108.

Ishida, T., Fujihara, N., Nishimura, T., Funabashi, H., Hirota, R., Ikeda, T., Kuroda, A. (2019). Live-cell imaging of macrophage phagocytosis of asbestos fibers under fluorescence microscopy. Genes and environment *41*, 1-11.

Jagaran, K., Singh, M. (2021). Nanomedicine for Neurodegenerative Disorders: Focus on Alzheimer's and Parkinson's Diseases. International Journal of Molecular Sciences *22*, 9082.

Jensen, K., Yahia, K., Christiansen, E., Jacobsen, N., Wallin, H., Guiot, C., Spalla, O., Witschger, O. (2011). Towards a method for detecting the potential genotoxicity of nanomaterials. Copenhagen, Denmark.

Jha, N.N., Kumar, R., Panigrahi, R., Navalkar, A., Ghosh, D., Sahay, S., Mondal, M., Kumar, A., Maji, S.K. (2017). Comparison of alpha-Synuclein Fibril Inhibition by Four Different Amyloid Inhibitors. ACS Chem Neurosci *8*, 2722-2733.

Jovičić, A., Mertens, J., Boeynaems, S., Bogaert, E., Chai, N., Yamada, S.B., Paul, J.W., Sun, S., Herdy, J.R., Bieri, G. (2015). Modifiers of C9orf72 dipeptide repeat toxicity connect nucleocytoplasmic transport defects to FTD/ALS. Nature neuroscience *18*, 1226-1229.

Jucaite, A., Svenningsson, P., Rinne, J.O., Cselényi, Z., Varnäs, K., Johnström, P., Amini, N., Kirjavainen, A., Helin, S., Minkwitz, M. (2015). Effect of the myeloperoxidase inhibitor AZD3241 on microglia: a PET study in Parkinson's disease. Brain *138*, 2687-2700.

Kakolyri, M., Margaritou, A., Tiligada, E. (2016). Dimethyl sulphoxide modifies growth and senescence and induces the non-revertible petite phenotype in yeast. FEMS Yeast Res *16*, fow008.

Kanhoush, R., Beenders, B., Perrin, C., Moreau, J., Bellini, M., Penrad-Mobayed, M. (2010). Novel domains in the hnRNP G/RBMX protein with distinct roles in RNA binding and targeting nascent transcripts. Nucleus *1*, 109-122.

Karakoti, A.S., Kuchibhatla, S.V.N.T., Babu, K.S., Seal, S. (2007). Direct synthesis of nanoceria in aqueous polyhydroxyl solutions. Journal of Physical Chemistry C *111*, 17232-17240.

Kaushik, A.C., Bharadwaj, S., Kumar, S., Wei, D.-Q. (2018). Nano-particle mediated inhibition of Parkinson's disease using computational biology approach. Scientific reports *8*, 1-8.

Keene, C.D., Rodrigues, C.M., Eich, T., Chhabra, M.S., Steer, C.J., Low, W.C. (2002). Tauroursodeoxycholic acid, a bile acid, is neuroprotective in a transgenic animal model of Huntington's disease. Proceedings of the National Academy of Sciences *99*, 10671-10676.

Khan, I., Saeed, K., Khan, I. (2019). Nanoparticles: Properties, applications and toxicities. Arabian journal of chemistry *12*, 908-931.

Khurana, V., Lindquist, S. (2010). Modelling neurodegeneration in Saccharomyces cerevisiae: why cook with baker's yeast? Nat Rev Neurosci *11*, 436-449.

Kilbourn, B.T. (2000). Cerium and cerium compounds. Kirk-Othmer Encyclopedia of Chemical Technology, 1-23.

Killinger, B.A., Melki, R., Brundin, P., Kordower, J.H. (2019). Endogenous alpha-synuclein monomers, oligomers and resulting pathology: let's talk about the lipids in the room. NPJ Parkinsons Dis. *5*, 23.

Kim, D., Yoo, J.M., Hwang, H., Lee, J., Lee, S.H., Yun, S.P., Park, M.J., Lee, M., Choi, S., Kwon, S.H. (2018). Graphene quantum dots prevent α-synucleinopathy in Parkinson's disease. Nature nanotechnology *13*, 812-818.

Kim, J.S., Adamcakova-Dodd, A., O'Shaughnessy, P.T., Grassian, V.H., Thorne, P.S. (2011). Effects of copper nanoparticle exposure on host defense in a murine pulmonary infection model. Part Fibre Toxicol *8*, 29.

Klein, G., Mathe, C., Biola-Clier, M., Devineau, S., Drouineau, E., Hatem, E., Marichal, L., Alonso, B., Gaillard, J.C., Lagniel, G., et al. (2016). RNA-binding proteins are a major target of silica nanoparticles in cell extracts. Nanotoxicology *10*, 1555-1564.

Klinge, S., Voigts-Hoffmann, F., Leibundgut, M., Arpagaus, S., Ban, N. (2011). Crystal structure of the eukaryotic 60S ribosomal subunit in complex with initiation factor 6. Science *334*, 941-948.

Knop, K., Hoogenboom, R., Fischer, D., Schubert, U.S. (2010). Poly(ethylene glycol) in Drug Delivery: Pros and Cons as Well as Potential Alternatives. Angewandte Chemie-International Edition *49*, 6288-6308.

Knott, G.J., Bond, C.S., Fox, A.H. (2016). The DBHS proteins SFPQ, NONO and PSPC1: a multipurpose molecular scaffold. Nucleic Acids Res *44*, 3989-4004.

Kobayashi, S. (2015). Choose Delicately and Reuse Adequately: The Newly Revealed Process of Autophagy. Biol Pharm Bull *38*, 1098-1103.

Kopac, T. (2021). Protein corona, understanding the nanoparticle-protein interactions and future perspectives: A critical review. International Journal of Biological Macromolecules *169*, 290-301.

Kopito, R.R. (2000). Aggresomes, inclusion bodies and protein aggregation. Trends Cell Biol *10*, 524-530.

Korecka, J.A., Thomas, R., Hinrich, A.J., Moskites, A.M., Macbain, Z.K., Hallett, P.J., Isacson, O., Hastings, M.L. (2020). Splice-Switching Antisense Oligonucleotides Reduce LRRK2 Kinase Activity in Human LRRK2 Transgenic Mice. Mol Ther Nucleic Acids *21*, 623-635.

Korsvik, C., Patil, S., Seal, S., Self, W.T. (2007). Superoxide dismutase mimetic properties exhibited by vacancy engineered ceria nanoparticles. Chem Commun (Camb), 1056-1058.

Kraft, C., Reggiori, F., Peter, M. (2009). Selective types of autophagy in yeast. Biochim Biophys Acta *1793*, 1404-1412.

Kreyling, W.G., Semmler-Behnke, M., Möller, W. (2006). Health implications of nanoparticles. Journal of Nanoparticle Research *8*, 543-562.

Kritzer, J.A., Hamamichi, S., McCaffery, J.M., Santagata, S., Naumann, T.A., Caldwell, K.A., Caldwell, G.A., Lindquist, S. (2009). Rapid selection of cyclic peptides that reduce α-synuclein toxicity in yeast and animal models. Nature chemical biology *5*, 655-663.

Kukalev, A., Nord, Y., Palmberg, C., Bergman, T., Percipalle, P. (2005). Actin and hnRNP U cooperate for productive transcription by RNA polymerase II. Nat Struct Mol Biol *12*, 238-244.

Kwon, H.J., Cha, M.-Y., Kim, D., Kim, D.K., Soh, M., Shin, K., Hyeon, T., Mook-Jung, I. (2016). Mitochondria-targeting ceria nanoparticles as antioxidants for Alzheimer's disease. ACS nano *10*, 2860-2870.

Landsiedel, R., Fabian, E., Ma-Hock, L., Wohlleben, W., Wiench, K., Oesch, F., van Ravenzwaay, B. (2012). Toxico-/biokinetics of nanomaterials. Archives of toxicology *86*, 1021-1060.

Lansbury, P.T., Lashuel, H.A. (2006). A century-old debate on protein aggregation and neurodegeneration enters the clinic. Nature *443*, 774-779.

Lashuel, H.A., Overk, C.R., Oueslati, A., Masliah, E. (2013). The many faces of alpha-synuclein: from structure and toxicity to therapeutic target. Nat. Rev. Neurosci. *14*, 38-48.

Lee, H.-J., Suk, J.-E., Patrick, C., Bae, E.-J., Cho, J.-H., Rho, S., Hwang, D., Masliah, E., Lee, S.-J. (2010). Direct transfer of α-synuclein from neuron to astroglia causes inflammatory responses in synucleinopathies. Journal of Biological Chemistry *285*, 9262-9272.

Lee, J.-S., Choi, S.-C. (2004). Crystallization behavior of nano-ceria powders by hydrothermal synthesis using a mixture of H2O2 and NH4OH. Materials Letters *58*, 390-393.

Lee, J.Y., Wasinger, V.C., Yau, Y.Y., Chuang, E., Yajnik, V., Leong, R.W. (2018). Molecular pathophysiology of epithelial barrier dysfunction in inflammatory bowel diseases. Proteomes *6*, 17.

Lee, S.S., Vizcarra, I.A., Huberts, D.H., Lee, L.P., Heinemann, M. (2012). Whole lifespan microscopic observation of budding yeast aging through a microfluidic dissection platform. Proceedings of the National Academy of Sciences *109*, 4916-4920.

Lee, V.M., Trojanowski, J.Q. (2006). Mechanisms of Parkinson's disease linked to pathological alpha-synuclein: new targets for drug discovery. Neuron *52*, 33-38.

Lesniak, A., Fenaroli, F., Monopoli, M.P., Aberg, C., Dawson, K.A., Salvati, A. (2012). Effects of the presence or absence of a protein corona on silica nanoparticle uptake and impact on cells. ACS nano *6*, 5845-5857.

Levy-Rimler, G., Viitanen, P., Weiss, C., Sharkia, R., Greenberg, A., Niv, A., Lustig, A., Delarea, Y., Azem, A. (2001). The effect of nucleotides and mitochondrial chaperonin 10 on the structure and chaperone activity of mitochondrial chaperonin 60. European journal of biochemistry *268*, 3465-3472.

Lew, A., Krutzik, P.O., Hart, M.E., Chamberlin, A.R. (2002). Increasing rates of reaction: microwave-assisted organic synthesis for combinatorial chemistry. J Comb Chem *4*, 95-105.

Li, S., Shu, F.J., Li, Z., Jaafar, L., Zhao, S., Dynan, W.S. (2017). Cell-type specific role of the RNA-binding protein, NONO, in the DNA double-strand break response in the mouse testes. DNA Repair (Amst) *51*, 70-78.

Li, Z., Liu, X., Ma, J., Zhang, T., Gao, X., Liu, L. (2018). hnRNPK modulates selective quality-control autophagy by downregulating the expression of HDAC6 in 293 cells. Int J Oncol *53*, 2200-2212.

Linder, S., Hufner, K., Wintergerst, U., Aepfelbacher, M. (2000). Microtubule-dependent formation of podosomal adhesion structures in primary human macrophages. J Cell Sci *113 Pt 23*, 4165-4176.

Linder, S., Wiesner, C. (2015). Tools of the trade: podosomes as multipurpose organelles of monocytic cells. Cellular and molecular life sciences *72*, 121-135.

Liu, R., Zhang, H.Y., Ji, Z.X., Rallo, R., Xia, T., Chang, C.H., Nel, A., Cohen, Y. (2013). Development of structure-activity relationship for metal oxide nanoparticles. Nanoscale *5*, 5644-5653.

Liu, S., Wang, Z., Jiang, X., Gan, J., Tian, X., Xing, Z., Yan, Y., Chen, J., Zhang, J., Wang, C., et al. (2021a). Denatured corona proteins mediate the intracellular bioactivities of nanoparticles via the unfolded protein response. Biomaterials *265*, 120452.

Liu, X., Lu, B., Fu, J., Zhu, X., Song, E., Song, Y. (2021b). Amorphous silica nanoparticles induce inflammation via activation of NLRP3 inflammasome and HMGB1/TLR4/MYD88/NF-kb signaling pathway in HUVEC cells. J Hazard Mater *404*, 124050.

Loftus Jr, E.V. (2004). Clinical epidemiology of inflammatory bowel disease: incidence, prevalence, and environmental influences. Gastroenterology *126*, 1504-1517.

Longhena, F., Faustini, G., Missale, C., Pizzi, M., Spano, P., Bellucci, A. (2017). The contribution of α-synuclein spreading to Parkinson's disease synaptopathy. Neural plasticity *2017*.

Longhena, F., Faustini, G., Brembati, V., Pizzi, M., Bellucci, A. (2020). The good and bad of therapeutic strategies that directly target α-synuclein. IUBMB life *72*, 590-600.

Lord, M.S., Berret, J.F., Singh, S., Vinu, A., Karakoti, A.S. (2021). Redox Active Cerium Oxide Nanoparticles: Current Status and Burning Issues. Small, e2102342.

Lu, X., Qian, J., Zhou, H., Gan, Q., Tang, W., Lu, J., Yuan, Y., Liu, C. (2011). In vitro cytotoxicity and induction of apoptosis by silica nanoparticles in human HepG2 hepatoma cells. Int J Nanomedicine *6*, 1889-1901.

Lundqvist, M., Stigler, J., Elia, G., Lynch, I., Cedervall, T., Dawson, K.A. (2008). Nanoparticle size and surface properties determine the protein corona with possible implications for biological impacts. Proc Natl Acad Sci U S A *105*, 14265-14270.

Lundqvist, M., Stigler, J., Cedervall, T., Berggard, T., Flanagan, M.B., Lynch, I., Elia, G., Dawson, K. (2011). The evolution of the protein corona around nanoparticles: a test study. ACS nano *5*, 7503-7509.

Mahmoudi, M., Shokrgozar, M.A., Sardari, S., Moghadam, M.K., Vali, H., Laurent, S., Stroeve, P. (2011). Irreversible changes in protein conformation due to interaction with superparamagnetic iron oxide nanoparticles. Nanoscale *3*, 1127-1138.

Mahmoudi, M., Sheibani, S., Milani, A.S., Rezaee, F., Gauberti, M., Dinarvand, R., Vali, H. (2015). Crucial role of the protein corona for the specific targeting of nanoparticles. Nanomedicine (Lond) *10*, 215-226.

Mahoney-Sánchez, L., Bouchaoui, H., Ayton, S., Devos, D., Duce, J.A., Devedjian, J.-C. (2021). Ferroptosis and its potential role in the physiopathology of Parkinson's Disease. Progress in neurobiology *196*, 101890.

Maiorano, G., Sabella, S., Sorce, B., Brunetti, V., Malvindi, M.A., Cingolani, R., Pompa, P.P. (2010). Effects of cell culture media on the dynamic formation of protein− nanoparticle complexes and influence on the cellular response. ACS nano *4*, 7481-7491.

Manzoni, C., Mamais, A., Dihanich, S., Abeti, R., Soutar, M.P.M., Plun-Favreau, H., Giunti, P., Tooze, S.A., Bandopadhyay, R., Lewis, P.A. (2013). Inhibition of LRRK2 kinase activity stimulates macroautophagy. Biochim Biophys Acta *1833*, 2900-2910.

Martin-Bastida, A., Ward, R.J., Newbould, R., Piccini, P., Sharp, D., Kabba, C., Patel, M.C., Spino, M., Connelly, J., Tricta, F. (2017). Brain iron chelation by deferiprone in a phase 2 randomised double-blinded placebo controlled clinical trial in Parkinson's disease. Scientific reports *7*, 1-9.

Masuda, S., Das, R., Cheng, H., Hurt, E., Dorman, N., Reed, R. (2005). Recruitment of the human TREX complex to mRNA during splicing. Genes Dev *19*, 1512-1517.

McNaught, K.S.P., Shashidharan, P., Perl, D.P., Jenner, P., Olanow, C.W. (2002). Aggresome-related biogenesis of Lewy bodies. European Journal of Neuroscience *16*, 2136-2148.

Melnik, A., Cappelletti, V., Vaggi, F., Piazza, I., Tognetti, M., Schwarz, C., Cereghetti, G., Ahmed, M.A., Soste, M., Matlack, K., et al. (2020). Comparative analysis of the intracellular responses to disease-related aggregation-prone proteins. J Proteomics *225*, 103862.

Mercado, G., Castillo, V., Soto, P., Lopez, N., Axten, J.M., Sardi, S.P., Hoozemans, J.J.M., Hetz, C. (2018). Targeting PERK signaling with the small molecule GSK2606414 prevents neurodegeneration in a model of Parkinson's disease. Neurobiol Dis *112*, 136-148.

Miceli, E., Kar, M., Calderon, M. (2017). Interactions of organic nanoparticles with proteins in physiological conditions. J Mater Chem B *5*, 4393-4405.

Milani, S., Bombelli, F.B., Pitek, A.S., Dawson, K.A., Radler, J. (2012). Reversible versus irreversible binding of transferrin to polystyrene nanoparticles: soft and hard corona. ACS nano *6*, 2532-2541.

Milowska, K., Grochowina, J., Katir, N., El Kadib, A., Majoral, J.-P., Bryszewska, M., Gabryelak, T. (2013). Viologen-phosphorus dendrimers inhibit α-synuclein fibrillation. Molecular pharmaceutics *10*, 1131-1137.

Min, H., Turck, C.W., Nikolic, J.M., Black, D.L. (1997). A new regulatory protein, KSRP, mediates exon inclusion through an intronic splicing enhancer. Genes & development *11*, 1023-1036.

Modrzynska, J., Berthing, T., Ravn-Haren, G., Kling, K., Mortensen, A., Rasmussen, R.R., Larsen, E.H., Saber, A.T., Vogel, U., Loeschner, K. (2018). In vivo-induced size transformation of cerium oxide nanoparticles in both lung and liver does not affect long-term hepatic accumulation following pulmonary exposure. PloS one *13*, e0202477.

Mohammad-Beigi, H., Hosseini, A., Adeli, M., Ejtehadi, M.R., Christiansen, G., Sahin, C., Tu, Z., Tavakol, M., Dilmaghani-Marand, A., Nabipour, I. (2019). Mechanistic understanding of the interactions between nano-objects with different surface properties and α-synuclein. ACS nano *13*, 3243-3256.

Mohammad-Beigi, H., Hayashi, Y., Zeuthen, C.M., Eskandari, H., Scavenius, C., Juul-Madsen, K., Vorup-Jensen, T., Enghild, J.J., Sutherland, D.S. (2020). Mapping and identification of soft corona proteins at nanoparticles and their impact on cellular association. Nature communications *11*, 1-16.

Molina, R.M., Konduru, N.V., Jimenez, R.J., Pyrgiotakis, G., Demokritou, P., Wohlleben, W., Brain, J.D. (2014). Bioavailability, distribution and clearance of tracheally instilled, gavaged or injected cerium dioxide nanoparticles and ionic cerium. Environmental Science: Nano *1*, 561-573.

Monopoli, M.P., Walczyk, D., Campbell, A., Elia, G., Lynch, I., Baldelli Bombelli, F., Dawson, K.A. (2011). Physical− chemical aspects of protein corona: relevance to in vitro and in vivo biological impacts of nanoparticles. Journal of the American Chemical Society *133*, 2525-2534.

Munusamy, S., Bhakyaraj, K., Vijayalakshmi, L., Stephen, A., Narayanan, V. (2014). Synthesis and characterization of cerium oxide nanoparticles using Curvularia lunata and their antibacterial properties. Int J Innov Res Sci Eng *2*, 318.

Murata, Y., Kotani, T., Ohnishi, H., Matozaki, T. (2014). The CD47–SIRPα signalling system: its physiological roles and therapeutic application. The Journal of Biochemistry *155*, 335-344.

Murugadoss, S., Lison, D., Godderis, L., Van Den Brule, S., Mast, J., Brassinne, F., Sebaihi, N., Hoet, P.H. (2017). Toxicology of silica nanoparticles: an update. Arch Toxicol *91*, 2967-3010.

Nabeshi, H., Yoshikawa, T., Arimori, A., Yoshida, T., Tochigi, S., Hirai, T., Akase, T., Nagano, K., Abe, Y., Kamada, H. (2011). Effect of surface properties of silica nanoparticles on their cytotoxicity and cellular distribution in murine macrophages. Nanoscale research letters *6*, 1-6.

Napierska, D., Thomassen, L.C., Lison, D., Martens, J.A., Hoet, P.H. (2010). The nanosilica hazard: another variable entity. Particle and fibre toxicology *7*, 1-32.

Naz, S., Beach, J., Heckert, B., Tummala, T., Pashchenko, O., Banerjee, T., Santra, S. (2017). Cerium oxide nanoparticles: a 'radical'approach to neurodegenerative disease treatment. Nanomedicine *12*, 545-553.

Nedelsky, N.B., Todd, P.K., Taylor, J.P. (2008). Autophagy and the ubiquitin-proteasome system: collaborators in neuroprotection. Biochim Biophys Acta *1782*, 691-699.

Nel, A.E., Mädler, L., Velegol, D., Xia, T., Hoek, E.M., Somasundaran, P., Klaessig, F., Castranova, V., Thompson, M. (2009). Understanding biophysicochemical interactions at the nano–bio interface. Nature materials *8*, 543-557.

Nikolaidis, A., Moschakis, T. (2017). Studying the denaturation of bovine serum albumin by a novel approach of difference-UV analysis. Food Chem *215*, 235-244.

Njoroge, J.M., Yourick, J.J., Principato, M.A. (2018). A flow cytometric analysis of macrophage–nanoparticle interactions in vitro: induction of altered Toll-like receptor expression. International journal of nanomedicine *13*, 8365.

O'Brien, J., Wilson, I., Orton, T., Pognan, F. (2000). Investigation of the Alamar Blue (resazurin) fluorescent dye for the assessment of mammalian cell cytotoxicity. Eur J Biochem *267*, 5421-5426.

Ogawa, T., Okumura, R., Nagano, K., Minemura, T., Izumi, M., Motooka, D., Nakamura, S., Iida, T., Maeda, Y., Kumanogoh, A. (2021). Oral intake of silica nanoparticles exacerbates intestinal inflammation. Biochemical and Biophysical Research Communications *534*, 540-546.

Olanow, C.W., Perl, D.P., DeMartino, G.N., McNaught, K.S.P. (2004). Lewy-body formation is an aggresome-related process: a hypothesis. The Lancet Neurology *3*, 496-503.

Ostrowski, P.P., Freeman, S.A., Fairn, G., Grinstein, S. (2019). Dynamic Podosome-Like Structures in Nascent Phagosomes Are Coordinated by Phosphoinositides. Dev Cell *50*, 397-410 e393.

Outeiro, T.F., Lindquist, S. (2003). Yeast cells provide insight into alpha-synuclein biology and pathobiology. Science *302*, 1772-1775.

Owens III, D.E., Peppas, N.A. (2006). Opsonization, biodistribution, and pharmacokinetics of polymeric nanoparticles. International journal of pharmaceutics *307*, 93-102.

Ozleyen, A., Yilmaz, Y.B., Tumer, T.B. (2021). Dataset on the differentiation of THP-1 monocytes to LPS inducible adherent macrophages and their capacity for NO/iNOS signaling. Data in Brief *35*, 106786.

Padmanabhan, P., Palanivel, M., Kumar, A., Mathe, D., Radda, G.K., Lim, K.L., Gulyas, B. (2020). Nanotheranostic agents for neurodegenerative diseases. Emerg Top Life Sci *4*, 645-675.

Palchetti, S., Colapicchioni, V., Digiacomo, L., Caracciolo, G., Pozzi, D., Capriotti, A.L., La Barbera, G., Lagana, A. (2016). The protein corona of circulating PEGylated liposomes. Biochim Biophys Acta *1858*, 189-196.

Passon, D.M., Lee, M., Rackham, O., Stanley, W.A., Sadowska, A., Filipovska, A., Fox, A.H., Bond, C.S. (2012). Structure of the heterodimer of human NONO and paraspeckle protein component 1 and analysis of its role in subnuclear body formation. Proc Natl Acad Sci U S A *109*, 4846-4850.

Peña, Á., Gewartowski, K., Mroczek, S., Cuéllar, J., Szykowska, A., Prokop, A., Czarnocki-Cieciura, M., Piwowarski, J., Tous, C., Aguilera, A. (2012). Architecture and nucleic acids recognition mechanism of the THO complex, an mRNP assembly factor. The EMBO journal *31*, 1605-1616.

Petroi, D., Popova, B., Taheri-Talesh, N., Irniger, S., Shahpasandzadeh, H., Zweckstetter, M., Outeiro, T.F., Braus, G.H. (2012). Aggregate clearance of α-synuclein in Saccharomyces cerevisiae depends more on autophagosome and vacuole function than on the proteasome. Journal of Biological Chemistry *287*, 27567-27579.

Pinals, R.L., Yang, D., Rosenberg, D.J., Chaudhary, T., Crothers, A.R., Iavarone, A.T., Hammel, M., Landry, M.P. (2020). Quantitative Protein Corona Composition and Dynamics on Carbon Nanotubes in Biological Environments. Angew Chem Int Ed Engl *59*, 23668-23677.

Pizzino, G., Irrera, N., Cucinotta, M., Pallio, G., Mannino, F., Arcoraci, V., Squadrito, F., Altavilla, D., Bitto, A. (2017). Oxidative Stress: Harms and Benefits for Human Health. Oxid Med Cell Longev *2017*, 8416763.

Poewe, W., Seppi, K., Tanner, C.M., Halliday, G.M., Brundin, P., Volkmann, J., Schrag, A.E., Lang, A.E. (2017). Parkinson disease. Nat Rev Dis Primers *3*, 17013.

Polymeropoulos, M.H., Lavedan, C., Leroy, E., Ide, S.E., Dehejia, A., Dutra, A., Pike, B., Root, H., Rubenstein, J., Boyer, R., et al. (1997). Mutation in the alpha-synuclein gene identified in families with Parkinson's disease. Science *276*, 2045-2047.

Radivojac, P., Obradovic, Z., Smith, D.K., Zhu, G., Vucetic, S., Brown, C.J., Lawson, J.D., Dunker, A.K. (2004). Protein flexibility and intrinsic disorder. Protein Sci *13*, 71-80.

Reed, K., Cormack, A., Kulkarni, A., Mayton, M., Sayle, D., Klaessig, F., Stadler, B. (2014). Exploring the properties and applications of nanoceria: is there still plenty of room at the bottom? Environmental Science: Nano *1*, 390-405.

Ritz, S., Schottler, S., Kotman, N., Baier, G., Musyanovych, A., Kuharev, J., Landfester, K., Schild, H., Jahn, O., Tenzer, S., et al. (2015). Protein corona of nanoparticles: distinct proteins regulate the cellular uptake. Biomacromolecules *16*, 1311-1321.

Rocca, A., Moscato, S., Ronca, F., Nitti, S., Mattoli, V., Giorgi, M., Ciofani, G. (2015). Pilot in vivo investigation of cerium oxide nanoparticles as a novel anti-obesity pharmaceutical formulation. Nanomedicine: nanotechnology, biology and medicine *11*, 1725-1734.

Rose, M.D., Misra, L.M., Vogel, J.P. (1989). KAR2, a karyogamy gene, is the yeast homolog of the mammalian BiP/GRP78 gene. Cell *57*, 1211-1221.

Ross, C.A., Poirier, M.A. (2004). Protein aggregation and neurodegenerative disease. Nat Med *10 Suppl*, S10-17.

Ruotolo, R., Pira, G., Villani, M., Zappettini, A., Marmiroli, N. (2018). Ring-shaped corona proteins influence the toxicity of engineered nanoparticles to yeast. Environmental Science: Nano *5*, 1428-1440.

Ruotolo, R., De Giorgio, G., Minato, I., Bianchi, M.G., Bussolati, O., Marmiroli, N. (2020). Cerium oxide nanoparticles rescue α-synuclein-induced toxicity in a yeast model of Parkinson's disease. Nanomaterials *10*, 235.

Saifi, M.A., Seal, S., Godugu, C. (2021). Nanoceria, the versatile nanoparticles: Promising biomedical applications. J Control Release *338*, 164-189.

Salton, M., Lerenthal, Y., Wang, S.Y., Chen, D.J., Shiloh, Y. (2010). Involvement of Matrin 3 and SFPQ/NONO in the DNA damage response. Cell cycle *9*, 1568-1576.

Salvati, A., Pitek, A.S., Monopoli, M.P., Prapainop, K., Bombelli, F.B., Hristov, D.R., Kelly, P.M., Åberg, C., Mahon, E., Dawson, K.A. (2013). Transferrin-functionalized nanoparticles lose their targeting capabilities when a biomolecule corona adsorbs on the surface. Nature nanotechnology *8*, 137-143.

Sanchez-Guajardo, V., Annibali, A., Jensen, P.H., Romero-Ramos, M. (2013). α-Synuclein vaccination prevents the accumulation of parkinson disease-like pathologic inclusions in striatum in association with regulatory T cell recruitment in a rat model. Journal of Neuropathology & Experimental Neurology *72*, 624-645.

Sanchez-Guzman, D., Giraudon--Colas, G.l., Marichal, L., Boulard, Y., Wien, F., Degrouard, J., Baeza-Squiban, A., Pin, S., Renault, J.P., Devineau, S. (2020). In situ analysis of weakly bound proteins reveals molecular basis of soft corona formation. ACS nano *14*, 9073-9088.

Sathe, A.G., Tuite, P., Chen, C., Ma, Y., Chen, W., Cloyd, J., Low, W.C., Steer, C.J., Lee, B.Y., Zhu, X.H. (2020). Pharmacokinetics, Safety, and Tolerability of Orally Administered Ursodeoxycholic Acid in Patients With Parkinson's Disease—A Pilot Study. The Journal of Clinical Pharmacology *60*, 744-750.

Sathyamurthy, S., Leonard, K.J., Dabestani, R.T., Paranthaman, M.P. (2005). Reverse micellar synthesis of cerium oxide nanoparticles. Nanotechnology *16*, 1960-1964.

Scaini, G., Fries, G.R., Valvassori, S.S., Zeni, C.P., Zunta-Soares, G., Berk, M., Soares, J.C., Quevedo, J. (2017). Perturbations in the apoptotic pathway and mitochondrial network dynamics in peripheral blood mononuclear cells from bipolar disorder patients. Transl Psychiatry *7*, e1111.

Schachtner, H., Calaminus, S.D., Thomas, S.G., Machesky, L.M. (2013). Podosomes in adhesion, migration, mechanosensing and matrix remodeling. Cytoskeleton (Hoboken) *70*, 572-589.

Schipper, M.L., Iyer, G., Koh, A.L., Cheng, Z., Ebenstein, Y., Aharoni, A., Keren, S., Bentolila, L.A., Li, J., Rao, J., et al. (2009). Particle size, surface coating, and PEGylation influence the biodistribution of quantum dots in living mice. Small *5*, 126-134.

Schlichtmann, B.W., Hepker, M., Palanisamy, B.N., John, M., Anantharam, V., Kanthasamy, A.G., Narasimhan, B., Mallapragada, S.K. (2021). Nanotechnology-mediated therapeutic strategies against synucleinopathies in neurodegenerative disease. Current Opinion in Chemical Engineering *31*, 100673.

Schwotzer, D., Ernst, H., Schaudien, D., Kock, H., Pohlmann, G., Dasenbrock, C., Creutzenberg, O. (2017). Effects from a 90-day inhalation toxicity study with cerium oxide and barium sulfate nanoparticles in rats. Part Fibre Toxicol *14*, 23.

Selvaraj, S., Sun, Y., Watt, J.A., Wang, S., Lei, S., Birnbaumer, L., Singh, B.B. (2012). Neurotoxin-induced ER stress in mouse dopaminergic neurons involves downregulation of TRPC1 and inhibition of AKT/mTOR signaling. J Clin Invest *122*, 1354-1367.

Selvarajan, V., Obuobi, S., Ee, P.L.R. (2020). Silica Nanoparticles—A Versatile Tool for the Treatment of Bacterial Infections. Frontiers in chemistry *8*, 602.

Shahmoradian, S.H., Lewis, A.J., Genoud, C., Hench, J., Moors, T.E., Navarro, P.P., Castaño-Díez, D., Schweighauser, G., Graff-Meyer, A., Goldie, K.N. (2019a). Lewy pathology in Parkinson's disease consists of crowded organelles and lipid membranes. Nature neuroscience *22*, 1099-1109.

Shahmoradian, S.H., Lewis, A.J., Genoud, C., Hench, J., Moors, T.E., Navarro, P.P., Castano-Diez, D., Schweighauser, G., Graff-Meyer, A., Goldie, K.N., et al. (2019b). Lewy pathology in Parkinson's disease consists of crowded organelles and lipid membranes. Nat. Neurosci. *22*, 1099-1109.

Shang, L., Wang, Y., Jiang, J., Dong, S. (2007). pH-dependent protein conformational changes in albumin:gold nanoparticle bioconjugates: a spectroscopic study. Langmuir *23*, 2714-2721.

Sharma, N., Brandis, K.A., Herrera, S.K., Johnson, B.E., Vaidya, T., Shrestha, R., DebBurman, S.K. (2006). α-synuclein budding yeast model. Journal of Molecular Neuroscience *28*, 161-178.

Sharma, V.P., Sharma, U., Chattopadhyay, M., Shukla, V. (2018). Advance applications of nanomaterials: a review. Materials Today: Proceedings *5*, 6376-6380.

Shaw, J.M., Nunnari, J. (2002). Mitochondrial dynamics and division in budding yeast. Trends Cell Biol *12*, 178-184.

Shen, D., Coleman, J., Chan, E., Nicholson, T.P., Dai, L., Sheppard, P.W., Patton, W.F. (2011). Novel cell-and tissue-based assays for detecting misfolded and aggregated protein accumulation within aggresomes and inclusion bodies. Cell biochemistry and biophysics *60*, 173-185.

Sheng, Y.H., Sali, A., Herzog, H., Lahnstein, J., Krilis, S.A. (1996). Site-directed mutagenesis of recombinant human beta(2)-glycoprotein I identifies a cluster of lysine residues that are critical for phospholipid binding and anti-cardiolipin antibody activity. Journal of Immunology *157*, 3744-3751.

Sigmund, W., Yuh, J., Park, H., Maneeratana, V., Pyrgiotakis, G., Daga, A., Taylor, J., Nino, J.C. (2006). Processing and structure relationships in electrospinning of ceramic fiber systems. Journal of the American Ceramic Society *89*, 395-407.

Singh, K.R.B., Nayak, V., Sarkar, T., Singh, R.P. (2020). Cerium oxide nanoparticles: properties, biosynthesis and biomedical application. RSC advances *10*, 27194-27214.

Singh, N., Marets, C., Boudon, J., Millot, N., Saviot, L., Maurizi, L. (2021). In vivo protein corona on nanoparticles: does the control of all material parameters orient the biological behavior? Nanoscale Advances *3*, 1209-1229.

Singh, R., Lillard Jr, J.W. (2009). Nanoparticle-based targeted drug delivery. Experimental and molecular pathology *86*, 215-223.

Singleton, A.B., Farrer, M., Johnson, J., Singleton, A., Hague, S., Kachergus, J., Hulihan, M., Peuralinna, T., Dutra, A., Nussbaum, R., et al. (2003). alpha-Synuclein locus triplication causes Parkinson's disease. Science *302*, 841.

Slowing, II, Wu, C.W., Vivero-Escoto, J.L., Lin, V.S. (2009). Mesoporous silica nanoparticles for reducing hemolytic activity towards mammalian red blood cells. Small *5*, 57-62.

Smith, M.G., Snyder, M. (2006). Yeast as a model for human disease. Current protocols in human genetics *48*, 15.16. 11-15.16. 18.

Spellman, P.T., Sherlock, G., Zhang, M.Q., Iyer, V.R., Anders, K., Eisen, M.B., Brown, P.O., Botstein, D., Futcher, B. (1998). Comprehensive identification of cell cycle–regulated genes of the yeast Saccharomyces cerevisiae by microarray hybridization. Molecular biology of the cell *9*, 3273-3297.

Spillantini, M.G., Schmidt, M.L., Lee, V.M., Trojanowski, J.Q., Jakes, R., Goedert, M. (1997). Alpha-synuclein in Lewy bodies. Nature *388*, 839-840.

Steckiewicz, K.P., Inkielewicz-Stepniak, I. (2020). Modified nanoparticles as potential agents in bone diseases: Cancer and implant-related complications. Nanomaterials *10*, 658.

Stefani, M., Dobson, C.M. (2003). Protein aggregation and aggregate toxicity: new insights into protein folding, misfolding diseases and biological evolution. Journal of molecular medicine *81*, 678-699.

Strain, J., Lorenz, C.R., Bode, J., Garland, S., Smolen, G.A., Ta, D.T., Vickery, L.E., Culotta, V.C. (1998). Suppressors of superoxide dismutase (SOD1) deficiency in Saccharomyces cerevisiae. Identification of proteins predicted to mediate iron-sulfur cluster assembly. J Biol Chem *273*, 31138-31144.

Su, L.J., Auluck, P.K., Outeiro, T.F., Yeger-Lotem, E., Kritzer, J.A., Tardiff, D.F., Strathearn, K.E., Liu, F., Cao, S., Hamamichi, S. (2010). Compounds from an unbiased chemical screen reverse both ER-to-Golgi trafficking defects and mitochondrial dysfunction in Parkinson's disease models. Disease models & mechanisms *3*, 194-208.

Sudha, P.N., Sangeetha, K., Vijayalakshmi, K., Barhoum, A. 2018. Nanomaterials history, classification, unique properties, production and market. *Emerging Applications of Nanoparticles and Architecture Nanostructures.* Elsevier.

Suen, D.F., Norris, K.L., Youle, R.J. (2008). Mitochondrial dynamics and apoptosis. Genes Dev *22*, 1577-1590.

Sun, H.P., Su, J.H., Meng, Q.S., Yin, Q., Chen, L.L., Gu, W.W., Zhang, Z.W., Yu, H.J., Zhang, P.C., Wang, S.L., et al. (2017). Cancer Cell Membrane-Coated Gold Nanocages with Hyperthermia-Triggered Drug Release and Homotypic Target Inhibit Growth and Metastasis of Breast Cancer. Advanced Functional Materials *27*, 1604300.

Sun, Y., Kakinen, A., Zhang, C., Yang, Y., Faridi, A., Davis, T.P., Cao, W., Ke, P.C., Ding, F. (2019). Amphiphilic surface chemistry of fullerenols is necessary for inhibiting the amyloid aggregation of alpha-synuclein NACore. Nanoscale *11*, 11933-11945.

Sutradhar, N., Sinhamahapatra, A., Pahari, S., Jayachandran, M., Subramanian, B., Bajaj, H.C., Panda, A.B. (2011). Facile Low-Temperature Synthesis of Ceria and Samarium-Doped Ceria Nanoparticles and Catalytic Allylic Oxidation of Cyclohexene. Journal of Physical Chemistry C *115*, 7628-7637.

Suzuki, H., Toyooka, T., Ibuki, Y. (2007). Simple and easy method to evaluate uptake potential of nanoparticles in mammalian cells using a flow cytometric light scatter analysis. Environmental science & technology *41*, 3018-3024.

Tarannum, N., Singh, M. (2013). Advances in synthesis and applications of sulfo and carbo analogues of polybetaines: a review. Reviews in Advanced Sciences and Engineering *2*, 90-111.

Tardiff, D.F., Tucci, M.L., Caldwell, K.A., Caldwell, G.A., Lindquist, S. (2012). Different 8-hydroxyquinolines protect models of TDP-43 protein, α-synuclein, and polyglutamine proteotoxicity through distinct mechanisms. Journal of Biological Chemistry *287*, 4107-4120.

Tassinari, R., Di Felice, G., Butteroni, C., Barletta, B., Corinti, S., Cubadda, F., Aureli, F., Raggi, A., Narciso, L., Tait, S., et al. (2020). Hazard identification of pyrogenic synthetic amorphous silica (NM-203) after sub-chronic oral exposure in rat: A multitarget approach. Food Chem Toxicol *137*, 111168.

Teichroeb, J.H., Forrest, J.A., Jones, L.W. (2008). Size-dependent denaturing kinetics of bovine serum albumin adsorbed onto gold nanospheres. Eur Phys J E Soft Matter *26*, 411-415.

Tenzer, S., Docter, D., Rosfa, S., Wlodarski, A., Kuharev, J.r., Rekik, A., Knauer, S.K., Bantz, C., Nawroth, T., Bier, C. (2011). Nanoparticle size is a critical physicochemical determinant of the human blood plasma corona: a comprehensive quantitative proteomic analysis. ACS nano *5*, 7155-7167.

Tenzer, S., Docter, D., Kuharev, J., Musyanovych, A., Fetz, V., Hecht, R., Schlenk, F., Fischer, D., Kiouptsi, K., Reinhardt, C., et al. (2013). Rapid formation of plasma protein corona critically affects nanoparticle pathophysiology. Nat Nanotechnol *8*, 772-781.

Terna, A.D., Elemike, E.E., Mbonu, J.I., Osafile, O.E., Ezeani, R.O. (2021). The future of semiconductors nanoparticles: Synthesis, properties and applications. Materials Science and Engineering: B *272*, 115363.

Terribile, D., Trovarelli, A., Llorca, J., de Leitenburg, C., Dolcetti, G. (1998). The synthesis and characterization of mesoporous high-surface area ceria prepared using a hybrid organic/inorganic route. Journal of Catalysis *178*, 299-308.

Thakkar, K.N., Mhatre, S.S., Parikh, R.Y. (2010). Biological synthesis of metallic nanoparticles. Nanomedicine *6*, 257-262.

Thakur, N., Manna, P., Das, J. (2019). Synthesis and biomedical applications of nanoceria, a redox active nanoparticle. J Nanobiotechnology *17*, 84.

Tian, Z.M., Li, J., Zhang, Z.Y., Gao, W., Zhou, X.M., Qu, Y.Q. (2015). Highly sensitive and robust peroxidase-like activity of porous nanorods of ceria and their application for breast cancer detection. Biomaterials *59*, 116-124.

Tira, R., De Cecco, E., Rigamonti, V., Santambrogio, C., Barracchia, C.G., Munari, F., Romeo, A., Legname, G., Prosperi, D., Grandori, R. (2020). Dynamic molecular exchange and conformational transitions of alpha-synuclein at the nano-bio interface. International Journal of Biological Macromolecules *154*, 206-216.

Tong, A.H., Evangelista, M., Parsons, A.B., Xu, H., Bader, G.D., Page, N., Robinson, M., Raghibizadeh, S., Hogue, C.W., Bussey, H., et al. (2001). Systematic genetic analysis with ordered arrays of yeast deletion mutants. Science *294*, 2364-2368.

Treusch, S., Hamamichi, S., Goodman, J.L., Matlack, K.E., Chung, C.Y., Baru, V., Shulman, J.M., Parrado, A., Bevis, B.J., Valastyan, J.S. (2011). Functional links between Aβ toxicity, endocytic trafficking, and Alzheimer's disease risk factors in yeast. Science *334*, 1241-1245.

Tsunekawa, S., Ishikawa, K., Li, Z.-Q., Kawazoe, Y., Kasuya, A. (2000). Origin of anomalous lattice expansion in oxide nanoparticles. Physical Review Letters *85*, 3440.

Tuite, M.F. (2019). Yeast models of neurodegenerative diseases. Prog Mol Biol Transl Sci *168*, 351-379.

Uetz, P., Giot, L., Cagney, G., Mansfield, T.A., Judson, R.S., Knight, J.R., Lockshon, D., Narayan, V., Srinivasan, M., Pochart, P. (2000). A comprehensive analysis of protein–protein interactions in Saccharomyces cerevisiae. Nature *403*, 623-627.

Uribe-Querol, E., Rosales, C. (2020). Phagocytosis: our current understanding of a universal biological process. Frontiers in immunology *11*, 1066.

van der Zande, M., Vandebriel, R.J., Groot, M.J., Kramer, E., Herrera Rivera, Z.E., Rasmussen, K., Ossenkoppele, J.S., Tromp, P., Gremmer, E.R., Peters, R.J., et al. (2014). Sub-chronic toxicity study in rats orally exposed to nanostructured silica. Part Fibre Toxicol *11*, 8.

van Kesteren, P.C., Cubadda, F., Bouwmeester, H., van Eijkeren, J.C., Dekkers, S., de Jong, W.H., Oomen, A.G. (2015). Novel insights into the risk assessment of the nanomaterial synthetic amorphous silica, additive E551, in food. Nanotoxicology *9*, 442-452.

Veillat, V., Spuul, P., Daubon, T., Egana, I., Kramer, I., Genot, E. (2015). Podosomes: Multipurpose organelles? Int J Biochem Cell Biol *65*, 52-60.

Vera, M., Pani, B., Griffiths, L.A., Muchardt, C., Abbott, C.M., Singer, R.H., Nudler, E. (2014). The translation elongation factor eEF1A1 couples transcription to translation during heat shock response. Elife *3*, e03164.

Vertegel, A.A., Siegel, R.W., Dordick, J.S. (2004). Silica nanoparticle size influences the structure and enzymatic activity of adsorbed lysozyme. Langmuir *20*, 6800-6807.

Viitanen, P.V., Lorimer, G.H., Seetharam, R., Gupta, R., Oppenheim, J., Thomas, J., Cowan, N. (1992). Mammalian mitochondrial chaperonin 60 functions as a single toroidal ring. Journal of Biological Chemistry *267*, 695-698.

Vijiaratnam, N., Simuni, T., Bandmann, O., Morris, H.R., Foltynie, T. (2021). Progress towards therapies for disease modification in Parkinson's disease. Lancet Neurol *20*, 559-572.

Virlan, M.J.R., Miricescu, D., Radulescu, R., Sabliov, C.M., Totan, A., Calenic, B., Greabu, M. (2016). Organic nanomaterials and their applications in the treatment of oral diseases. Molecules *21*, 207.

Vitali, M., Rigamonti, V., Natalello, A., Colzani, B., Avvakumova, S., Brocca, S., Santambrogio, C., Narkiewicz, J., Legname, G., Colombo, M., et al. (2018). Conformational properties of intrinsically disordered proteins bound to the surface of silica nanoparticles. Biochim Biophys Acta Gen Subj *1862*, 1556-1564.

Vucic, S., Kiernan, M.C., Menon, P., Huynh, W., Rynders, A., Ho, K.S., Glanzman, R., Hotchkin, M.T. (2021). Study protocol of RESCUE-ALS: A Phase 2, randomised, double-blind, placebo-controlled study in early symptomatic amyotrophic lateral sclerosis patients to assess bioenergetic catalysis with CNM-Au8 as a mechanism to slow disease progression. BMJ open *11*, e041479.

Walkey, C.D., Chan, W.C. (2012). Understanding and controlling the interaction of nanomaterials with proteins in a physiological environment. Chem Soc Rev *41*, 2780-2799.

Walkey, C.D., Olsen, J.B., Song, F., Liu, R., Guo, H., Olsen, D.W., Cohen, Y., Emili, A., Chan, W.C. (2014). Protein corona fingerprinting predicts the cellular interaction of gold and silver nanoparticles. ACS nano *8*, 2439-2455.

Wang, C.H., Lin, S.S. (2004). Preparing an active cerium oxide catalyst for the catalytic incineration of aromatic hydrocarbons. Applied Catalysis a-General *268*, 227-233.

Wang, H., Zhu, J.J., Zhu, J.M., Liao, X.H., Xu, S., Ding, T., Chen, H.Y. (2002). Preparation of nanocrystalline ceria particles by sonochemical and microwave assisted heating methods. Physical Chemistry Chemical Physics *4*, 3794-3799.

Wang, T., Bai, J., Jiang, X., Nienhaus, G.U. (2012). Cellular uptake of nanoparticles by membrane penetration: a study combining confocal microscopy with FTIR spectroelectrochemistry. ACS nano *6*, 1251-1259.

Wang, X., Huang, T., Bu, G., Xu, H. (2014). Dysregulation of protein trafficking in neurodegeneration. Mol Neurodegener *9*, 31.

Wang, Y., Meriin, A.B., Zaarur, N., Romanova, N.V., Chernoff, Y.O., Costello, C.E., Sherman, M.Y. (2009). Abnormal proteins can form aggresome in yeast: aggresome-targeting signals and components of the machinery. The FASEB Journal *23*, 451-463.

Williams-Gray, C.H., Wijeyekoon, R., Yarnall, A.J., Lawson, R.A., Breen, D.P., Evans, J.R., Cummins, G.A., Duncan, G.W., Khoo, T.K., Burn, D.J. (2016). S erum immune markers and disease progression in an incident P arkinson's disease cohort (ICICLE-PD). Movement disorders *31*, 995-1003.

Winzeler, E.A., Shoemaker, D.D., Astromoff, A., Liang, H., Anderson, K., Andre, B., Bangham, R., Benito, R., Boeke, J.D., Bussey, H., et al. (1999). Functional characterization of the S. cerevisiae genome by gene deletion and parallel analysis. Science *285*, 901-906.

Wong, L.L., Pye, Q.N., Chen, L., Seal, S., McGinnis, J.F. (2015). Defining the catalytic activity of nanoceria in the P23H-1 rat, a photoreceptor degeneration model. PloS one *10*, e0121977.

Wu, H., Ng, B.S., Thibault, G. (2014). Endoplasmic reticulum stress response in yeast and humans. Biosci Rep *34*, e00118.

Wu, J., Xie, H. (2016). Effects of titanium dioxide nanoparticles on α-synuclein aggregation and the ubiquitin-proteasome system in dopaminergic neurons. Artificial cells, nanomedicine, and biotechnology *44*, 690-694.

Xiao, B., Deng, X., Zhou, W., Tan, E.-K. (2016). Flow cytometry-based assessment of mitophagy using MitoTracker. Frontiers in cellular neuroscience *10*, 76.

Xiao, R., Tang, P., Yang, B., Huang, J., Zhou, Y., Shao, C., Li, H., Sun, H., Zhang, Y., Fu, X.D. (2012). Nuclear matrix factor hnRNP U/SAF-A exerts a global control of alternative splicing by regulating U2 snRNP maturation. Mol Cell *45*, 656-668.

Yadav, I., Aswal, V.K., Kohlbrecher, J. (2016). Size-dependent interaction of silica nanoparticles with lysozyme and bovine serum albumin proteins. Phys Rev E *93*, 052601.

Yan, Y., Gause, K.T., Kamphuis, M.M., Ang, C.-S., O'Brien-Simpson, N.M., Lenzo, J.C., Reynolds, E.C., Nice, E.C., Caruso, F. (2013). Differential roles of the protein corona in the cellular uptake of nanoporous polymer particles by monocyte and macrophage cell lines. ACS nano *7*, 10960-10970.

Yang, J.A., Johnson, B.J., Wu, S., Woods, W.S., George, J.M., Murphy, C.J. (2013). Study of wild-type α-synuclein binding and orientation on gold nanoparticles. Langmuir *29*, 4603-4615.

Yin, L.X., Wang, Y.Q., Pang, G.S., Koltypin, Y., Gedanken, A. (2002). Sonochemical synthesis of cerium oxide nanoparticles - Effect of additives and quantum size effect. Journal of Colloid and Interface Science *246*, 78-84.

Yokel, R.A., Florence, R.L., Unrine, J.M., Tseng, M.T., Graham, U.M., Wu, P., Grulke, E.A., Sultana, R., Hardas, S.S., Butterfield, D.A. (2009). Biodistribution and oxidative stress effects of a systemically-introduced commercial ceria engineered nanomaterial. Nanotoxicology *3*, 234-248.

Yokel, R.A., Hussain, S., Garantziotis, S., Demokritou, P., Castranova, V., Cassee, F.R. (2014). The Yin: An adverse health perspective of nanoceria: uptake, distribution, accumulation, and mechanisms of its toxicity. Environ Sci Nano *1*, 406-428.

Yoshida, T., Yoshioka, Y., Takahashi, H., Misato, K., Mori, T., Hirai, T., Nagano, K., Abe, Y., Mukai, Y., Kamada, H. (2014). Intestinal absorption and biological effects of orally administered amorphous silica particles. Nanoscale research letters *9*, 1-7.

Zesiewicz, T., Salemi, J.L., Perlman, S., Sullivan, K.L., Shaw, J.D., Huang, Y., Isaacs, C., Gooch, C., Lynch, D.R., Klein, M.B. (2018). Double-blind, randomized and controlled trial of EPI-743 in Friedreich's ataxia. Neurodegener Dis Manag *8*, 233-242.

Zhang, H., Dunphy, D.R., Jiang, X., Meng, H., Sun, B., Tarn, D., Xue, M., Wang, X., Lin, S., Ji, Z., et al. (2012). Processing pathway dependence of amorphous silica nanoparticle toxicity: colloidal vs pyrolytic. J Am Chem Soc *134*, 15790-15804.

Zhang, Q.L., Yang, Z.M., Ding, B.J. Synthesis of cerium oxide nanoparticles by the precipitation method. Materials Science Forum, 2009. Trans Tech Publ, 233-238.

Zhang, S., Gao, H., Bao, G. (2015). Physical Principles of Nanoparticle Cellular Endocytosis. ACS nano *9*, 8655-8671.

Zhou, F., Zhao, X.M., Xu, H., Yuan, C.G. (2007). CeO2 spherical crystallites: Synthesis, formation mechanism, size control, and electrochemical property study. Journal of Physical Chemistry C *111*, 1651-1657.

Zhou, K.B., Wang, X., Sun, X.M., Peng, Q., Li, Y.D. (2005). Enhanced catalytic activity of ceria nanorods from well-defined reactive crystal planes. Journal of Catalysis *229*, 206-212.

Zhu, H., Bilgin, M., Bangham, R., Hall, D., Casamayor, A., Bertone, P., Lan, N., Jansen, R., Bidlingmaier, S., Houfek, T. (2001). Global analysis of protein activities using proteome chips. Science *293*, 2101-2105.

Zhu, M., Fink, A.L. (2003). Lipid binding inhibits α-synuclein fibril formation. Journal of Biological Chemistry *278*, 16873-16877.

Zoungrana, T., Findenegg, G.H., Norde, W. (1997). Structure, Stability, and Activity of Adsorbed Enzymes. J Colloid Interface Sci *190*, 437-448.